I. Magnesium Promoted Coupling of Carbodiimides and Terminal Acetylenes

II. Bismuth Compounds Supported by Di(amido) Chelating Ligands

by

Ryan James Schwamm

Victoria
UNIVERSITY OF WELLINGTON
Te Whare Wānanga
o te Ūpoko o te Ika a Māui

A thesis
submitted to Victoria University of Wellington
in fulfilment of the
requirements for the degree of
Masters of Science
in Chemistry

Victoria University of Wellington

2014

Abstract

The work presented in this thesis is divided into two parts, both of which investigate the chemistry of main group elements supported by N,N'-donor ligands.

Part 1 investigates the use of Mg(mesC{NCy}$_2$)(N{SiMe$_3$}$_2$)(THF) (mes = 2,4,6-Me$_3$C$_6$H$_3$, Cy = C$_6$H$_{11}$) as a pre-catalyst for the coupling of terminal acetylenes to carbodiimides. A catalytic cycle for the reaction is proposed, based on a series of stoichiometric reactions. Ligand redistribution via Schlenk equilibria is a prominent feature of the proposed catalytic cycle. The scope of catalysis was also investigated, indicating a strong dependence on the sterics and electronics of both the carbodiimide and the terminal acetylene. Investigation of other magnesium species identified other pathways into the catalytic cycle.

Part 2 explores the derivitisation of Bi(Me$_2$Si{NAr})Cl (Ar = 2,6-i-Pr$_2$C$_6$H$_3$) to form a number of novel bismuth(III) species of the general formula Bi(Me$_2$Si{NAr})X (X = alkyl, aryl, amide, aryloxide, phosphide). In addition, a number of cationic bismuth species have been isolated from the reaction of Bi(Me$_2$Si{NAr})Cl with ECl$_3$ (E = Al, Ga). Preliminary investigations reveal that the amide and aryloxide derivatives are active as initiators for the ring-opening polymerisation of lactide and ε-caprolactone. A number of bismuth(III) compounds bearing the related di(amido)ether ligands [O(Me$_2$Si{NAr})$_2$]$^{2-}$ have also been synthesised.

Acknowledgements

Table of Contents

List of Figures

Bismuth Compounds Supported by Di(amido) Chelating Ligands   74

List of Tables

List of Schemes

Magnesium Promoted Coupling of Carbodiimides and Terminal Acetylenes

Bismuth Compounds Supported by Di(amido) Chelating Ligands

List of Equations

xiv

Glossary

δ	Chemical shift
Δ	Difference in . . .
$\sum$	Sum of . . .
%cov	Percentage of the sum of covalent radii.
σ_p	Hammett value (*para*)
1,8-napthalene	1,8-$C_{10}H_6\{NSiMe_3\}_2$
Ar	2,6-di-*iso*-propylphenyl, 2,6-i-$Pr_2C_6H_3$
Ar'	2,6-di-*tert*-butylphenyl, 2,6-t-$Bu_2C_6H_3$
Ar"	2,6-di-*iso*-propylphenyl (2,6-i-$Pr_2C_6H_3$) or 2,6-dimethylphenyl (2,6-$Me_2C_6H_3$)
Ar†	2-methylphenyl (2-MeC_6H_2) or 4-methylphenyl, 4-MeC_6H_2
BSS	Bismuth subsilacylate
BDI_{DIPP}	β-diketiiminate (2,6-di-*iso*-propylphenyl derivative), $[HC(CMeNAr)_2]^-$
CN	Coordination Number
Cp	Cyclopentadienyl ligand, C_5H_5
Cp*	Pentamethylcyclopentadienyl ligand, C_5Me_5
Cy	Cyclohexyl, C_6H_{11}
cy-salen	2,2'-cyclohexylbis(nitriomethylidene)diphenol
DOP	Degree of Pyramidalisation
EI-MS	Electron Ionisation Mass Spectrometry
eq.	Equation
Et	Ethyl, CH_2CH_3
Et_2O	Diethyl ether, $O(CH_2CH_3)_2$
HMBC	Heteronuclear Multiple Bond Correlation
Hz	Hertz
i-Pr	*iso*-propyl, $CH(CH_3)_2$

Ln	Lanthanide
m-	*meta-*
m/z	Mass to charge ratio
Me	Methyl, CH_3
mes	2,4,6-trimethylphenyl, $Me_3C_6H_2$
n-Bu	Butyl, $(CH_2)_3CH_3$
nOe	Nuclear Overhauser effect
NMR	Nuclear Magnetic Resonance
o-	*ortho-*
p-	*para-*
Ph	Phenyl, C_6H_5
PLA	Poly-lactic Acid (poly lactide)
ppm	Parts per million
r_{cov}	Covalent radius
ROP	Ring-opening Polymerisation
t-Bu	*tert*-Butyl, $C(CH_3)_3$
THF	Tetrahydrofuran, $O(CH_2CH_2)_2$
VT	Variable Temperature

Part I

Magnesium Promoted Coupling of Carbodiimides and Terminal Acetylenes

Chapter 1

Introduction

1.1 Alkaline Earth Metals (Mg, Ca, Sr, Ba)

The high natural abundance and low toxicity of the group 2 (alkaline earth) elements make them attractive for a wide range of important applications.[1] The chemistry of group 2 metals is dominated by the +2 oxidation state, with compounds largely inactive towards redox processes. Group 2 organometallic compounds are often described as intermediates between the highly polarising nature of the group 1 organometallic compounds (e.g. alkyl lithium) and the high Lewis acidity of the group 3 metals (e.g. aluminium) (Figure 1.1).[2] The reactivity of organometallic alkaline earth metal species generally increases down the group, as the metal centres become increasingly electropositive.[3]
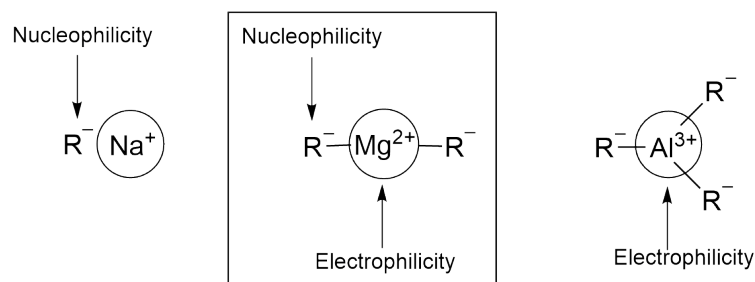
Figure 1.1: General reactivity of group 1, 2 and 3 organometallic species.

Group 2 metals share many properties with the lanthanides, governed by similar bonding interactions, which are highly ionic and non-directional.[2] This has resulted in proposed links between the reactivity of the two classes of compound. Organolanthanide(III) compounds have a versatile chemistry and have been utilised in a wide range of reactions. These compounds demonstrate two fundamental types of reactivity: (i) σ-bond metathesis and (ii) insertion of an unsaturated bond into a M-X σ-bond (X = C, N, O, P) (Figure 1.2).
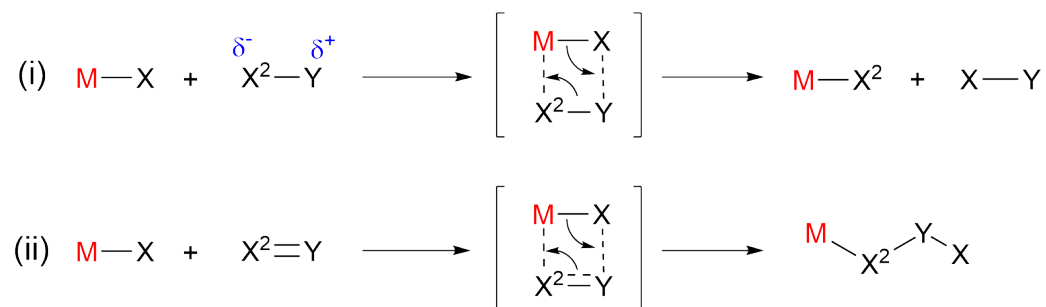
Figure 1.2: Reactivity of organolanthanide(III) compounds.

A number of catalytic reactions incorporating these key steps have been developed using lanthanide(III) compounds.[4] The similar reactivity of lanthanide(III) compounds and the alkaline earth metal species has recently led to investigations into the catalytic activity of compounds of the group 2 elements.

1.1.1 Heavy alkaline earth metal catalysis

A series of recent publications by Hill and co-workers has demonstrated the effectiveness of a number of β-diketiminate stabilised heavy alkaline earth amides as pre-catalysts for hydroamination and hydrophosphination of a range of different unsaturated substrates (Figure 1.3).[5–9]

In related studies, Harder and co-workers reported that heavy alkaline earth benzyl complexes, $M(\{2\text{-}(Me_2N)C_6H_4\}CHSiMe_3)_2(THF)$ (M = Ca, Sr), are catalytically active for hydrosilylation reactions with unsaturated substrates.[10] Calcium compounds have also been extensively explored as catalysts for the polymerisations of

$Ca(BDI_{DIPP})(N\{SiMe_3\}_2)(THF)$
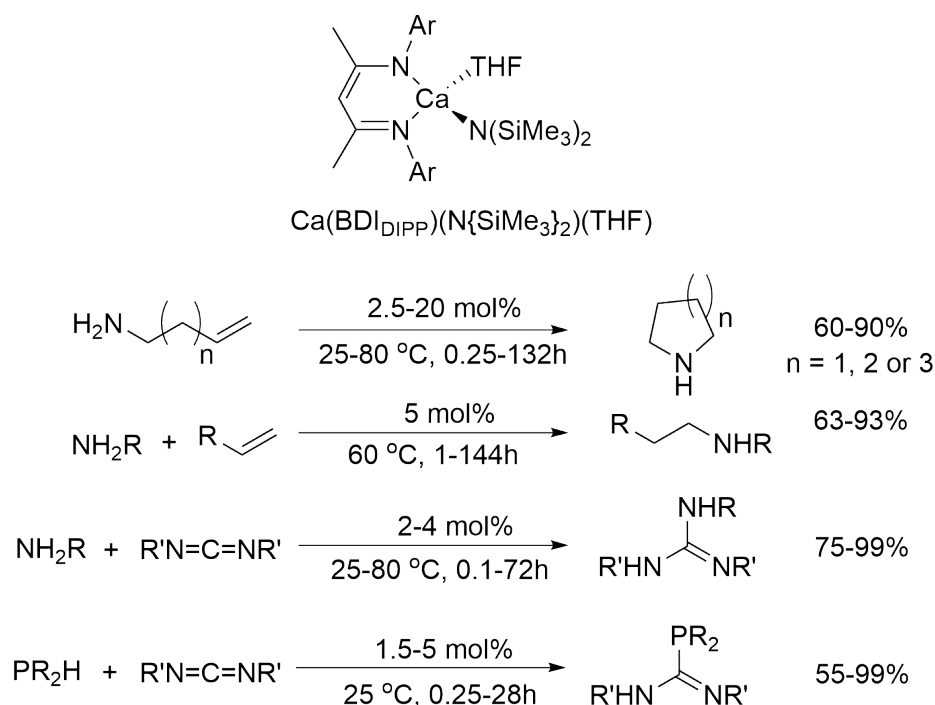
Figure 1.3: $Ca(BDI_{DIPP})(N\{SiMe_3\}_2)(THF)$ catalysed heterofunctionalisation of unsaturated substrates $(BDI_{DIPP} = [CH(C(Me)\{NAr\})_2]^-,\ Ar = 2,6\text{-}i\text{-}Pr_2C_6H_3)$.

activated alkenes and the ring-opening polymerisation of lactide.[11–13]

1.1.2 Magnesium catalysis

Magnesium compounds have been implemented as one of the most important tools in synthetic laboratories since the discovery of Grignard reagents. Grignard reagents are typically viewed as a source of nucleophilic carbon, due to the highly polarising nature of the Mg-R bond. Reaction of Grignard reagents with electrophilic carbon centres results in stoichiometric C-C bond formation via nucleophilic attack (Scheme 1.1). These reactions are strictly stoichiometric in metal.
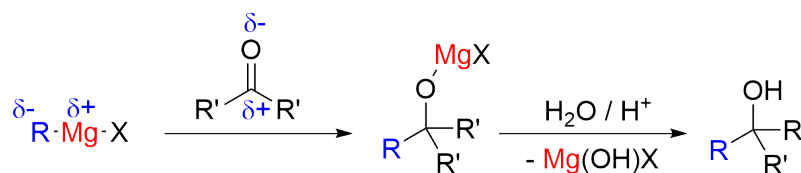
Scheme 1.1: Nucleophilic attack of a Grignard reagent with an electrophilic carbonyl functionality.

4

Catalytically active magnesium compounds remain an attractive target for industrial and small scale operations due to the commercial availability of many magnesium compounds and relatively low toxicity of magnesium. A number of groups have reported the use of catalytically active magnesium compounds for the hydroamination of unsaturated substrates.[14–17] Recent work by Coles and co-workers has explored the catalysis of the Tishchenko reaction by magnesium amidinate and guanidinate compounds.[18,19] In a closely related investigation to the work presented in this thesis, Hill et al. recently reported the use of $MgBu_2$ for the magnesium mediated reaction between alkynes and isocyanates to form bis(imidazolidine-2,4-diones) (eq. 1.1).[20]
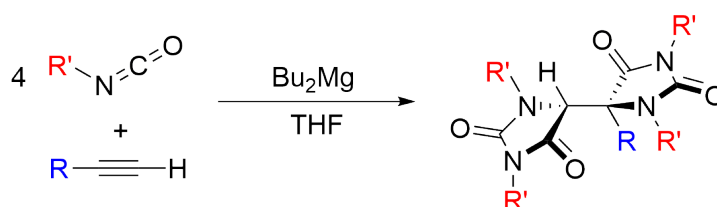
eq. 1.1: Magnesium facilitated synthesis of bis(imidazolidine-2,4-dione).

1.1.3 Schlenk equilibrium

An important consideration when dealing with heteroleptic alkaline earth metal compounds is the propensity for these compounds to undergo Schlenk-like equilibria, whereby the ligands redistribute to form the corresponding homoleptic species (eq. 1.2). These equilibria can result in complications in the application of alkaline earth species in catalysis; for example (1) loss of the ancillary ligand from the metal centre may result in reduced solubility; (2) a reduction in the control of the environment of the reactive centre.

$$2\ RMgX \rightleftharpoons MgR_2 + MgX_2$$
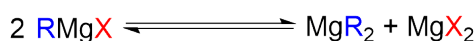
eq. 1.2: Schlenk equilibrium in organomagnesium halides.

Ligand redistribution can generally be limited through the use of bulky ancilliary ligands capable of sterically destabilising the formation of the homoleptic species

(eq. 1.3).

$$2 \quad R\!-\!Mg\!-\!X \quad \rightleftharpoons \quad MgR_2 + MgX_2$$
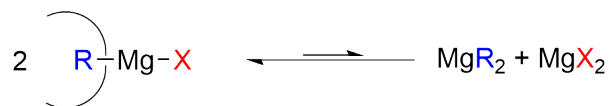
eq. 1.3: Steric destabilisation of the Schlenk equilibrium.

Although not specific to the work presented in this thesis, we note that Schlenk equilibria pose a greater problem for the heavier alkaline earth metals (Ca, Sr and Ba) due to the increased size of the metal centres. Therefore these metals require greater steric protection, with a lot of the research in this field being focussed on finding suitable ligands.[21]

1.2 Amidinate and Guanidinate Ligands

Amidinate ligands ($[RC\{NR'\}_2]^-$) have been employed as ancilliary ligands in a wide range of metal complexes, spanning all groups of the periodic table.[22] One attractive property of amidinate ligands is the range of different derivatives that are accessible through substitution at both the nitrogen and backbone-carbon positions, with substitution at the carbon centre dictating nomenclature. Amidinate and guanidinate (R = amine) ligands have received significant attention for their stabilising properties, relatively simple synthesis and tunability.[22] These ligands contain conjugated π-systems, allowing for delocalisation of electron density and charge over
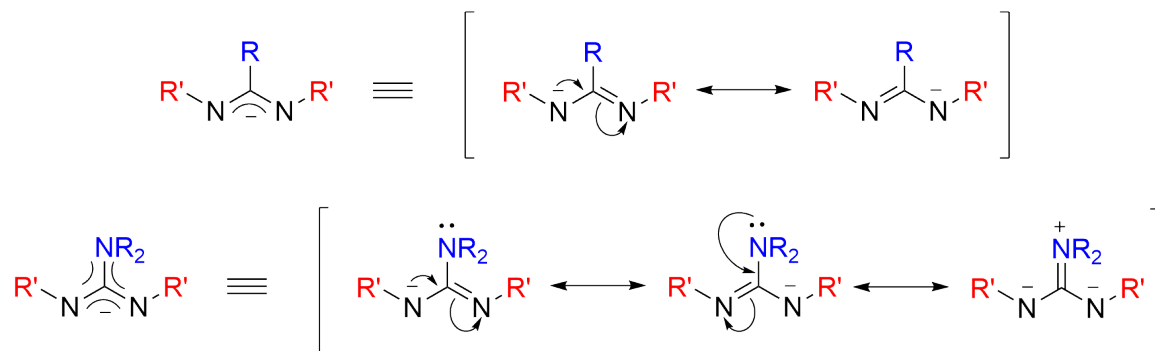
Figure 1.4: Resonance structures for amidinate (top) and guanidinate (bottom).

the CN_2 sub-unit (Figure 1.4). While the amidinate ligand is stabilised by two resonance structures, the guanidinate ligand has the potential to form three resonance structures via donation of the lone pair from the tertiary amine, resulting in greater electronic stabilisation.

Many bonding modes for amidinate and guandinate ligands have been observed. Mono-dentate binding of the amidinate to the metal centre (Figure 1.5, A) results when electron density is localised in a C=N bond. Chelation to a single metal centre affords a four-membered metallacycle (B), while bridging between two-, three- and four- metal centres has been utilised in the synthesis of multi-metallic clusters (C, D and E).
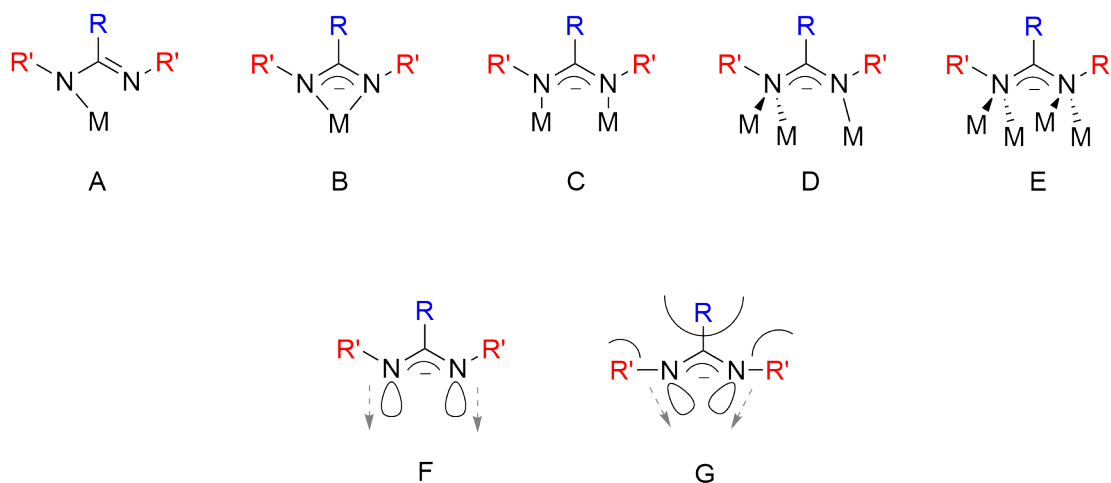
Figure 1.5: Possible bonding modes (top) and dependence of sp^2 orbital position on R/R' (bottom).

Jordan and co-workers proposed that in an idealised amidinate structure, 120° bond angles at the carbon and nitrogen centres result in parallel projection of the sp^2 donor obitals (F), favouring a bridging bonding mode.[23] Increasing the R-C-N and C-N-R' bond angles, achieved through the incorporation of sterically demanding groups at the nitrogen and backbone-carbon, results in projection of the lone pair nitrogen orbitals towards the centre of the amidinate (G), favouring a chelating bonding mode.

Guanidinate ligands have been shown to provide significant steric protection to

smaller metal centres. Jones and co-workers recently demonstrated this stability in the formation of the first Mg(I) species $[\{i\text{-}Pr_2N\}C\{NAr\}_2Mg]_2$ (Ar = 2,6-i-Pr$_2$C$_6$H$_3$).[24] Previous work in the Coles group has illustrated the effectiveness of the amidinate ligand $[(\text{mes})C\{NCy\}]^-$ (mes = 2,4,6-Me$_3$C$_6$H$_2$) for the stabilisation of heteroleptic magnesium compounds.[18] This work identified Mg(mesC$\{NCy\}_2$)(N$\{SiMe_3\}_2$)(THF) (**1**) as a pre-catalyst for the Tishchenko reaction. No evidence of ligand redistribution was observed during catalytic studies, consistent with significant steric protection at the magnesium centre.

1.3 Catalytic Coupling of Terminal Acetylenes and Carbodiimides

The catalytic coupling of terminal acetylenes to carbodiimide substrates, via C-C bond formation, provides an atom economic route to the corresponding propargylamidine compounds (eq. 1.4). While this reaction does not occur spontaneously, formation of the corresponding propargylamidines can be achieved in the presence of a catalyst.
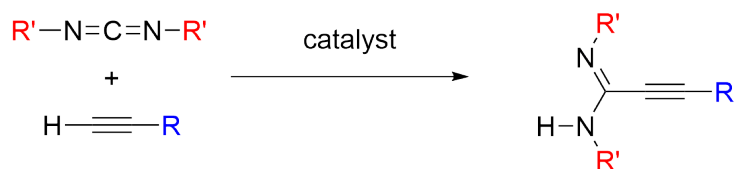
eq. 1.4: Catalytic coupling of terminal acetylenes and carbodiimides.

Ong et al. reported amido- and organo-lithium reagents as pre-catalysts for the coupling of terminal acetylenes and carbodiimides.[25] Hou and co-workers recently reported the catalytic coupling of terminal acetylenes to carbodiimides promoted by the half-sandwich yttrium complex (Me$_2$Si$\{C_5Me_4\}\{NPh\}$)Y(CH$_2$SiMe$_3$)(THF)$_2$.[26] No catalytic activity was observed for the tris(alkyl) complex Y(CH$_2$SiMe$_3$)$_3$(THF)$_2$, highlighting the importance of the correct combination of ligands in this process.

A catalytic cycle for the reaction was proposed (Figure 1.6). Entry into the catalytic cycle is achieved via the protonolysis of the alkyl substituent by a terminal acetylene. Subsequent insertion of the carbodiimide into the Y-C$_{acetylide}$ bond results in formation of the corresponding propargylamidinate species. Protonolysis of the propargylamidinate by the terminal acetylene liberates the propargylamidine and regenerates the acetylide species.
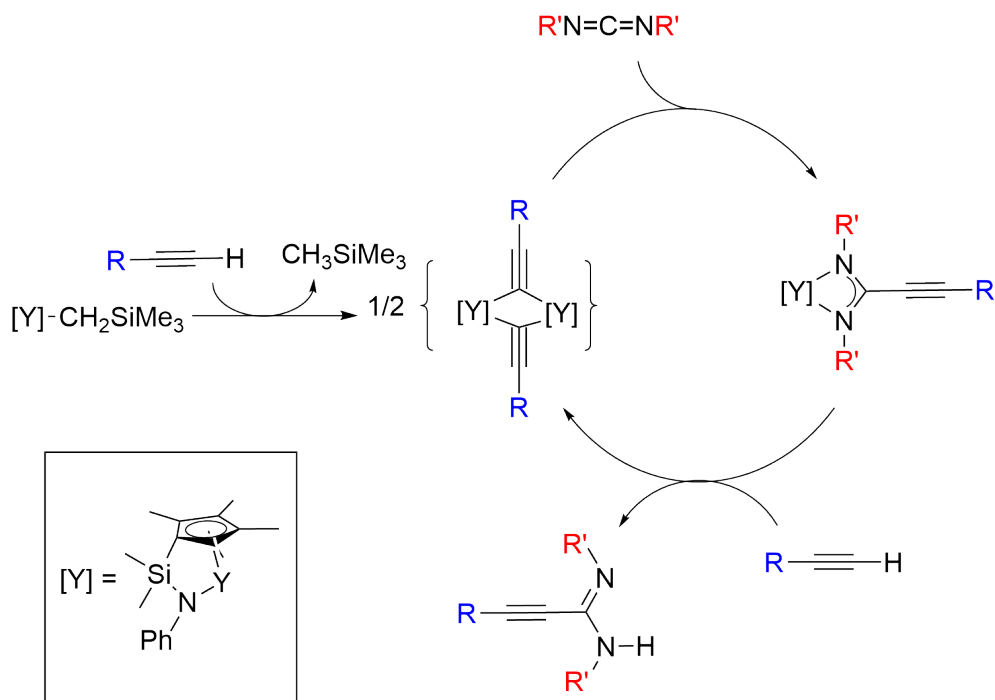
Figure 1.6: Proposed catalytic cycle for the catalytic coupling of terminal acetylenes and carbodiimides.

Hill and co-workers have exploited the similarities between the heavy alkaline earth metals and the lanthanides to extend this catalytic activity to calcium.[27] An analogous catalytic cycle was proposed for the reaction, based on the similar reactivity of Ln(III) and Ca(II).

1.4 Research Outlook

Preliminary evidence indicated that Mg(mesC{NCy}$_2$)(N{SiMe$_3$}$_2$)(THF) (**1**) is active for the catalytic coupling of terminal acetylenes with carbodiimides, showing

comparable yields to those seen for the calcium-based system.[28] The aim of the work presented in Part 1 was to investigate the catalytic properties of the established magnesium pre-catalyst **1** for the catalytic coupling of terminal acetylenes with carbodiimides (eq. 1.5). Investigation of the conditions and scope of the catalysis was planned through the use of NMR spectroscopy. Identification of key intermediates in the reaction pathway was targeted to provide information about the catalytic cycle.
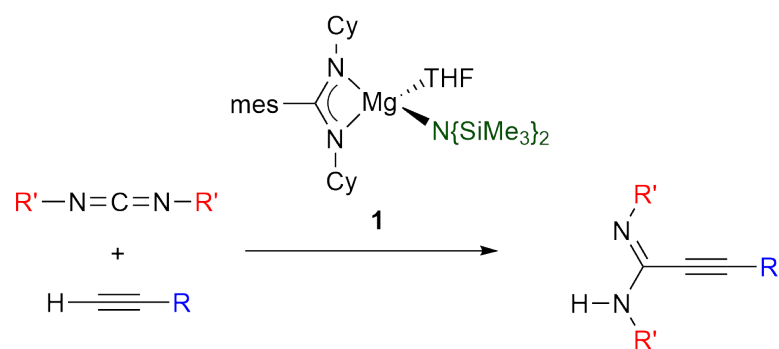
eq. 1.5: Magnesium facilitated coupling of terminal acetylenes and carbodiimides.

Chapter 2

Results and Discussion

2.1   Outline

This chapter describes a detailed analysis of the magnesium promoted catalytic coupling of terminal acetylenes and carbodiimides.

Section 2.2 investigates the effect of changing the reaction conditions (temperature, catalyst loading, solvent, time) on the catalytic activity. A series of catalytic reactions were performed on an NMR scale to determine optimal conditions. The optimal results were obtained when the reaction mixture was heated to 80 °C for 24 hours in C_6D_6. These conditions were retained throughout this investigation.

Section 2.3 investigates the catalytic cycle of the magnesium promoted coupling of terminal acetylenes and carbodiimides. A series of stoichiometric reactions were performed in order to elucidate the individual steps of the catalysis.

Section 2.4 explores the scope of catalysis with respect to the acetylene and carbodiimide substrates. Substrate dependence was monitored for a range of terminal acetylenes and carbodiimides. The dependence on the sterics and electronics of substrates was used to provide information about the reaction mechanism.

Section 2.5 explores the activity of a range of magnesium reagents, including Grignard reagents, as possible pre-catalysts for this reaction.

Section 2.6 details the independent synthesis and isolation of a number of compounds identified in the catalytic cycle.

Section 2.7 provides a comparison of the solid-state structures of magnesium species isolated in Section 2.6. An investigation into the effect of the geometry on the delocalisation of electron density over the amidinate CN_2 unit is presented.

2.2   Reaction Conditions

The effectiveness of **1** in the catalytic addition of terminal alkynes to carbodiimides was initially investigated using *N,N'*-diisopropylcarbodiimide and phenylacetylene as standard substrates. Reactions were performed on an NMR scale in C_6D_6 and monitored by ^{1}H NMR spectroscopy. A stock solution of **1** in C_6D_6 (0.0034 M) was used to administer the pre-catalyst. A range of potential internal standards (1,5-cyclooctadiene, mesitylene, 1,4-dimethoxybenzene, ferrocene and *p*-xylene) were tested, but were unsuitable due to overlap with other resonances. Reported yields were therefore determined by comparison of the integral of the *iso*-propyl methine resonance of PhC≡CC{NH*i*-Pr}{N*i*-Pr} (**5**) in the ^{1}H NMR spectrum, with the integral of the THF from **1** after 24 hours, unless stated otherwise (Figure 2.1).

Preliminary reactions using a catalyst loading of 10 mol% **1** yielded 44% of the corresponding propargylamidine at room temperature (Table 2.1, entry 1). Reducing the catalyst loading to 1 mol% resulted in a significantly lower yield (24%) (entry 2). Heating the reaction mixture resulted in improved yields (entries 3 and 4), with good yields (∼70 %) obtained at 80 °C. As a control reaction, it was determined that there was no formation of the corresponding propargylamidine in the absence of **1** under the same conditions.

Table 2.1: Dependence of catalytic activity on reaction conditions.

entry	catalyst loading (mol%)	solvent	temp (°C)	yield (%)
1	10	C_6D_6	25	44
2	1	C_6D_6	25	24
3	1	C_6D_6	50	53
4	1	C_6D_6	80	72
5	5	toluene	80	73[a]
6	5	THF	80	51[a]

[a]Isolated yield.

The catalysis was repeated on a preparative scale using standard substrates and 5 mol% **1** (entries 5 and 6). Using toluene as the solvent gave better yields than using THF, consistent with competitive binding of THF to the active Mg centre during catalysis.
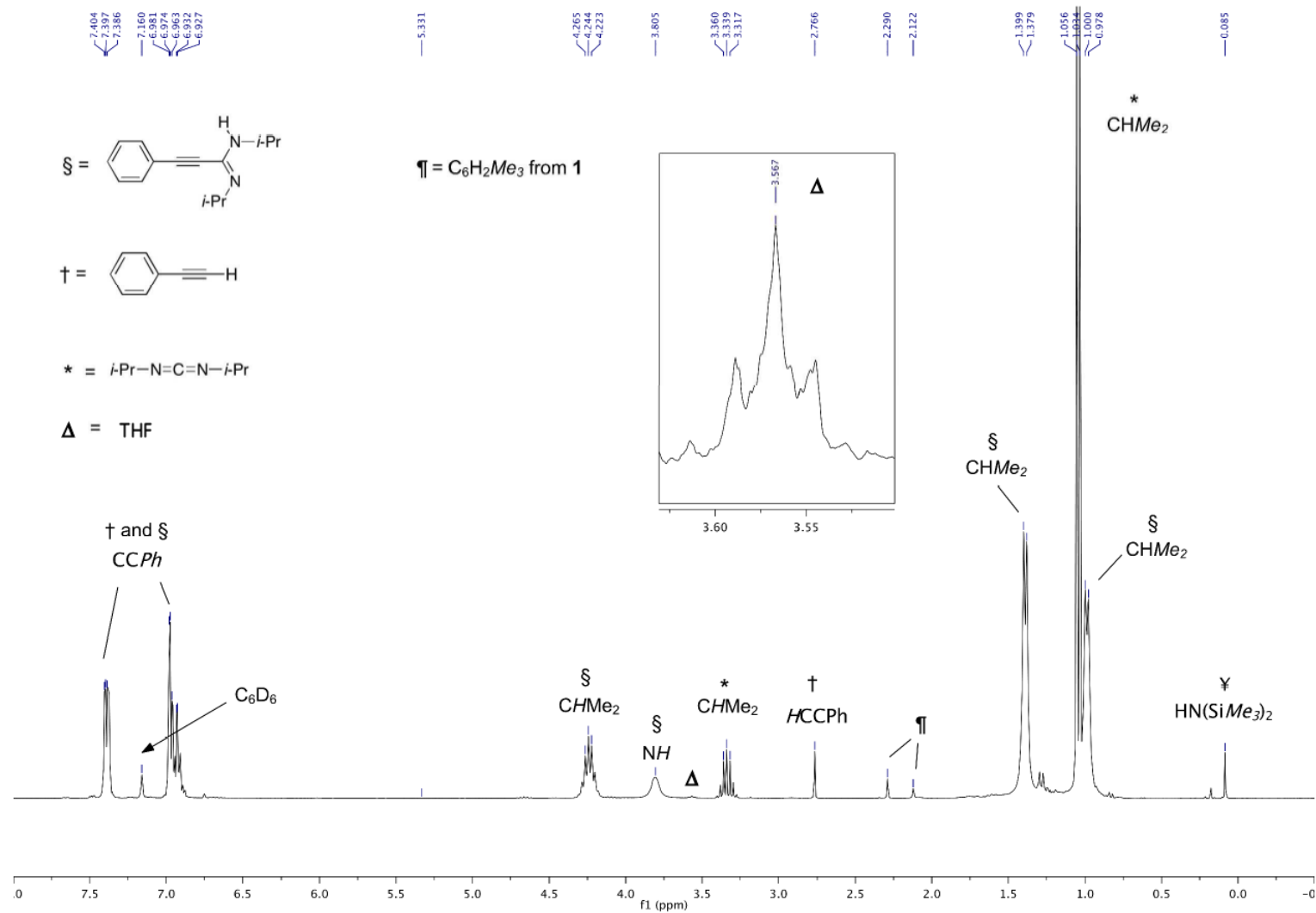
Figure 2.1: Assigned ^{1}H NMR spectrum for NMR scale catalytic study at 80 °C after 24h (entry 4).

2.3 Catalytic Cycle

The proposed catalytic cycle for the alkaline earth promoted coupling of terminal acetylenes to carbodiimide substrates involves initial protonolysis of the amide group (Figure 2.2, Step I), followed by insertion of the carbodiimide into the M-C bond (Step II) and finally protonolysis of the propargylamidinate by a terminal acetylene (StepIII).[27]
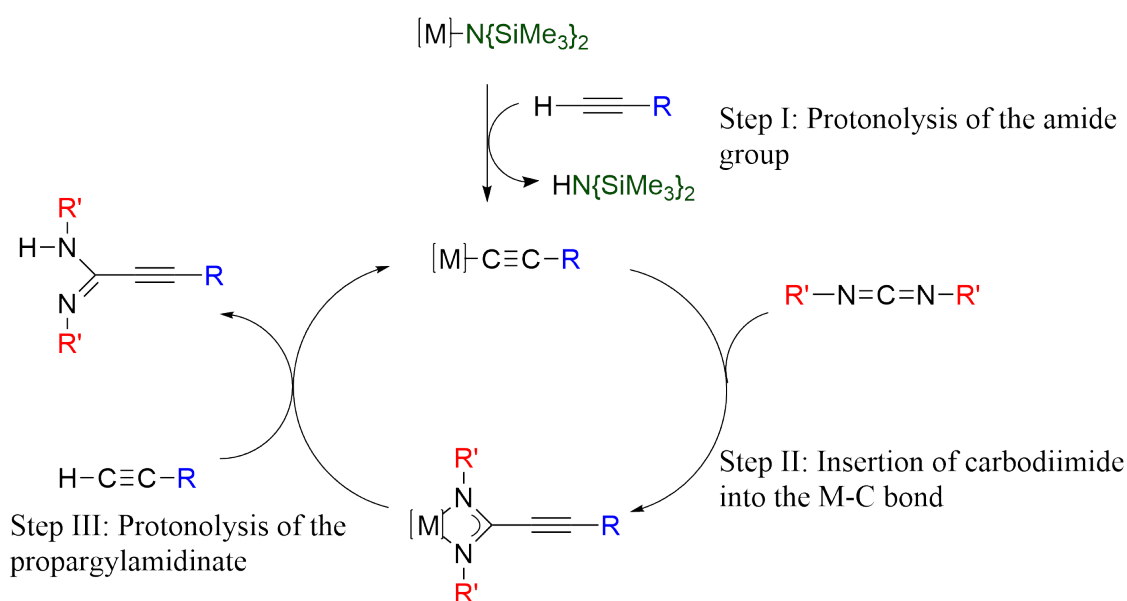
Figure 2.2: Generic catalytic cycle for alkaline earth promoted coupling of terminal acetylene and carbodiimide substrates.

While this catalytic cycle is widely accepted for lanthanide catalysis, little research has been performed towards the understanding of the mechanism for the alkaline earth metal promoted reaction. As mentioned in Chapter 1, one key difference between lanthanides and the alkaline earth metals is the inherent tendency for the latter to undergo ligand redistribution via a Schlenk-like equilibrium (*vide supra*).

To investigate the catalytic cycle of the magnesium mediated coupling of terminal acetylenes to carbodiimides, a series of stoichiometric studies were performed on an NMR scale. These were then repeated on a preparative scale using *N,N'*-diisopropylcarbodiimide and phenylacetylene as standard substrates.

2.3.1   NMR studies

Step I: Initiation

All catalytic studies described in Section 2.2 were performed by the addition of **1** to a 1:1 pre-mixed solution of phenylacetylene and *N,N'*-diisopropylcarbodiimide. Therefore, pre-catalyst **1** can enter into the proposed catalytic cycle via two possible pathways; (i) protonolysis of the amide by the terminal acetylene, or (ii) insertion of the carbodiimide substrate into the Mg-N bond followed by protonolysis of the guanidinate ligand by phenylacetylene (Figure 2.3). Previous reports of insertion of unsaturated substrates in Mg-N bonds indicate that this is a viable reaction pathway.[14,29] To investigate these two possible initiation pathways, a series of NMR scale experiments were performed.
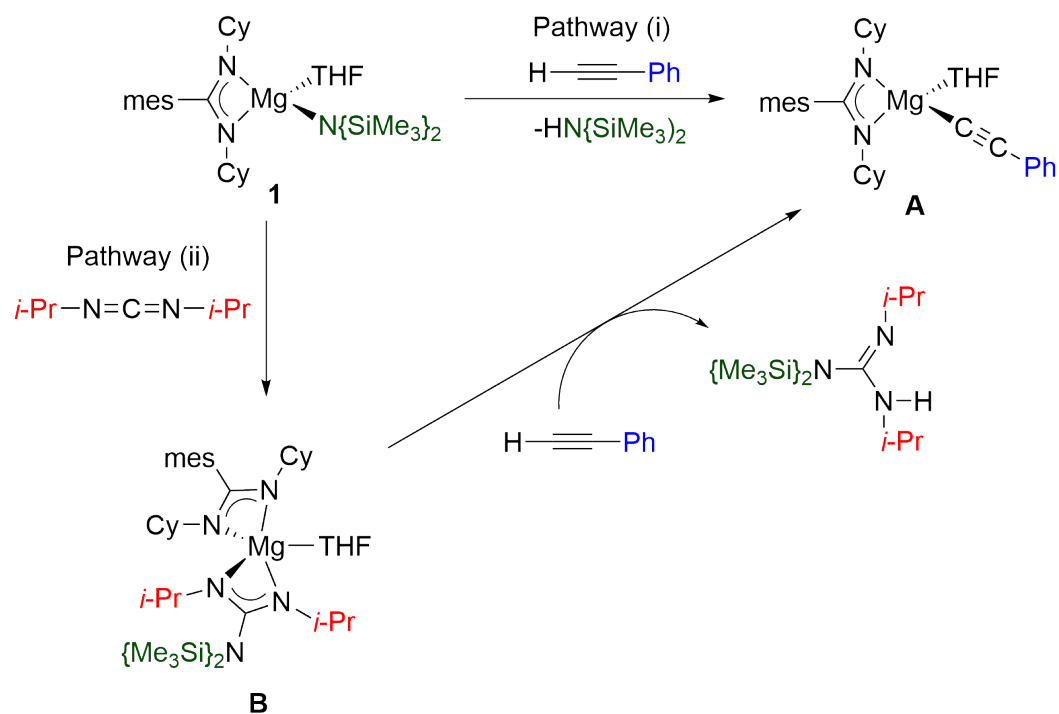
Figure 2.3: Step I: Initiation pathways for the formation of **A**.

Pathway (i) ^{1}H NMR analysis of an NMR-scale reaction of **1** and one equivalent of phenylacetylene in C_6D_6 shows quantitative formation of a new species (Figure 2.4). Loss of the singlet corresponding to the terminal proton of phenylacetylene (δ_H 2.72 ppm) indicates complete consumption of the starting material, with liberation of one equivalent of HN{SiMe$_3$}$_2$ noted (sharp singlet at δ_H 0.09 ppm). A single set of resonances for the amidinate and acetylide ligands are observed. The resonance corresponding to the o-C_6H_5 proton (δ_H 7.85 ppm) indicates significant deshielding compared to free phenylacetylene, consistent with close proximity to the electropositive magnesium centre.
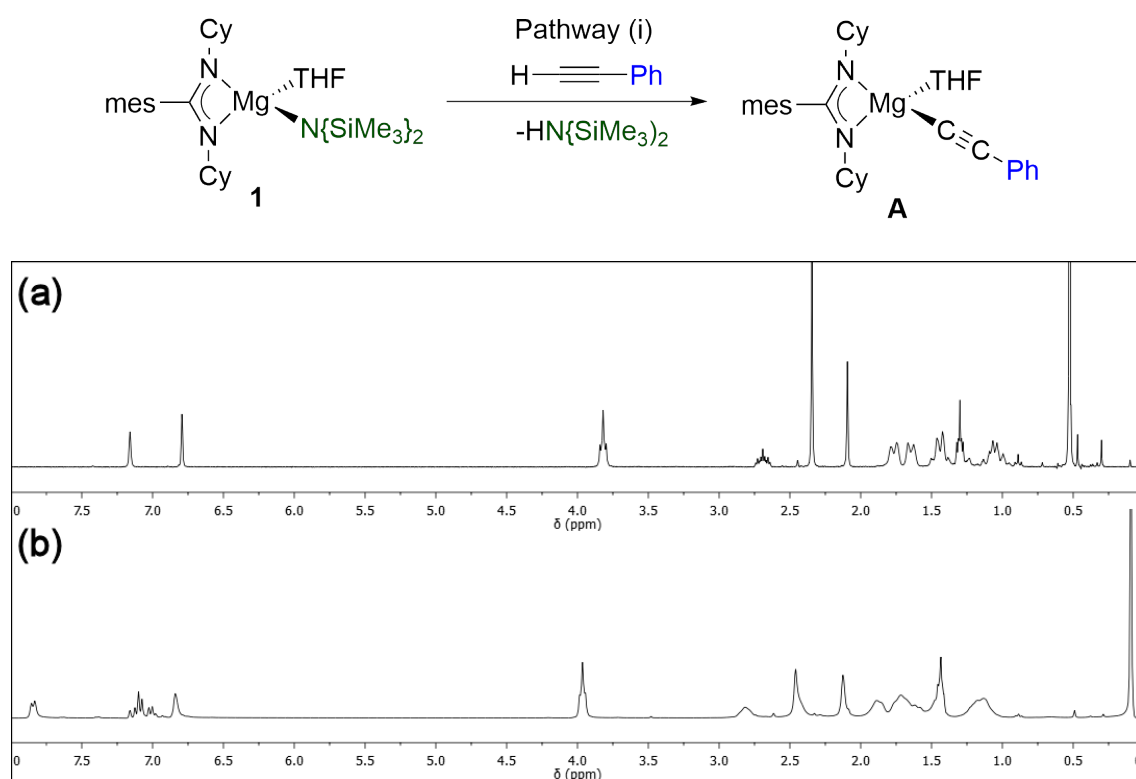
Figure 2.4: Reaction of **1** and phenylacetylene. ^{1}H NMR spectra of **1** (a) and **1** + HC≡CPh (b) in C_6D_6.

Nuclear Overhauser effect (nOe) analysis of the reaction mixture shows through space coupling of the THF OCH_2 to both the α-cyclohexyl and *ortho*-phenyl protons. Coupling is also observed between the *ortho*-phenyl (δ_H 7.83 ppm) protons and the α-cyclohexyl (δ_H 2.87 ppm) and mesityl *ortho*-methyl (δ_H 2.46 ppm) protons. This suggests that all three ligands are in close proximity, consistent with the terminal acetylide compound, **A**.

17

Significant broadening of signals corresponding to the amidinate and acetylide groups suggest the presence of equilibria in solution. Variable temperature NMR (VT-NMR) spectroscopy was used to analyse the reaction mixture in C_7D_8 (Figure 2.5). As the reaction mixture is cooled to -80 °C, the broad doublet corresponding to the o-C_6H_5 of the phenyl group resolves into two distinct peaks. Broadening of the signal corresponding to the THF is also observed as the temperature is lowered. At -80 °C, the THF resolves into two distinct resonances. This is consistent with the presence of fluxional processes in solution, however it is unclear whether this corresponds to ligand redistribution, or other fluxional processes (e.g. THF dissociation/association, restricted rotation).

In contrast to the single ligand environment observed in the ^{1}H NMR spectrum, the ^{13}C NMR spectrum displays two low field resonances for the metallacyclic carbon (δ_C 173.9 and 173.7 ppm), suggesting the presence of multiple amidinate environments in the reaction mixture. Two resonances are also noted for the α-cyclohexyl proton (δ_C 55.9 and 55.2 ppm), consistent with a mixture of multiple species in solution. Broad signals corresponding to the acetylene triple bonded carbon centres are observed at δ_C 120.1 ppm and 117.6 ppm, significantly downfield from free phenylacetylene (δ_C 83.5 and 77.1 ppm). Overlapping peaks complicate the rest of the ^{13}C NMR spectrum.

Comparison of the resonances in the ^{1}H and ^{13}C NMR spectra of the reaction mixture to independently synthesised $Mg((mes)C\{NCy\}_2)_2(THF)$ (**2**) and $Mg(C\equiv CPh)_2(THF)_4$ (**6**.$(THF)_4$) (*vide infra*) suggest that **2** (δ_C 173.9 and 55.2 ppm) and the bis(acetylide) **6**.$(THF)_n$[i] are present in solution. Resonances that do not correspond to these species are assigned to **A**. The presence of these species indicates that ligand redistribution is occurring in solution (eq. 2.1).

To test this hypothesis, a mixture of independently synthesised **2** and **6**.$(THF)_4$ was examined by ^{1}H NMR spectroscopy in C_6D_6. The resulting spectrum was consistent

---

[i]The number of THF molecules bound to the bis(acetylide) $Mg(C\equiv CPh)_2$ (**6**) is unknown in solution. n = 0, 1 or 2
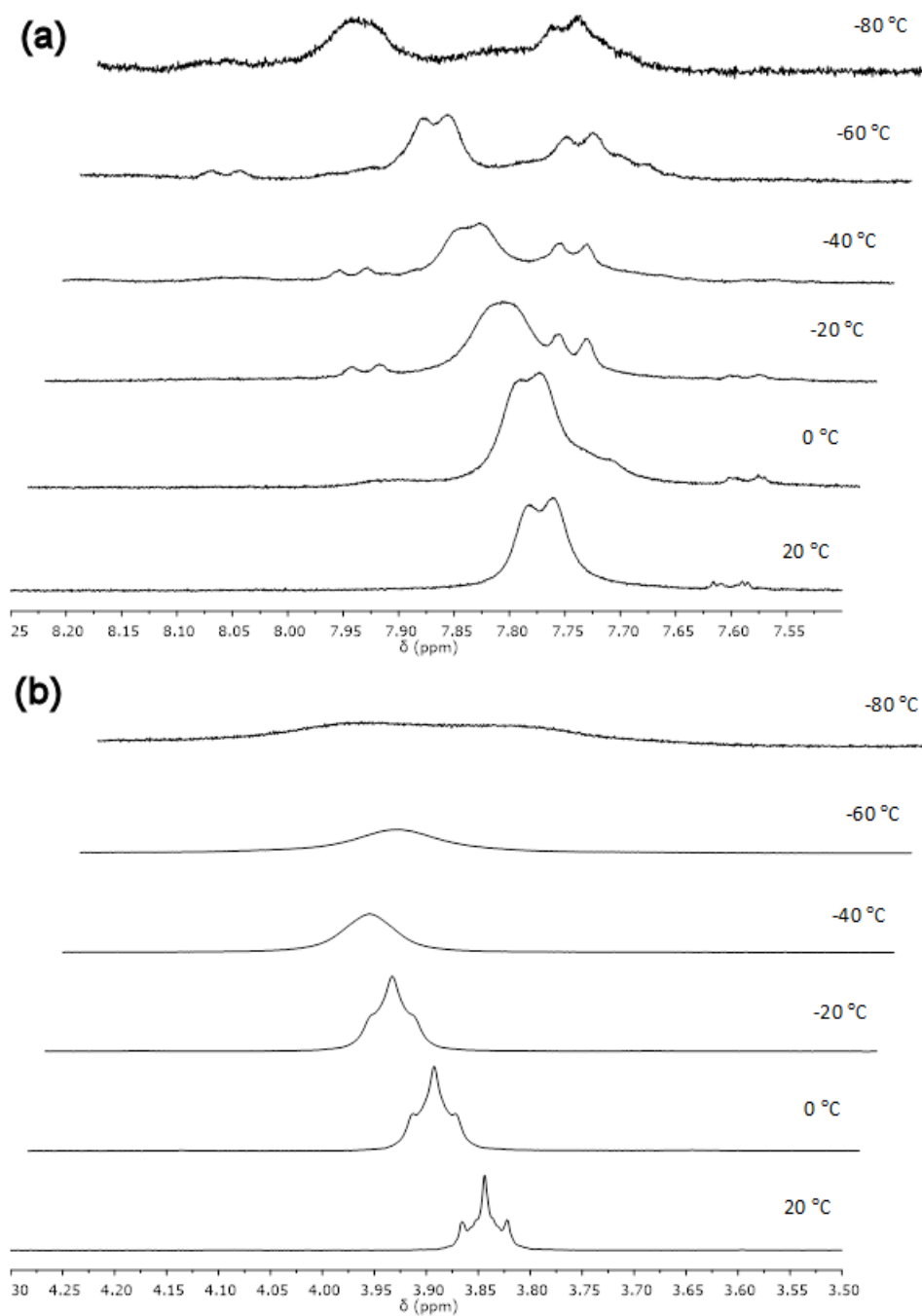
Figure 2.5: Variable Temperature ^{1}H NMR spectrum of **1** + HC≡CPh. (a) o-C$_6$H$_5$ proton resonance; (b) THF OCH_2 proton resonance.
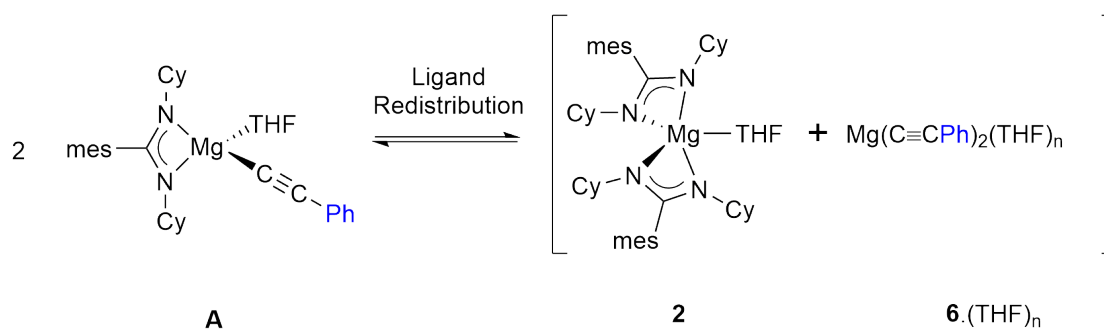
eq. 2.1: Ligand redistribution of **A**.

with the formation of an equilibrium in solution. Significant broadening of the ^{1}H NMR signals corresponding to the amidinate ligand (δ_H 6.83 (C$_6$H$_2$), 2.84 (α-Cy), 2.47 (o-Me) and 2.11 (p-Me) ppm) was observed (Figure 2.6). While **6** is only sparingly soluble in C$_6$D$_6$, addition of **2** to a suspension of **6**.(THF)$_4$ results in complete dissolution of all precipitates.
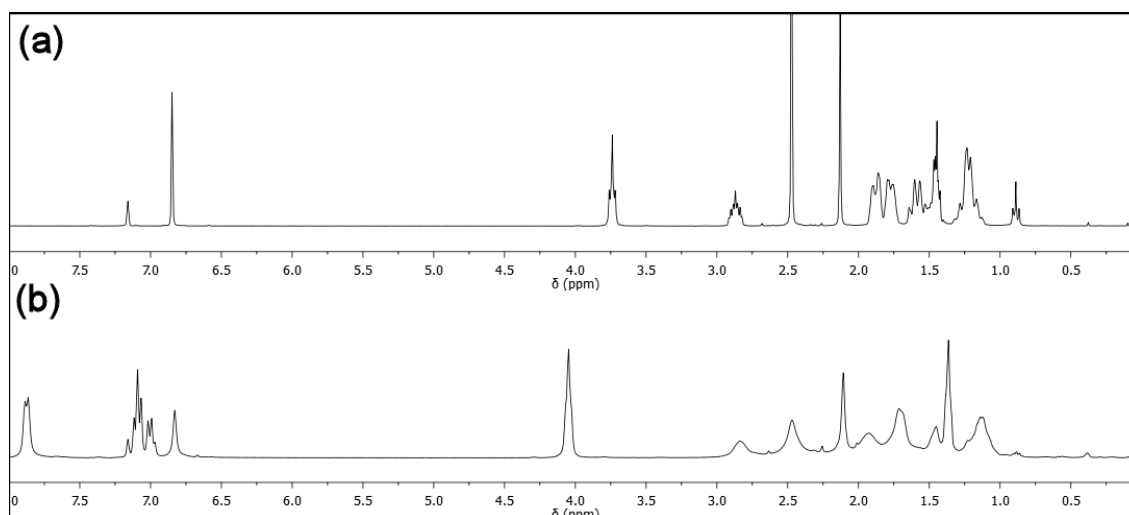
Figure 2.6: ^{1}H NMR spectra of **2** (a) and **2** + **6**.(THF)$_4$ (b) in C$_6$D$_6$.

Treatment of either **A** or **2** with excess phenylacetylene (2-5 equivalents) at 80 °C in C$_6$D$_6$ does not liberate the amidinate ligand from the magnesium centre. No new signals attributable to the free amidine were present in the ^{1}H NMR spectrum, with retention of both starting materials observed.

Pathway (ii)   Reaction of **1** with one equivalent of *N,N'*-diisopropylcarbodiimide (Scheme 2.1) resulted in quantitative consumption of the starting amide, generating a mixture of species.
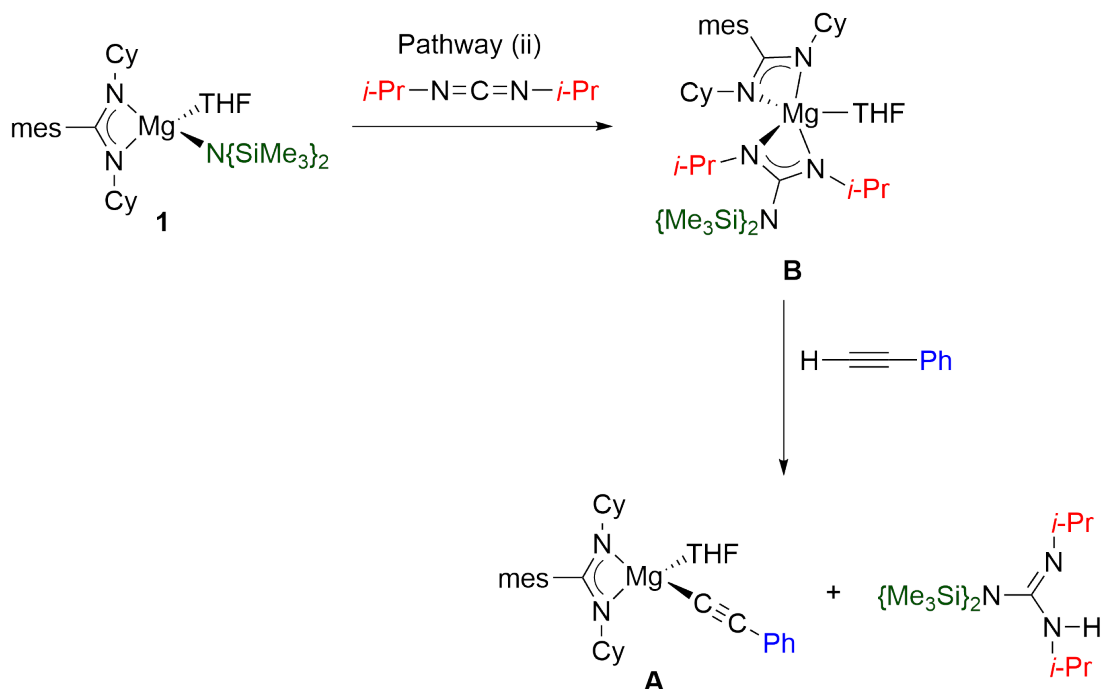
Scheme 2.1: Insertion of *N,N'*-diisopropylcarbodiimide into Mg-N bond followed by protonolysis of the guanidinate (pathway (ii)).

Two sets of resonances corresponding to the C_6H_2 (δ_H 6.85 and 6.82 ppm), *o*-Me (δ_H 2.47 and 2.41 ppm) and *p*-Me (δ_H 2.13 and 2.12 ppm) protons of the mesityl substituent are observed. Two SiMe$_3$ proton environments are also observed (δ_H 0.37 and 0.32 ppm). The signal corresponding to the α-cyclohexyl proton resonance appears as a broad multiplet (δ_H 2.78 ppm). The integral of this multiplet is consistent with overlapping signals. Resonances corresponding to the *iso*-propyl methine and methyl protons overlap with THF and cyclohexyl proton resonances, respectively.

Resonances at δ_H 6.85, 2.47 and 2.13 ppm correspond to the bis(amidinate) species Mg(mesC{NCy}$_2$)$_2$(THF) (**2**), while the resonance at δ_H 0.32 ppm corresponds to bis(guanidinate) Mg({Me$_3$Si}$_2$NC{N*i*-Pr}$_2$)$_2$(THF) (**3**). The identity of these species was confirmed by independent synthesis (*vide infra*). Signals at δ_H 6.82, 2.41, 2.12 and 0.37 ppm are attributed to mixed amidinate/guanidinate **B**.

The ^{13}C NMR spectrum of the reaction mixture displays two low field resonances for the metallacyclic carbon of the amidinate ligand (δ_C 174.0 and 173.8 ppm), consistent with two distinct amidinate environments. A single low field resonance is observed for the metallacyclic guanidinate carbon (δ_C 166.4 ppm), presumed to be due to overlapping signals from **B** and **3**. Resonances at δ_C 6.63 and 2.76 ppm, corresponding to the SiMe$_3$ carbon atoms, confirm the presence of two guanidinate environments.

The presence of compounds **2** and **3** in the mixture were confirmed by comparison to independently synthesised samples (*vide infra*). The resonance at δ_C 174.0 ppm corresponds to compound **2**, while the resonances at δ_C 166.4 and 2.76 ppm correspond to compound **3**. Peaks that do not correspond to these species were attributed to mixed amidinate/guanidinate species **B**. Formation of this mixture of products provides strong evidence supporting the presence of ligand redistribution in this system (eq. 2.2).
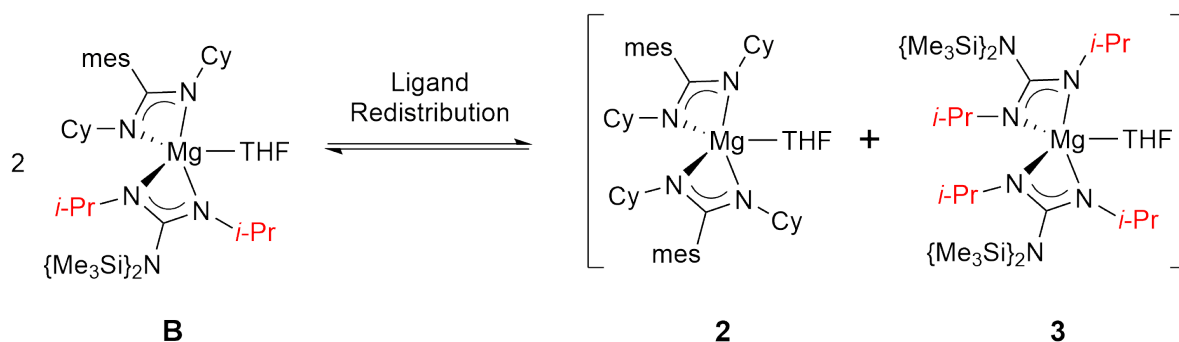
eq. 2.2: Ligand redistribution between **B** and **2/3**.

Ligand redistribution to form a mixture of **2** and **3** was confirmed in an independent experiment. Equimolar amounts of **2** and **3** were dissolved in C$_6$D$_6$ and examined by ^{1}H NMR. The relative integration of peaks at δ_H 6.85 and 6.82 ppm and δ_H 0.37 and 0.32 ppm show a statistical 2:1:1 ratio of **B:2:3**.

Initiation pathway The results from the the investigation of pathway (i) and pathway (ii) prove that both are viable reactions when **1** is added to the phenylacetylene/carbodiimide mixture during catalysis. To determine which pathway

predominates, a competition experiment was performed.

The stoichiometric addition of **1** in C_6D_6 to a mixture containing 1:1 equivalent of phenylacetylene and *N,N'*-diisopropylcarbodiimide was performed. Analysis of the mixture by ^{1}H NMR demonstrated that both pathways were operating at room temperature, showing formation of both HN{SiMe₃}₂ and the guanidine {Me₃Si}₂NC{NH*i*-Pr}{N*i*-Pr}. Pathway (i) is the dominant reaction pathway with formation of HN{SiMe₃}₂ and {Me₃Si}₂NC{NH*i*-Pr}{N*i*-Pr} in a 9:1 ratio, determined from integration of the SiMe₃ resonances.

Step II: Insertion into the Mg-C Bond

The addition of one equivalent of *N,N'*-diisopropylcarbodiimide to the reaction mixture of **A** in C_6D_6 results in complete consumption of the carbodiimide and formation of a new species, **C** (eq. 2.3).
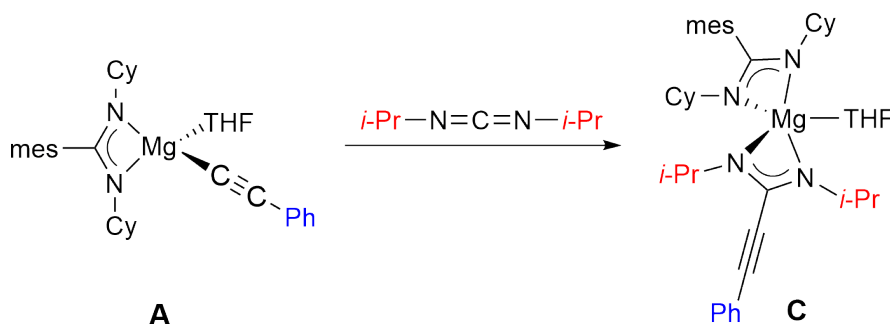
eq. 2.3: Step II: Insertion of *N,N'*-diisopropylcarbodiimide into **A**.

Significant upfield shifts in the phenyl proton signals (δ_H 7.46 and 6.97 ppm) are consistent with an increased distance between the phenyl ring and the magnesium centre. Resonances corresponding to the *iso*-propyl methine and methyl protons (δ_H 4.35 and 1.48 ppm, respectively) are also shifted upfield compared to the carbodiimide starting material, consistent with a change in the environment of the nitrogen groups. Two sets of resonances corresponding to the mesityl *o*-Me (δ_H 2.45 and 2.44 ppm) and *iso*-propyl methyl (δ_H 1.48 and 1.41 ppm) protons are observed, once again indicating formation of a mixture of species. The resonance for the α-cyclohexyl pro-

ton is observed as a broad multiplet (δ_H 2.81 ppm). The multiplet corresponding to the THF protons (δ_H 3.77 ppm) is downfield from free THF, consistent with an interaction with a magnesium centre.

The ^{13}C NMR spectrum indicates the generation of a mixture of compounds, with two sets of resonances present for all carbon environments. This is most clearly represented by two distinct low-field resonances for each of the metallacyclic carbons of the amidinate (δ_C 174.0 and 173.8 ppm) and propargylamidinate (δ_C 157.9 and 157.7 ppm) ligands. Two sets of signals for the triple bonded carbon centres (δ_C 95.9, 95.8, 81.0 and 80.8 ppm) are observed as sharp resonances.

These data are consistent with ligand redistribution between the mixed amidinate/propargylamidinate species **C** and **2** (δ_H 2.45 and 1.48 ppm; δ_C 174.0 ppm) / bis(propargylamidinate) Mg(PhC≡C{Ni-Pr}$_2$)$_2$(THF) (**4**) (δ_C 157.9, 95.9 and 80.8 ppm) (eq. 2.4). The identity of these species was confirmed by independent synthesis (*vide infra*).
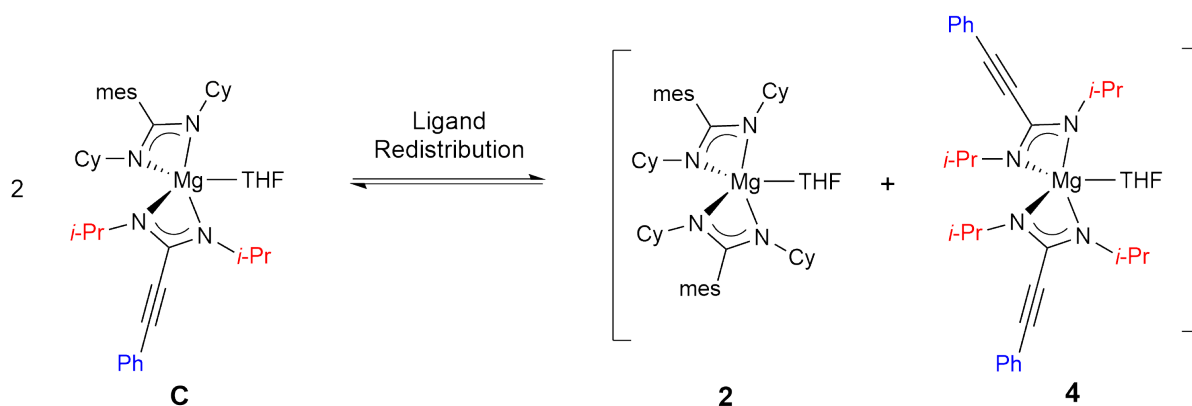
eq. 2.4: Ligand redistribution between **C** and **2/4**

The ability of a mixture of **2** and **4** to undergo ligand redistribution was determined by ^1H NMR analysis of a 1:1 mixture of independently synthesised samples. The results clearly show formation of **C** in solution, most evident by the resonance at δ_H 2.44 ppm for the o-Me protons of the mesityl.[ii]

Insertion of a carbodiimide into the Mg-C$_{acetylide}$ bond was shown to be non-

---

[ii]**4** was isolated and added to the reaction as the bis(THF) adduct **4**.(THF).

reversible. The addition of *N,N'*-dicyclohexylcarbodiimide to **C** did not result in formation of a mixture of different insertion products and no consumption of the *N,N'*-dicyclohexylcarbodiimide was observed.[iii]

If insertion of the *N,N'*-diisopropylcarbodiimide into **A** was reversible, we would expect to see consumption of the *N,N'*-dicyclohexylcarbodiimide and formation of the corresponding insertion product as it competes with the *N,N'*-diisopropylcarbodiimide for insertion into the Mg-$C_{acetylide}$ bond (Scheme 2.2, (a)). This would result in formation of a mixture of the different insertion products. Alternatively, if the insertion of *N,N'*-diisopropylcarbodiimide is irreversible, addition of *N,N'*-dicyclohexylcarbodiimide would not result in the formation of a mixture of the different insertion products (Scheme 2.2, (b)). The lack of reactivity observed when *N,N'*-dicyclohexylcarbodiimide is added to **C** is consistent with Scheme (b).

[iii]The tendency of compounds **A** and **C** to undergo ligand redistribution has been excluded in this case for simplicity.
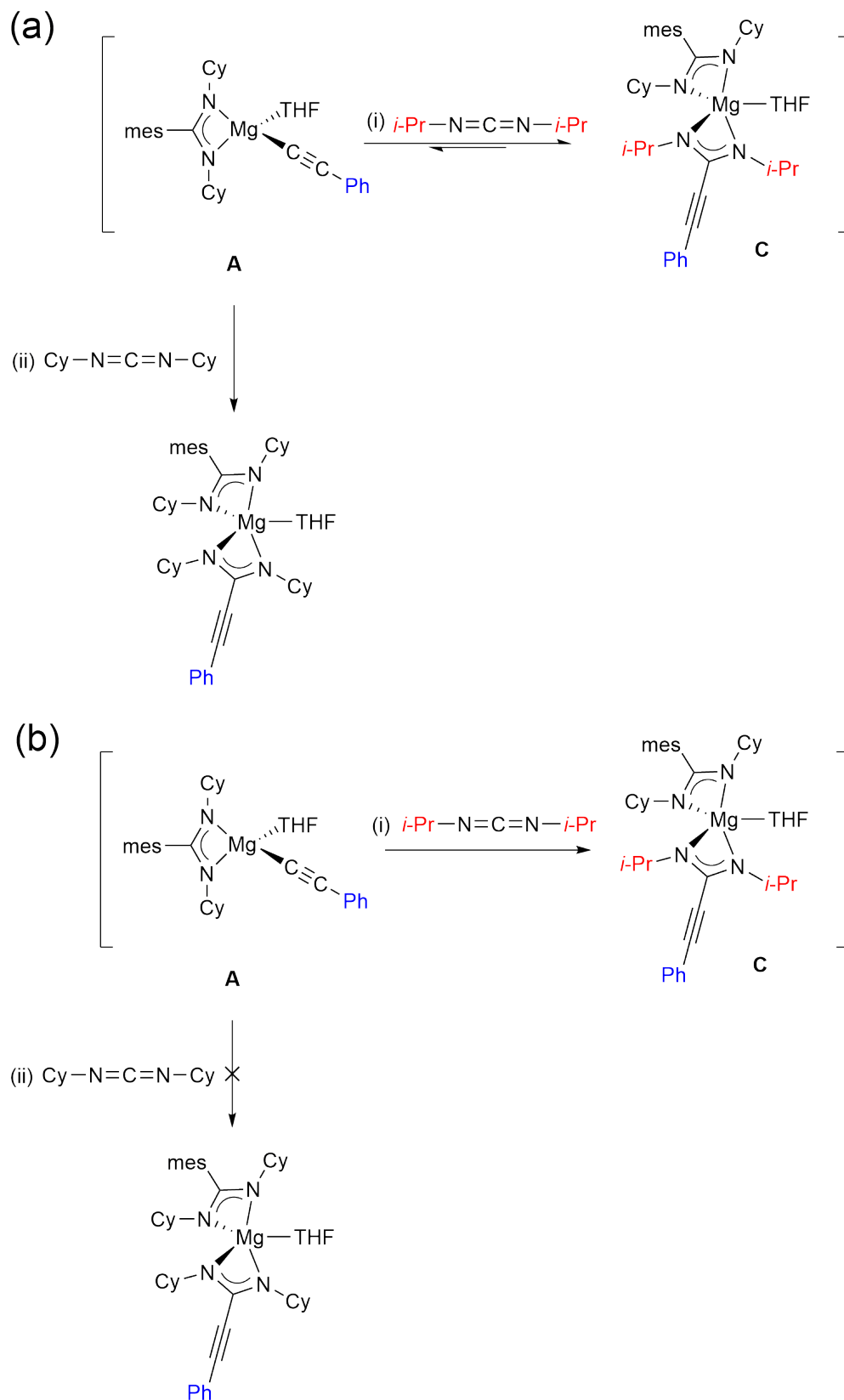
Scheme 2.2: Reversibility of the insertion step; (a) Reversible insertion of *N,N'*-diisopropylcarbodiimide into Mg-C$_{acetylide}$, (b) Non-reversible insertion of *N,N'*-diisopropylcarbodiimide into Mg-C$_{acetylide}$.[iii]

Step III: Protonolysis of the Propargylamidinate

Attempts to form the corresponding propargylamidine PhC≡CC{NHi-Pr}{Ni-Pr} (**5**) by the protonolysis of the propargylamidinate ligand by phenylacetylene proved unsuccessful (eq. 2.5). Addition of excess phenylacetylene (5 eq.) to the reaction mixture of **C**, **2** and **4** resulted in no observable reaction, even after heating to 80 °C.
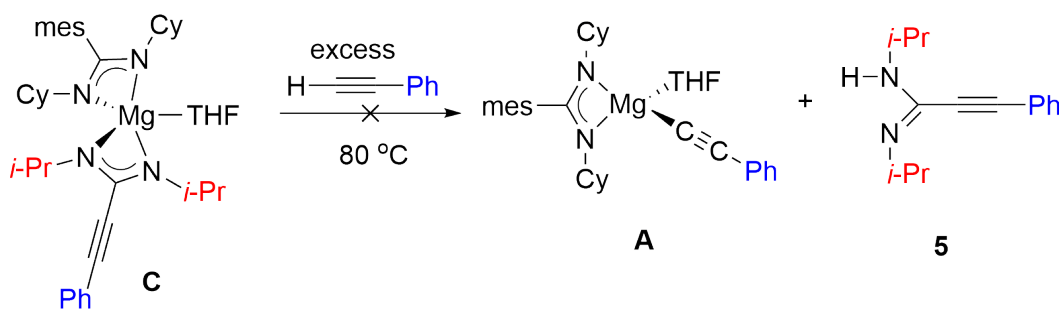
eq. 2.5: Step III: Protonolysis of the propargylamidinate by phenylacetylene.

This apparent lack of reactivity was investigated further as the result is counter to the observed catalytic results (Section 2.2), where protonation must be occurring to generate the product and complete catalytic turnover. No observable reaction was observed upon addition of one equivalent of phenylacetylene to independently synthesised **4**.(THF)(*vide infra*) when heated to 80 °C, suggesting the propargylamidinate ligand is unreactive towards phenylacetylene. Previous studies using lanthanide-based catalysts have reported the protonolysis of the propargylamidinate as the rate determining step.[26]

To more closely represent catalytic conditions, one equivalent of *N,N'*-diisopropylcarbodiimide was added to a pre-mixed sample of **C**, **2**, **4** and phenylacetylene. Under these conditions, formation of the corresponding propargylamidine was observed, completing the catalytic cycle. *N,N'*-diisopropylcarbodiimide is unreactive with **C**, **2** and **4** in the absence of phenylacetylene.

These observations can be explained by reversible protonolysis of the propargylamidinate, where the equilibrium heavily favours formation of **C**, **2** and **4** (Figure 2.7).
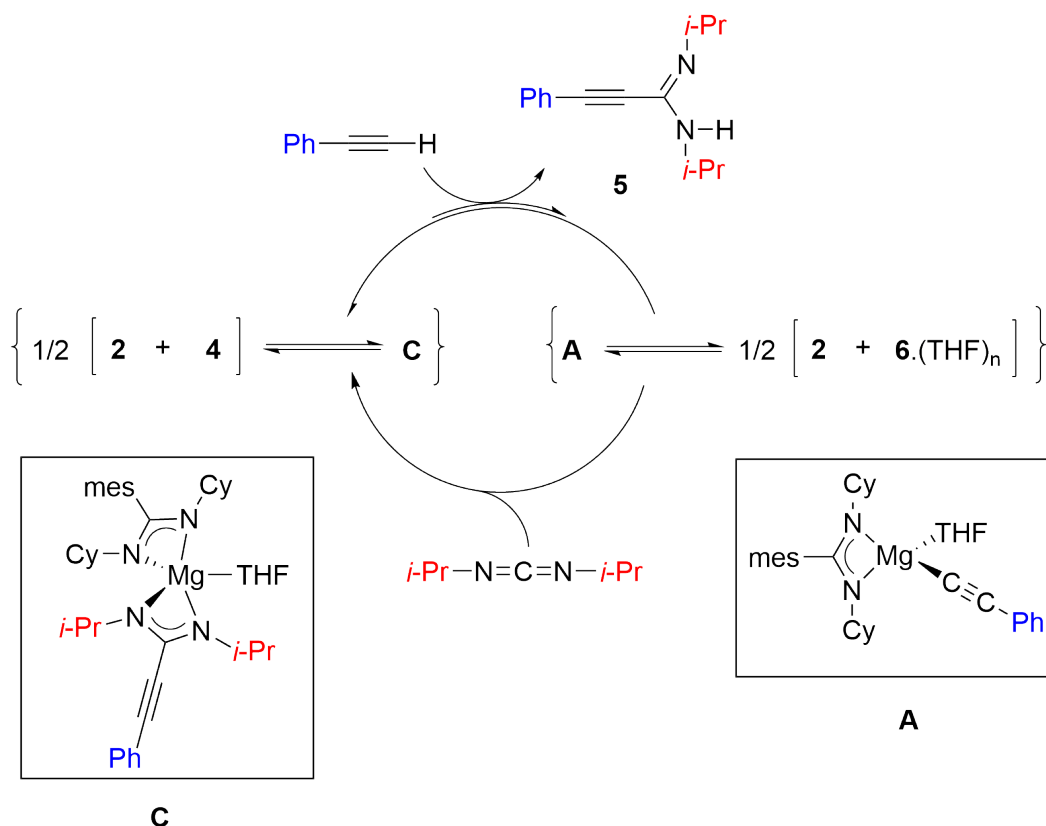
Figure 2.7: Reversible protonolysis of **C**. **2** = Mg(mesC{NCy}$_2$)$_2$(THF), **4** = Mg(PhC≡CC{Ni-Pr}$_2$)$_2$(THF), **6**.(THF)$_n$ = Mg(C≡CPh)$_2$(THF)$_n$.

Addition of the *N,N'*-diisopropylcarbodiimide acts to trap formation of **A** and drive the reaction forward.

To test the reversibility of this step of the reaction, two equivalents of propargylami-dine **5** were added to an independently synthesised sample of Mg(C≡CPh)$_2$(THF)$_4$ (**6**.(THF)$_4$) (*vide infra*). This resulted in quantitative formation of the corresponding bis(propargylamidinate) **4**.(THF), with liberation of phenylacetylene, shown by the formation of a sharp singlet in the ^{1}H NMR spectrum corresponding to the phenylacetylene terminal proton (δ_H 2.72 ppm) (eq. 2.6). This indicates that, under these conditions, protonolysis can occur in both directions, consistent with formation of an equilibrium.

Crimmin et al. reported an analogous system for the calcium catalysed hydrophos-phination of carbodiimide substrates, whereby reversible protonolysis of the phos-phaguanidinate ligand was overcome by trapping formation of the phosphide by
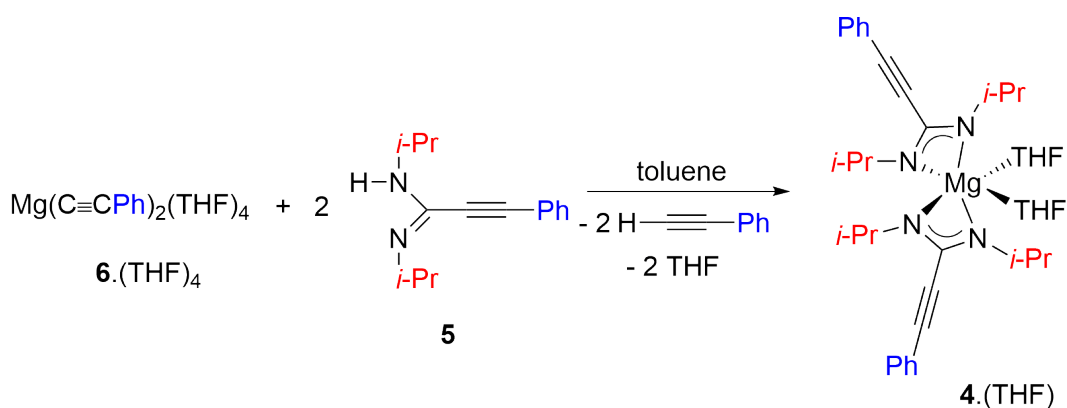
eq. 2.6: Protonolysis of the acetylide ligand by propargylamidine **5**.

insertion of a carbodiimide into the Ca-P bond.[8]

2.3.2 Preparative scale reactions

Attempted Isolation of A

Attempts to isolate the amidinate acetylide **A** from the reaction of **1** and phenylacetylene in toluene were unsuccessful. Removal of the volatiles yielded a white solid which, upon recrystallisation from a mixture of THF/hexane, afforded the bis(acetylide) $Mg(C{\equiv}CPh)_2(THF)_4$ (**6**.$(THF)_4$; first crop, yield 16%) and bis(amidinate) **2** (second crop, yield 26 %). This is consistent with Schlenk-like ligand redistribution between **A** and **2**/**6**.$(THF)_4$ when in the presence of excess THF (Scheme 2.3). Independent synthesis of **6**.$(THF)_4$ confirmed formation of the bis(acetylide) adduct (*vide infra*). Attempts to isolate species from non-coordinating solvents were prevented by low solubility of the products.

Compound **2** was obtained as a colourless crystalline solid. ^{1}H NMR analysis of **2** indicates a single ligand environment for the amidinate, consistent with a symmetric environment in solution. Integration of the THF signals is consistent with a single THF molecule associated with the magnesium centre.

The ^{13}C NMR spectrum shows a single low field resonance consistent with the
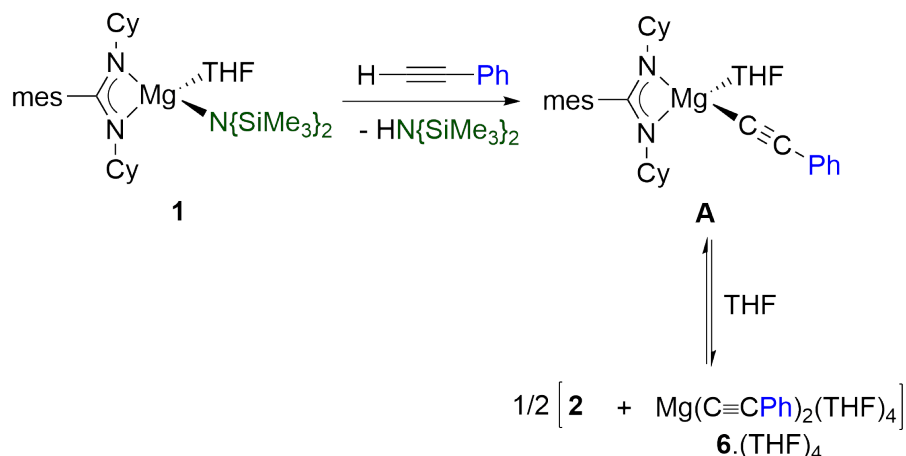
Scheme 2.3: Synthesis of **2** and **6**.(THF)$_4$.

metallacyclic carbon centre (δ_C 174.3). The α-cyclohexyl resonance (δ_C 54.8 ppm) is significantly downfield compared to the free carbodiimide, consistent with the close proximity to the resonance stabilised metallacyclic ring. Elemental analysis data is consistent with the calculated values for compound **2**.

Single crystal X-ray analysis confirmed **2** as the monomeric bis(amidinate) complex, Mg(mesC{NCy}$_2$)$_2$(THF) (Figure 2.8). Compound **2** crystallises in the $P4_32_12$ space group and lies on a two-fold rotation axis (C_2).

Addison et al. reported a convenient method for describing the geometry of 5-coordinate metal compounds based on the difference between the largest angle about the metal centre (α) and the second largest angle (β) (Figure 2.9).[30] In an idealised trigonal bipyramid geometry, the difference in angles is 60°, while an idealised square-based pyramid geometry would have a difference of 0°. The τ value is calculated by dividing the difference between α and β by 60°. A τ value of >0.5 indicates bias towards a trigonal bipyramid geometry, while a τ value of <0.5 corresponds to bias towards a square-based pyramid geometry.

Using this classification, the geometry about the magnesium centre in **2** is described as a distorted square-pyramidal geometry ($\tau = 0.41$). The bidentate chelating amidinate ligands are related by symmetry, forming the basal plane, with the THF molecule occupying the axial position. The four membered metallacycle ring is
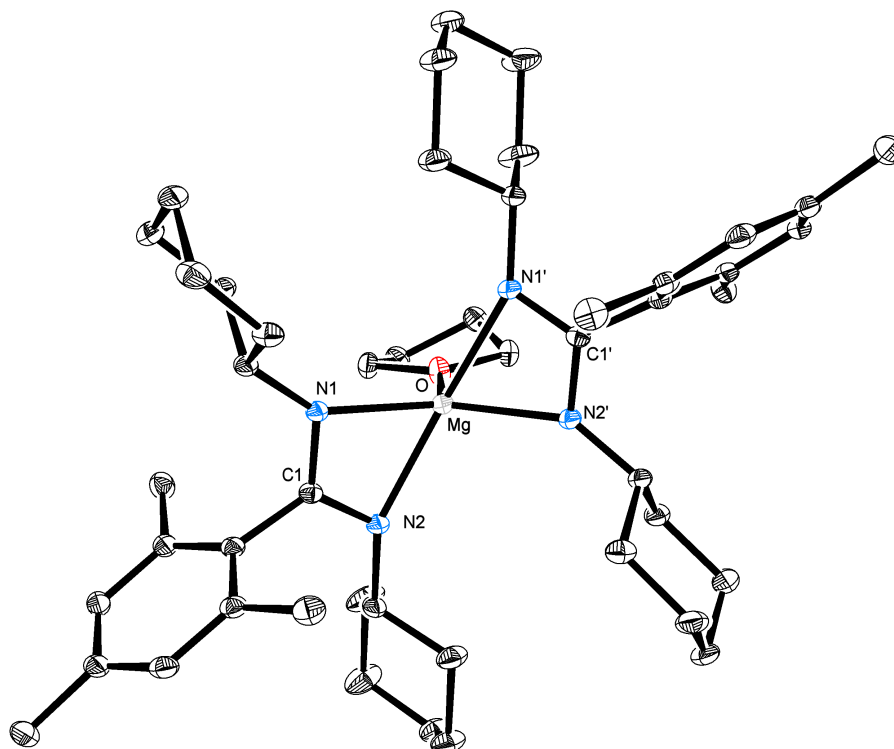
Figure 2.8: ORTEP representation of **2**. 30% Thermal ellipsoid. Hydrogens omitted for clarity. Selected bond lengths (Å) and angles (°) are reported in Table 2.2.

Table 2.2: Selected bond lengths (Å) and angles (°) in **2**.

Mg-N(1)	2.0957(12)	N(1)-C(1)-N(2)	115.42(13)
Mg-N(2)	2.1982(12)	N(1)-Mg-N(1)'	142.58(7)
N(1)-C(1)	1.3345(18)	N(2)-Mg-N(2)'	167.38(7)
N(2)-C(1)	1.3212(19)	C(1)-N(1)-Mg	92.80(9)
Mg-O	2.0456(16)	C(1)-N(2)-Mg	88.68(9)
N(1)-Mg-N(2)	62.99(5)		

planar (sum of internal angles = 359.9°) with an acute bite angle (62.99(4)°), significantly smaller than observed for tetrahedral compound **1** (65.54(7)°).[18]

The mesityl ring is approximately orthogonal so that the *o*-Me groups lie above and below the CN$_2$Mg plane, with an interplanar angle of 80.31(6)°. This is consistent with the structure of **1** and [Mg(mesC{NCy}$_2$)(Br)(Et$_2$O)]$_2$.[18] The Mg-N(1) and Mg-N(2) distances, (2.0957(12) Å and 2.1982(12) Å, respectively) are consistent with σ-bonding interactions of the amidinate with the magnesium centre. The N(1)-

$$\tau = (\alpha - \beta)/ 60^{\mathrm{o}}$$

Trigonal bipyramid
$\alpha = 180^{\mathrm{o}}$, $\beta = 120^{\mathrm{o}}$
$\tau = 1$

Square-based pyramid
$\alpha = 180^{\mathrm{o}}$, $\beta = 180^{\mathrm{o}}$
$\tau = 0$
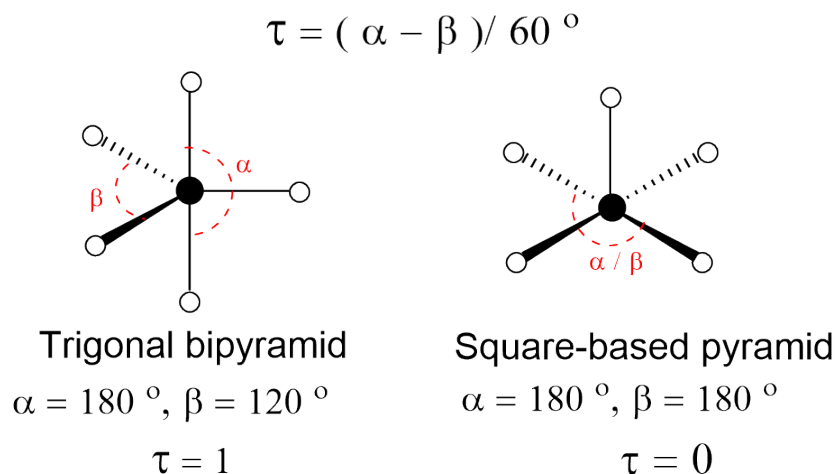
Figure 2.9: τ values for trigonal bipyramid (left) and sqaure-based pyramid (right) geometries.

C(1) and N(2)-C(1) bond distances (1.3345(18) Å and 1.3212(19) Å, respectively) are intermediate between typical C-N (1.47 Å) and C=N (1.27 Å), indicating a bond order greater than 1. The difference in the Mg-N bond lengths is noted and discussed in greater detail in Section 2.7.

Attempted Isolation of C
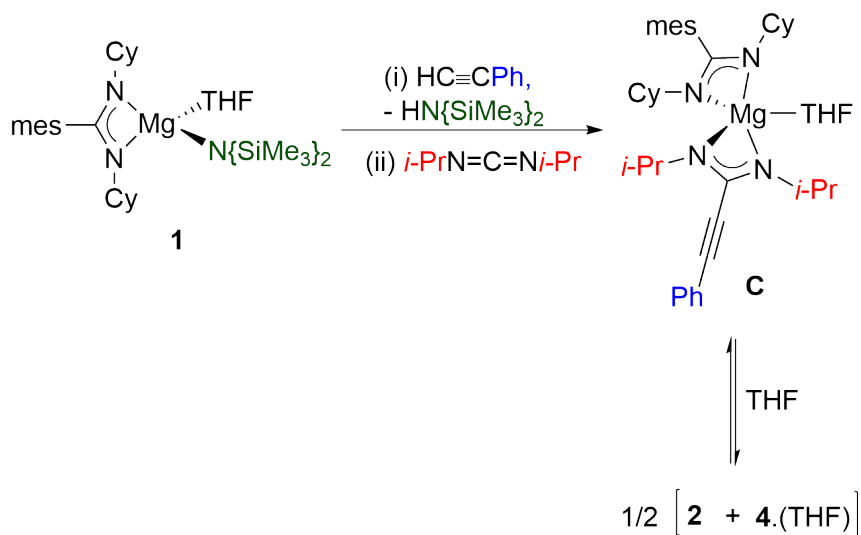
Scheme 2.4: Synthesis of **2** and **4**.(THF).

The isolation of **C** from the sequential addition of one equivalent of phenylacetylene to **1**, followed by one equivalent of *N,N'*-diisopropylcarbodiimide

in toluene was also unsuccessful. Removal of the volatiles and recrystallisation from a mixture of THF/hexane afforded **2** (first crop, yield 47 %) and bis(propargylamidinate) **4**.(THF) (second crop, yield 36 %), consistent with ligand redistribution (Scheme 2.4). The identity of these compounds was confirmed through independent synthesis and comparison of NMR data.

2.4   Scope of Catalysis

Investigation of the scope of catalysis was performed for a range of terminal alkyne (R) and carbodiimide (R') substituents using a catalyst loading of 1 mol% and heating to 80 °C for 24h (Table 2.3). All catalytic experiments were performed twice, with the reported yield representing the average of two runs. Yields were again calculated using the THF resonances as an internal standard (Section 2.2). Varying the R' substituent of the carbodiimide had a significant effect on the catalytic activity of **1**. The *i*-Pr and Cy derivatives gave similar yields after 24h (entries 1 and 2), consistent with the similar steric profile of the two nitrogen substituents. Increasing the steric bulk at the nitrogen substituents to *t*-Bu resulted in significantly lower yields (entry 3).

This is consistent with an associative mechanism that involves interaction with the metal centre prior to bond formation (Figure 2.10). The *i*-Pr and Cy substituents can rotate to prevent steric clashing of the carbon centres with the substrate (α). This is not possible for *t*-Bu substituents which do not have the methine hydrogen (β). It should be noted that while α and β in Figure 2.10 represent the transition state of the protonolysis step, increasing the steric bulk at the nitrogen will also influence the insertion step. Protonolysis of the propargylamidinate has previously been reported as the rate-determining step for this reaction.[26,27] While this is in agreement with our observations for the *i*-Pr derivative (Section 2.3), the rate determining step for the *t*-Bu derivative is unknown.

Table 2.3: Substrate scope for the coupling of terminal acetylenes and carbodiimides.
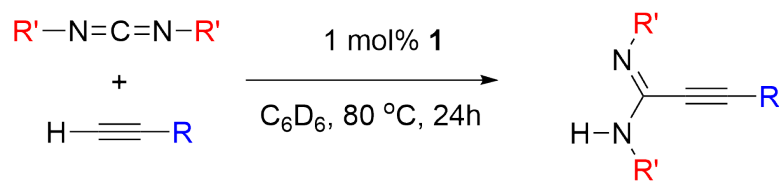
entry	R	R'	yield (%)
1	Ph	i-Pr	72
2	Ph	Cy	74
3	Ph	t-Bu	7
4	Ph	Ar[a]	0
5	4-t-BuC$_6$H$_4$	i-Pr	76
6	4-MeC$_6$H$_4$	i-Pr	77
7	SiMe$_3$	i-Pr	63
8	Si(i-Pr)$_3$	i-Pr	42
9	CH$_3$(CH$_2$)$_3$	i-Pr	41
10	t-Bu	i-Pr	12

[a] Ar = 2,6-i-Pr$_2$C$_6$H$_3$.

No amidine was produced when using *N,N'*-di(2,6-diisopropylphenyl)carbodiimide (entry 4), consistent with previous results from the lanthanides systems discussed earlier.[26] The lack of catalysis was attributed to the high acidity of the aryl-substituted propargylamidinate; however sterics will also play a role.

Para-substitution of the phenyl ring had little effect on the catalysis (entries 5 and 6) compared to phenylacetylene. The trimethylsilyl-substituted acetylene gave a reduced yield (entry 7), with the tri-*iso*-propylsilyl substituted acetylene exhibiting further reduced activity (entry 8). This suggests that there is some dependence of the activity on the steric bulk of the acetylene.

Further reduced yields were observed for alkyl-substituted acetylenes (entries 9 and 10), with the *t*-Bu derivative exhibiting much lower yields. These results indicate a dependence of the catalytic activity on both the sterics and electronics of the
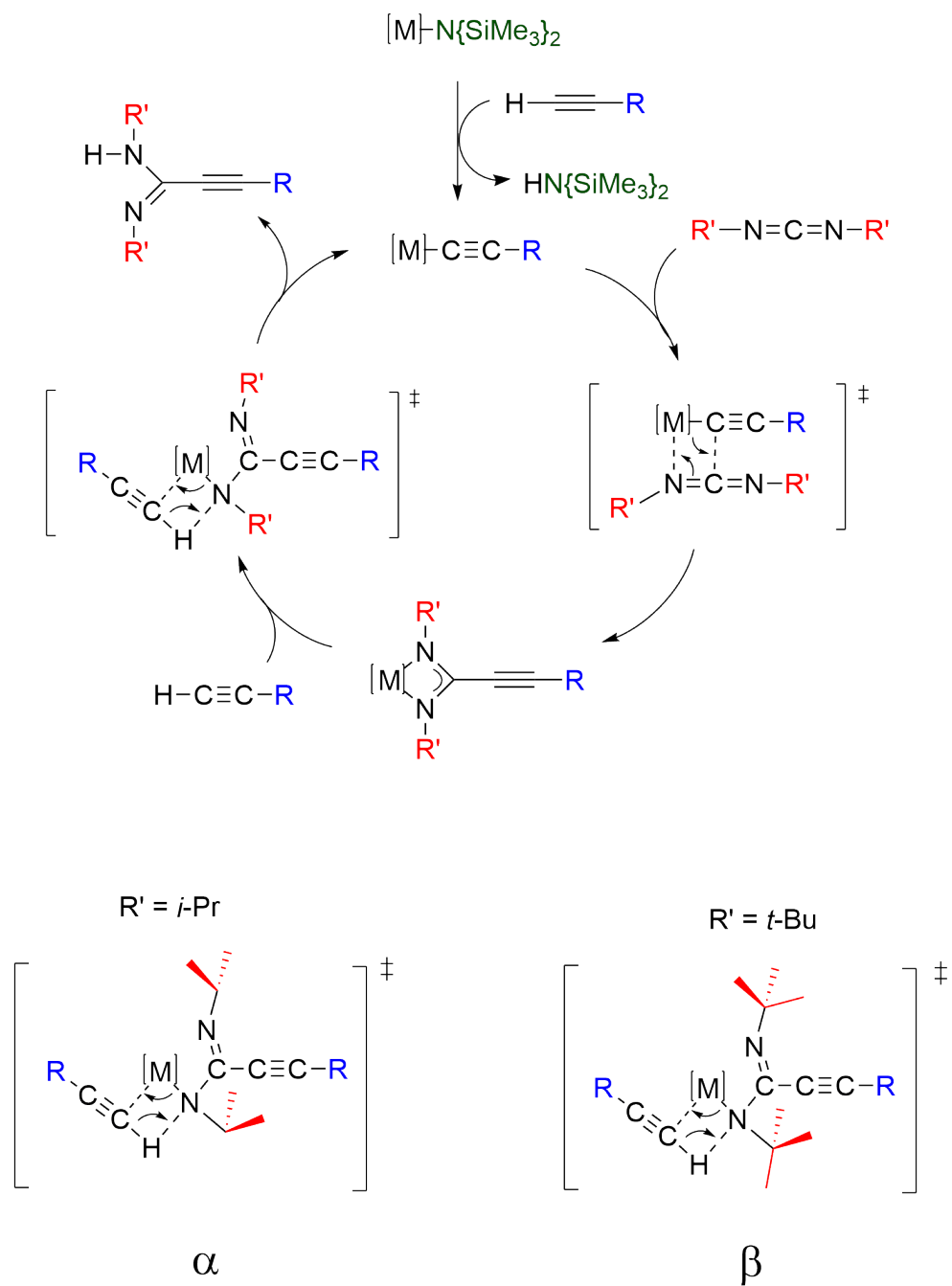
Figure 2.10: Associative mechanism for individual steps of the catalytic cycle. Proposed transition state for the protonolysis step, R' = *i*-Pr (α) and *t*-Bu (β).

acetylene and carbodiimide substrates.

Assuming that the protonolysis of the propargylamidinate is the rate-determining step (Step III, Figure 2.2), the relationship between the acetylene R-group and the reactivity of the terminal proton was investigated. The Hammett values (σ_p) for the R substituents were used to investigate the electron withdrawing/donating properties of these substituents, where a more positive σ_p value corresponds to greater electron withdrawing properties and *vice versa.*[31] A weak correlation (R^2 = 0.807) is observed between the σ_p value of R and the reported yield (Figure 2.11).
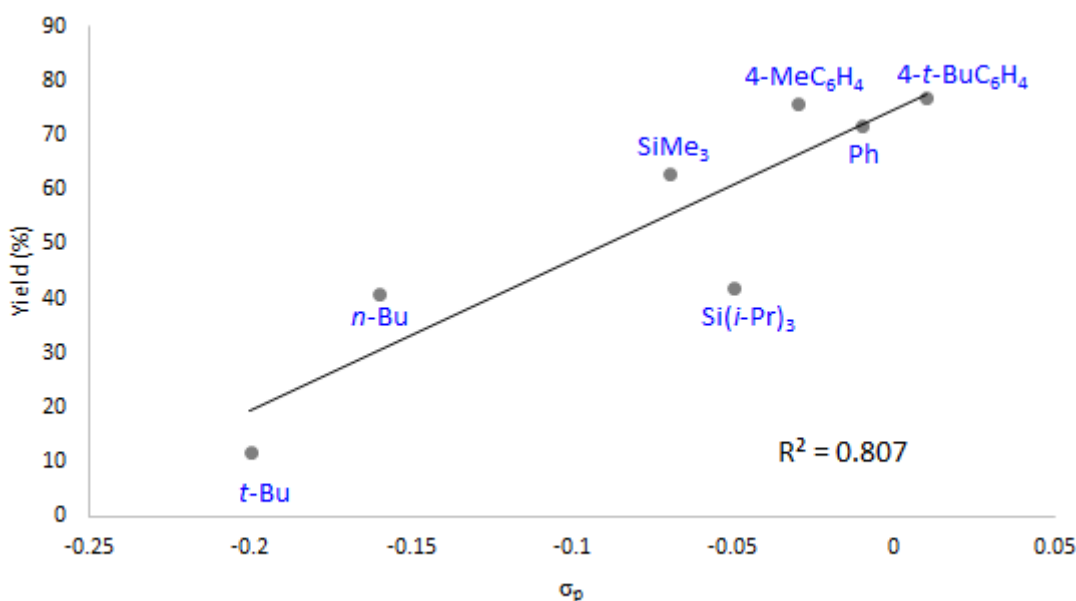
Figure 2.11: Plot of Hammett values (σ_p) vs. NMR yields. R^2 = 0.807.

As the electron withdrawing properties of R increase (i.e. σ_p becomes more positive), there is a linear increase in the yield. More electron withdrawing R groups are expected to result in a more acidic terminal proton on the acetylene, effecting the rate of the rate-determining protonolysis step. The relatively weak correlation likely indicate a contribution from the sterics of the R group. Indeed, removal of the sterically bulky t-Bu and Si(i-Pr)$_3$ derivatives from the plot results in a much better fit of the data to a linear relationship (R^2 = 0.947). It should be noted that Hammett values are determined at room temperature, while yields were determined at 80 °C in a sealed system.

2.5 Alternative Pre-catalysts

The prevalence of ligand redistribution in the catalytic cycle analysis prompted an investigation into the possible activity of other magnesium compounds (Table 2.4). All catalytic studies were performed on an NMR scale, under standard conditions (Section 2.2), unless stated otherwise. The reported yields in Table 2.4 represent the average of two catalytic runs, and were determined from the integration ^{1}H resonances of the product relative to the THF or Et_2O solvent molecule, unless stated otherwise.

Table 2.4: Alternative magnesium based pre-catalysts.

entry	catalyst	yield (%)
1	Mg(mesC{NCy}$_2$)(N{SiMe$_3$}$_2$)(THF) (**1**)	72
2	Mg(mesC{NCy}$_2$)$_2$(THF) (**2**)	74
3	Mg({Me$_3$Si}$_2$NC{Ni-Pr}$_2$)$_2$(THF) (**3**)	73
4	Mg(PhC≡CC{Ni-Pr}$_2$)$_2$(THF) (**4**.(THF))	72[a]
5	Mg(C≡CPh)$_2$(THF)$_4$ (**6**.(THF)$_4$)	73[a]
6	MgBu$_2$ (1.0 M, heptane)	74[a]
7	Mg(N{SiMe$_3$}$_2$)$_2$	70
8	MgMeBr (3.0 M, Et$_2$O)	63[a]
9	MgMeBr·nEt$_2$O (solid)	59[a]
10	MgPhBr·nEt$_2$O (solid)	63[a]
11	Mg(PhC≡CC{Ni-Pr}$_2$)Br(Et$_2$O) (**7**)	60[a]
12	MgBr$_2$.Et$_2$O	0
13	Mg(BPh$_4$)$_2$	0
14	MgMeBr, 5 mol % (3.0 M, Et$_2$O)[b]	56[c]
15	MgMeBr, 5 mol % (3.0 M, Et$_2$O)[d]	53[c]

[a]Yield calculated from consumption of carbodiimide. [b]Toluene. [c]Isolated yield. [d]THF.

Initially attempts were made to enter into the catalytic cycle via other possible intermediates in the catalytic cycle. Entries 2-4 demonstrate that it is possible to enter the catalytic cycle via bis(amidinate) **2**, bis(guanidinate) **3** and bis(propargylamidinate) **4**.(THF), providing comparable yields to **1**. This demonstrates that during catalysis the loss of one or more bidentate ligands is occurring.

As loss of the bidentate ligand is a possibility in this catalysis, entry into the catalytic cycle using pre-cursors to the bis(*N,N'*-ligand) systems was investigated. The reactivity of Mg-C/Mg-N bonds indicate that these species may gain entry into the catalytic cycle either by protonolysis of the alkyl/amido substituent by the acetylene, or by insertion of the carbodiimide into the Mg-C/Mg-N bonds to form the corresponding bis(*N,N'*-ligand) species *in situ* (Figure 2.12). Entries 5-7 show the activity of bis(acetylide) (**6**.(THF)$_4$), bis(alkyl) (MgBu$_2$) and bis(amide) (Mg(N{SiMe$_3$}$_2$)$_2$) magnesium species. Yields comparable to **1** were obtained, consistent with removal of the ancillary ligand early on in catalysis.
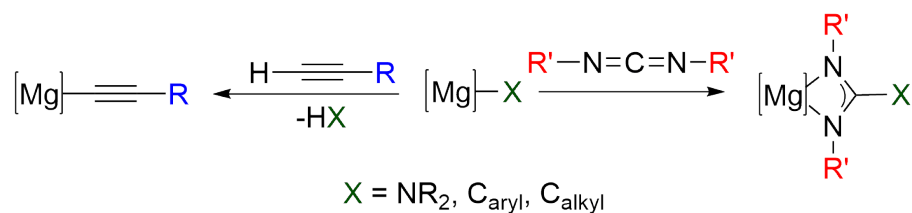
Figure 2.12: Entry into the catalytic cycle from organo- and amido-magnesium compounds.

Expanding on this reactivity, a number of Grignard reagents were tested for catalytic activity (entries 9-11). Catalytic turnover was observed, however lower yields (∼60%) were obtained compared to **1**. No change in the activity was observed upon partial removal of the Et$_2$O solvent and addition of the catalyst as a solid. Compound **7** exhibited similar activity to MeMgBr and PhMgBr, suggesting the reduced yields are due to the presence of the Mg-Br bond. To confirm this hypothesis, entry into the catalytic cycle by magnesium dibromide etherate (MgBr$_2$.Et$_2$O) was attempted. No catalytic C-C bond formation was observed after 24 hours at 80 °C, confirming that the Mg-Br bond does not provide entry into the catalytic cycle

(entry 12). $Mg(BPh_4)_2$ was also shown to be inactive towards the catalytic coupling of terminal alkynes to carbodiimide substrates (entry 13), indicating catalysis is unlikely to occur via Lewis acid catalysis.

Catalysis was demonstrated on a preparative scale using 5 mol% MgMeBr in toluene and THF (entries 14 and 15), with isolated yields of 56 % and 53 %, respectively. While previous catalytic studies suggested a dependence of catalytic activity on the solvent (Section 2.2), this is not observed in this case.

2.6 Independent Synthesis of Compounds Identified in the Catalytic Cycle

2.6.1 Synthesis and Characterisation of 3

Compound **3** was synthesised by the addition of two equivalents of *N,N'*-diisopropylcarbodiimide to $Mg(N\{SiMe_3\}_2)_2$ in THF (eq. 2.7). The ^1H NMR spectrum shows the expected resonances for a single symmetric $[\{Me_3Si\}_2NC\{Ni\text{-}Pr\}_2]^-$ guanidinate ligand. Integration of the THF peaks is consistent with a single THF molecule bound to the magnesium centre.
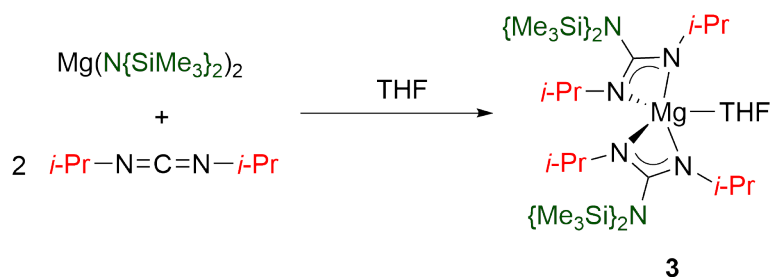
eq. 2.7: Synthesis of **3**.

The ^{13}C NMR spectrum displays a single low field resonance (δ_C 167.2 ppm), consistent with the metallacyclic carbon centre. The $SiMe_3$ carbons are observed as a single high field resonance (δ_C 2.5 ppm). The elemental analysis data of compound **3** is in good agreement with the calculated values.

Single crystal X-ray crystallography shows that compound **3** crystallises in the $P2_1/c$ space group. The compound exists as a 5-coordinate monomeric bis(guanidinate) species in the solid-state, containing a single molecule of THF bound to the metal centre. The geometry of the metal centre is described as intermediate between square pyramidal and trigonal bipyramidal ($\tau = 0.50$).[30] Both guanidinate ligands chelate to the magnesium centre with acute bite angles (63.04(7)°and 63.00(7)°). The Mg-N bond lengths (range = 2.0646(18) - 2.1842(18) Å) are consistent with σ-bonding interactions. The N-C bond distances of the metallacyclic CN_2 unit (range = 1.317(3) - 1.331(3) Å) indicate a bond order greater than 1. Analogous to **2**, differences in the Mg-N and N-C bond lengths are noted.

The bis(trimethylsilyl)amino group consists of a planar nitrogen (sum of angles = 359.9°) with N-C bond distances (N(3)-C(1) 1.457(3) Å and N(6)-C(14) 1.447(3) Å). The NSi_2:metallacycle inter-planar angles are 79.76(6)°and 80.65(6)°. These data are consistent with single C-NSi_2 bonds with no overlap of the N lone pair and the empty p-orbital on the central carbon, and confirm that there is no resonance contribution from the third (zwitterionic) resonance form (Chapter 1, Figure 1.4).

Figure 2.13: ORTEP representation of **3**. 30% Thermal ellipsoid plot. Hydrogens omitted for clarity. Selected bond lengths (Å) and angles (°) are reported in Table 2.5.

Table 2.5: Selected bond lengths (Å) and angles (°) in **3**.

Mg-N(1)	2.1842(18)	N(1)-Mg-N(2)	61.08(8)
Mg-N(2)	2.0655(18)	N(4)-Mg-N(5)	63.01(8)
Mg-N(4)	2.1831(18)	N(1)-C(1)-N(2)	113.88(18)
Mg-N(5)	2.0646(18)	N(4)-C(14)-N(5)	114.15(19)
N(1)-C(1)	1.3345(18)	N(1)-Mg-N(4)	166.00(6)
N(2)-C(1)	1.3212(19)	N(2)-Mg-N(5)	136.20(7)
N(3)-C(1)	1.444(3)	C(1)-N(1)-Mg	89.04(13)
N(4)-C(14)	1.317(3)	C(1)-N(2)-Mg	94.03(15)
N(5)-C(14)	1.329(3)	C(14)-N(4)-Mg	93.84(16)
N(6)-C(14)	1.447(3)	C(14)-N(5)-Mg	88.97(13)
Mg-O	2.0804(17)		

2.6.2   Synthesis and Characterisation of 4.(THF)

Compound **4**.(THF) was isolated from the reaction of two equivalents of propargylamidine **5** with MgBu$_2$ in THF. An alternative synthesis for this compound involves the addition of two equivalents of *N,N'*-diisopropylcarbodiimide to compound **6**.(THF)$_4$ in THF (Scheme 2.5).
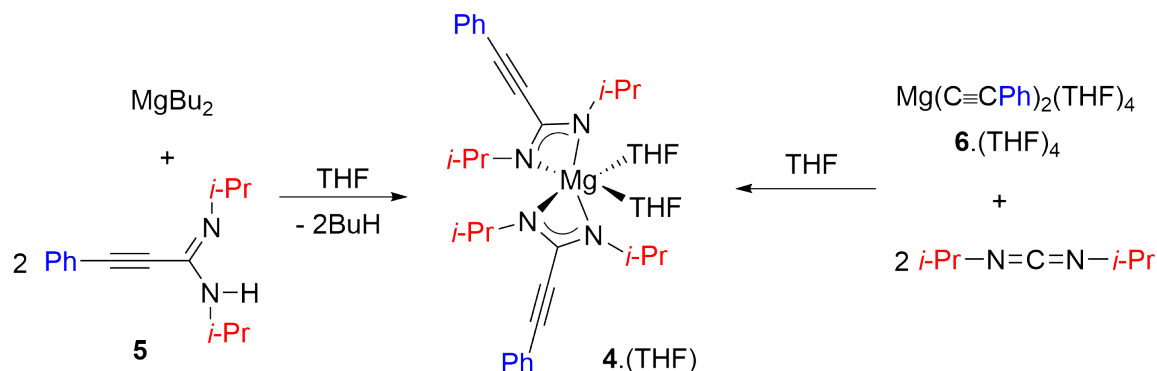
Scheme 2.5: Synthesis of **4**.(THF).

The ^{1}H NMR spectrum of **4**.(THF) displays a multiplet at δ_H 7.48 ppm corresponding to the o-C$_6$H$_5$ protons of the propargylamidinate. Integration of the THF resonances relative to the amidinate indicates a 1:1 ratio, suggesting two THF molecules

at the magnesium.

The ^{13}C NMR spectrum displays a single set of peaks corresponding to the propargylamidinate ligand. A single low field resonance (δ_C 157.9 ppm) represents the metallacyclic carbon centre. The triply bonded carbon centres appear as sharp resonances at δ_C 95.9 and 80.0 ppm. Elemental analysis data is consistent with calculated values for compound **4**.(THF).

Compound **4**.(THF) crystallises in the $P\bar{1}$ space group and lies on an inversion centre. The solid-state structure shows a 6-coordinate, monomeric bis(propargylamidinate) species, and confirms that two THF molecules are bound to the magnesium centre. The metal centre has a distorted octahedral geometry, with the THF molecules trans to each other. The bidentate propargylamidinate ligands chelate to the magnesium centre, forming planar four membered metallacycles (sum of internal angles = 359.9°). The main distortion in the metal geometry is due to the acute bite angle of the chelating propargylamidinate ligands (62.77(3)°). The N-Mg-O angles (range of angles = 88.94(3)°- 91.06(3)°) are consistent with a distorted octahedral geometry.
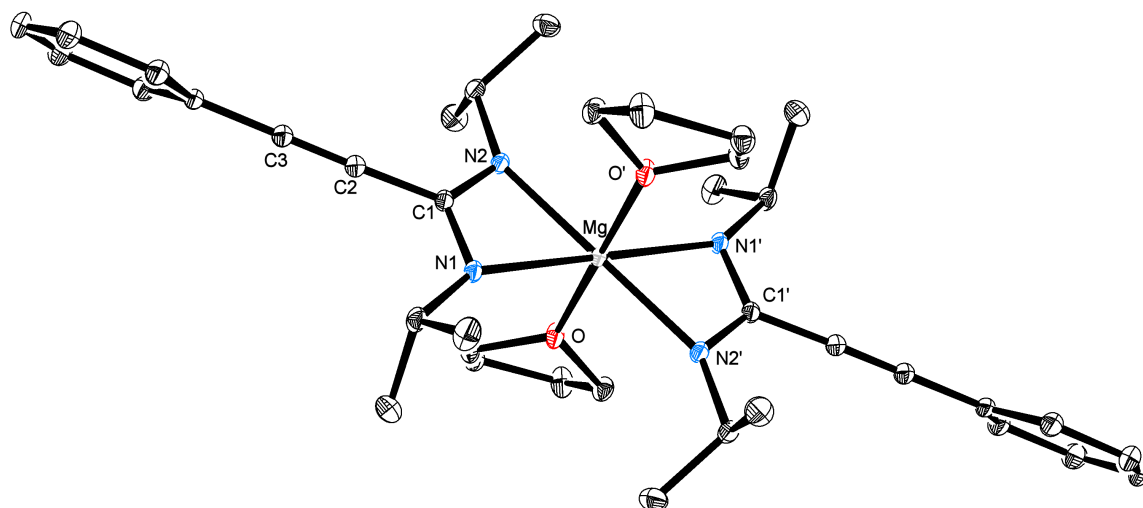
Figure 2.14: ORTEP representation of **4**.(THF). 30% Thermal ellipsoid plot. Hydrogens omitted for clarity. Selected bond lengths (Å) and angles (°) are reported in Table 2.6.

42

Table 2.6: Selected bond lengths (Å) and angles (°) in **4**.(THF).

Mg-N(1)	2.1691(8)	N(1)-C(1)-N(2)	116.33(8)
Mg-N(2)	2.1644(8)	Mg-N(2)-C(13)	148.44(6)
N(1)-C(1)	1.3288(13)	Mg-N(1)-C(10)	148.45(8)
N(2)-C(1)	1.3279(13)	C(1)-C(2)-C(3)	178.57(13)
Mg-O	2.1814(7)	C(2)-C(3)-C(4)	179.41(11)
C(2)-C(3)	1.1964(14)	C(1)-N(1)-Mg	90.34(7)
N(1)-Mg-N(2)	62.77(3)	C(1)-N(2)-Mg	90.56(5)

Mg-N(1) and Mg-N(2) bond distances (2.1691(8) and 2.1644(8) Å, respectively) are consistent with σ-bonding interactions of the propargylamidinate with the magnesium centre. The N(1)-C(1) and N(2)-C(1) bond distances (1.3288(13) and 1.3279(13) Å, respectively) are consistent with delocalisation of π-electron density over the metallacyclic CN_2 unit. The C(2)-C(3) bond distance (1.196 Å) and the C(1)-C(2)-C(3) (178.57(11)°) and C(2)-C(3)-C(4) (179.41(12)°) bond angles, are consistent with localisation of electron density to form a triple bond.

2.6.3   Synthesis and Characterisation of 6.(THF)$_4$

The synthesis of compound **6**.(THF)$_4$ has previously been reported in the literature, however full crystallographic and NMR data for this compound were not reported.[32] Addition of two equivalents of phenylacetylene to a THF solution of $MgBu_2$ results in the quantitative formation of **6**.(THF)$_4$ (eq. 2.8).

$$MgBu_2 \quad \xrightarrow[\text{THF}]{2\,H\text{—}\!\!\equiv\!\!\text{—}Ph} \quad Mg(C\!\equiv\!CPh)_2(THF)_4$$
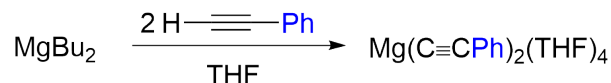
eq. 2.8: Synthesis of **6**.(THF)$_4$.

The ^{1}H NMR spectrum of **6**.(THF)$_4$ displays three resonances corresponding to the aromatic protons. The $o\text{-}C_6H_5$ protons are observed as a relatively low field doublet (δ_H 7.89 ppm), consistent with a close proximity to the magnesium centre.

Integration of the peaks indicate the presence of four THF molecules in **6**.$(THF)_4$. The ^{13}C NMR spectrum provided limited information due to poor solubility of **6** in C_6D_6. A single set of resonances was observed in the aromatic region (δ_C 132.2, 129.3, 128.5 and 127.0 ppm), accounting for all carbon centres. Peaks corresponding to the THF carbons are observed at δ_C 68.0 and 25.8 ppm. No resonances were observed for the C≡C carbons.

6.$(THF)_4$ crystallises in the $C2/c$ space group, with the molecule lying on a 2-fold rotation axis (C_2). The solid-state structure confirms the presence of a terminal bis(acetylide) species and four coordinated THF molecules (Figure 2.15). Two of the THF molecules are disordered over two positions. The geometry at the metal centre can be best described as a distorted octahedral, where the acetylide substituents are trans to each other. The remaining positions are occupied by four THF molecules bound to the magnesium centre.
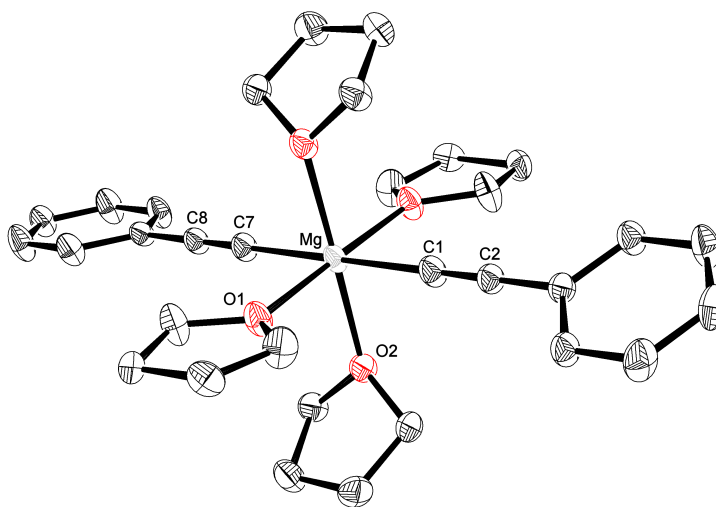
Figure 2.15: ORTEP representation of **6**.$(THF)_4$. 30% Thermal ellipsoid plot. Hydrogens omitted for clarity. Selected bond lengths (Å) and angles (°) are reported in Table 2.7.

Table 2.7: Selected bond lengths (Å) and angles (°) in **6**.$(THF)_4$.

Mg-C(1)	2.187(2)	C(1)-C(2)	1.224(3)
Mg-C(7)	2.191(2)	C(7)-C(8)	1.220(3)

The Mg-C(1) and Mg-C(7) bond lengths (2.187(2) and 2.191(2) Å, respectively) are within the expected range for terminal magnesium (bis)acetylide species (2.092(2)-2.348(2) Å)[33] and are comparable to the Mg-C bond distances in the six-coordinate terminal (bis)phenylacetylide $Mg(C{\equiv}CPh)_2(tmeda)_2$ (2.176(6) and 2.200(6) Å).[34] The C(1)-C(2) and C(7)-C(8) bond lengths (1.224(3) and 1.220(3) Å, respectively) similar to the expected value for a C$\equiv$C triple bond (*ca.* 1.203 Å). Disorder in two of the THF molecules prevents discussion of the bond lengths and angles of the THF groups.

2.6.4   Synthesis and Characterisation of 7

As part of the catalytic studies, the mono-propargylamidinate bromide **7** was synthesised (Section 2.5). Compound **7** was synthesised from the addition of one equivalent of methylmagnesium bromide (MeMgBr) to a stirring solution of propargylamidine **5** in Et_2O (eq. 2.9). Recrystallisation from Et_2O yielded clear yellow crystals of **7**.
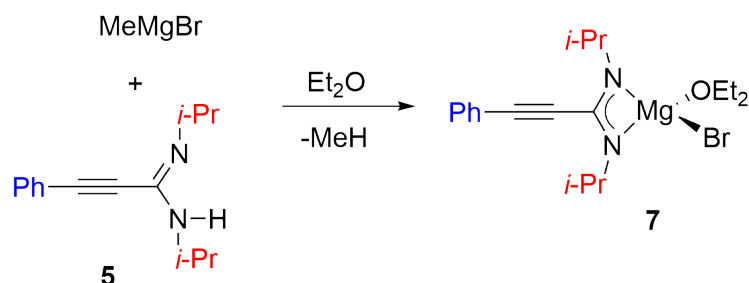
eq. 2.9: Synthesis of **7**.

The ^{1}H NMR spectrum of **7** displays resonances in the aromatic region corresponding to the o-C_6H_5 protons at δ_H 7.38 ppm. The presence of coordinated Et_2O is confirmed by a quartet and triplet (δ_H 3.53 and 1.07 ppm, respectively) upfield from free Et_2O. Integration of the signals relative to the propargylamidinate peaks indicates a 1:1 ratio of Et_2O to amidinate in the compound.

The ^{13}C NMR spectrum shows a single low field resonance (δ_C 158.9 ppm) consistent with the metallacyclic carbon of the propargylamidinate. The quaternary C$\equiv$C

carbons appear as sharp resonances at δ_C 97.1 and 80.1 ppm. Elemental analysis is consistent with the calculated values for **7**.

X-ray crystallography indicates that **7** crystallises in the $Pca2_1$ space group. Compound **7** dimerizes in the solid-state through μ-Br bridges, generating two five-coordinate magnesium centres (Figure 2.16). The geometry of both metal centres is intermediate between square pyramidal and trigonal bipyramid ($\tau = 0.56$ (Mg(1)) and 0.48 (Mg(2))).[30] The bromides bridge the magnesium centres to form a planar four-membered Mg_2Br_2 core (sum of internal angles = 360.0°). The Mg-Br bonds are unsymmetrical, with Mg(1)-Br(2) and Mg(2)-Br(1) bonds (2.5364(9) and 2.5406(9) Å, respectively) being significantly shorter than the Mg(1)-Br(1) and Mg(2)-Br(2) (2.7202(9) and 2.7181(9) Å, respectively).
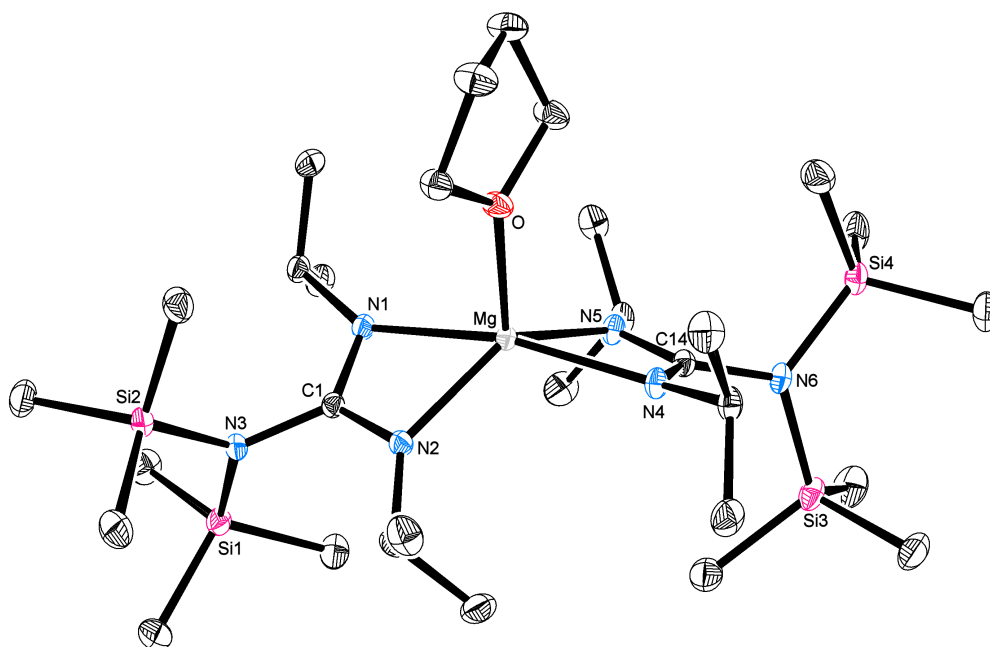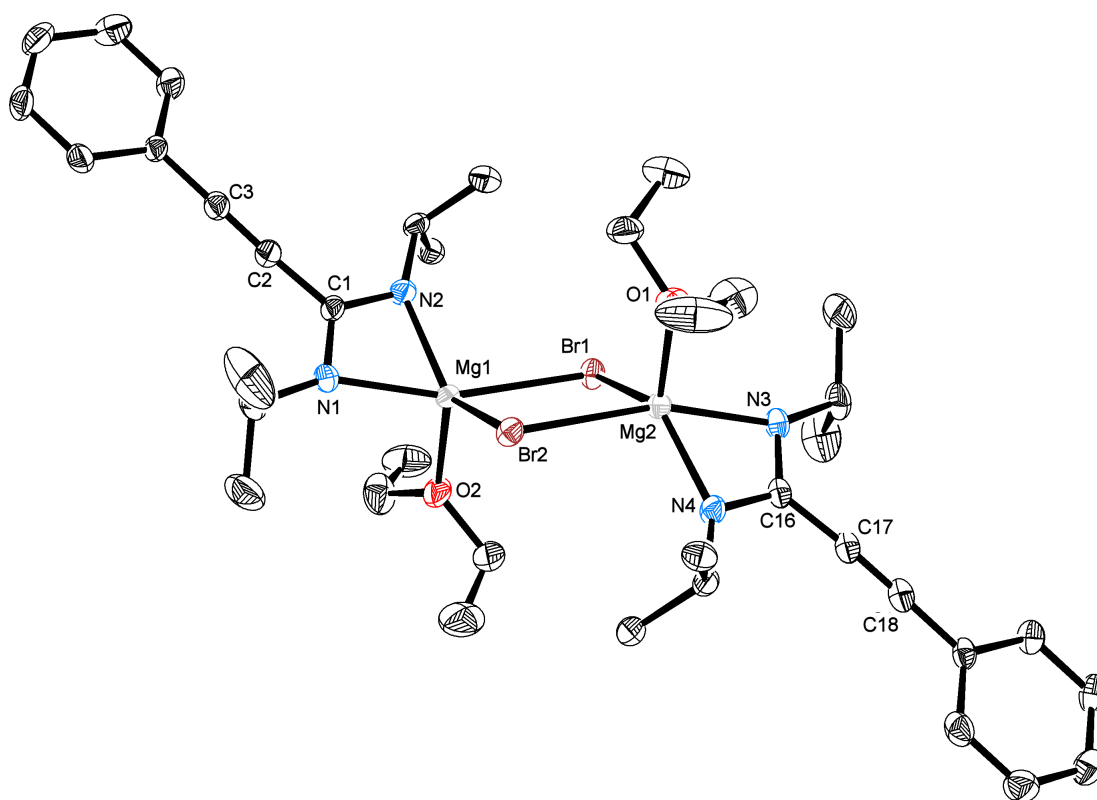

Figure 2.16: ORTEP representation of [**7**]$_2$. 30% Thermal ellipsoid plot. Hydrogens omitted for clarity. Selected bond lengths (Å) and angles (°) are reported in Table 2.8

Table 2.8: Selected bond lengths (Å) and angles (°) in [**7**]$_2$.

Mg(1)-Br(1)	2.7202(9)	Mg(2)-Br(1)	2.5406(9)
Mg(1)-Br(2)	2.5364(9)	Mg(2)-Br(2)	2.7181(9)
Mg(1)-N(1)	2.138(2)	Mg(2)-N(3)	2.119(2)
Mg(1)-N(2)	2.060(2)	Mg(2)-N(4)	2.071(2)
N(1)-C(1)	1.324(4)	N(3)-C(16)	1.331(3)
N(2)-C(1)	1.333(3)	N(4)-C(16)	1.340(3)
C(2)-C(3)	1.203(4)	C(17)-C(18)	1.206(4)
N(1)-Mg(1)-N(2)	64.51(9)	N(3)-Mg(2)-N(4)	64.74(9)
Mg(1)CN$_2$:Mg$_2$Br$_2$ inter-planar angle			52.67(7)
Mg(2)CN$_2$:Mg$_2$Br$_2$ inter-planar angle			47.29(7)

The propargylamidinate ligands bind to the magnesium centre in a bidentate fashion, forming planar metallacycles (sum of internal angles = 360.0° (Mg(1)) and 359.9° (Mg(2))). The bite angle of the propargylamidinate ligands represent the most acute internal angles of these metallacycles (64.51(9)° (Mg(1)) and 64.74(9)° (Mg(2))). The plane of the CN$_2$Mg metallacycles intersect the Mg$_2$Br$_2$ plane at similar angles (dihedral angles = 52.67(7)° (CN$_2$Mg(1)/Mg$_2$Br$_2$) and 47.29(7)° (CN$_2$Mg(2)/Mg$_2$Br$_2$)), and may be considered trans across the Mg$_2$Br$_2$ plane.

The Mg-N bond distances (range = 2.060(2) - 2.138(2) Å) are consistent with σ-bonding interactions. The N-C bond distances (range = 1.324(4) - 1.340(3) Å) and Mg-N bond distances reflect delocalization of electron density on the CN$_2$ moiety. Short bond distances for C(2)-C(3) and C(17)-C(18) (1.203(4) and 1.206(4) Å, respectively) reflect the presence of a carbon-carbon triple bond.

2.7 Comparison of Solid-state Structures of Magnesium Amidinate/Guandinate Compounds

Magnesium compounds supported by amidinate and guanidinate ligands are relatively common. A number of bis(amidinate) and bis(guanidinate) magnesium compounds have been structurally characterised as four-, five- or six-coordinate species, with neutral donor ligands (L) occupying the remaining sites in five- and six-coordinate species (Figure 2.17).
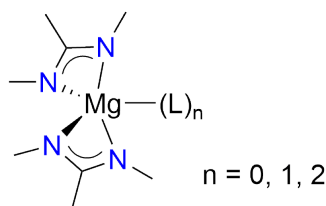
Figure 2.17: Representation of a generic bis(amidinate)/bis(guanidinate) magnesium compound.

The coordination number of these species is dependent on the sterics and electronics of the substituents at both the nitrogen and backbone carbon. Compounds containing sterically demanding substituents (e.g. t-Bu,[35,36] 2,6-i-$Pr_2C_6H_3$[37] and 2,4,6-$Me_3C_6H_2$[35]) at either the nitrogen atoms or the backbone carbon commonly form four-coordinate species with no solvent molecules (L) coordinated to the magnesium centre. Reducing the steric bulk at these positions can allow neutral donor ligands to coordinate, increasing the coordination number of the magnesium centre. Therefore, the coordination number of the magnesium species can be used to identify amidinate ligands with similar steric profiles.

2.7.1 Five-Coordinate Magnesium bis(amidinate/guanidinate) Compounds

Structurally characterised five-coordinate magnesium bis(amidinate)/bis(guanidinate) compounds are rare, with most existing as four- and six-coordinate

species in the solid-state. The only other structurally characterised five-coordinate bis(amidinate)/ bis(guanidinate) magnesium compounds reported in the literature are Mg(({i-Pr}$_2$NC{Ni-Pr}$_2$)$_2$(THF)[38] (**I**), Mg(PhC{NCy}{NSiMe$_3$})$_2$(Et$_2$O)[39] (**II**) and Mg(PhC{NSiMe$_3$}$_2$)$_2$(N≡CPh)[40] (**III**).

Comparison of the solid-state structures of compounds **2** and **3** to these compounds indicate a dependence of the geometry of the metal centre on the substituents at the nitrogen and metallacyclic carbon (Table 2.9). Using the system developed by Addison et al.,[30] bias towards square pyramidal and trigonal bipyramid geometries have been determined and utilised to classify the geometry of these species.

Both **2** and **3** form heavily distorted geometries, with τ values close to 0.5, suggesting only slight bias towards one geometry over the other. Mg({i-Pr}$_2$NC{Ni-Pr}$_2$)$_2$(THF) (**I**) also forms a heavily distorted geometry, which may reflect the similar steric profiles of the nitrogen substituents. Mg(PhC{NCy}{NSiMe$_3$})$_2$(Et$_2$O) (**II**) and Mg(PhC{NSiMe$_3$}$_2$)$_2$(N≡CPh) (**III**), which have SiMe$_3$ substituents at the nitrogens, are biased towards a trigonal bipyramidal geometry (tbp).

Differences in the Mg-N ($\Delta_{\text{Mg}-\text{N}}$) and N-C bond distances ($\Delta_{\text{N}-\text{C}}$) of the metallacycle reflect partial localisation of electron density within the CN$_2$ moiety. This is most prominent in compounds **2**, **3** and **I**. In an idealised trigonal bipyramidal structure, M-N$_{\text{axial}}$ bonds are significantly longer than M-N$_{\text{equitorial}}$ bonds.[41] The chelating nature of the amidinate/guanidinate ligands prevent idealised geometries from forming, and may cause the τ value to be a misrepresentation of the true geometries. The partial localisation of electron density over the CN$_2$ unit may indicate that **2**, **3** and **I** adopt a distorted trigonal bipyramidal geometry, with the longer Mg-N bonds corresponding to the nitrogen atoms in the pseudo-axial positions and the shorter Mg-N bonds corresponding to the nitrogen atoms in the pseudo-equatorial positions. Despite having a greater τ value, compounds **II** and **III** have much smaller $\Delta_{\text{Mg}-\text{N}}$ values than **2**, **3** and **I**.

Coordination of an amidinate ligand to a metal centre can be represented by reso-

nance structures α and β in Figure 2.18.[23] The deviation from symmetrical coordination of the amidinate ligands is consistent with increased contribution from one of the resonance structures over the other. Differences in the Mg-N and N-C bond distances in **2**, **3** and **I** are consistent with a greater resonance contribution from resonance structure α. The nitrogen associated with the longer Mg-N bond has the shorter N-C bond, consistent with this assessment.

α β
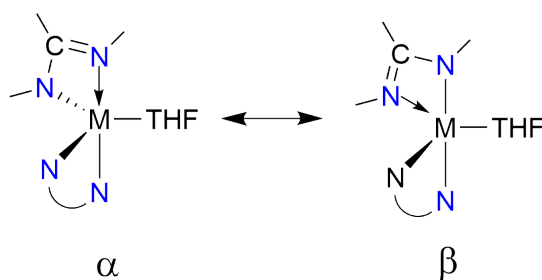
Figure 2.18: Resonance structures of amidinate bonding to a metal centre.

Table 2.9: Selected structural data for five-coordinate bis(amidinate)/ bis(guanidinate) magnesium species.

	2	**3**[c]	**I**	**II**	**III**
τ (geometry bias[a])	0.41 (sq. pyr.)	0.5	0.57 (tbp)	0.74 (tbp)	0.92 (tbp)
N-Mg-N' angle (°)	63.0(1)	63.0	63.0(3)	64.1(1)	64.8(1)
Mg-N (Å)	2.096(1) , 2.198(1)	2.184 , 2.065	2.066(7), 2.184(6)	2.158(3), 2.103(3)	2.139(3), 2.110(3)
$\Delta_{\mathrm{Mg-N}}$ (Å)	0.103	0.119	0.118	0.055	0.029
N-C[b] (Å)	1.335(2), 1.321(2)	1.320, 1.330	1.363(12), 1.306(12)	1.350(5), 1.319(5)	1.320(5), 1.324(5)
$\Delta_{\mathrm{N-C}}$ (Å)	0.013	0.010	0.057	0.031	0.004
Mg-N-C angle (°)	145.3(10), 150.9(10)	146.7, 139.9	142.3(6), 146.9(5)	142.7(2), 141.0(17)	140.9(17), 138.8(18)

[a]Square-based pyramid (sq. pyr.), Trigonal bipyramid (tbp). [b]Metallacyclic carbon centre. [c]Average values of both amidinate ligands.
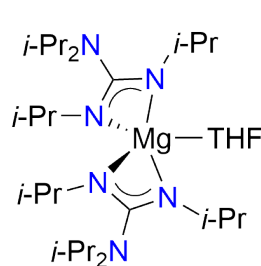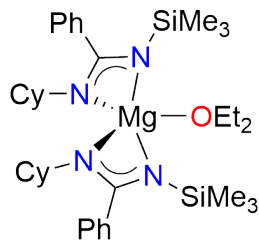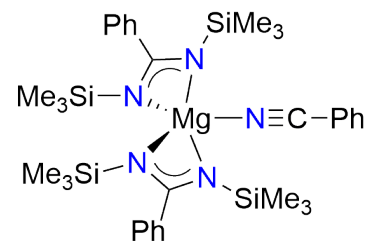
I   **II**   **III**

2.7.2 Six-Coordinate Magnesium bis(amidinate/guanidinate) Compounds

In contrast to five-coordinate species **2** and **3**, compound **4**.(THF) crystallises as a six-coordinate magnesium species, incorporating two molecules of THF in the coordination sphere. This indicates that the propargylamidinate ligand has a smaller steric profile than the amidinate and guanidinate ligands of **2** and **3**, and illustrates the effect of changing the metallacyclic carbon substituent on the coordination number of the metal.

A number of structurally characterised six-coordinate bis(amidinate) species have been reported in the literature with most incorporating small substituents at either the nitrogen or metallacycic carbon. Srinivas et al. reported the solid-state structure of the six-coordinate bis(benzamidinate) compound, Mg(PhC{Ni-Pr}$_2$)$_2$(THF)$_2$ (**IV**).[38] The solid-state structure of six-coordinate bis(benzamidinate) species, Mg(PhC{NSiMe$_3$}$_2$)$_2$(THF)$_2$ (**V**) was reported by Walther and co-workers.[42] Junk and co-workers reported the solid-state structure of two related six-coordinate bis(formamidinate) compounds, Mg(HC{N-4-MeC$_6$H$_4$}$_2$)$_2$(THF)$_2$ (**VI**) and Mg(HC{N-2-MeC$_6$H$_4$}$_2$)$_2$(THF)$_2$ (**VII**).[43] All of these compounds have the THF molecules arranged in a trans-conformation.

Comparison of these compounds to **4**.(THF) (Table 2.10) indicate a relatively narrow range of N-Mg-N' bite angles (62.30° - 63.24°) for 6-coordinate trans species. The Mg-N bond distances in **4**.(THF) are identical (within 3σ) to the Mg-N bond distances of **IV**, consistent with both compounds containing i-Pr substituents at the nitrogens. Significantly shorter Mg-N bond distances are observed for the aryl-substituted formamidinate species **V** and **VI**, while **VII** displays significantly longer Mg-N bonds. The difference in the Mg-N (Δ_{Mg-N}) and N-C (Δ_{N-C}) bond lengths within the amidinate ligands suggest only minor localisation of electron density within the CN$_2$ unit.

Comparison of the Mg-N-C angles of **4**.(THF) and **IV** indicate a much larger angle for **4**.(THF). These two species only differ in the substitution at the metallacycle carbon, with **4**.(THF) containing an acetylene linker between the metallacycle carbon and the phenyl group. The increased Mg-N-C angle in **4**.(THF) is likely a result of a reduction in the steric profile at the metallacyclic carbon as the phenyl group is further removed from the nitrogen substituents (Figure 2.19).
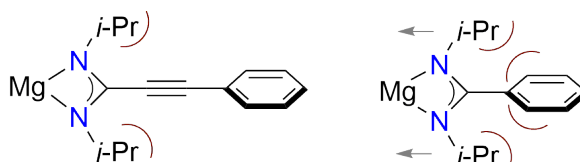
Figure 2.19: Comparison of the different metallacycle carbon substituents in **4**.(THF) and **IV**.

Table 2.10: Selected structural data for six-coordinate bis(amidinate) species

	4.(THF)	IV	V	VI[b]	VII[b,c]
N-Mg-N' angle (°)	62.77(3)	62.3(2)	62.71(10)	62.77	63.24
Mg-N (Å)	2.1691(10), 2.1645(7)	2.169(6), 2.161(6)	2.188(3), 2.208(3)	2.164, 2.150	2.165
δ_{Mg-N} (Å)	0.0046	0.008	0.02	0.0145	0
N-C[a] (Å)	1.3288(12), 1.3280(15)	1.324(9), 1.338(9)	1.328(5), 1.329(5)	1.321, 1.315	1.319
δ_{N-C} (Å)	0.0008	0.014	0.001	0.0065	0
Mg-N-C (°)	148.44(6), 148.45(8)	146.6(5), 146.7(6)	138.76(15), 142.03(14)	147.39, 149.46	152

[a]Metallacyclic carbon centre. [b]Average values of both amidinate ligands. [c]N atoms of the amidinate ligand are related by symmetry.
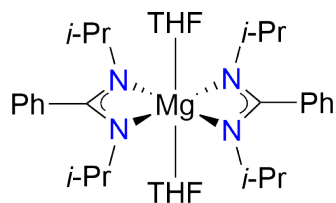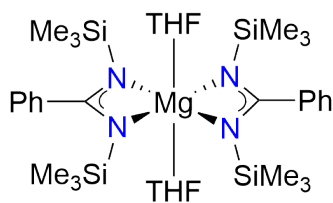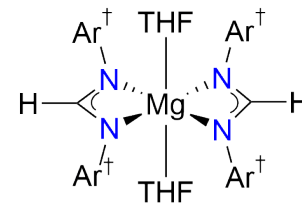
IV   **V**   Ar†= 4-MeC$_6$H$_4$ (**VI**), 2-MeC$_6$H$_4$ (**VII**)

2.7.3 Magnesium halides supported by amidinate and guanidinate ligands

Despite the ready availability of numerous Grignard reagents, magnesium halides supported by amidinate and guanidinate ligands are surprisingly rare. Compound **7** forms a dimeric structure in the solid-state, whereby the two molecules are linked through bridging bromide interactions. The only other structurally characterised magnesium bromide species supported by an amidinate ligand is [Mg(mesC{NCy}$_2$)Br(Et$_2$O)]$_2$[18] (**VIII**). The solid-state structures of the related magnesium chloride species [Mg({SiMe$_3$}$_2$NC{NCy}$_2$)Cl(THF)]$_2$[44] (**IX**) and [Mg(HC{NAr}$_2$)Cl(THF)]$_2$[45] (**X**) have also been reported (Figure 2.21). These species also exist as dimers in the solid-state, with two 5-coordinate magnesium centres with structures similar to that observed in [**7**]$_2$. The amidinate ligands are arranged trans to each other across the plane of the Mg$_2$X$_2$ metallacycle (X = halide).

According to the τ values for these compounds, a range of geometries are possible (Table 2.11). The amidinate/guanidinate ligands bind to the magnesium centre with characteristically acute bite angles to form planar metallacycles. While [**7**]$_2$, **VIII** and **IX** have relatively similar bite angles, **X** has a significantly smaller bite angle. This may be a reflection of the similar steric profile at the nitrogen centers for [**7**]$_2$, **VII** and **IX**, and the increased steric bulk at the nitrogens of **X**. In addition the bite angles in these compounds (range = 63.62°- 64.78°) are notably higher than that observed for both 5- and 6-coordinate bis(amidinate) and bis(guanidinate) systems.

Partial localisation of electron density is observed in all of these species, represented by large $\Delta_{\text{Mg}-\text{N}}$ and $\Delta_{\text{N}-\text{C}}$ values. The nitrogen atom of the longer Mg-N bond corresponds to the shorter N-C bond, analogous to the 5-coordinate bis(amidinate)/ bis(guanidinate) systems. Significant differences are also observed for the Mg-X bonds.

The large Δ_{Mg-N} and Δ_{Mg-X} values in $[\mathbf{7}]_2$, **VII** and **IX** are consistent with a trigonal bipyramidal geometry (as in Section 2.7.1), with significant elongation of the Mg-N and Mg-X bonds of the nitrogen (N*) and halide (X) atoms in the pseudo-axial position. The other nitrogen occupies the pseudo-equitorial position, and has a much shorter Mg-N bond length. The nitrogen in the pseudo-axial position (N*) is defined by the largest angle about the magnesium centre (α), and corresponds to the nitrogen with the longer bond in all cases.
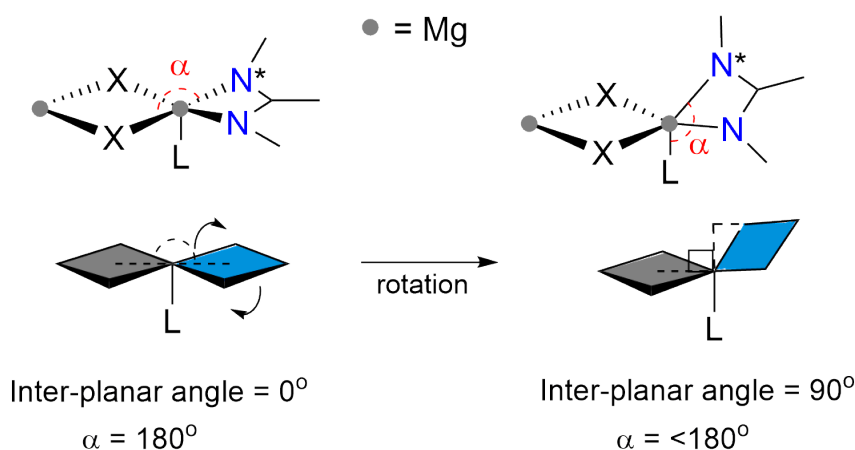
Figure 2.20: Representation of the effect of inter-planar angles on α. α = largest angle about Mg, L = solvent molecule.

The CN_2Mg : Mg_2X_2 inter-planar angles determines whether the axial nitrogen atom (N*) sits trans to the solvent molecule or a halide atom (Figure 2.20). Compound **X** has a significantly larger inter-planar angle (mean = 87.4°) than $[\mathbf{7}]_2$, **VII** and **IX**, forming an almost perpendicular arrangement. As a result, the N*-Mg-O bond angle becomes larger than the N*-Mg-X bond angle, consistent with the solvent molecule occupying the pseudo-axial position. This is consistent with the relatively small Δ_{Mg-X} value in addition to a relatively long Mg-O bond (mean = 2.082 Å).

Compounds $[\mathbf{7}]_2$, **VII** and **IX** display small inter-planar angles (range = 42.01°-57.90°), resulting in the pseudo-axial positions being occupied by N* and X atoms. This is represented by the largest angle about the magnesium centre corresponding to N*-Mg-Br, shorter Mg-O bond distances (range = 2.024(2)-2.046(2) Å) and significantly larger Δ_{Mg-X} values.

VIII

mes — Cy, N, L, Br, Mg, Mg, Cy, N, mes ... L, Cy

IX

{Me₃Si}₂N ... Cy, L, Cl, Mg, Mg, Cy, N{SiMe₃}₂ ... L, Cy

X

Ar, L, Cl, H, Mg, Mg, Ar, H ... L, Ar
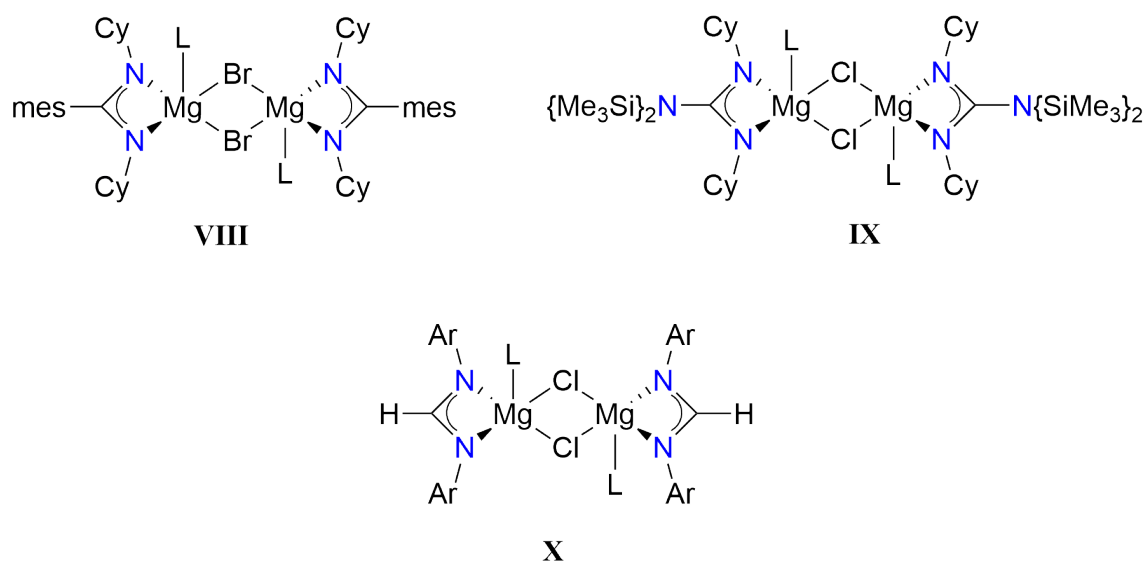
Figure 2.21: Bridged halide species supported by amdinate/guanidinate ligands. L = Et_2O (**VII**), THF (**IX**, **X**).

57

Table 2.11: Structural data for five-coordinate magnesium halides supported by amdinate/guandinate ligands

	$[7]_2$		**VIII**	**IX**	$\mathbf{X}^d$
	Mg(1)	Mg(2)			
τ (geometry bias^a)	0.56, 0.48	0.48	0.70 (tbp)	0.43 (sq. pyr.)	0.075 (sq. pyr.)
N-Mg-N angle (°)	64.51(9)	64.74(9)	64.78(9)	64.10(8)	63.62
Mg-X (X = Br,Cl) (Å)	2.720(1),2.536(1)	2.718(1),2.541(1)	2.553(1), 2.679(1)	2.417(1), 2.495(1)	2.404, 2.440
$\delta_{\text{Mg}-\text{X}}$ (Å)	0.18	0.18	0.13	0.078	0.036
Mg-N (Å)	2.138(2), 2.060(2)	2.119(2),2.071(2)	2.122(2), 2.050(3)	2.073(2), 2.125(2)	2.081, 2.187
$\delta_{\text{Mg}-\text{N}}$ (Å)	0.078	0.048	0.072	0.051	0.106
N-C^b (Å)	1.333(3), 1.324(4)	1.340(3), 1.331(3)	1.332(4), 1.338(3)	1.334(3), 1.321(3)	1.313, 1.320
$\delta_{\text{N}-\text{C}}$ (Å)	0.009	0.009	0.006	0.013	0.007
CN_2Mg:Mg_2Br_2 interplanar angle	52.67(7)	47.29(7)	57.90(7)	42.01(5)	87.4
Mg-O	2.024(2)	2.030(2)	2.046(2)	2.033(2)	2.082
Largest angle^c	N*-Mg-Br	N*-Mg-Br	N*-Mg-Br	N*-Mg-Cl	N*-Mg-O

^{a}Square-based pyramid (sq. pyr.), Trigonal bipyramid (tbp). ^{b}Metallacyclic carbon centre. ^{c}Atoms corresponding to α. ^{d}Average of four 5-coordinate Mg centres.

2.7.4 Summary

A recurring theme in this comparison is the dependence of resonance stabilisation on the geometry of the metal centre. Five-coordinate bis(amidinate)/bis(guanidinate) magnesium species and magnesium halides supported by amidinate/guanidinate ligands exhibit partial localisation of electron density. In contrast, six-coordinate bis(amidinate)/bis(guanidinate) species show only minor localisation in the CN_2 unit. This is thought to be associated with the formation of trigonal bipyramidal geometries, where the nitrogen atoms occupy the axial or equitorial positions. Nitrogen atoms in the axial positions have significantly longer Mg-N bonds and shorter N-C bonds, consistent with bias towards one resonance form (Section 2.7.1, Figure 2.18).

The geometry of five-coordinate metal species containing bidentate ligands with acute bite angles is difficult to determine, often forming distorted structures. The τ value reported by Addison et al.[30] has been employed for the classification of 5-coordinate species, however assignments based on this value do not fit with experimental observations of the bond lengths and angles. This suggests that this rule breaks down when using bidentate ligands that form constrained four-membered metallacycles.

Chapter 3

Conclusion

Following on from preliminary reports of catalytic addition of terminal acetylenes to carbodiimides facilitated by **1**, this research has explored the dependence on reaction conditions and substrate scope. A detailed investigation into the catalytic cycle has been performed in addition to the identification of a range of magnesium-based pre-catalysts.

The overall yield of the reaction was shown to be dependent on the catalyst loading, temperature and solvent. At higher catalyst loading and temperatures, the catalytic activity is significantly higher. Using THF as a solvent decreased catalytic activity compared to toluene, possibly due to competitive binding to the active site.

Catalysis was also observed to be dependent on the sterics and electronics of both the acetylene and carbodiimide substrates. Significant dependence on the steric bulk at the nitrogen of the carbodiimide was attributed to the presence of an associative mechanism. The sterics and electronics of the acetylene substituent were also contributing factors in determining catalytic activity, with a linear relationship between the electron withdrawing properties of the acetylene substituent (R) and the catalytic activity.

The catalytic cycle studies show a clear deviation from the mechanism proposed for

the lanthanides. Identification of important intermediates in the reaction pathway was performed through the use of a series of NMR scale reactions. A number of potential intermediates were investigated, however facile ligand redistribution inhibited the isolation of these compounds. In contrast to the proposed mechanism, Step III of the catalytic cycle (protonolysis of the propargylamidinate ligand) was observed to be reversible. A summary of the findings from the catalytic cycle studies has been compiled in Figure 3.1.

The propensity for intermediates to undergo ligand redistribution led to the catalytic testing of a range of magnesium compounds. Bis(amidinate)/ bis(guanidinate)/ bis(propargylamidinate) species were catalytically active, suggesting loss of the ligand. Homoleptic organo- and amido-magnesium compounds were also observed to be catalytically active, showing similar yields to **1**. Finally, Grignard reagents showed reduced catalytic activity, due to the lack of reactivity of the Mg-Br bond.

The identity of important species in the reaction mixtures were determined through the independent synthesis and isolation of these or related compounds. Compounds were fully characterised using ^{1}H and ^{13}C NMR spectroscopy, single crystal X-ray crystallography and elemental analysis. Comparison of the solid-state structures of these compounds to similar species reported in the literature indicated a tendency for five-coordinate magnesium amidinate species to undergo significant localisation of electron density in the CN_2 unit. The τ value was used to determine bias in the geometry of five-coordinate magnesium compounds, however it was found to be unsuitable for compounds containing multiple constrained metallacycles.

LMg−N{SiMe₃}₂

R'−N=C=N−R'

H≡R
− HN{SiMe₃}₂

LMg⟨N,N⟩−N{SiMe₃}₂ (R' on N's) ⇌ 1/2 [N{SiMe₃}₂ / R'−N N−R' / Mg / R'−N N−R' / N{SiMe₃}₂ + MgL₂]

H≡R
− {SiMe₃}₂NC{NR'}{NHR'}

LMg−C≡C−R ⇌ 1/2 [MgL₂ + Mg(−C≡C−R)₂]   R'−N=C=N−R'

−RC≡CC{NR'}{NHR'}
H−C≡C−R

LMg⟨N,N⟩≡R (R' on N's) ⇌ 1/2 [R / R'−N N−R' / Mg / R'−N N−R' / R + MgL₂]
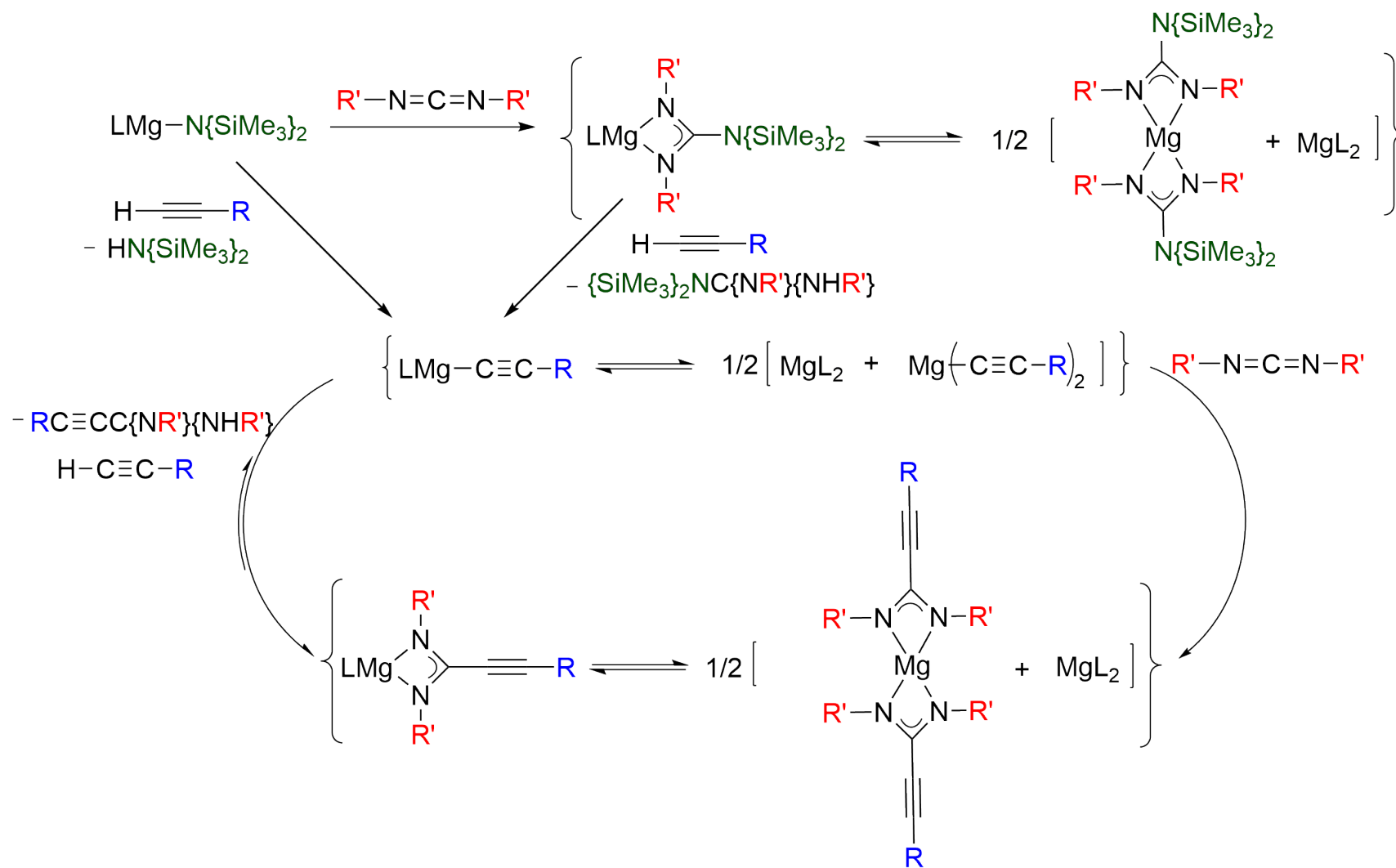
Figure 3.1: Proposed catalytic cycle for magnesium-based catalytic addition of terminal acetylenes to carbodiimides. THF solvent omitted for simplification. L = [mesC{NCy}]²⁻

Chapter 4

Experimental

4.1 General Procedures

All manipulations were performed under a dry and oxygen-free atmosphere of N_2 using Schlenk-line and cannula techniques, or in a conventional nitrogen glovebox. Solvents were dried using a Puresolv. system (Innovative Technologies). NMR spectra were recorded in C_6D_6 at 298K using a Bruker Avance DPX 300 MHz at 300.1 (^{1}H) and 75.4 (^{13}C) MHz. All ^{1}H and ^{13}C chemical shifts are referenced internally to residual solvent resonances. Elemental analyses were performed by S. Boyer at London Metropolitan University. All compounds were purchased from the Sigma-Aldrich chemical company and used as received, unless stated otherwise. Liquids were subjected to 3x freeze-pump-thaw cycles, and stored under nitrogen in the glovebox. $Mg(mesC\{NCy\}_2)(N\{SiMe_3\}_2(THF)$ (**1**)[18] and $Mg(N\{SiMe_3\}_2)_2$[46] were synthesised according to literature procedures.

4.1.1 Crystal Structure Data

X-ray diffraction data (Appendix C) were collected by the X-ray Crystallography Laboratory at the University of Canterbury using an Agilent SuperNova diffractome-

ter fitted with an Atlas detector. Crystals were covered in inert oil and suitable single crystals were selected. Data was collected at 120.01(10)K using Cu Kα radiation at 1.5418 Å. The structures were solved using the program package WinGX and refined using SHELXL97. ORTEP representations were prepared using ORTEP-III.[47]

4.2 General Procedure for Catalytic Study
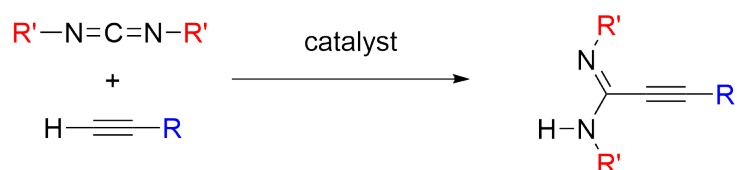
4.2.1 NMR scale

To a J. Young NMR tube charged with a mixture of phenylacetylene (0.022 mL, 0.17 mmol.) and *N,N*-diisopropylcarbodiimide (0.028 mL, 0.17 mmol.) was added a solution of **1** in C$_6$D$_6$ (0.5 mL of a 0.0034 M standard solution, 1.7 μmol.). The NMR tube was heated to 80 °C for 24h with regular monitoring of the progress of the catalysis using ^{1}H NMR spectroscopy. The yield of propargylamidine **5** was determined using peaks corresponding to the THF of **1** as an internal standard. Yield 72 %.

4.2.2 Preparative scale

A solution of **1** (0.05 g, 0.085 mmol.) in toluene (2.5 mL) was added to a stirring solution of phenylacetylene (0.22 mL, 1.7 mmol.) and N,N-diisopropylcarbodiimide (0.28 mL, 1.7 mmol.) in toluene (2.5 mL). The solution was heated to 80 °C and allowed to stir for 24h, followed by removal of the volatiles *in vacuo* to give a yellow oil. Clear, yellow crystals of propargylamidine **5** were obtained by recrystallisation from hexane. Yield 0.28 g, 73 %.

4.3 Catalytic Cycle Studies

4.3.1 Mg(mesC{NCy}$_2$)(C≡CPh)(THF) (A)

NMR scale

Phenylacetylene (0.0045 mL, 0.034 mmol.) was added to a J. Young NMR tube charged with a solution of **1** (20 mg, 0.034 mmol.) in C_6D_6 (0.5 mL). The solution was allowed to sit for 10 mins at room temperature followed by ^{1}H NMR analysis.

^{1}H NMR (C_6D_6, 300MHz) δ 7.84 (d, $J_{HH} = 7.2$ Hz, 2H, o-C_6H_5), 7.10 (t, $J_{HH} = 7.2$ Hz, 2H, m-C_6H_5), 7.01 (d, $J_{HH} = 6.9$ Hz, 1H, p-C_6H_5), 6.84 (s, 2H, C_6H_2), 3.96 (t, $J_{HH} = 6.1$ Hz, 4H, THF-CH_2), 2.81 (br m, 2H, α-C_6H_{11}), 2.46 (br s, 6H, o-Me_2), 2.13 (br s, 3H, p-Me), 1.95-1.00 (m, 24H, C_6H_{11} and THF-CH_2), 0.09 (s, 18H, HN(SiMe_3)$_2$);

^{13}C NMR (C_6D_6, 75 MHz) δ 173.9 (CN$_2$), 136.6, 136.5, 134.5, 134.3, 132.2, 128.40, 127.4, 126.4(C_6H_5 and C_6H_2), 119.9, 117.7 (C≡C), 68.9 (THF-CH$_2$), 55.9, 55.2 (α-C_6H_{11}), 37.9, 26.4 (br), 26.1, 25.6 (α-C_6H_{11}), 21.2 (p-Me), 20.8 (o-Me_2), 2.7 (HN(SiMe_3)$_2$).

Preparative scale

Phenylacetylene (0.065 mL, 0.62 mmol.) was added drop wise to a rapidly stirring solution of **1** (0.36 g, 0.62 mmol.) in toluene (10 mL). The resulting solution was left to stir for 24h at room temperature, followed by removal of volatiles *in vacuo* to give a yellow oil. The addition of hexane (5 mL) and THF (1 mL) to the oil, followed by storage at -30 °C for 24 h yielded a white powder, identified as **6**.(THF)$_4$ by ^{1}H NMR spectroscopy. Yield 0.027 g, 16 %. Additional crops of clear, colourless crystals were obtained by further concentration of the solution identified as **2**. Yield 0.060 g, 26 %.

4.3.2   Mg(mesCNCy$_2$)({Me$_3$Si}$_2$NC{Ni-Pr}$_2$)(THF)$_n$ (B)

NMR scale

N,N-diisopropylcarbodiimide (0.0056 mL, 0.034 mmol.) was added to a J. Young NMR tube charged with a solution of **1** (20 mg, 0.034 mmol.) in C$_6$D$_6$ (0.5 mL). The solution was allowed to sit for 2 h at room temperature followed by ^{1}H NMR analysis, showing formation of a mixture of **2**, **3** and **B**.

^{1}H NMR (C$_6$D$_6$, 300MHz) δ 6.85 (s, C$_6$*H$_2$* {**2**}), 6.82 (s, C$_6$*H$_2$* {**B**}), 3.79 (m, (C*H*(CH$_3$)$_2$ {**3/B**}), 3.71 (m, THF-C*H$_2$* {**2/3/B**}), 2.87 (m, α-C$_6$H$_{11}$ {**2/B**}), 2.47 (s, 6H, *o-Me$_2$* {**2**}), 2.42, 2.41 (s, *o-Me$_2$* {**B**}), 2.13 (s, *p-Me* {**2**}), 2.12 (s, *p-Me* {**B**}), 1.95-1.10 (m, C$_6$*H$_{11}$* and CH(C*H$_3$*)$_2$ {**2/3/B**}), 1.42 (m, THF-C*H$_2$*), 0.36 (s, (Si*Me$_3$*) {**B**}), 0.32 (s, (Si*Me$_3$* {**3**}));

^{13}C NMR (C$_6$D$_6$, 75 MHz) δ 174.0 (*C*N$_2$ {**2**}), 173.8 (*C*N$_2$ {**B**}), 166.4 (overlapping *C*N$_3$ {**3/B**}), 136.5, 136.4, 134.6, 134.3, 134.2, 128.4 (*C$_6$*H$_2$ {**2/B**}), 68.1 (THF-*C*H$_2$ {**2/3/B**}), 55.3 (α-*C$_6$*H$_{11}$ {**B**}), 54.9 (α-*C$_6$*H$_{11}$ {**2**}), 45.3 (overlapping *C*H(CH$_3$)$_2$ {**3/B**}), 37.9, 37.8, 27.5, 27.4, 27.0, 26.5, 26.4, 26.3, 26.2, 25.9, 25.6, 25.3, 24.8 (*C$_6$*H$_{11}$, CH(*C*H$_3$)$_2$ and THF-*C*H$_2$ {**2/3/B**}), 21.2 (*p-Me* **2/B**}), 20.8 (*o-Me$_2$* **B**}), 20.7 (*o-Me$_2$* {**2**}).

4.3.3   Mg(mesC{NCy}$_2$)(PhC≡CC{Ni-Pr}$_2$) (THF) (C)

NMR scale

Phenylacetylene (0.0045 mL, 0.034 mmol.) was added to a J. Young NMR tube charged with a solution of **1** (20 mg, 0.034 mmol.) in C$_6$D$_6$ (0.5 mL). The solution was allowed to sit for 2h at room temperature followed by the addition of *N,N*-diisopropylcarbodiimide (0.0056 mL, 0.034 mmol.).^{1}H NMR analysis showed formation of a mixture of **2**, **4** and **C**.

^{1}H NMR (C$_6$D$_6$, 300MHz) δ 7.48 (m, o-C$_6$$H_5$ {**4)**}), 7.46 (m, o-C$_6$$H_5$ {**C**}), 6.98 (m, m-/p-C$_6$$H_5$ {**C**}), 6.95 (m, m-/p-C$_6$$H_5$ {**4**}), 6.84 (s, C$_6$H$_2$ {**2**}), 6.81 (s, C$_6$H$_2$ {**C**}), 4.37 (overlapping sept, CH(CH$_3$)$_2$ {**4/C**}), 3.77 (m, THF-CH_2 {**2/4/C**}), 2.79 (m, α-C$_6$$H_{11}$ {**2/C**}), 2.45 (s, o-Me {**2**}), 2.44 (s, o-Me {**C**}), 2.13 (s, p-Me {**2/C**}), 1.84-1.12 (m, C$_6$H$_{11}$ and THF-CH_2 {**2/4/C**}), 1.44 (d, CH(CH_3)$_2$ {**4**}), 1.41 (d, CH(CH$_3$)$_2$ {**C**}), 0.09 (s, 18H, (HN{SiMe_3)}).

^{13}C NMR (C$_6$D$_6$, 75MHz) δ 174.0 (CN$_2$ {**2**}), 173.8 (CN$_2$ {**C**}), 157.9 (CN2 {**4**}), 157.7 (CN2 {**C**}), 136.5, 136.4, 134.7, 134.3, 132.3, 132.2, 128.9, 128.7, 123.1 (C_6H$_5$ and C_6H$_2$ **2/4/C**}), 95.9, 95.8, 81.0, 80.8 ($C{\equiv}C$ {**4/C**}), 68.0 (THF-CH$_2$ {**2/4/C**}), 55.7, 55.1 (α-C_6H$_{11}$ {**2/C**}), 48.9, 48.8 (CH(CH$_3$)$_2$ {**4/C**}), 37.9, 37.8, 27.5, 27.3, 26.9, 26.7, 26.5, 26.4, 26.1, 25.6, 24.8 (C_6H$_{11}$, CH(CH$_3$)$_2$ and THF-CH$_2$ {**2/4/C**}), 21.2 (overlapping p-Me {**2/C**}), 20.8, 20.7 (o-Me {**2/C**}), 2.68 (HN(SiMe_3)$_2$).

Preparative scale

Phenylacetylene (0.065 mL, 0.62 mmol.) was added drop wise to a rapidly stirring solution of **1** (0.36 g, 0.62 mmol.) in toluene (10 mL). The solution was allowed to stir for 4h at room temperature, followed by the addition of N,N-diisopropylcarbodiimide (0.10 mL, 0.62 mmol.). The resulting solution was stirred for 24h followed by removal of volatiles *in vacuo* to give a crude yellow solid. The addition of hexane (5 mL) to the solid, followed by storage at -30 °C for 24 h yielded clear colourless crystals, identified as **2**. Yield 0.11 g, 47 %. Additional crops of clear, yellow crystals were obtained by further concentration of the solution and storage at -30 °C, identified as **4**.THF by ^{1}H NMR spectroscopy. Yield 0.070 g, 36 %.

4.3.4 Protonolysis of 2/5/C by phenyl acetylene

Phenylacetylene was added dropwise to a pre-formed mixture of **2**, **5** and **C** (*vide supra*) in C_6D_6. ^1H NMR analysis showed no change after 2h at 80 °C. Addition of *N,N*-diisopropylcarbodiimide to the reaction mixture resulted in loss of phenylacetylene and formation of **5** (An electronic copy of ^1H NMR spectrum is available on the attached CD).

4.3.5 General procedure for equilibria studies

A solution of **2** (0.020 g, 0.027 mmol.) in C_6D_6 (0.5 mL) was added to a vial containing **6**.$(THF)_4$ (0.014 g, 0.027 mmol.). The resulting mixture was transferred to a J. Young NMR tube. Formation of products was monitored by ^1H NMR spectroscopy at room temperature.

Results:

2 + **6**.$(THF)_4$ resulted in formation of **A**, **2** and **6**.$(THF)_n$

2 + **3** resulted in formation of a mixture of **B**, **2** and **3**

2 + **4**.(THf) resulted in formation of a mixture of **C**, **2** and **4**.(THF)

4.3.6 Reaction of 1 with a 1:1 mixture of phenylacetylene and *N,N'*-diisopropylcarbodiimide

A solution of **1** (0.020 g, 0.034 mmol.) in C_6D_6 was added to a mixture of phenylacetylene (4.4 μL, 0.034 mmol.) and *N,N'*-diisopropylcarbodiimide (5.6 μL, 0.034 mmol.). The mixture was analysed by ^1H NMR spectroscopy, showing formation of a mixture of **A**, **2**, **6**.$(THF)_n$, $HN\{SiMe_3\}_2$ and $\{SiMe_3\}_2NC\{Ni\text{-}Pr\}\{NHi\text{-}Pr\}$.

4.4 Compounds Identified in the Catalytic Cycle

4.4.1 Mg(mesC{NCy$_2$}$_2$)$_2$(THF)(2)

Compound **2** was isolated from the attempted preparation of **A** (*vide infra*).

Anal. Calcd. for C$_{48}$H$_{74}$MgN$_4$O (*747.43*): C, 77.13; H, 9.98; N, 7.50 %. Found: C, 76.86; H, 10.12; N, 7.56 %.

^{1}H NMR (C$_6$D$_6$, 300MHz) δ 6.85 (s, 4H, C$_6$H$_2$), 3.74 (m, 4H, THF-CH_2), 2.87 (m, 4H, α-C$_6$H$_{11}$), 2.46 (s, 12H, o-Me_2), 2.12 (s, 6H, p-Me), 1.90-1.10 (m, 40H, C$_6$H$_{11}$), 1.43 (m, 4H, THF-CH_2);

^{13}C NMR (C$_6$D$_6$, 75 MHz) δ 174.3 (CN$_2$), 136.7, 134.2, 134.1, 128.8 (C_6H$_2$), 67.9 (THF-CH$_2$), 54.8 (α-C_6H$_{11}$), 37.8, 26.5 (C_6H$_{11}$), 25.9 (THF-CH$_2$), 25.8 (C_6H$_{11}$), 21.2 (p-Me), 20.7 (o-Me_2).

4.4.2 Mg({Me$_3$Si}$_2$NC{Ni-Pr}$_2$)$_2$(THF) (3)

A solution of *N,N*-diisopropylcarbodiimide (0.12 mL, 0.73 mmol.) in THF (5 mL) was added dropwise to a stirring solution of Mg(N{SiMe$_3$}$_2$)$_2$ (0.25 g, 0.73 mmol.) in THF (5 mL). The resulting solution was stirred at room temperature for 24h followed by concentration of the solution *in vacuo*. Clear, colourless crystals suitable for X-ray diffraction were obtained upon storage of the solution at -30 °C for 24h. Yield 0.31 g, 78 %

Anal. Calcd. for C$_{30}$H$_{72}$MgN$_6$OSi$_4$ (*699.58*): C, 53.81; H, 10.84; N, 12.55 %. Found: C, 53.60; H, 10.78; N, 12.54 %.

^{1}H NMR (C$_6$D$_6$, 300MHz) δ 3.69 (sept, J_{HH} = 6.2 Hz, 4H, CH(CH$_3$)$_2$), 3.59 (m, 4H, THF-CH_2), 1.41 (m, 4H, THF-CH_2), 1.17 (d, J_{HH} = 6.2 Hz, 24H, CH(CH_3)$_2$), 0.32 (s, 36H, N{SiMe_3}$_2$);

^{13}C NMR (C$_6$D$_6$, 75 MHz) δ 167.2 (CN$_2$), 67.9 (THF-CH$_2$), 44.7 (CH(CH$_3$)$_2$), 27.4 (CH(CH$_3$)$_2$), 25.7 (THF-CH$_2$), 2.5 (SiMe_3).

4.4.3   Mg(PhC≡CC{Ni-Pr}$_2$)$_2$(THF)$_2$ (4.(THF))

Method 1: Reaction of MgBu$_2$ with 2 equiv. of **5**

A solution of MgBu$_2$ in heptane (0.88 mL of a 1.0 M solution, 0.88 mmol.) was added drop wise to a stirring solution of PhC≡CC{Ni-Pr}{NHi-Pr} (0.40 g, 1.8 mmol.) in THF (5 mL). The solution was allowed to stir for 24 h followed by removal of the volatiles. Clear yellow crystals suitable for X-ray analysis were obtained by recrystallization from hexane at -30 °C. Yield 0.36 g, 66 %.

Method 2: Reaction of **6**.(THF)$_4$ with 2 equiv. *N,N'*-diisopropylcarbodiimide

A solution of **6**.(THF)$_4$ (0.10 g, 0.19 mmol.) in THF (10 mL) was added drop wise to a stirring solution of *N,N'*-diisopropylcarbodiimide (0.05 mL, 0.38 mmol.) in THF (5 mL) at -30 °C. The solution was allowed to stir for 24 h followed by removal of the volatiles. Clear yellow crystals were obtained by recrystallization from hexane at -30 °C. Yield 0.094 g, 71 %.

Anal. Calcd. for C$_{38}$H$_{54}$MgN$_4$O$_2$ (*623.18*): C, 73.24; H, 8.73; N, 8.99 %. Found: C, 73.15; H, 8.61; N, 9.05 %.

^{1}H NMR (C$_6$D$_6$, 300MHz) δ 7.48 (m, 4H, *o*-C$_6$$H$$_5$), 6.95 (m, 6H, *m-/p*-C$_6$$H$$_5$), 4.38 (sept, J_{HH} = 6.4 Hz, 4H, CH(CH$_3$)$_2$), 3.62 (m, 4H, THF-CH_2), 1.44 (d, J_{HH} = 6.4 Hz, 24H, CH(CH_3)$_2$), 1.34 (m, 4H, THF-CH_2);

^{13}C NMR (C$_6$D$_6$, 75 MHz) δ 157.9 (CN$_2$), 132.3, 128.9, 128.7, 123.1 (C_6H$_5$), 95.9, 80.8 (C≡C), 68.0 (THF-CH$_2$), 48.9 (CH(CH$_3$)$_2$), 26.7 (CH(CH$_3$)$_2$), 25.6 (THF-CH$_2$).

4.4.4 Mg(C≡CPh)$_2$(THF)$_4$ (6.(THF)$_4$)

A solution of MgBu$_2$ in heptane (1.2 mL of a 1.0M solution, 1.2 mmol.) was added dropwise to a stirring solution of phenylacetylene (0.31 mL, 2.4 mmol.) in THF (5 mL). The resultant solution was stirred for 24h followed by removal of the solvent *in vacuo* to give a white powder. Clear colourless crystals were obtained by recrystallisation from a hexane/THF solution. Yield 0.54 g, 84 %.

^{1}H NMR (C$_6$D$_6$, 300MHz) δ 7.89 (d, J_{HH} = 7.2 Hz, 2H, o-C$_6$H$_5$), 7.10 (t, J_{HH} = 7.2 Hz, 2H, p-C$_6$H$_5$), 7.00 (d, J_{HH} = 7.2 Hz, 4H, m-C$_6$H$_5$), 3.61 (t, J_{HH} = 6.6 Hz, 16H, THF-CH_2), 1.40 (t, J_{HH} = 6.6 Hz, 16H, THF-CH_2);

^{13}C NMR (C$_6$D$_6$, 75MHz) δ * 132.2, 129.3, 128.5, 127.0 (C_6H$_5$), 68.0 (THF-CH$_2$), 25.8 (THF-CH$_2$).

*Resonances for the C≡C carbons not observed.

4.4.5 Mg(PhC≡CC{Ni-Pr}$_2$)Br(OEt$_2$) (7)

A solution of MeMgBr in Et$_2$O (0.48 mL of a 3.0 M solution, 1.45 mmol.) was added drop wise to a stirring solution of PhC≡CC{Ni-Pr}{NHi-Pr} (0.33 g, 1.45 mmol.) in Et$_2$O (5 mL). The resultant solution was left to stir for 24h, followed by concentration and storage at -30 °C. Yellow crystals of **7** were obtained after 24h at -30 °C. Yield 0.47 g, 81 %.

Anal. Calcd. for C$_{19}$H$_{29}$MgN$_2$OBr (*405.66*): C, 56.26; H, 7.21; N, 6.91 %. Found: C, 56.05; H, 7.27; N, 6.75 %.

^{1}H NMR (C$_6$D$_6$, 300MHz) δ 7.38 (br, 2H, o-C$_6$H$_5$), 6.95 (s, 2H, m-C$_6$H$_5$), 6.92 (s, 1H, p-C$_6$H$_5$), 4.34 (br, 2H, CH(CH$_3$)$_2$), 3.53 (t, J_{HH} = 6.9 Hz, 4H, CH_2CH$_3$), 1.52 (br, 12H, CH(CH_3)$_2$), 1.10 (t, J_{HH} = 6.9 Hz, 6H, CH$_2$CH_3);

^{13}C NMR (C$_6$D$_6$, 75 MHz) δ 158.9 (CN$_2$), 132.3, 129.3, 128.7, 122.4 (C_6H$_5$),

97.13, 80.05 ($C{\equiv}C$), 65.6 (CH$_2$CH$_3$), 49.1 (CH(CH$_3$)$_2$), 26.1 (CH(CH$_3$)$_2$), 14.7 (CH$_2$$CH_3$).

Part II

Bismuth Compounds Supported by Di(amido) Chelating Ligands

Chapter 1

Introduction

1.1 Bismuth

Bismuth is the heaviest stable element in the periodic table, with an electron configuration of $[Xe]4f^{14}5d^{10}6s^{2}6p^{3}$. The most common oxidation state for bismuth compounds is +3, although a large number of organobismuth compounds occupying the +5 oxidation state are also known.[48] Bismuth(III) maintains a large ionic radius (Shannon ionic radii Bi^{3+}: 6-coordinate = 1.03 Å; 8-coordinate = 1.17 Å)[49] and also contains a stereochemically active lone pair which has a significant effect on the geometry of the bismuth.[48]

In contrast to the majority of heavy main group elements (Sn, Pb, Te, Sb and Tl), bismuth is relatively non-toxic. Bismuth compounds are attracting increasing attention due to their application in medicine (e.g bismuth subsalicylate, the active ingredient in Pepto-Bismol©).[50] Other uses of bismuth compounds include superconducting materials,[51] and catalysts for organic transformations.[52] Bismuth has also been applied as a non-toxic alternative to lead in radioprotective shielding material for X-ray computed tomography (CT) scanning.[53]

While the majority of studies performed on bismuth compounds have focused on

trivalent species, the general coordination chemistry of bismuth(III) compounds remains relatively unexplored compared to the chemistry of the other main group elements.

1.1.1 Low-Coordinate Bismuth(III) Cations

Simple bismuth(III) compounds (BiX$_3$, X = Cl, NO$_3$, OTf and OAc) are active Lewis acid catalysts for a range of organic transformations such as the Friedel-Crafts acylation, Diels-Alder reactions and Aldol condensations.[52] Cationic bismuth compounds are expected to have increased electrophilicity associated with a positively charged metal centre that may further enhance the Lewis acidity.

Low coordinate bismuth compounds (CN<4) have received very little attention, with the majority of research focussing on 4-, 6- and 8-coordinate cationic bismuth. Veith and co-workers reported the synthesis of a number of formally two-coordinate bismuth cations supported by the divalent bis(amido)silyl scaffold [Me$_2$Si{Nt-Bu}$_2$]$^{2-}$.[54] These compounds were made via abstraction of the chloride from the neutral Bi(III) pre-cursor Bi(Me$_2$Si{Nt-Bu}$_2$)Cl by ECl$_3$ (E = Al, Ga, In) affording the corresponding tetrachlorometallate salt, [Bi(Me$_2$Si{Nt-Bu}$_2$)][ECl$_4$] (eq. 1.1).
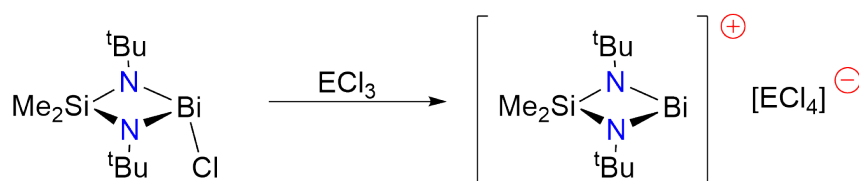
eq. 1.1: Synthesis of [Bi(Me$_2$Si{Nt-Bu}$_2$][ECl$_4$], (E = Al, Ga, In).

The solid-state structure of the tetrachloroaluminate salt [Bi(Me$_2$Si{Nt-Bu}$_2$)][AlCl$_4$] confirms abstraction of the chloride and formation of the cationic species. The structure is, however, stabilised by long range Bi$\cdots$Cl interactions, where each [Bi(Me$_2$Si{Nt-Bu}$_2$)]$^+$ cation interacts with two [AlCl$_4$]$^-$ anions to form a polymeric chain (Figure 1.1).
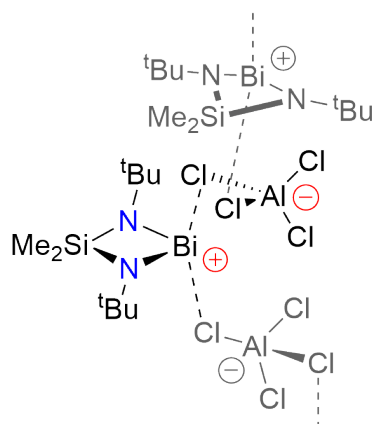
Figure 1.1: Polymeric solid-state structure of [Bi(Me$_2$Si{Nt-Bu}$_2$)][AlCl$_4$].

Chloride-abstraction by ECl$_3$ has been utilised in the synthesis of a range of bismuth cations, with the majority of these studies using AlCl$_3$ as the reagent.[54–57] Only a few examples of chloride-abstraction using GaCl$_3$[54,58] and InCl$_3$[54] have been reported for the synthesis of bismuth cations. Bi$\cdots$Cl stabilising interactions are common in these tetrachlorometallate bismuth salts.

Cationic bismuth compounds that do not have stabilising interactions with either the counter-ion or solvent molecules are rare. Evans and co-workers recently reported that the bis(aryl) bismuth compound Bi(2,6-{Me$_2$NCH$_2$}$_2$C$_6$H$_3$)$_2$Cl reacts with NaBPh$_4$ to form the corresponding tetraphenylborate salt, [Bi(2,6-{Me$_2$NCH$_2$}$_2$C$_6$H$_3$)$_2$][BPh$_4$] (Scheme 1.1). Formation of the bismuth cation was also achieved by the addition of [HNEt$_3$][BPh$_4$] to the allyl compound Bi(2,6-{Me$_2$NCH$_2$}$_2$C$_6$H$_3$)$_2$(CH$_2$CH=CH$_2$).[59] The tetraphenylborate acts as an outer-sphere anion and has no close interactions with the bismuth cation.
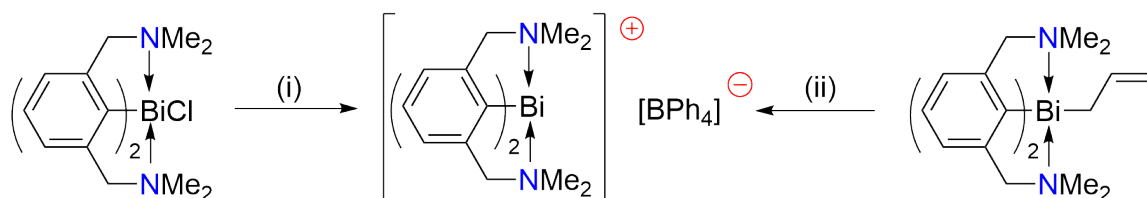
Scheme 1.1: Formation of [Bi(2,6-{Me$_2$NCH$_2$}$_2$C$_6$H$_3$)$_2$][BPh$_4$]: (i) NaBPh$_4$, -NaCl; (ii) [HNEt$_3$][BPh$_4$], -NEt$_3$, -CH$_3$HC=CH$_2$.

1.1.2 Compounds containing Bi-X bonds (X = NR$_2$, OR, PR$_2$).

Bismuth Amides, Alkoxides and Aryloxides

Compounds containing one or more Bi-X bonds (X = NR$_2$, OR) are attracting attention for their interesting reactivity and potential applications. For example, homoleptic bismuth(III) amides, Bi(NR$_2$)$_3$ (R = alkyl, aryl, silyl), have been used as pre-cursors for metal-organic chemical vapor deposition (MOCVD) of bismuth-containing thin films due to their low M-N bond strength.[60] These compounds are extremely sensitive to the reaction conditions (temperature, solvent, light), and readily decompose at room temperature.

Roesky and co-workers recently reported the synthesis of the 1,8-napthalene supported amide Bi(1,8-C$_{10}$H$_6$\{NSiMe$_3$\}$_2$)(NMe$_2$) from the reaction of the free ligand 1,8-C$_{10}$H$_6$\{NHSiMe\}$_2$ with the homoleptic tris(amide) Bi(NMe$_2$)$_3$. The Bi-NMe$_2$ bond is stable to relatively harsh temperature and light conditions, but was shown to react with a range of unsaturated substrates, including carbodiimides and isocyanates. The principal mode of reactivity was via insertion into the Bi-NMe$_2$ bond (Scheme 1.2).[61]
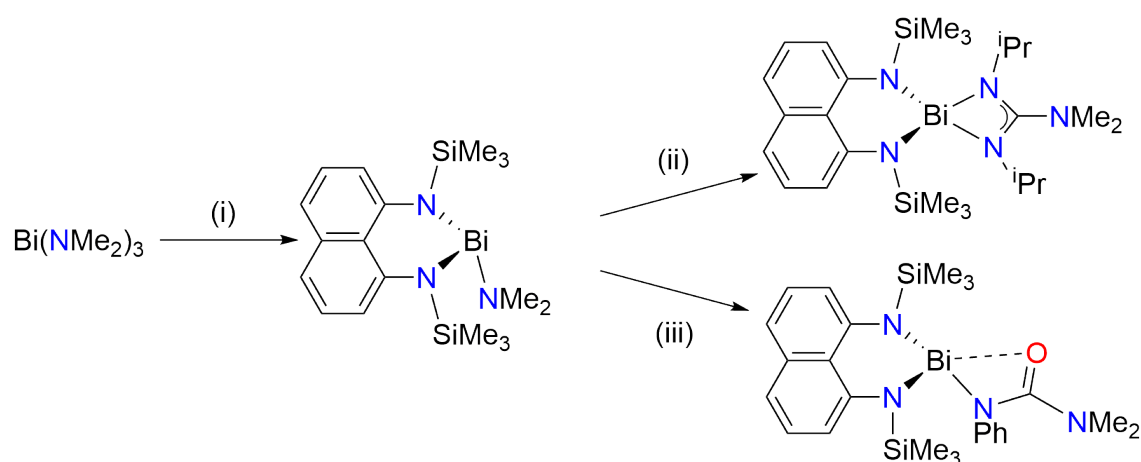
Scheme 1.2: Synthesis of Bi(1,8-C$_{10}$H$_6$\{NSiMe$_3$\}$_2$)(NMe$_2$) and reactivity with carbodiimide and isocyanate substrates. (i) 1,8-C$_{10}$H$_6$\{NHSiMe\}$_2$, - 2NHMe$_2$; (ii) *i*-Pr-N=C=N-*i*-Pr; (iii) PhN=C=O.

The related compound $Bi(Me_2Si\{NAr\}_2)(N\{SiMe_3\}_2)$ (Ar = 2,6-i-Pr$_2$C$_6$H$_3$) (**16**) has been synthesised in the Coles group from the reaction of $Bi(Me_2Si\{NAr\}_2)Cl$ (**9**) with $LiN\{SiMe_3\}_2$ (eq. 1.2).[62] This compound shows increased stability towards high temperatures compared to the corresponding homoleptic tris(amide) $Bi(N\{SiMe_3\}_2)_3$, which decomposes readily at room temperature.
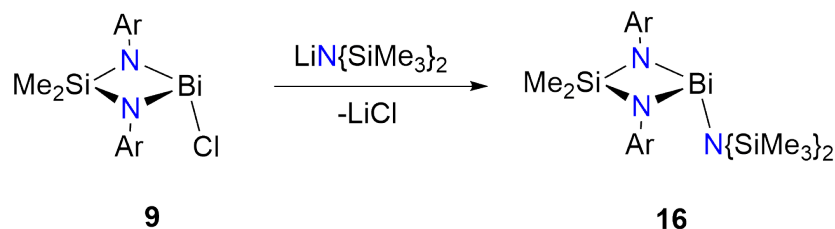
eq. 1.2: Reaction of **9** with $LiN\{SiMe_3\}_2$.

Bismuth alkoxides and aryloxides are also of interest. Bismuth tris(alkoxides), $Bi(OR)_3$, have been studied as model systems for understanding the Standard Oil of Ohio Company (SOHIO) process for the oxidation (Figure 1.2, A) and ammoxidation (B) of propene, which currently uses a bismuth molybdate catalyst.[63] Bismuth(III) alkoxides have also shown significant activity for the ring-opening polymerisation of cyclic esters (*vide infra*).
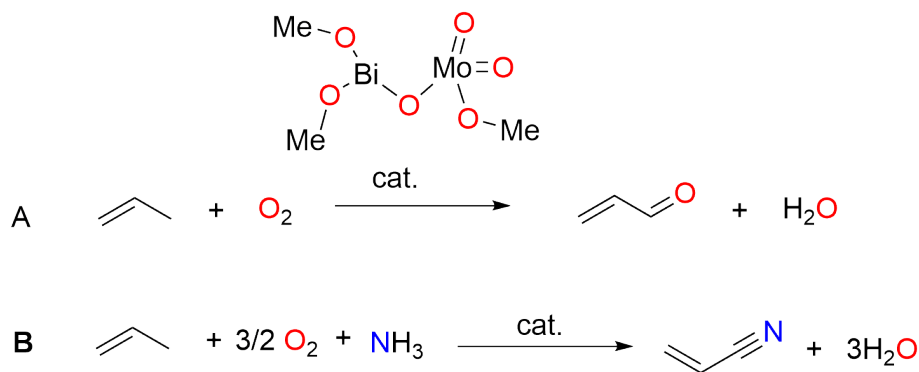
Figure 1.2: SOHIO process: (**A**) Oxidation of propene; (**B**) Ammoxidation of propene.

Bismuth Phosphides

Bismuth phosphide, BiP, is of interest in materials science as an isoelectronic analogue of PbS, a common semiconducting material.[64] Despite this, few examples of

structurally characterised bismuth phosphide compounds have been reported in the literature (Figure 1.3), and the majority contain silyl-substituted phosphides. The only structurally characterised terminal bismuth phosphide is $[Bi(P\{SiPh_2t\text{-}Bu\}]_2$, where bismuth is in the +1 oxidation state.[65] In contrast to Bi-N and Bi-O bonds, no investigation into the reactivity of Bi-P bonds has been reported. Insertion of unsaturated substrates into M-P bonds has been observed for a number of main group,[66,67] transition metal[68] and rare earth metal[69–71] compounds.
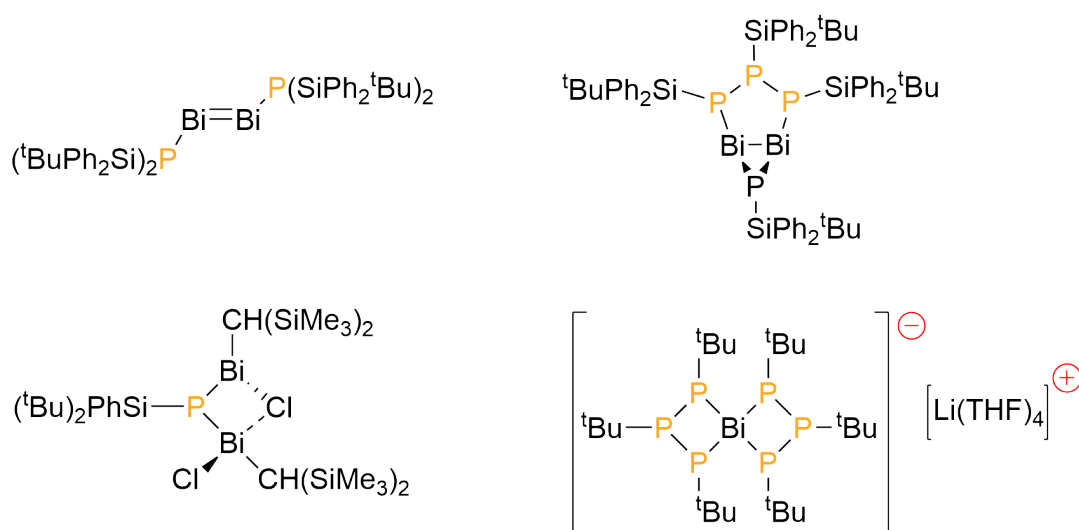
Figure 1.3: Examples of different structurally characterised bismuth phosphides.[65,72,73]

1.1.3 Ring-Opening Polymersiation of Lactide

Polyesters are attracting increasing attention as a environmentally friendly biodegradable plastics.[74] The most common method for the synthesis of these polymers is by the metal catalysed ring-opening polymerisation (ROP) of cyclic ester monomers. Tin(II) octanoate ($Sn(Oct)_2$, Oct = 2-ethylhexanoate) has been employed as an initiator for the ROP of lactide, to form poly-lactic acid (PLA) (eq. 1.3). The high activity and air/moisture stability of $Sn(Oct)_2$ has led to it being considered the benchmark catalyst for this polymerisation.

Significant work has gone into the development of alternative catalyts for this re-

eq. 1.3: Sn(Oct)$_2$ initiated ring-opening polymerisation (ROP) of lactide.
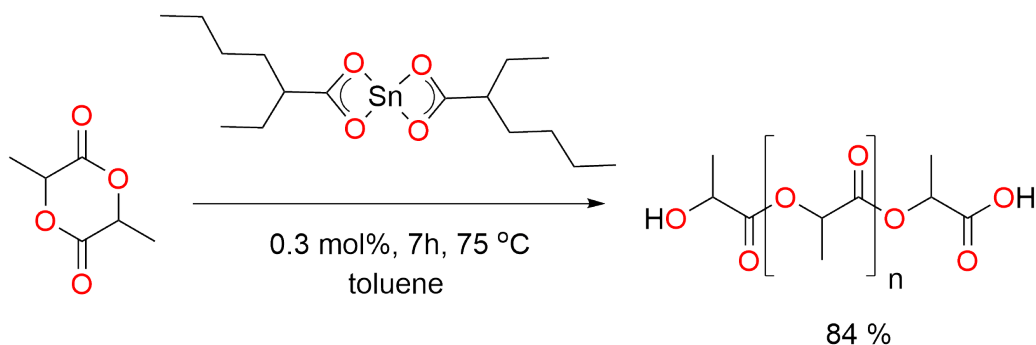
action, with examples of catalytically active main group compounds based on aluminium,[75] germanium,[76] calcium,[77] magnesium,[71,78] and zinc.[71,78] Over the last few years, the use of bismuth(III) compounds as initiators has gained interest. Krichel-dorf and co-workers reported that bismuth alkanoates are active as initiators for the ROP of cyclic esters, albeit with a much lower activity than Sn(Oct)$_2$.[79] Since this work, catalytic ROP of cyclic esters has been achieved using a range of simple Bi(III) salts as initiators (e.g. halides,[80] carboxylates[81] and triflate[79]). Chisholm and co-workers have recently reported that bismuth subsalicylate (BSS), the active ingredient of commercially available Pepto Bismol$^©$, is highly active in the ring-opening polymerisation of lactide (eq. 1.4) and ε-caprolactone, showing comparable activity to the industrial standard Sn(Oct)$_2$.[82] In contrast to the Sn(Oct)$_2$ systems, BSS exists as a poorly defined aggregate and was insoluble in the reaction solvent (CHCl$_3$).
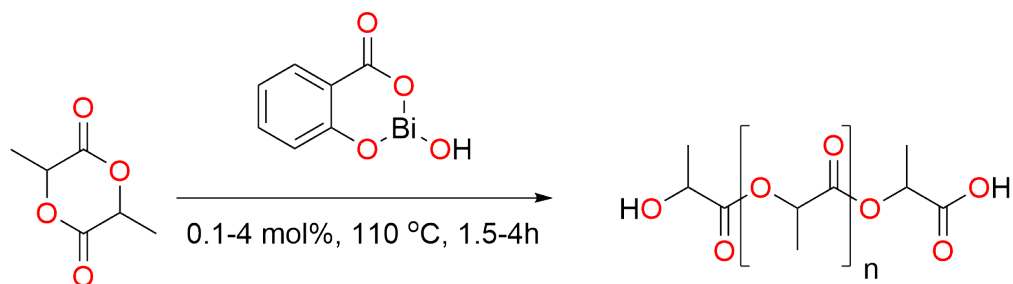
eq. 1.4: Bismuth subsalicylate (BSS) initiated ring-opening polymerisation of lactide.

A subsequent investigation reported that cy-salen bismuth alkoxides are active single-site initiators for the ROP of lactide (1 mol%, 1-1.5 h, room temperature, 74-

92 % conversion), giving predominantly heterotactic PLA and showing much greater activity than Sn(Oct)$_2$.[83] The alkoxide species were reactive towards water, resulting in deactivation of the catalysts. In a related study, Vuorinen et al. reported that homoleptic bismuth alkoxide complexes, Bi(OR)$_3$ (R = t-Bu, CMe$_2$$i$-Pr), are active initiators for living ROP of rac-lactide in toluene (0.3 mol%, 2.5 h, 75 °C, 95-98 % conversion), whereas the less sterically encumbered alkoxide derivative Bi(Oi-Pr)$_3$ showed considerably lower activity (0.3 mol%, 4 h, 75 °C, 16 % conversion), presumed to be due to oligomerization of the initiating species.[84]

1.2 Di(amido)silyl Ligands

N,N'-chelating ligands provide an attractive scaffold for the formation of low valent metal compounds. The divalent N,N'-acilliary ligand, [Me$_2$Si{NR}$_2$]$^{2-}$ has been utilised in the synthesis of a wide range of metal complexes. These ligands can be thought of as non-resonance stabilised isostructural analogues of amidinate ligands (see Part 1, Chapter 1), which occupy two of the available valencies of the metal to which they are bound.

A wide range of di(amido)silane Me$_2$Si{NHR}$_2$ derivatives have been synthesised through either (a) the in $situ$ reaction of two equivalents of the corresponding lithium amide salt, LiNHR, with SiMe$_2$Cl$_2$ or (b) the reaction of four equivalents of the amine with SiMe$_2$Cl$_2$, where the excess amine acts as a base and removes HCl to form the corresponding ammonium salt (Scheme 1.3).[85,86]
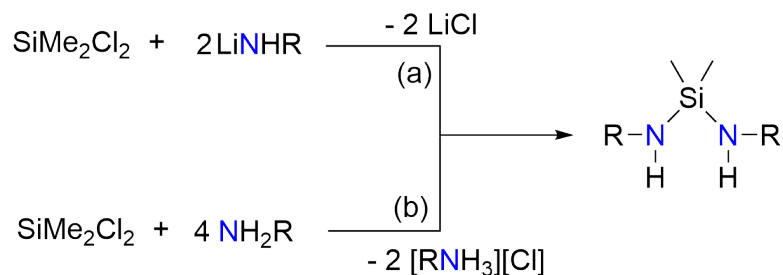
Scheme 1.3: Synthetic pathways to Me$_2$Si{NHR}$_2$.

Di(amido)silyl ligands containing sterically bulky nitrogen substituents (R) are commonly employed as kinetically stabilising ligands for main group,[87–90] transition metal[91] and rare earth metal[92,93] complexes. A number of bonding modes have been observed for both monoanionic and dianionic analogues (Figure 1.4) including monodentate (**A**), bidentate chelate (**B** and **C**) and bridging (**D**) bonding modes.
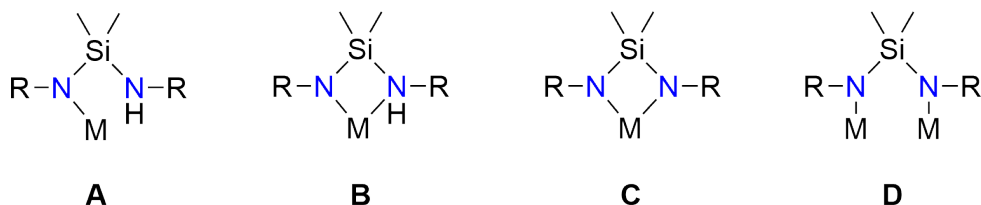
Figure 1.4: Bonding modes of di(amido)silane ligand.

1.3 Research Outlook

The di(amido)silyl bismuth compound $Bi(Me_2Si\{NAr\}_2)Cl$ (Ar = 2,6-i-$Pr_2C_6H_3$) (**9**) has previously been reacted with $AlCl_3$ and LiR (R = N$\{SiMe_3\}_2$, Cp, Cp*).[62] The aim of this work was to expand this area to give additional compounds containing Bi-X bonds (X = NR_2, OR, PR_2). In addition, we aimed to investigate the formation of low-coordinate cationic bismuth compounds via reaction of **9** with the metal trichlorides ECl_3 (E = Al, Ga, In) and examine the role of Bi$\cdots$Cl intermolecular interactions through the synthesis of cations containing outer-sphere anions.

Chapter 2

Results and Discussion

2.1   Outline

The work presented in this chapter leads on from research reported by Day et al.[62] Me$_2$Si{NHAr}$_2$ (**8**),[94] Bi(Me$_2$Si{NAr}$_2$)Cl (**9**),[95] Bi(Me$_2$Si{NAr}$_2$)(N{SiMe$_3$}$_2$) (**16**)[62] (Ar = 2,6-i-Pr$_2$C$_6$H$_3$) and O(Me$_2$SiNHAr")$_2$ (Ar" = 2,6-i-Pr$_2$C$_6$H$_3$) (**19a**)[96] were synthesised according to literature procedures.

Section 2.2 describes the synthesis of the bismuth dichloride complex Bi(Me$_2$Si{NHAr}{NAr})Cl$_2$ (**11**) from the reaction of the mono-metallated ligand, Me$_2$Si{N(M)Ar}{NHAr} (M = Na, K), with BiCl$_3$. The attempted synthesis of **9** by reaction of **11** with a Lewis base is described.

Section 2.3 details the formation of low-coordinate bismuth cations supported by the di(amido)silyl scaffold by reaction of **9** with ECl$_3$ (E = Al, Ga, In) or NaBR$_4$ (R = Ph, Et).

Section 2.4 reports the synthesis and reactivity of Bi(Me$_2$Si{NAr}$_2$)X (X = N{SiMe$_3$}$_2$ (**16**), O-2,6-t-Bu$_2$C$_6$H$_3$ (**17**), PCy$_2$ (**18**)). The ring-opening polymerisation of lactide and ε-caprolactone was achieved using amide and aryloxide derivatives. The reactivity of the amide and phosphide derivatives with heterocumulenes

was also briefly investigated.

Section 2.5 explores the synthesis of bismuth(III) compounds containing the related ligand O{Me$_2$SiNHAr"}$_2$ (Ar" = 2,6-i-Pr$_2$C$_6$H$_3$, 2,6-Me$_2$C$_6$H$_3$).

2.2   Synthesis of Bi(Me$_2$Si{NHAr}{NAr})Cl$_2$

2.2.1   Synthesis of Me$_2$Si{N(M)Ar}{NHAr} (M = Na (10a), K (10b); Ar = 2,6-i-Pr$_2$C$_6$H$_3$)

Reaction of Me$_2$Si{NHAr}$_2$ (Ar = 2,6-i-Pr$_2$C$_6$H$_3$) (**8**) with one equivalent of MH (M = Na, K) in toluene resulted in formation of the corresponding mono-metallated ligand salt, Me$_2$Si{N(M)Ar}{NHAr} (M = Na (**10a**) and K (**10b**)). **10b** was soluble in toluene allowing the isolation by crystallisation from the reaction mixture. **10a** was insoluble in the reaction solvent and was recrystallised from a solution of THF as **10a**.(THF)$_n$. Attempts to react these species with further equivalents of MH to form the di-sodium and di-potassium salts, Me$_2$Si{N(M)Ar}$_2$, proved unsuccessful in both toluene and THF, even when the reaction mixture was heated to 80 °C for 24 hours (Scheme 2.1). This contrasts with the reaction of **8** with two equivalents of n-BuLi, where formation of Me$_2$Si{NArLi}$_2$ occurs readily at room temperature, and may reflect the differences in size of the group 1 metals.[94]
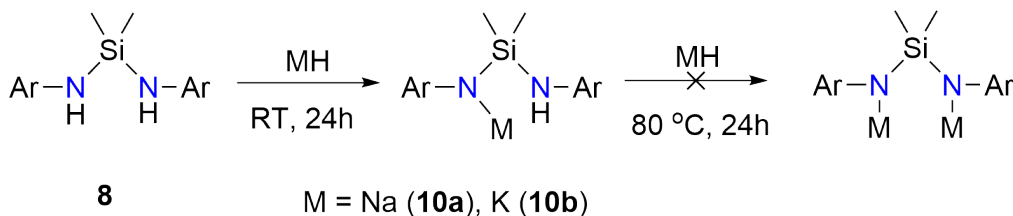
Scheme 2.1: Reaction of **8** with MH to form Me$_2$Si{N(M)Ar}{NHAr} (M = Na (**10a**), K (**10b**)).

The ^{1}H NMR spectra of both **10a**.(THF)$_n$ and **10b** display two sets of resonances corresponding to the 2,6-i-Pr$_2$C$_6$H$_3$ substituent, consistent with formation of the

mono-metallated species. This is most clearly illustrated by the resonances corresponding to the *iso*-propyl methine protons. The ^{1}H NMR spectrum of **10a**.(THF)$_n$ displays two distinct septets for the *iso*-propyl methine protons (δ_H 4.23 and 3.87 ppm), while the ^{1}H NMR spectrum of **10b** displays a multiplet (δ_H 3.81 ppm) corresponding to four protons, consistent with overlapping signals. A single resonance for the SiMe$_2$ protons is observed for both **10a**.(THF)$_n$ and **10b** (δ_H 0.47 and 0.56 ppm, respectively). The N-H resonances for **10a**.(THF)$_n$ and **10b** are observed as singlets at δ_H 3.18 and 3.08 ppm, respectively, downfield from the N-H resonance of **8** (δ_H 2.63 ppm). Integration of the ^{1}H NMR spectrum shows that **10a**.(THF)$_n$ has at least 4 THF molecules contained in the isolated crystals.

The ^{13}C NMR spectra of both **10a**.(THF)$_3$ and **10b** display two distinct environments for the N-aryl substituents, also consistent with formation of the mono-metallic species. A single high field resonance for the SiMe$_2$ carbons is observed in both cases, appearing at δ_C 4.6 and 5.9 ppm for **10a**.(THF)$_3$ and **10b**, respectively. A single ^{29}Si NMR resonance at δ_{Si} -32.1 ppm is observed for **10b**, appearing significantly upfield from both the free ligand and the di-lithiated ligand salt Me$_2$Si{ArNLi}$_2$ (δ_{Si} -8.3 and -15.9 ppm, respectively).[94]

Single crystal X-ray crystallography identified **10a**.(THF)$_3$ as the tris-THF adduct, Me$_2$Si{N[Na(THF)$_3$]Ar}{NHAr} (**10a**.(THF)$_3$), crystallising in the $P\bar{1}$ space group (Figure 2.1). The unit cell contains one molecule of **10a**.(THF)$_3$, and one molecule of non-coordinated THF. One of the coordinated THF molecules is disordered over two positions, with half occupancy at each site.

The tetrahedral sodium centre is coordinated to three THF molecules, with the mono-dentate di(amido) ligand occupying the final position (bonding mode A, Figure 1.4). The Na-N(1) bond length (2.3144(11) Å) is consistent with a σ-bonding interaction. The N(1)-Si bond length (1.6673(10) Å) is significantly shorter than the N(2)-Si bond length (1.7716(11) Å), consistent with a stronger interaction between silicon and the formally anionic amido nitrogen.
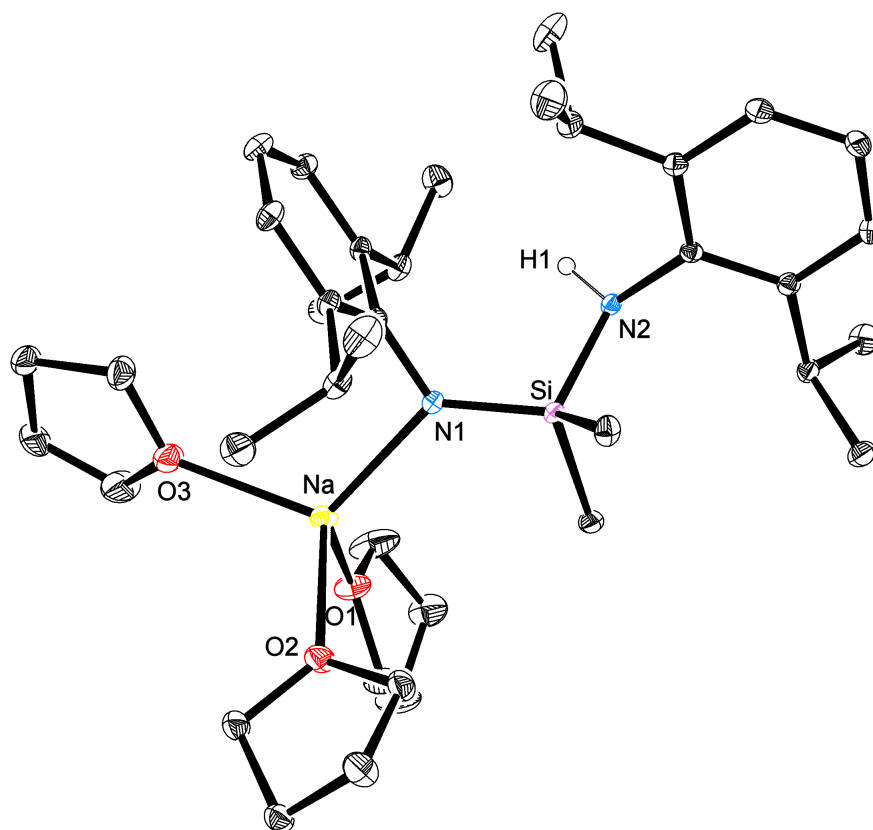
Figure 2.1: ORTEP representation of **10a**.(THF)$_3$+THF. 30% Thermal ellipsoid. Selected hydrogens and THF solvate omitted. Selected bond lengths (Å) and angles (°) are reported in Table 2.1.

Table 2.1: Selected bond lengths (Å) and angles (°) in **10a**.(THF)$_3$.

Na-N(1)	2.3144(11)	N(1)-C(1)	1.3874(15)
Na-C(1)	3.0036(13)	N(2)-C(13)	1.4249(14)
N(1)-Si	1.6672(10)	Na-N(1)-C(1)	105.72(9)
N(2)-Si	1.7716(11)	N(1)-Si-N(2)	109.73(5)

2.2.2 Synthesis of Bi(Me$_2$Si{NAr}{NHAr})Cl$_2$ (11)

Reaction of one equivalent of Me$_2$Si{N(M)Ar}{NHAr} (M = Na (**10a**), K (**10b**)) with BiCl$_3$ followed by work-up resulted in the isolation of Bi(Me$_2$Si{NAr}{NHAr})Cl$_2$ (**11**) as a yellow powder (Scheme 2.2). Alternatively, the sequential reaction of **8** with one equivalent of *n*-BuLi followed by the *in situ* reaction with BiCl$_3$ also resulted in formation of **11**. Attempts to obtain crystals from a mixture of hexane/toluene suitable for single crystal X-ray crystallography

R−N−Si−N−R
M   H

BiCl₃ →

Me₂Si{NAr}... Bi Cl Cl (structure 11)

← (i) *n*-BuLi (ii) BiCl₃

R−N−Si−N−R
H   H

M = Na (**10a**), K (**10b**)   **11**   **8**
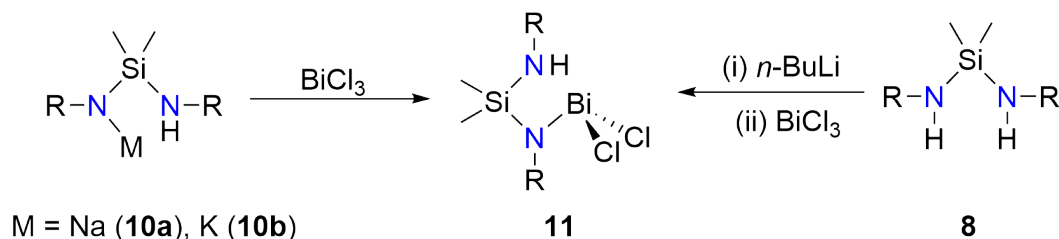
Scheme 2.2: Synthesis of Bi(Me₂Si{NAr}{NHAr})Cl₂ (**11**).

were unsuccessful.

The ^{1}H NMR spectrum of **11** displays two sets of resonances corresponding to *iso*-propyl methine (δ_H 3.79 and 3.26 ppm) and methyl protons (δ_H 1.40 and 1.09 ppm). In contrast to the broad resonances observed for the bismuth mono-chloride **9**, these signals are clearly defined at room temperature.[95] The more deshielded *iso*-propyl methyl protons appear as two separate doublets, consistent with restricted rotation for the aryl substituent adjacent to the bismuth centre. The other *iso*-propyl methyl resonance does not display this splitting pattern and is represented by a single doublet, consistent with two distinct aryl environments. A single high field resonance is observed for the SiMe₂ protons (δ_H 0.1 ppm). The N-H resonance appears at δ_H 4.61 ppm, similar to that observed for the antimony dichloride analogue Sb(Me₂Si{NAr}{NHAr})Cl₂ (N-H δ_H 4.64 ppm, CDCl₃).[97]

The ^{13}C NMR spectrum displays two sets of resonances for the N-aryl substituent, consistent with two distinct 2,6-*i*-Pr₂C₆H₃ groups. A single high field resonance corresponding to the SiMe₂ carbons is observed at δ_C 3.8 ppm. Elemental analysis is in agreement with the calculated values for **11**.

2.2.3 Reaction of 11 with a Lewis Base

In an attempt to form the mono-chloride species **9** from **11**, a number of Lewis bases were added to an NMR sample in C₆D₆ and monitored by ^{1}H NMR spectroscopy. The reaction of one equivalent of NEt₃ with **11** did not result in abstraction of HCl and formation of **9**, with no reaction observed after 24 hours at 80 °C. Reacting **11**

with one equivalent of n-BuLi at -30 °C resulted in formation of an unidentifiable mixture of products.

2.3 Synthesis and Characterisation of Low-Coordinate Bismuth Cations

2.3.1 Reaction of Bi(Me$_2$Si{NAr}$_2$)Cl (9) with ECl$_3$ (E = Al, Ga, In)

The reaction of Bi(Me$_2$Si{NAr}$_2$)Cl (Ar = 2,6-i-Pr$_2$C$_6$H$_3$) (**9**) with one equivalent of ECl$_3$ (E = Al, Ga) in toluene results in formation of the corresponding cation [Bi(Me$_2$Si{NAr}$_2$)]$^+$ as the [AlCl$_4$]$^-$ (**12a**) and [GaCl$_4$]$^-$ (**12b**) salts.[i] No reaction was observed upon addition of InCl$_3$ to **9** at room temperature and heating the reaction mixture to 80 °C for 24h resulted in an intractable mixture of products. The lack of chloride abstraction for the indium reagent contrasts with previous reports by Veith and co-workers, where [Bi(Me$_2$Si{Nt-Bu }$_2$)][InCl$_4$] was synthesised by reaction of the neutral chloride with InCl$_3$.[54]

The reaction of **9** with one equivalent of AlCl$_3$ in toluene proceeds with a change in the colour of the solution from yellow to dark red. Deep red crystals of **12a** were obtained upon concentration and cooling of the mother liquor to -30 °C (eq. 2.1).
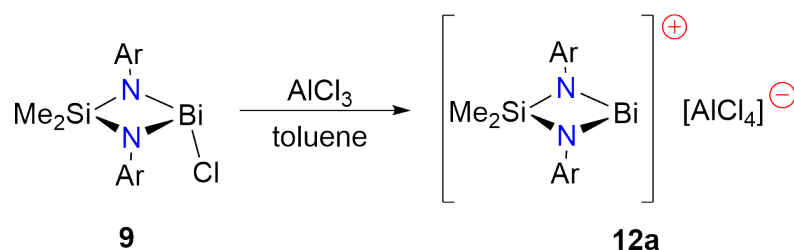
eq. 2.1: Reaction of **9** with AlCl$_3$.

---

[i] **12a** has previously been synthesised by Ben Day[62], however has only been characterised by crystallography. The solid-state structure of **12a** has multiple Bi···Cl-AlCl$_3$ interactions, dimerising to form ([Bi(Me$_2$Si{NAr}$_2$)][AlCl$_4$])$_2$

The ^{1}H NMR spectrum of **12a** shows a single set of resonances for the SiMe$_2$, *iso*-propyl methyl and *iso*-propyl methine protons (δ_H 0.13, 1.21 (br) and 3.49 (br) ppm, respectively). This contrasts with the spectra of **9**, where two sets of resonances are observed for these protons,[95] and is consistent with a loss of the C_S symmetry imposed by the pyramidal geometry of the bismuth in **9** and formation of a C_{2h} symmetric centre in **12a**. The simplest interpretation of these data is formation of the two coordinate cation, with a mirror plane passing through the metallacycle, although other possible solution-state structures may also correspond to this new symmetry (see Appendix A).

The ^{13}C NMR spectrum shows a single set of resonances for the ligand, consistent with a C_{2h} symmetry. The SiMe$_2$ carbons appear as a single resonance at a δ_C 10.4 ppm. The ^{29}Si NMR spectrum of **12a** has a single resonance at δ_{Si} 38.0, downfield from the ^{29}Si NMR resonance of **9** (δ_{Si} 29.7 ppm, difference in chemical shift ($\Delta\delta_{Si}$) = 8.3 ppm). These data and elemental analysis agree with the previously determined solid-state structure, which showed formation of the two coordinate bismuth cation **12a'** with a planar SiN$_2$Bi metallacycle.[i]

The analogous reaction of **9** with one equivalent of GaCl$_3$ was performed on an NMR scale, proceeding in a similar manner with an immediate colour change to afford a deep red solution. The ^{1}H NMR spectrum is similar to **12a**, with resonances at δ_H 0.13, 1.24 and 3.51 ppm corresponding to the SiMe$_2$, *iso*-propyl methine and *iso*-propyl methyl protons, respectively. This is consistent with formation of [Bi(Me$_2$Si{NAr}$_2$)][GaCl$_4$] (**12b**).

Repeating the reaction on a preparative scale gave a ^{1}H NMR spectrum of the crude product consistent with formation of **12b**. Attempts to isolate **12b** by crystallisation at -30°C were however unsuccessful, resulting in the co-crystallisation of two visually distinct species consisting of an off-white precipitate, and deep red crystals. The off-white precipitate was ^{1}H NMR inactive, with a melting point of 78-79 °C, consistent with GaCl$_3$ (mp 77.9 ± 0.2 °C).[1] Single crystal X-ray analysis identified

the deep red crystals as the di-bismuth cation $[\{Bi(Me_2Si\{NAr\}_2)\}_2(\mu\text{-}Cl)][GaCl_4]$ (**13b**) (Scheme 2.3).
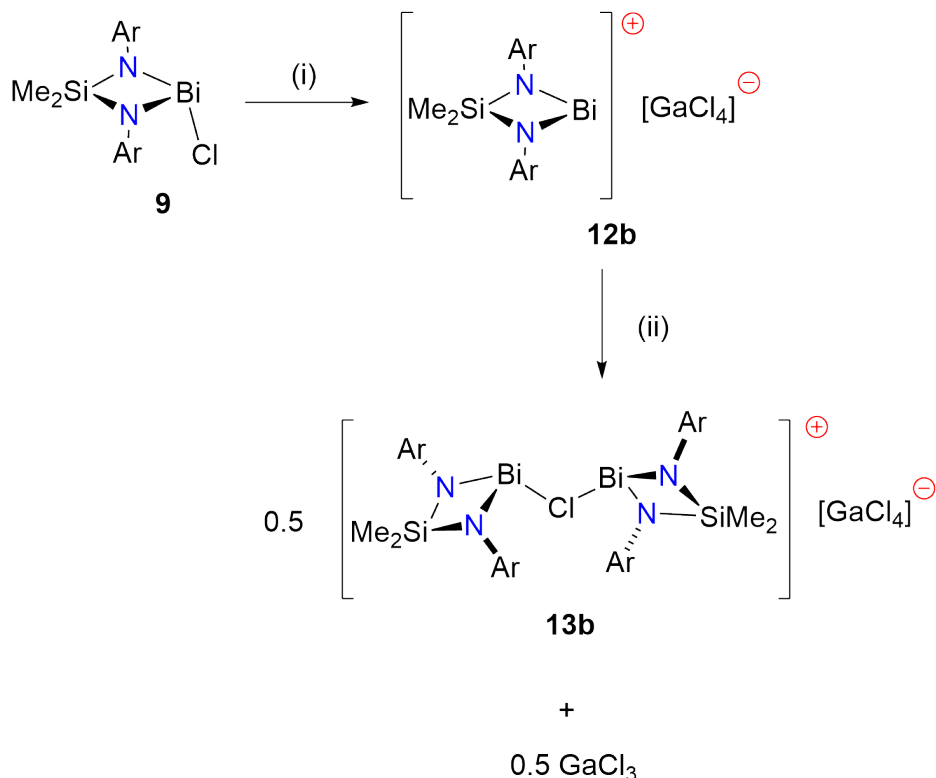
Scheme 2.3: Synthesis of **13b**; (i) $GaCl_3$, toluene (ii) recrystallisation from a mixture of toluene and hexane solution at -30 °C.

The ^{1}H NMR spectrum of an isolated sample of **13b** displays a single set of resonances for the $SiMe_2$, *iso*-propyl methine and $p\text{-}C_6H_3$ protons (δ_H 0.21, 3.90 and 6.74 ppm, respectively), shifted downfield from the corresponding signals for **12a/12b** (Figure 2.2). These data are consistent with a C_{2h} symmetric structure in solution which contrasts the solid-state structure (*vide infra*) and implies fluxionality in solution. Similar to **12a**, the ^{29}Si NMR resonance of **13b** (δ_{Si} 31.2 ppm) appears downfield from **9**, however the difference in chemical shift is much smaller for **13b** ($\Delta\delta_{Si}$ = 1.5 ppm).

Single crystal X-ray diffraction shows that **13b** crystallises in the $P\bar{1}$ space group. The unit cell contains one molecule of **13b**, in addition to one molecule of hexane (Figure 2.3). The cationic component of **13b** consists of two bismuth atoms linked by a μ-chloride bridge with both bismuth atoms adopting a pyramidal geometry
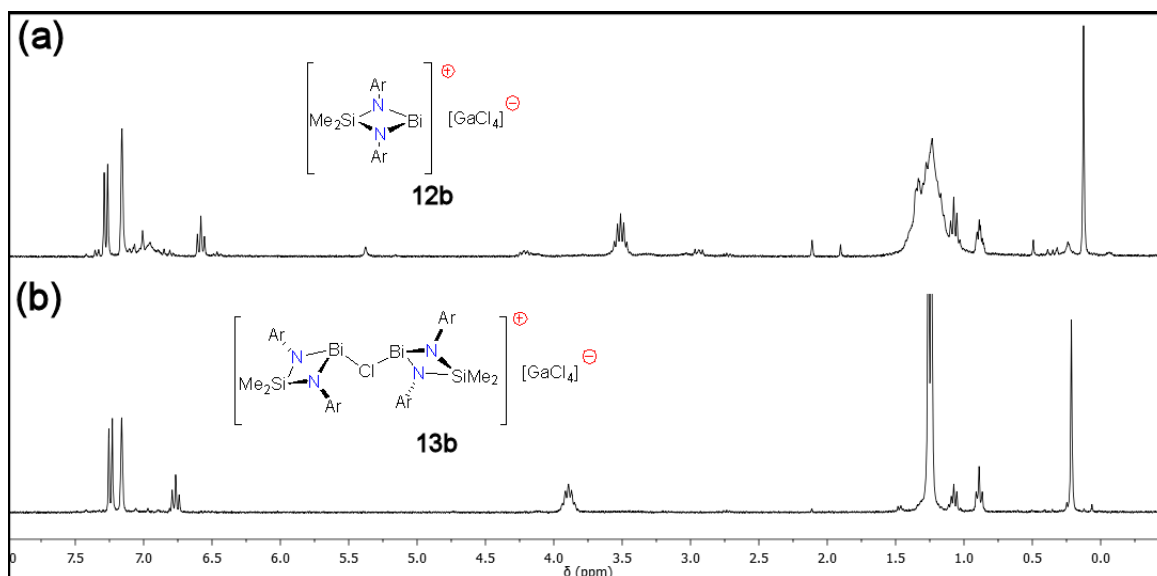
Figure 2.2: ^{1}H NMR Spectra of **12b** (a) and **13b** (b).

(sum of angles = Bi(1) 267.40°; Bi(2) 267.61°). The di(amido) ligands chelate to the bismuth centres forming planar metallacycles (sum of internal angles = Bi(1) 359.9°; Bi(2) 360.0°), with relatively large bite angles (Bi(1) 72.08(15)°; Bi(2) 72.21(15)°) compared to **9** (average = 71.26°). The inter-planar angle between the SiN$_2$Bi metallacycles is 144.03(11)°, occupying the same face of the molecule to form a trans-trans arrangement. This arrangement is stabilised by Bi$\cdots$Cl interactions with the [GaCl$_4$]$^-$ anion at the opposite face of the molecule. The Bi(1)-Cl(3), Bi(2)-Cl(2) and Bi(2)-Cl(5) bond distances (3.3168(14), 3.5373(16) Å and 3.5618(14) Å, respectively) are within the sum of the van der Waals radii of Bi and Cl atoms (4.1 Å).[58]

The μ-chloride bridge has a bent geometry (126.80(4)°). The Bi(1)-Cl(1) bond length (2.7888(12) Å) is significantly longer than the Bi(2)-Cl(1) bond length (2.6902(12) Å), indicating unsymmetrical bonding of the bridging Cl(1) atom (Δ_{BiCl} = 0.10 Å). The difference in bond lengths is attributed to a greater cationic character for Bi(1). Both bismuth chlorine bond distances are longer than the terminal chloride bond of **9** (2.556(1) Å and 2.4857(16) Å) and shorter than the closest Bi$\cdots$Cl interaction in **12a** (2.953(3) Å). The only other structurally characterised mono-chloride bridged bismuth cation, [{t-BuN(CH$_2$C$_6$H$_4$)$_2$Bi}$_2$(μ-Cl)][B(C$_6$F$_5$)$_4$],[98] also

exhibits asymmetry at the Bi-Cl-Bi bridge ($\Delta_{\text{BiCl}} = 0.11$ Å). The Bi-N bond lengths (range = 2.121(4)-2.153(3) Å) are consistent with σ-bonding interactions. No shortening of the bond lengths compared with the neutral compound **9** are observed upon formation of the cationic species.
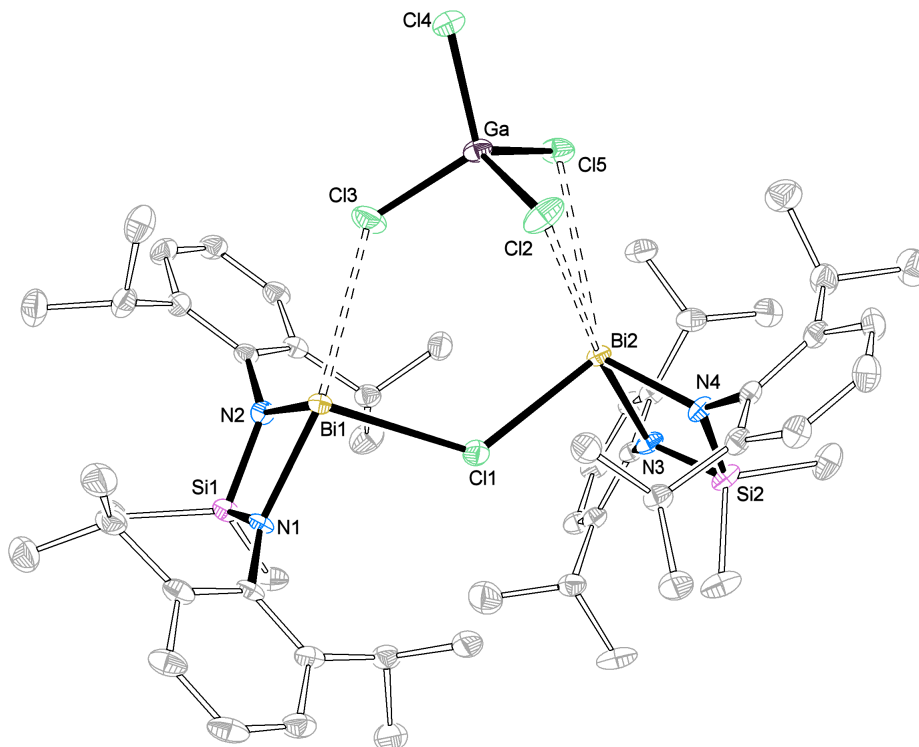
Figure 2.3: ORTEP representation of [**13b**].hexane. 30% Thermal ellipsoid. Hydrogens and hexane solvate omitted for clarity. Selected bond lengths (Å) and angles (°) are reported in Table 2.2.

Table 2.2: Selected bond lengths (Å) and angles (°) in **13b**.

Bi(1)-Cl(1)	2.7888(12)	Bi(2)-Cl(1)	2.6902(12)
Bi(1)-N(1)	2.152(3)	Bi(2)-N(3)	2.143(3)
Bi(1)-N(2)	2.131(3)	Bi(2)-N(4)	2.121(4)
Bi(1)-Cl(3)	3.3168(14)	Bi(2)-Cl(2)	3.5373(16)
Bi(1)-Cl(4)'	3.3277(13)	Bi(2)-Cl(5)	3.5618(14)
N(1)-Bi(1)-N(2)	72.09(13)	N(3)-Bi(2)-N(4)	72.22(18)
N(1)-Si(1)-N(2)	92.68(19)	N(3)-Si(2)-N(4)	92.2(2)
Ga-Cl(2)	2.1878(14)	Ga-Cl(4)	2.1770(13)
Ga-Cl(3)	2.1689(15)	Ga-Cl(5)	2.1622(14)

13b dimerizes in the solid-state, with two $[GaCl_4]^-$ units bridging between two $[\{Bi(Me_2Si\{NAr\}_2)\}_2(\mu\text{-Cl})]$ units via additional $Bi\cdots Cl$ interactions (Figure 2.4). In contrast to the solid-state structure of **12a**, the Ga-Cl bond distances within the anion are similar, consistent with all four chlorides being involved in inter-ion interactions. This is confirmed in the dimer, where Cl(4) is associating with a second cation (Bi(1)'-Cl(4) 3.3277(1) Å). The only other structurally characterised bismuth tetrachlorogallate salt, $[(\{SiMe_3\}_2N=N\{SiMe_3\})_2Bi][GaCl_4]$, does not exhibit $Bi\cdots Cl$ interactions, instead interacting with the two ligands via three-centre four-electron bonds.[58]
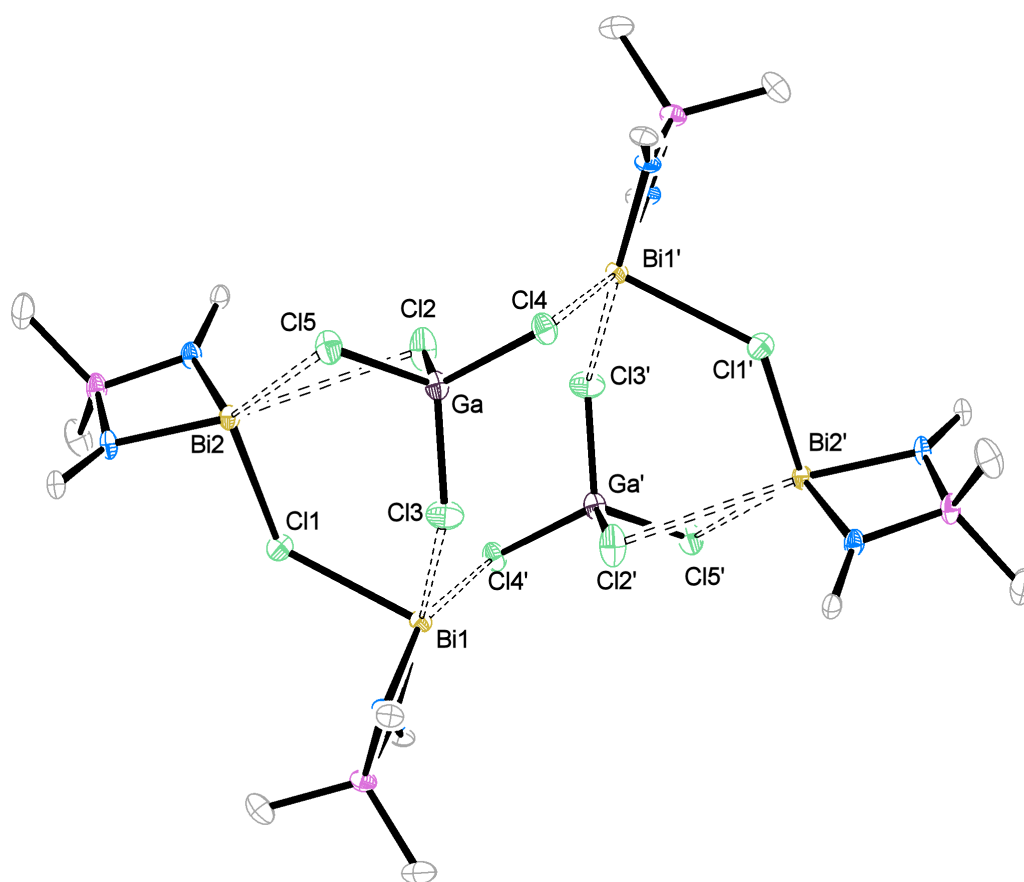
Figure 2.4: ORTEP representation of [**13b**]$_2$. 30% Thermal ellipsoid. Hydrogens and selected carbons are omitted for clarity.

Addition of 0.5 equivalents of $GaCl_3$ to an NMR sample of **13b** in C_6D_6 resulted in conversion to **12b**, demonstrating the presence of an equilibrium between **13b** and **12b** (eq. 2.2). Upon crystallisation, differential solubilities and precipitation of $GaCl_3$ from the solution is thought to drive the equilibrium towards the left,

resulting in the crystallisation of both $GaCl_3$ and **13b**. The reaction of **9** with 0.5 equivalents of $GaCl_3$ also resulted in formation of **13b**, with no evidence of the $GaCl_3$ precipitation.
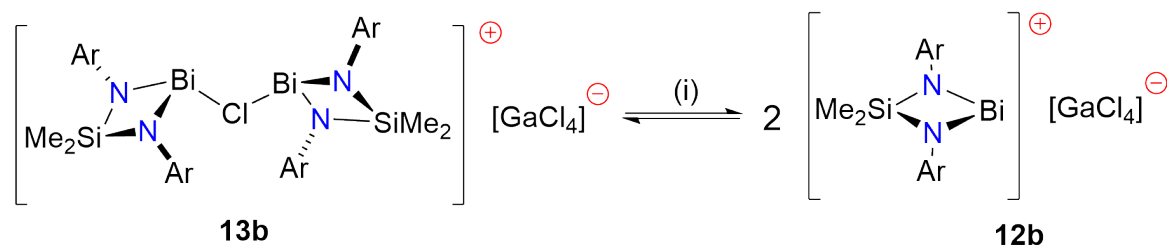
eq. 2.2: Synthesis of **12b**. (i) 0.5 equivalents of $GaCl_3$.

To test whether this equilibrium was also occurring for the tetrachloroaluminate system, the NMR scale addition of one equivalent of **9** to **12a** in C_6D_6 was performed (eq. 2.3). The ^{1}H NMR spectrum displays significant shifts in all of the peaks compared to **12a** (Figure 2.5). Comparison of the data to the ^{1}H NMR spectrum of **13b** show very similar shifts, with key resonances at δ_H 0.20, 3.86 and 6.74 ppm corresponding to the $SiMe_2$, *iso*-propyl methine and p-C_6H_3 protons. This is consistent with formation of the di-bismuth cation, $[\{Bi(Me_2Si\{NAr\}_2)\}_2(\mu\text{-}Cl)][AlCl_4]$ (**13a**).
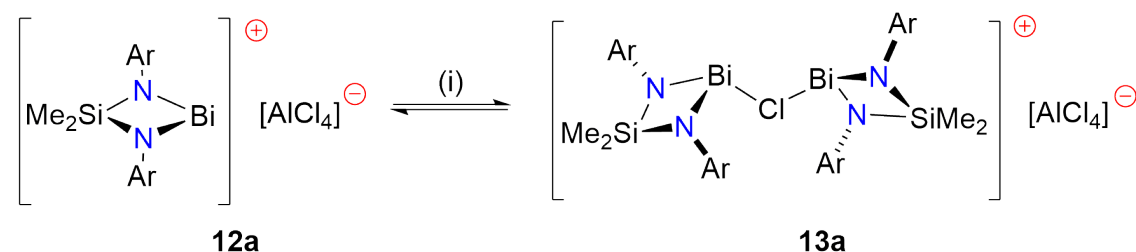
eq. 2.3: Synthesis of **13a**. (i) 1 equivalent of **9**.

94
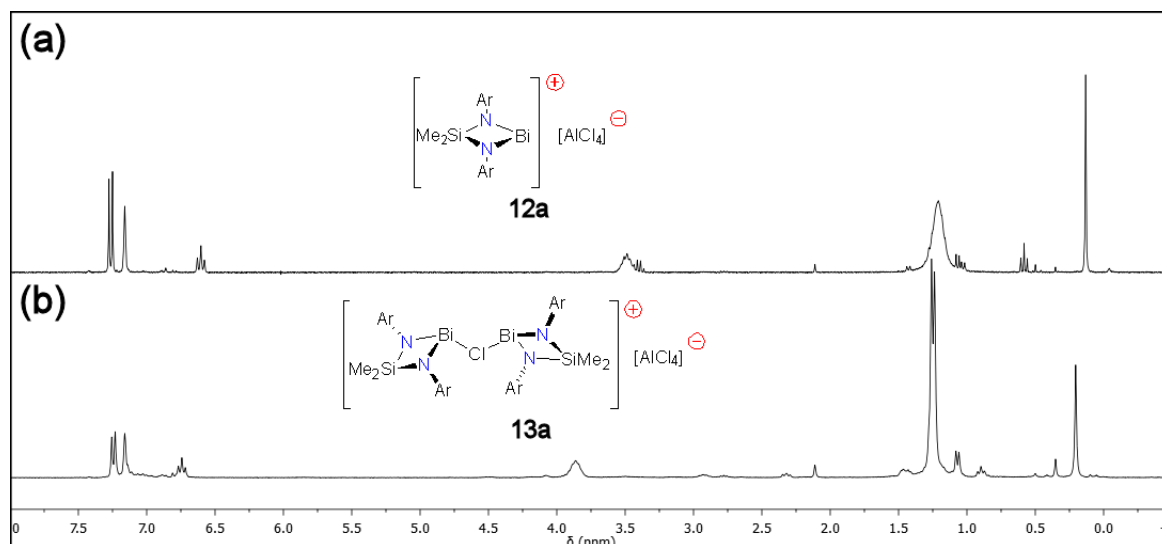
Figure 2.5: ^{1}H NMR Spectra of **12a** and **13a**.

2.3.2 Reaction of 9 with NaBR$_4$ (R = Ph, Et)

^{1}H NMR analysis of the reaction of NaBPh$_4$ and **9** in toluene showed no reaction at room temperature. Heating the mixture to 90 °C for three days gave a yellow solution which, upon crystallisation of the reaction products from toluene, afforded clear colourless crystals of BPh$_3$ (first crop) followed by a mixture of colourless crystals of BPh$_3$ and yellow crystals of Bi(Me$_2$Si{NAr}$_2$)Ph (**14**) (eq. 2.4) (second crop). The identity of the colourless crystals as BPh$_3$ was confirmed by unit cell measurements using X-ray diffraction[99] and ^{11}B NMR spectroscopy (δ_B 68.0 ppm[100]). Mechanical separation of the colourless and yellow crystals allowed for full characterisation of **14**.
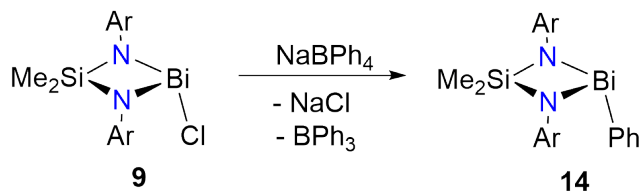
eq. 2.4: Synthesis of **14**.

The ^{1}H NMR spectrum of **14** in C$_6$D$_6$ shows two resonances corresponding to the SiMe$_2$ protons (δ_H 0.63 and 0.15 ppm), consistent with a C_S symmetric structure. A single set of resonances corresponding to the *iso*-propyl methyl and methine protons

95

is observed (δ_H 1.29 and 4.30 ppm, respectively), explained by rapid rotation of the Ar substituents, resulting in equivalent environments for the *iso*-propyl protons (i.e. the observed resonance corresponds to the average signal of the two distinct environments). The o-C_6H_5 protons of the phenyl substituent appear as a low field doublet (δ_H 8.49 ppm), significantly downfield from the o-C_6H_5 protons of BiPh$_3$ (δ_H 7.73 ppm, C_6D_6) and also significantly downfield from the [BPh$_4$]$^-$ anion of [Bi(2,6-$\{Me_2NCH_2\}_2C_6H_3$)]$^+$ reported by Evans and co-workers (δ_H 6.99 ppm, CD_3CN[59]). The ^{13}C NMR spectrum is consistent with the formation of **14**, showing two signals corresponding to the SiMe$_2$ protons at 17.5 and 4.8 ppm. The ^{29}Si NMR resonance appears at δ_{Si} 19.5 ppm, shifted significantly upfield from **9** ($\Delta\delta_{Si}$ = -10.2 ppm). Elemental analysis data was consistent with the calculated values for **14**.

X-ray diffraction studies of single crystals of **14** show that it is monomeric in the solid-state and crystallises in the $P\bar{1}$ space group (Figure 2.6). The unit cell contains two independent molecules of **14** and a single molecule of toluene. The toluene solvate molecule lies on a centre of inversion and is disordered over two positions.

The geometry at both three-coordinate bismuth centres is pyramidal (sum of angles = Bi(1) 269.02°; Bi(2) 268.62°), with bond angles ranging between 70.5(7)°and 100.5(9)°. The metallacycles are planar (sum of internal angles = Bi(1) 359.8°; Bi(2) 360.0°), with the most acute bond angle corresponding to the bite angle of the di(amido)silyl ligand (N-Bi-N' = 70.50(7)°and 70.86(7)°, respectively). The Bi-C$_{ipso}$ bond distances (Bi(1) 2.253(3) Å; Bi(2) 2.252(3) Å) are typical for a phenyl bound to bismuth.[101] The Bi-N bond distances (2.168(2) - 2.1790(19) Å) are consistent with σ-bonding interactions.
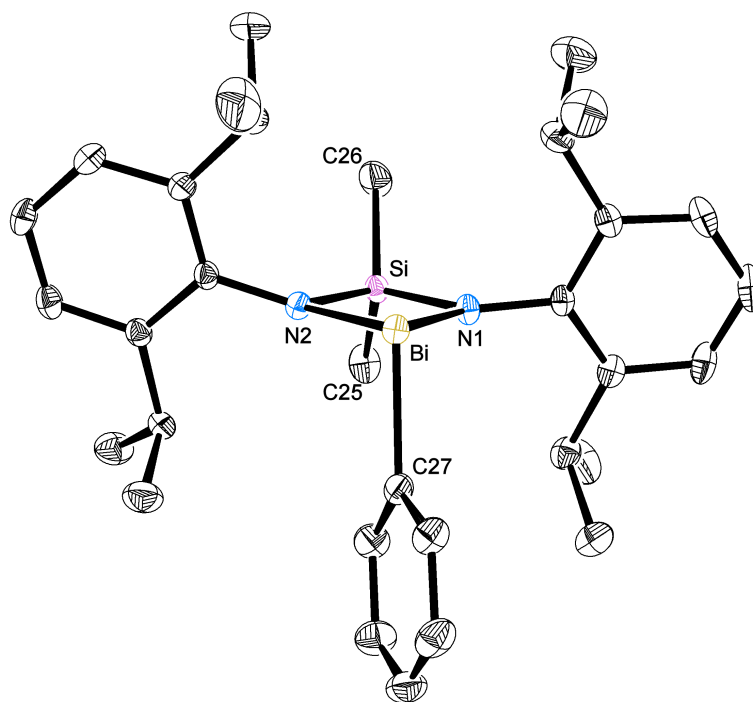
Figure 2.6: ORTEP representation of [2(**14**)].0.5toluene. 30% Thermal ellipsoid. Hydrogens, one molecule of **14** and toluene solvate omitted. Selected bond lengths (Å) and angles (°) are reported in Table 2.3.

Table 2.3: Selected bond lengths (Å) and angles (°) of both molecules of **14**.

Bi(1)-N(1)	2.168(2)	Bi(2)-N(3)	2.1790(19)
Bi(1)-N(2)	2.177(2)	Bi(2)-N(4)	2.172(2)
Bi(1)-C(27)	2.253(3)	Bi(2)-C(58)	2.252(3)
N(1)-Bi(1)-N(2)	70.86(8)	N(3)-Bi(2)-N(4)	70.50(8)
N(1)-Si(1)-N(2)	93.65(11)	N(3)-Si(2)-N(4)	93.91(11)
Bi(1)-N(1)-Si(1)	98.21(10)	Bi(2)-N(3)-Si(2)	97.63(9)
Bi(1)-N(2)-Si(1)	97.49(9)	Bi(2)-N(4)-Si(2)	97.59(8)

Comparison of the two molecules of **14** in the unit cell indicate that they differ in the orientation of the phenyl substituent. In both cases, the phenyl substituent approaches a perpendicular arrangment with respect to the metallacycle plane (Si$\cdots$Bi-C$_{ipso}$ = Bi(1) 102.92(8)°; Bi(2) 100.45(8)°). The phenyl groups are rotated in opposite directions along the Bi-C$_{ipso}$ bond relative to the plane bisecting the metallacycle through the Si, Bi and C$_{ipso}$ atoms (Bi(1) = +14.85(7)°; Bi(2) = -29.56(11)°, where positive = clockwise and negative = anti-clockwise) (Figure 2.7).
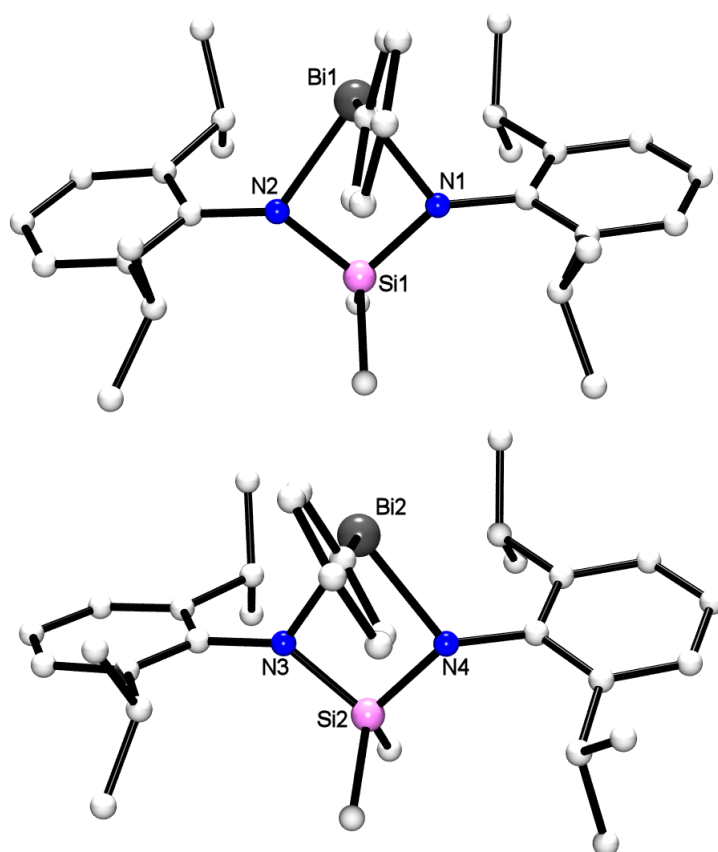
Figure 2.7: Schematic representation of different molecules of **14**; top = Bi(1), bottom = Bi(2). Hydrogens omitted for clarity.

The close proximity of the phenyl substituent to the *i*-Pr groups of the aryl substituent results in distortion of the metallacyclic ring in order to relieve steric strain, with the nitrogen aryl-substituent twisting above the plane of the metallacycle. The geometry of the nitrogen centres is significantly distorted from trigonal planar (sum of angles = 353.87°- 358.71°). Distortion of the nitrogen geometry is observed to be larger for N(2) and N(4) (sum of angles = 354.94°and 353.87°, respectively), where

the phenyl substituents are closer to the *i*-Pr groups. The distortion is more pronounced in the second molecule, where the phenyl substituent show greater rotation from the Si, Bi and C_{ipso} plane.

Analysis of the packing suggests the presence of intermolecular interactions with the symmetry-generated molecule (Bi(2)') (Figure 2.8). The distance between the *para*-carbon of the phenyl substituent (C(61)) and Bi(2)' is 3.629(3) Å, within the range of distances previously attributed to bonding interactions within $[BiCl_3.C_6H_{6-n}Me_n]$ (Bi-C = 3.168(7) - 3.751(8) Å).[102–106] The phenyl rings experience large slippage (2.57 Å), consistent with dominating π-π stacking effects between the two phenyl rings (centroid-centroid distance = 3.827(3) Å). It is also noted that crystal packing forces may account for the formation of the dimer.
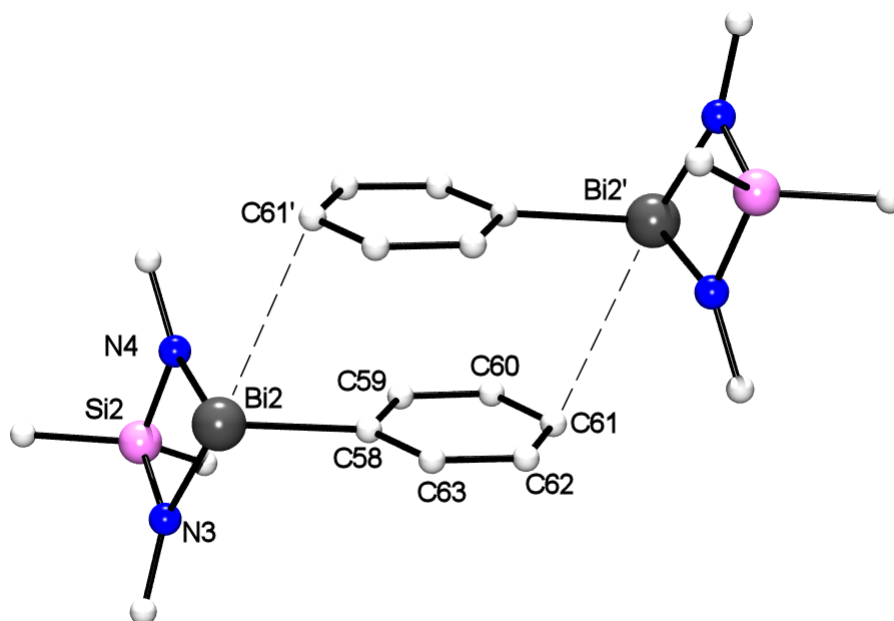
Figure 2.8: Schematic representation of the dimerization of **14**. Hydrogens and selected carbons are omitted for clarity.

Reaction of the previously isolated tetrachloroaluminate cation **12a** (*vide supra*) with one equivalent of $NaBPh_4$ on an NMR scale also resulted in a mixture of **14** and BPh_3. This suggests that formation of the bismuth cation may be occurring prior to abstraction of the phenyl group from the $[BPh_4]^-$ anion (Scheme 2.4).

Abstraction of aryl substituents from tetraarylborate anions is well documented.[107]
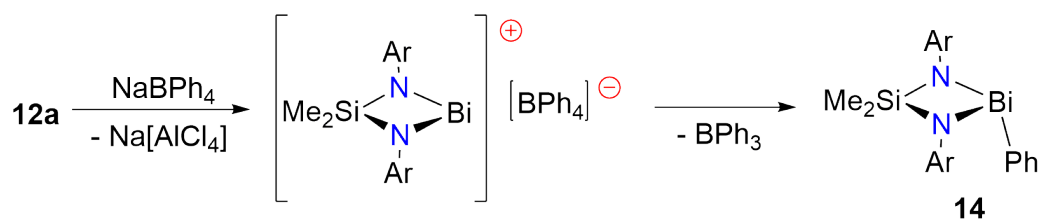
Scheme 2.4: Abstraction of a phenyl group from the tetraphenylborate anion.

Stavila et al. recently reported the reaction of sodium tetraarylborate salts with bismuth(III) carboxylates as a convenient route to triarylbismuth compounds.[108] In order to further investigate this reactivity, the reaction of the tetraalkylborate $NaBEt_4$ with **9** was performed, resulting in formation of the corresponding alkyl bismuth compound $Bi(Me_2Si\{NAr\}_2)Et$ (**15**) in addition to the presumed reaction side products, BEt_3[ii] and NaCl (eq. 2.5). Tetraalkylborates are significantly more nucleophilic than tetraarylborates, and are commonly used in the synthesis of a wide range of alkyl-metal compounds.[109]
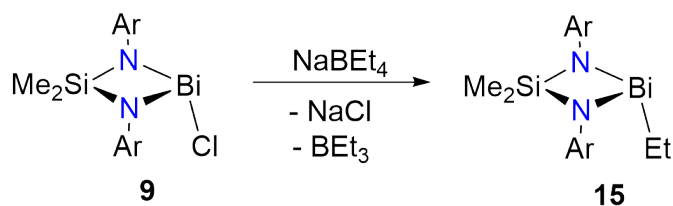
eq. 2.5: Synthesis of **15**.

The ^1H NMR spectrum of **15** displays two resonances corresponding to the $SiMe_2$ protons (δ_H 0.42 and 0.04 ppm), consistent with C_S symmetry. As observed for **14**, a single set of resonances are displayed for the *iso*-propyl methine and methyl protons (δ_H 4.28 and 1.31 ppm, respectively), attributed to the rapid rotation of $2,6$-i-$Pr_2C_6H_3$ substituents resulting in averaged signals. The peaks corresponding to the ethyl substituent appear as a triplet and quartet at δ_H 2.47 and 2.04 ppm, respectively. The integrals of these resonances indicate the presence of a single ethyl substituent, consistent with abstraction of the ethyl group from the tetraethylborate anion.

[ii]BEt_3 is a volatile liquid and was removed on work-up

The ^{13}C NMR spectrum shows two resonances for the SiMe$_2$ carbons (δ_C 15.6 and 5.2 ppm). The ethyl terminal carbon, CH$_2$CH$_3$ appears as a high field resonance (δ_C 8.7 ppm), confirmed by HSQC analysis. No resonance was observed for the remaining ethyl carbon (BiCH$_2$CH$_3$), likely due to quadrupolar broadening caused by the proximity to bismuth (^{209}Bi = 100% abundant, spin I = $^9/_2$).[110] Elemental analysis data is consistent with the calculated values for **15**. The ^{29}Si NMR resonance appears at δ_{Si} 17.8 ppm, significantly upfield from **9** ($\Delta\delta$ = - 11.9 ppm) and very similar to that observed in **14**. The relatively large upfield shift in the ^{29}Si NMR resonances for both **14** and **15** reflect the relatively electron rich metallacycle after exchanging the electronegative chloride for an aryl/alkyl group.

Single crystal X-ray crystallography was used to determine the solid-state structure of **15**. Unfortunately, significant disorder prevents detailed discussion of bond lengths and angles (Appendix B), however the connectivity is unambiguous, showing the formation of **15** .

2.4 Reactivity of Compounds Containing Bi-X Bonds (X = NR$_2$, OAr', PR$_2$)

Bi(Me$_2$Si{NAr}$_2$)(N{SiMe$_3$}$_2$) (**16**) was synthesised from the reaction of one equivalent of LiN{SiMe$_3$}$_2$ with **9** via literature procedures.[62] Attempts to synthesise this compound via addition of the di(amido) ligand Me$_2$Si{NHAr}$_2$ (**8**) to Bi(N{SiMe$_3$}$_2$)$_3$ proved unsuccessful with no reaction at room temperature after 24 hours (Scheme 2.5).
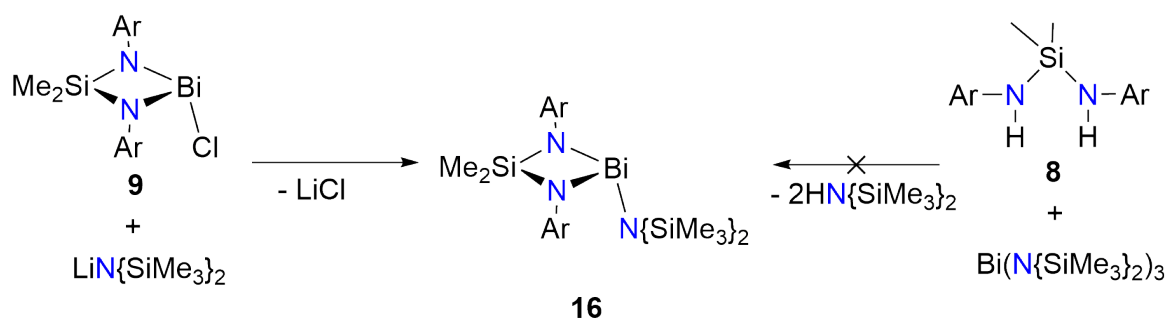
Scheme 2.5: Synthesis of **16**.

2.4.1 Synthesis of Bi(Me₂Si{NAr}₂)(OAr') (Ar' = 2,6-(*t*-Bu)₂C₆H₃) (17)

Reaction of one equivalent of KOAr' (Ar' = 2,6-*t*-Bu₂C₆H₃) with **9** in toluene results in formation of a dark green solution. The corresponding aryloxide, Bi(Me₂Si{NAr}₂)(OAr') (**17**) was isolated from the reaction mixture after 24 hours at -30 °C as dark green crystals (eq 2.6).
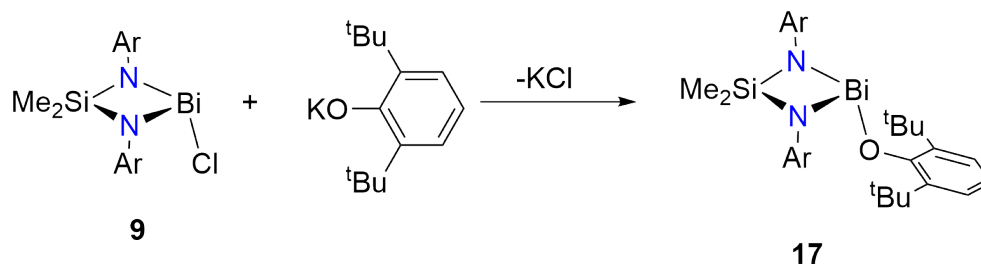
eq. 2.6: Synthesis of **17**.

The ^{1}H NMR of **17** displays two singlets at δ_H 0.70 and 0.01 ppm for the SiMe₂ protons, consistent with a C_S symmetric bismuth centre. The *iso*-propyl methyl protons appear as two sets of doublets (δ_H 1.13 and 1.34 ppm), one of which overlaps with the *tert*-butyl methyl groups (δ_H 1.39 ppm). The *iso*-propyl methine protons appear as a single broad resonance at δ_H 3.88 ppm, similar to that observed in compounds **14** and **15**. The ^{13}C NMR spectrum is consistent with the formation of **17**, showing eight aromatic resonances. Two high field resonances are observed for the SiMe₂ carbon atoms (δ_C 15.5 and 2.8 ppm). Elemental analysis data is consistent with the calculated values for **17**.

Single crystal X-ray crystallography confirmed **17** as the monomeric aryloxide crystallising in the $P\bar{1}$ space group. The bismuth centre adopts a pyramidal geometry (sum of angles = 273.71°) with the di(amido) ligand chelating to the bismuth to form a planar four-membered metallacycle (sum of internal angles = 359.93°, bite angle = 71.63(10)°). The oxygen atom sits almost perpendicular to the plane of the metallacycle (Si$\cdots$Bi-O = 104.41(6)°). The Bi-O-C27 angle (119.14(16)°) indicates a bent geometry. Chisholm and co-workers attributed this bent geometry in Bi(cy-salen)(OAr') to the hybridisation of the oxygen pπ orbitals toward sp^2 in order to minimise interaction of the lone pairs of the oxygen with the bismuth lone pair (Figure 2.10).[83] This cy-salen derivative has a much larger Bi-O-C$_{ipso}$ bond angle (130.7(2)°) compared with **17**, consistent with greater sp^2 hybridisation in **17**. The plane of the aromatic component of 2,6-t-Bu$_2$C$_6$H$_3$ sits rotated with respect to the plane of the metallacycle (inter-planar angle = 131.50(12)°).
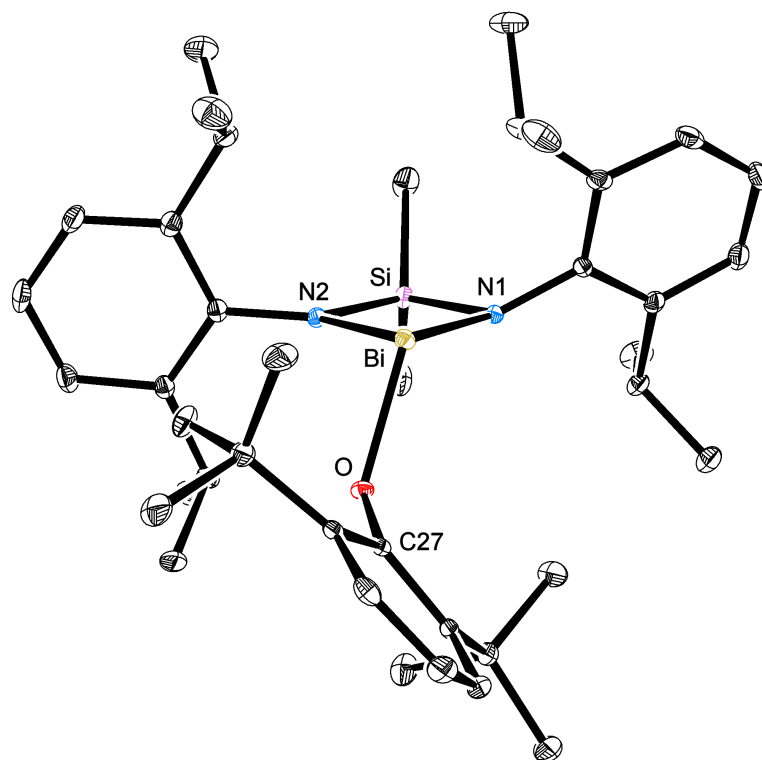
Figure 2.9: ORTEP representation of **17**. 30% Thermal ellipsoid. Hydrogens omitted for clarity. Selected bond lengths (Å) and angles (°) are reported in Table 2.4.

Table 2.4: Selected bond lengths (Å) and angles (°) in **17**.

Bi-O	2.142(2)	Bi-O-C(27)	119.14(16)
O-C(27)	1.359(4)	N(1)-Si-N(2)	93.62(13)
Bi-N(1)	2.188(3)	Bi-N(1)-Si	96.31(14)
Bi-N(2)	2.136(3)	Bi-N(2)-Si	98.37(13)
N(1)-Si	1.738(3)	N(1)-Bi-O	110.86(10)
N(2)-Si	1.732(3)	N(2)-Bi-O	91.22(9)
N(1)-Bi-N(2)	71.63(10)		
SiN$_2$Bi : 2,6-t-Bu$_2$C$_6$H$_3$ inter-planar angle			131.50(12)
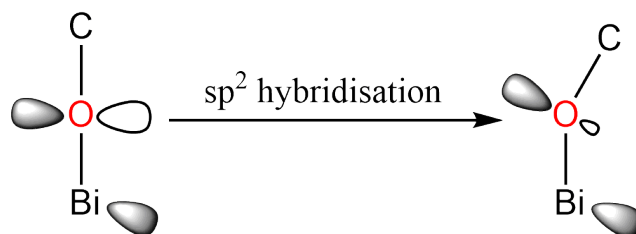
Figure 2.10: sp^2 hybridisation of the oxygen πp orbitals.

The Bi-N bond distances (N(1) 2.188(3) Å; N(2) 2.136(2) Å) are typical for this system, consistent with σ-bonding interactions. While N(2) is approximately planar (sum of angles = 359.6°), N(1) exhibits significant distortion (sum of angles = 348.31°), with the aryl substituent being pushed above the plane of the metallacycle. There does not appear to be any close contacts between the Ar' substituent and the aromatic group on N(1). The cause of this distortion may therefore be the result of intermolecular packing forces.

The Bi-O bond distance (2.142(2) Å) is within the sum of the covalent radii for bismuth and oxygen (2.18 Å) indicating the formation of a covalent interaction. The related three-coordinate bismuth aryloxide complex containing t-Bu groups in the $ortho$-positions, Bi(O-2,4,6-t-Bu$_3$C$_6$H$_3$)$_2$Cl, has significantly shorter Bi-O bond lengths (average = 2.093(3) Å).[111] This demonstrates that the ligand strongly influences the coordination of the aryloxide group. Indeed, Evans and co-workers reported spontaneous formation of the bismuth cation [(2,6-(Me$_2$NCH$_2$)C$_6$H$_3$)$_2$Bi][OAr'], where

close interaction of the bismuth centre with the bulky aryloxide is prevented by the aryl ligands (Bi-O = 3.455(2) Å), resulting in the formation of an outer-sphere aryloxide anion.

2.4.2 Synthesis of $Bi(Me_2Si\{NAr\}_2)(PCy_2)$ (18)

The reaction of **9** with one equivalent of $LiPCy_2$ in toluene yields $Bi(Me_2Si\{NAr\}_2)(PCy_2)$ (**18**) as a red crystalline solid after work up (eq. 2.7).
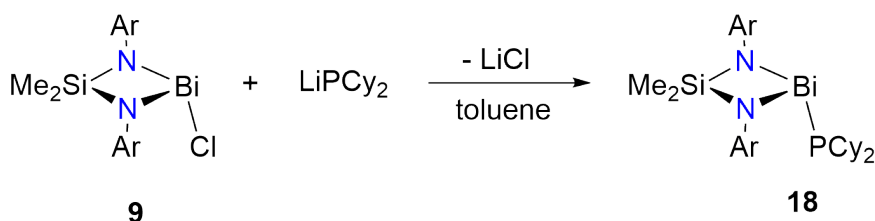
eq. 2.7: Synthesis of **18**.

The ^{1}H NMR spectrum of **18** displays two singlets corresponding to the $SiMe_2$ protons (δ_H 0.51 and 0.16 ppm), consistent with a C_s symmetric molecule. A single set of broad resonances are observed for each of the *iso*-propyl methine and α-cyclohexyl protons (δ_H 4.35 and 3.53 ppm, respectively). Two high field resonances are observed in the ^{13}C NMR spectrum, corresponding to $SiMe_2$ carbons (δ_C 15.4 and 4.3 ppm). The ^{31}P NMR spectrum shows a single peak at δ_P 56.3 ppm, significantly downfield from $LiPCy_2$ (δ_P 21.9 ppm). The ^{29}Si NMR resonance for **18** (δ_{Si} 16.4 ppm) appears upfield from **9** ($\Delta\delta_{Si}$ = -13.3 ppm). Elemental analysis data is consistent with the calculated values for **18**.

Single crystal X-ray crystallography shows that **18** crystallises in the $P\bar{1}$ space group. The unit cell incorporates half a molecule of toluene which lies on an inversion centre, where the CH_3 group is disordered over two positions, with half occupancy at each position.
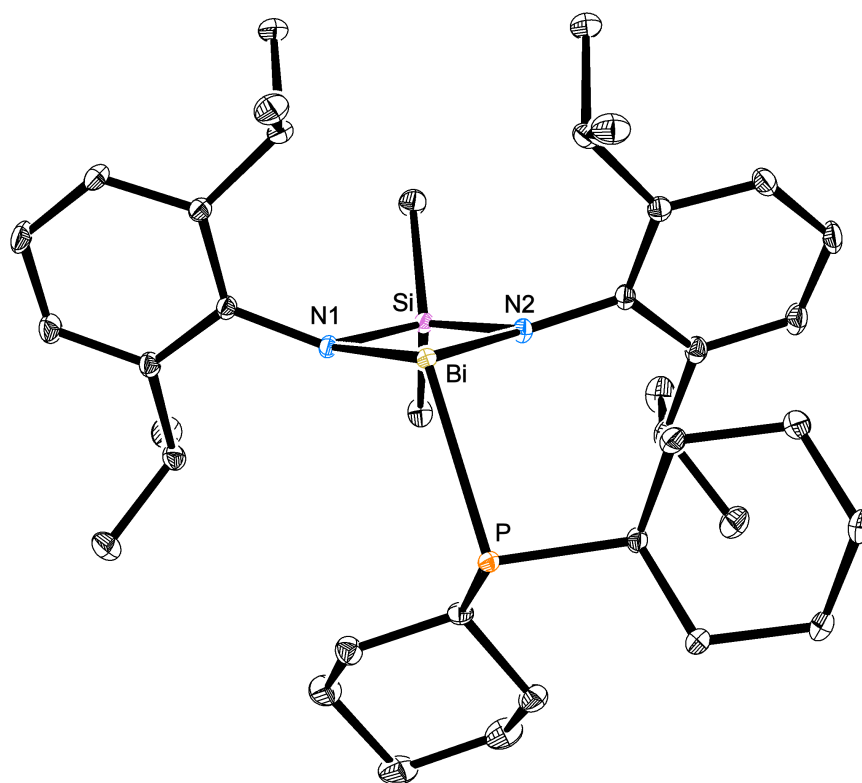
Figure 2.11: ORTEP representation of [**18**].0.5toluene. 30% Thermal ellipsoid. Hydrogens and toluene solvate omitted for clarity. Selected bond lengths (Å) and angles (°) are reported in Table 2.5.

Table 2.5: Selected bond lengths (Å) and angles (°) in **18**.

Bi-P	2.6796(6)	N(1)-Bi-N(2)	70.13(6)
Bi-P'	3.2407(6)	N(1)-Si-N(2)	95.69(8)
Bi-N(1)	2.2022(18)	Bi-N(1)-Si	97.69(8)
Bi-N(2)	2.2605(18)	Bi-N(1)-Si	96.42(8)
N(1)-Si	1.7439(19)	N(1)-Bi-P	109.92(7)
N(2)-Si	1.7150(19)	N(2)-Bi-P	95.50(6)

The three-coordinate bismuth centre is pyramidal (sum of angles = 275.55°). The di(amido) ligand chelates to the bismuth centre with an acute bite angle (70.13(7)°) to form a planar metallacyclic ring (sum of internal angles = 359.9°). Analogous to **17**, the phosphorus is not centred between the two nitrogens, and is closer to N(2) compared to N(1) (P$\cdots$N(1) distance 4.006(2) Å (N(1)-Bi-P 109.92(7)°); P$\cdots$N(2) distance 3.668(2) Å (N(1)-Bi-O 95.50(6)°). Greater pyramidalisation is observed at the more distant nitrogen centre, N(1) (sum of angles = 349.49° and 356.51° for N(1) and N(2), respectively).

The terminal Bi-P bond distance (2.6796(6) Å) in **18** is slightly longer than the bridging Bi-P-Bi bond lengths observed in [t-Bu$_2$PhSiP](BiCH(SiMe$_3$)$_2$Cl)$_2$[73] and terminal Bi-P bond lengths of the dibismuthine [BiP(SiPh$_2$$t$-Bu)$_2$]$_2$[65] (range = 2.630(13) - 2.6482(17) Å). The phosphorus atom sits almost perpendicular to the plane of the metallacycle (Si$\cdots$Bi-P = 106.43(2)°), adopting a pyramidal geometry (sum of angles = 305.6°) with the cyclohexyl substituents pointing towards the bismuth centre. This contrasts with the structure of the related group 14 terminal phosphides M(BDI$_{DIPP}$)(PCy$_2$) (M = Ge, Sn, Pb; BDI$_{DIPP}$ = [CH(C(Me){NAr})$_2$]$^-$), where the Cy groups point away from the metal centre (Figure 2.12).[112]

18   (BDI$_{DIPP}$)M(PCy$_2$)
M = Ge, Sn, Pb

Figure 2.12: Schematic representation of the positioning of the cyclohexyl groups in **18** (left) and M(BDI$_{DIPP}$)(PCy$_2$) (M = Ge, Sn, Pb) (right).

The position of the cyclohexyl substituents in **18** is attributed to the formation of a dimer in the solid-state (Figure 2.13). Analysis of the solid-state packing of **18**

indicates a relatively close interaction with a symmetry generated molecule of **18**. The intermolecular Bi-P' distance (3.2407(6) Å) is much longer than the intramolecular Bi-P bond distance (2.6795(8) Å), however it is within the sum of the van der Waal's radii for these two atoms (4.25 Å), suggesting a bonding interaction. The more distorted N(1) atom sits closer to the PCy$_2$ group of the symmetry related molecule than N(2), which may explain the greater degree of distortion observed at N(1).

Figure 2.13: ORTEP representation of [**18**]$_2$ dimer. 30% Thermal ellipsoid. Hydrogens are omitted for clarity.

2.4.3 Comparison of Solid-state Structures of Three-Coordinate Di(amido) Bismuth Compounds

Comparison of the solid-state structures of Bi(Me$_2$Si{NAr}$_2$)X (X = Cl, Ph, N{SiMe$_3$}$_2$, OAr', PCy$_2$) (Table 2.6) indicate significant differences in the position of the functional group (X) with respect to the 'Me$_2$Si{NAr}$_2$Bi' unit and the

geometry of the Bi- and N-atoms depending on the functional group.

The Bi-X bond distance of chloride (**9**), phenyl (**14**), amide (**16**) and aryloxide (**17**) derivatives are closely related to the corresponding sum of the covalent radii ($\%_{cov}$ = 99.9% - 102%). The Bi-P bond of **18** is comparatively longer than the sum of the covalent radii ($\%_{cov}$ = 105%), likely due to formation of the dimer $[\mathbf{18}]_2$ in the solid-state.

The di(amido) ligand chelates via a bidentate bonding mode to form a planar four-membered metallacycle in all cases. The bite angles for these compounds appear in a relatively narrow range (70.13(6)°- 71.63(10)°). The Bi-N bond lengths of the ligand, however, change significantly depending on the X substituent. Chloride **9** has significantly shorter Bi-N bond lengths than the heteroatom and phenyl derivatives, possibly reflecting the increased electronegativity of the halide.

Amide **16**, aryloxide **17** and phosphide **18** all show significant shortening of one Bi-N bond, compared to the other Bi-N bond (Difference in Bi-N bond lengths (Δ_{Bi-N}) = 0.027, 0.052, 0.058 Å, respectively). This is not observed for the chloride (**9**) or phenyl (**14**) derivatives. The nitrogen atom of the longer Bi-N bond experiences a greater loss of planarity, compared to the shorter Bi-N bond, with greater pyramidalisation observed for the N atoms in **16**, **17** and **18**, which may be a reflection of the sterics of the X substituents.

The position of X with respect to the metallacycle is noted to play a significant role in determining the geometry at both the nitrogen and bismuth centres.[62] As all of these compounds exhibit planar metallacycles, the Si···Bi-X angle can be used to describe the position of X with respect to the metallacycle (Figure 2.14). The Si···Bi-X angle is significantly larger for **17** and **18** compared to the chloride and phenyl derivatives, indicating that the X substituent sits further from the bismuth centre. Increased Si···Bi-X angles coincide with larger sum of angles about bismuth ($\sum_{Bi}$ values), and therefore greater planar character of the bismuth centre (smaller degree of pyramidalisation (DOP)).

Figure 2.14: Representation of the Si-Bi-X bond angle in determining the position of X.

Another measurement that can be used to compare where X sits with respect to the $Me_2Si\{NAr\}_2Bi$ unit is θ, the difference between N-Bi-X angles, measuring how far X sits to one side of the molecule (Figure 2.15). Positive θ values correspond to anti-clockwise shift of X, while negative θ values correspond to clockwise shift.

Figure 2.15: Representation of positive shift of θ.

While chloride, phenyl and amide derivatives do not experience large distortions, significant deviations are observed for the phosphide and aryloxide derivatives. **17** exhibits a large clockwise shift in the position of the oxygen atom (θ = -9.82°), resulting in it being situated closer to N(2) than N(1). The PCy_2 group of **18** is rotated in the opposite direction, exhibiting a large anti-cloackwise shift in the position of the phosphorus atom (θ = -7.21°).

Table 2.6: Comparison of selected bond lengths and angles within Bi(Me$_2$Si{NAr}$_2$)X complexes

	X = Cl, **9**[a,b]	Ph, **14**[b]	N{SiMe$_3$}$_2$, **16**[a,b]	O-2,6-t-Bu$_2$C$_6$H$_3$, **17**	PCy$_2$, **18**
Bi-X bond length (Å) (%$_{cov}$ (%)[c])	2.552 (102)	2.253 (102)	2.187 (99.9)	2.142(2) (100)	2.680(1) (105)
Bite angle (°)	71.26	70.68	71.19	71.63(10)	70.13(6)
Bi-N bond length (Å)	2.132, 2.144	2.170, 2.178	2.166, 2.193	2.136(2), 2.188(3)	2.202(2), 2.261(2)
$\sum_N$ (°)	359.0, 359.8	354.4, 358.7	353.6, 353.2	348.3, 359.6	349.5, 356.5
Si$\cdots$Bi-X (°)	94.84	101.69	109.96	104.41(6)	106.43(2)
$\sum_{Bi}$ (°) (DOP (%)[d])	264.9 (106)	269.0 (101)	280.5 (88.3)	273.7 (95.9)	275.6 (93.8)
θ (°)[e]	0.388	1.345	-0.004	-9.82	7.21

[a]Literature values[62], [b]Average values of all molecules in the unit cell, [c]Percentage of the sum of covalent radii[113] (%$_{cov}$) = [Bi-X/Σr$_{cov}$] x 100. [d]Degree of pyramidalisation (DOP, %) = [360-Σ_{Bi}]/0.9; DOP = 100 % is equivalent to Σ_{Bi} = 270°, DOP = 0% = planar geometry.[e]θ = difference in N-Bi-X bond angles within the molecule.

2.4.4 Insertion of RN=C=Y (R = *i*-Pr, Cy or Ph, Y = NR or O) into Bi-N and Bi-P bonds

Insertion of unsaturated substrates into Bi-X bonds remains relatively unexplored, with few examples reported in the literature. A series of reactions were performed to investigate the reactivity of compounds containing Bi-N and Bi-P bonds towards the insertion of heterocummulenes. ^{1}H and ^{31}P NMR spectroscopy was used to monitor the insertion reactions.

Reaction of 16 and Bi(N{SiMe$_3$}$_2$)$_3$ with *N,N'*-dicyclohexylcarbodiimide

The NMR scale reaction of the homoleptic species Bi(N{SiMe$_3$}$_2$)$_3$ with three equivalents of *N,N'*-dicyclohexylcarbodiimide in C$_6$D$_6$ affords a new species after 10 minutes at room temperature. Analysis of the ^{1}H NMR spectrum indicates the presence of significant quantities of unreacted *N,N'*-dicyclohexylcarbodiimide, represented by the α-cyclohexyl proton resonance at δ_H 3.15 ppm. Resonances at δ_H 0.34 and 3.38 ppm correspond to the SiMe$_3$ and α-cyclohexyl protons of a new species. Integration of the α-cyclohexyl resonances indicates a 2:1 ratio of *N,N'*-dicyclohexylcarbodiimide to the new species. These results are consistent with mono-insertion into Bi(N{SiMe$_3$}$_2$)$_3$ to form Bi({SiMe$_3$}$_2$NC{NCy})(N{SiMe$_3$}$_2$)$_2$.

Repeating this reaction on a preparative scale, using one equivalent of *N,N'*-dicyclohexylcarbodiimide, results in complete consumption of the starting materials and formation of the mono-insertion product (eq. 2.8). Resonances at δ_H 3.38, 0.37 and 0.34 ppm correspond to the α-cyclohexyl, guanidinate SiMe$_3$ and amido SiMe$_3$ protons, respectively.

eq. 2.8: Reaction of Bi(N{SiMe$_3$}$_2$)$_3$ with *N,N'*-dicyclohexylcarbodiimide.

The reaction of *N,N'*-dicyclohexylcarbodiimide with **16** in C_6D_6 did not result in insertion of the carbodiimide into the Bi-N{SiMe$_3$}$_2$ bond, even when heated to 80 °C for 24 hours (eq. 2.9). This may reflect the significant steric protection provided by the di(amido) ligand.

eq. 2.9: Reaction of **16** with *N,N'*-dicyclohexylcarbodiimide.

The lack of insertion with **16** also contrasts with a recent result by Roesky and co-workers, where insertion of *N,N'*-diisopropylcarbodiimide and phenyl isocyanate into the Bi-NMe$_2$ bond of Bi(1,8-C$_{10}$H$_6${NSiMe$_3$})(NMe$_2$) was observed (*vide supra*).[61] This is due to significant differences in the steric profile of the ligands. Indeed, analysis of the solid-state structure of (1,8-C$_{10}$H$_6${NSiMe$_3$})BiNMe$_2$ indicates that the bismuth sits well below the plane of the metallacycle and the SiMe$_3$ groups point above the plane of the metallacycle. This contrasts with the solid-state structure of **16**, where the bismuth is held in the plane of the metallacycle and the N-aryl substituents sit much closer.[62]

Reaction of 18 with *N,N'*-dicyclohexylcarbodiimide and phenyl isocyanate

The NMR scale reaction of **18** with one equivalent of *N,N'*-dicyclohexylcarbodiimide in C_6D_6 did not result in the corresponding insertion product, with no consumption of starting materials even when heated to 80 °C for 2 hours (eq. 2.10). This is analogous to the lack of reactivity observed for **16**.

The NMR scale reaction of **18** with one equivalent of phenyl isocyanate, however, resulted in quantitative consumption of starting materials and formation of a new

eq. 2.10: Reaction of **18** with *N,N'*-dicyclohexylcarbodiimide

species. The ^{1}H NMR spectrum of the reaction shows two resonances corresponding to the SiMe$_2$ (δ_H 0.54 and 0.04 ppm), shifted from **18**. The *iso*-propyl methine and α-cyclohexyl protons appear as a single set of broad signals (δ_H 4.31 and 3.89 ppm, respectively), significantly downfield from **18**. This is consistent with identical environments for the N-aryl substituents, suggesting insertion into Bi-N bonds is not occurring. The ^{31}P NMR spectrum shows a single resonance at δ_P 0.2 ppm, significantly upfield compared to **18**. These data provide preliminary evidence for the formation of the Bi-P insertion product (eq. 2.11). Further work is ongoing to definitively establish the structure of this new product.

eq. 2.11: Reaction of **18** with phenyl isocyanate.

2.4.5 Catalytic Ring-Opening Polymerisation of Lactide and ϵ-Caprolactone by 16 and 17

Bismuth compounds containing Bi-O bonds form highly active initiators for the ring-opening polymerisation (ROP) of cyclic esters (*vide supra*). A series of NMR scale reactions were performed to investigate whether amide **16** and aryloxide **17**

are active initiators for the ROP of rac-lactide and ε-caprolactone. Catalytic studies were performed at 80 °C, using a catalyst loading of 1 mol%. Reactions were monitored over time using ^{1}H NMR spectroscopy.

Compounds **16** and **17** were both found to be active as initiators for the ring-opening polymerisation of lactide and ε-caprolactone, albeit much slower than the current industry standard (Sn(Oct)_2).[84] Similar activities were observed for both species, showing complete conversion of starting materials within 72 hours when heated to 80 °C (Figure 2.16).

Figure 2.16: ROP of lactide and ε-caprolactone initiated by **16** and **17**.

The polymerisation is significantly slower than the rate observed for the single site bismuth catalyst Bi(cy-salen)(OAr') (Ar'= 2,6-t-Bu$_2$C$_6$H$_3$), where $\sim$70 % conversion of monomer was observed after 1h at room temperature.[83] The slower rate observed for **16** and **17** may reflect an increased steric profile around the bismuth centre.

2.5 Synthesis of Bismuth Compounds Supported by Di(amido)ether Ligands

A class of ligand that is closely related to the di(amido)silyl ligands investigated in this research is the di(amidosilyl)ether ligand, $[O(SiMe_2NR)_2]^{2-}$ (Figure 2.17).

Figure 2.17: Divalent di(amido)ether ligand $[O(SiMe_2NR)_2]^{2-}$.

These ligands have recieved little attention despite their tunability and stabilising properties. Compared to the di(amido)silyl ligand, these ligands provide significantly more flexibility in the OSi_2 backbone, and can be considered isostructural to the commonly employed β-diketiminate (BDI) ligand. In contrast to the di(amido)silane ligands, upon ligation to a metal, the R substituents point forward from the nitrogen substituents to provide significantly more steric protection to the metal centre, a result of the reduced ring strain associated with the 6-membered metallacycle.

Figure 2.18: Differing positions of the R substituents in 6- and 4-membered metallacycles.

Both bi-dentate (Figure 2.19, A and B) and tri-dentate (C) (via coordination through the O) bonding modes have been observed, with the latter occurring frequently in actinide compounds.[114,115]

The synthesis for a number of derivatives containing bulky R groups has been reported. Bochmann and co-workers reported the synthesis of the alkyl derivatives $O(SiMe_2NHR)_2$ (R = Cy and t-Bu) from the addition of $O(SiMe_2Cl)_2$ to a solution

Figure 2.19: Observed bonding modes of divalent, di(amido) ether ligands.

containing four equivalents of the corresponding amine at 0 °C (Figure 2.20, pathway (a)). The excess amine acts as a base to remove two equivalents of HCl as the ammonium salt. Alternatively, aryl derivatives (R = 2,6-i-Pr$_2$C$_6$H$_3$ (**19a**), 2,4,6-Me$_3$C$_6$H$_2$, 3,5-(CF$_3$)$_2$C$_6$H$_3$) have been synthesised through the reaction of O(SiMe$_2$Cl)$_2$ with two equivalents of the corresponding lithium amide at -80 °C (pathway (b)).[96]

Figure 2.20: Synthesis of di(amido)ether ligands.

This section focusses on the use of the 2,6-i-Pr$_2$C$_6$H$_3$ (**19a**) and 2,6-Me$_2$C$_6$H$_3$ (**19b**) derivatives for the stabilisation of bismuth compounds.

2.5.1 Synthesis of O{Me$_2$SiNHAr"}$_2$ (Ar" = 2,6-i-Pr$_2$C$_6$H$_3$ (19a), 2,6-Me$_2$-C$_6$H$_3$ (19b))

19a was synthesised according to the literature procedure.[96] **19b** was synthesised via an analogous method through the generation of the lithium amide salt LiNHAr" (Ar" = 2,6-Me$_2$C$_6$H$_3$) followed by the *in situ* reaction with 0.5 equivalents of O(SiMe$_2$Cl)$_2$ (eq. 2.12). The reaction proceeded cleanly, yielding pure **19b** as a colourless oil after work-up.

The ^{1}H NMR spectrum of **19b** displays two singlets at δ_H 2.22 and 0.09 ppm,

$$2\ NH_2Ar'' \quad \xrightarrow[\text{(ii) } O(SiMe_2Cl)_2]{\text{(i) } 2.2\ n\text{-BuLi}} \quad \text{[O(SiMe}_2\text{NHAr'')}_2\text{]} \quad + \quad 2\ LiCl$$
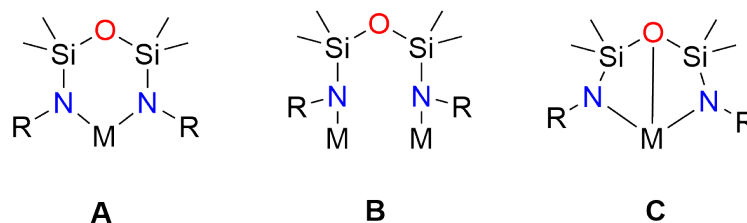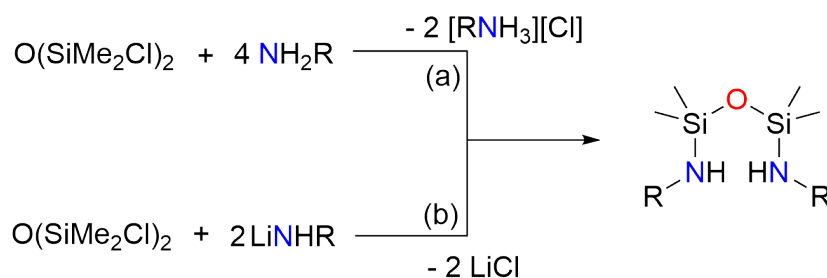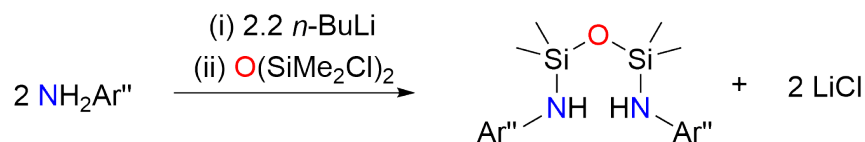
Ar" = 2,6-i-Pr$_2$C$_6$H$_3$ (**19a**), 2,6-Me$_2$C$_6$H$_3$ (**19b**)

eq. 2.12: Synthesis of O(SiMe$_2$NHAr")$_2$.

corresponding to the o-Me and SiMe$_2$ protons, respectively. The ^{13}C NMR spectrum is also consistent with formation of **19b**, with a single high field resonance at δ_C 0.8 ppm corresponding to the SiMe$_2$ carbons. The mass spectrum of **19b** displays a peak at m/z 373.21 corresponding to $[O\{Me_2SiNHAr''\}_2 + H]^+$. The base peak at m/z 122.10 is consistent with $[Ar''NH_3]^+$ via cleavage of the N-Si bond.

2.5.2 Synthesis of Bi(O{Me$_2$SiNAr"}$_2$)Cl (Ar" = 2,6-i-Pr$_2$C$_6$H$_3$ (20a) and 2,6-Me$_2$C$_6$H$_3$ (20b))

The reaction of **19a** or **19b** with 2.2 equivalents of n-BuLi to generate the corresponding di-lithium salt, followed by an *in situ* reaction with BiCl$_3$ resulted in formation of the corresponding di(amido) bismuth chloride species, Bi(O{Me$_2$SiNAr"}$_2$)Cl (Ar" = 2,6-^{i}Pr$_2$C$_6$H$_3$ (**20a**), 2,6-Me$_2$C$_6$H$_3$ (**20b**)) (eq. 2.13). Clear colourless crystals of **20a** were obtained from a toluene/hexane solution at -30 °C. Attempts to isolate **20b** were unsuccessful, however enough sample was obtained to investigate the ^{1}H NMR spectrum. Previous work in the Coles group has characterised **20b** in the solid-state.[iii]

The ^{1}H NMR spectrum of **20a** displays two singlets for the SiMe$_2$ protons (δ_H 0.60 and 0.20 ppm). The *iso*-propyl methine protons are represented by two distinct septets at δ_H 4.22 and 3.66 ppm. Four doublets are displayed for the *iso*-propyl methyl protons (δ_H 1.45, 1.28, 1.26, and 1.05 ppm), resulting from the combination

---

[iii]20b exists as a monomer in the solid state, with the di(amido)ether coordinated in a bidentate fashion to form a six-membered metallacycle. The metallacycle has a boat conformation. No NMR or elemental analysis data were obtained.[116]
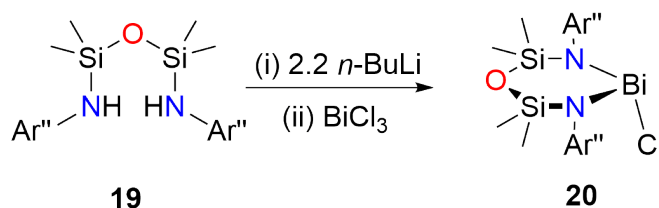
eq. 2.13: Synthesis of Bi(O{Me$_2$SiNAr"}$_2$)Cl (Ar" = 2,6-i-Pr$_2$C$_6$H$_3$ (**20a**) and 2,6-Me$_2$C$_6$H$_3$ (**20b**))

of a pyramidal bismtuh centre and restricted rotation. At low temperatures, **9** displayed a similar splitting pattern, forming four doublets for the *iso*-propyl methyl protons.[95]

The ^{13}C NMR spectrum is consistent with the formation of **20a**, showing two sets of resonances for the N-aryl substituents. The SiMe$_2$ carbons are represented by two high field resonances at δ_C 4.5 and 3.2 ppm. The ^{29}Si NMR spectrum of **20a** has a single resonance at δ_{Si} 5.9 ppm, significantly downfield from previously synthesised bismuth compounds containing the related [Me$_2$Si{NAr}$_2$]$^{2-}$ ligand (range of δ_{Si} = 16.4 to 38.0 ppm, *vide supra*). Elemental analysis data is consistent with the calculated values for **20a**.

The ^{1}H NMR for **20b** is consistent with formation of a pyramidal bismuth centre, represented by two singlets corresponding to the SiMe$_2$ protons (δ_H 0.59 and 0.17 ppm). The shifts of these two peaks appear close to those observed for **20a**. The *o*-Me protons are also represented by two singlets at δ_H 2.73 and 2.46 ppm.

Single crystal X-ray crystallography revealed that **20a** crystallises in the $P\bar{1}$ space group (Figure 2.21). **20a** crystallises as a three-coordinate monomeric chloride, with the bismuth centre forming a trigonal pyramidal geometry (sum of angles = 293.26°). The ligand binds to the bismuth in a bidentate chelate fashion to give a six-membered metallacycle in the chair conformation. This contrasts with the solid-state structure of **20b**, where the metallacycle adopts a boat conformation, with the O and Bi atoms occupying the same face of the molecule.[iii]
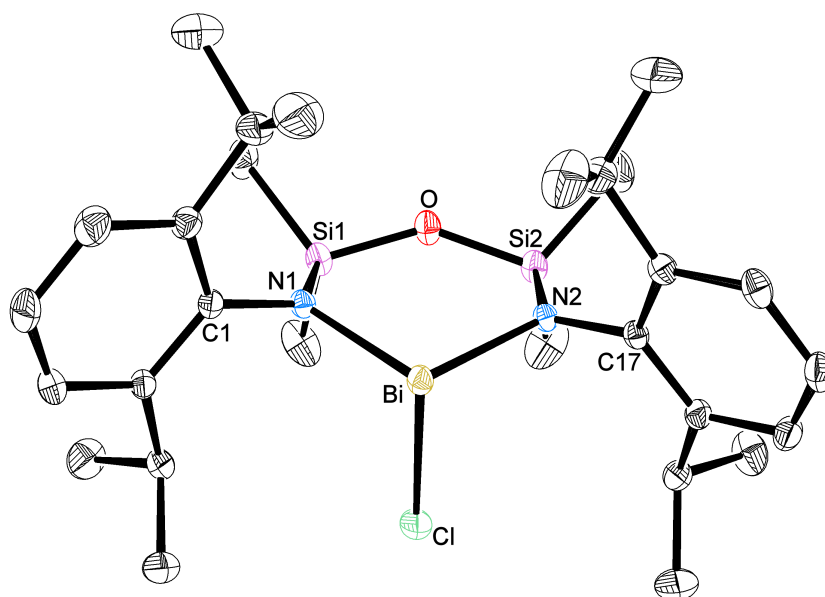
Figure 2.21: ORTEP representation of **20a**. 30% Thermal ellipsoid. Hydrogens omitted for clarity. Selected bond lengths (Å) and angles (°) are reported in Table 2.7.

Table 2.7: Selected bond lengths (Å) and angles (°) in **20a**.

Bi-Cl	2.5033(10)	N(1)-Bi-N(2)	102.47(9)
Bi-N(1)	2.136(2)	Si(1)-O-Si(2)	142.92(18)
Bi-N(2)	2.149(2)	Bi-N(1)-C(1)	111.91(17)
N(1)-Si	1.731(3)	Bi-N(2)-C(17)	109.70(18)
N(2)-Si	1.718(3)	Bi-N(1)-Si(1)	121.55(12)
O-Si(1)	1.631(2)	Bi-N(2)-Si(2)	122.34(13)
O-Si(2)	1.633(2)	N(1)-Bi-Cl	96.50(9)
Bi-O	3.395(2)	N(2)-Bi-Cl	94.31(9)

As expected, the bite angle of the di(amido) ligand (102.47(9)°) is much larger than that observed for $[Me_2Si\{NAr\}_2]^{2-}$ (range = 70.13° - 71.63°) , consistent with the reduced ring strain. In contrast to **9**, the bulky aryl groups project forward from the ligand backbone due to the reduced strain associated with the 6-membered metallacycle. This is represented by acute Bi-N-C_{aryl} bond angles (N(1) 109.69(17)°; N(2) 111.93(18)°), much smaller than the angles observed in **9** (range = 121.7(5)° - 129.1(5)°).[95]

The Bi-Cl (2.5033(10) Å) and Bi-N bond distances (N(1) 2.136(2); N(2) 2.149(2) Å) are consistent with σ-bonding interactions and are within the range observed in **9** (range Bi-Cl = 2.4857(16) - 2.556(1) Å); Bi-N = 2.132(3) - 2.181(3) Å). The Bi-O distance (3.395(2) Å) is significantly longer than observed in systems where the ligand binds tri-dentate (2.479(12) - 2.529(17) Å)[114,115] and is closer to the distances observed in bi-dentate bonding modes (3.025(4) - 3.229(7) Å),[117,118] suggesting that the oxygen atom is not participating in coordination. The geometry at both N(1) and N(2) is planar (sum of angles = 359.9°in both cases).

2.5.3   Reaction of 20a with AlCl$_3$

The reaction of one equivalent of **20a** with AlCl$_3$ in toluene results in formation of a deep red solution after 2 hours stirring at room temperature. Concentration of the solution followed by storage at -30 °C resulted in the formation of deep red crystals of [Bi(O{Me$_2$SiNAr"}$_2$)][AlCl$_4$] (**21**) (eq. 2.14).
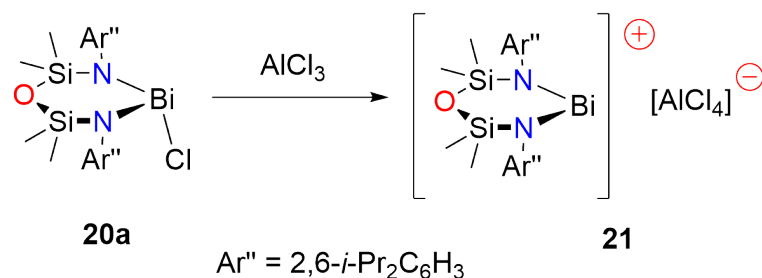
eq. 2.14: Reaction of **20a** with AlCl$_3$

The ^{1}H NMR spectrum of **21** shows loss of the C_S symmetry, most clearly evident from a single set of resonances for the SiMe$_2$ and *iso*-propyl methine protons (δ_H 0.22 and 3.42 ppm, respectively). This is consistent with formation of a C_{2h} symmetric cation. A single molecule of toluene is also observed in the ^{1}H NMR spectrum. The ^{13}C NMR spectrum is consistent with the formation of **21**, displaying a single set of resonances for each of the carbon environments. A single high field resonance is observed at δ_C 3.8 ppm, corresponding to the SiMe$_2$ carbon centres.

Compound **21** crystallises in the $P\bar{1}$ space group as a monomeric four-coordinate

bismuth species (Figure 2.22). A single toluene molecule interacts with the bismuth centre through π-interactions (Bi$\cdots$centroid distance = 3.2414(9) Å) with significant slippage with respect to the bismuth (0.51 Å). Interestingly, interaction with the toluene molecule appears to be more favourable than forming dimeric/polymeric structures with multiple Bi$\cdots$Cl-Al bridging chlorides as observed in the di(amido) bismuth tetrachloroaluminate salts described elsewhere in this thesis. The toluene molecule occupies the apical position, where the stereochemically active lone pair would be expected.
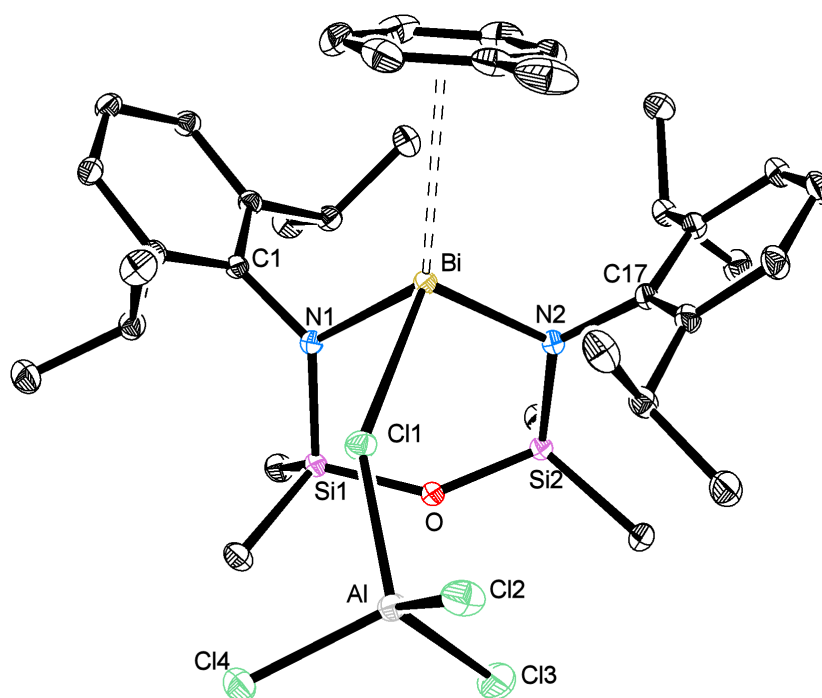
Figure 2.22: ORTEP representation of [**21**].toluene. 30% Thermal ellipsoid. Hydrogens omitted for clarity. Selected bond engths (Å) and angles (°) are reported in Table 2.8.

The bismuth centre adopts a tetrahedral geometry with the ligand coordinating in a bidentate chelate fashion. The 6-membered metallacycle adopts a boat conformation with the Bi and O atoms occupying the same face of the ring. This contrasts with the chair conformation observed in **20a** (Figure 2.23). The Bi-O distance (3.2492(11) Å) is significantly shorter than that observed for **20a**, however it is still not within the range for tri-dentate coordination and may be a reflection of the change of the metallacycle from the chair to boat conformation.

Table 2.8: Selected bond lengths (Å) and angles (°) in **21**.

Bi-Cl(1)	3.0708(4)	O-Si(1)	1.6405(11)
Bi-N(1)	2.1136(12)	O-Si(2)	1.6832(11)
Bi-N(2)	2.1111(12)	Bi-O	3.2492(11)
N(1)-Si(1)	1.7499(13)	N(1)-Bi-N(2)	100.29(5)
N(2)-Si(2)	1.7632(13)	Si(1)-O-Si(2)	138.90(7)
Al-Cl(1)	2.1900(6)	Al-Cl(3)	2.1134(7)
Al-Cl(2)	2.1290(6)	Al-Cl(4)	2.1214(6)
Bi-centroid	3.2414(9)		

Figure 2.23: ORTEP representation of the metallacycles for **20a** (left) and **21** (right). 30% Thermal ellipsoid.

The Bi-N bond distances (N(1) 2.1136(12) Å; N(2) 2.1111(12) Å) are significantly shorter than the Bi-N bond distances in **20a**, consistent with formation of a cationic bismuth centre. Both N(1) and N(2) retain planarity (sum of angles = 358.9°and 359.9°, respectively), with the aryl substituents again pointing forward from the metallacycle, represented by acute Bi-N-C$_{aryl}$ angles.

The Bi-Cl bond length (3.0708(4) Å) is significantly longer than that observed in the neutral chloride **20a** (2.5033(10) Å) and similar to that observed in **12a** (shortest Bi$\cdots$Cl distance = 2.953(3) Å). The Al-Cl(1) bond length (2.1900(6) Å) is significantly longer than the other Al-Cl bonds (2.1134(8) - 2.1290(7) Å), consistent with the bridging interaction.

Elemental analysis data is consistent with the calculated values for **21** without the toluene molecule. This indicates that the toluene molecule can be lost relatively easily under reduced pressure.

Chapter 3

Conclusion

The coordination chemistry of mono- and di-anionic ligands derived from $Me_2Si\{NHAr\}_2$ has been explored through the synthesis of a number of bismuth compounds.

The monovalent derivative $Bi(Me_2Si\{NAr\}\{NHAr\})Cl_2$ (**11**) has been synthesised from the reaction of $Me_2Si\{N(M)Ar\}\{NHAr\}$ (M = Na (**10a**), K (**10b**)) with $BiCl_3$.

The reaction of $Bi(Me_2Si\{NAr\}_2)Cl$ (**9**) with ECl_3 (E = Al, Ga) results in formation of the cationic bismuth species $[Bi(Me_2Si\{NAr\}_2)]^+$ as the corresponding tetrachlorometallate salt (E = Al (**12a**), Ga (**12b**)). Attempts to isolate the tetrachlorogallate salt resulted in isolation of $[\{Bi(Me_2Si\{NAr\}_2)\}_2(\mu\text{-}Cl)][GaCl_4]$ (**13b**), confirmed by single crystal X-ray crystallography. Attempts to isolate $[Bi(Me_2Si\{NAr\}_2)]^+$ as the tetraphenylborate and tetraethylborate salts were unsuccessful, resulting in abstraction of the aryl/alkyl group from the borate anion to form $Bi(Me_2Si\{NAr\}_2)Ph$ (**14**) and $Bi(Me_2Si\{NAr\}_2)Et$ (**15**), respectively.

A number of derivatives of the general form $Bi(Me_2Si\{NAr\}_2)X$ (X = $N\{SiMe_3\}_2$ (**16**), O-2,6-t-$Bu_2C_6H_3$ (**17**), PCy_2 (**18**)) have been synthesised from the reaction of **9** with the corresponding group 1 salt MX (M = Li or K, X = $N\{SiMe_3\}_2$, O-2,6-t-$Bu_2C_6H_3$, PCy_2). The amide (**16**) and aryloxide (**17**) derivatives were active

as initiators for the catalytic ROP of cyclic esters. In addition, insertion of *N,N'*-dicyclohexylcarbodiimide into Bi-N or Bi-P bonds was investigated where as no reaction was observed for compounds **16** and **18**, attributed to the steric bulk of the ligand. Preliminary results suggest insertion of phenyl isocyanate into the Bi-P bond of **18** was achieved.

Finally, a number of bismuth compounds supported by the related di(amido)ether ligands [O{Me$_2$SiNAr"}$_2$]$^{2-}$ (Ar" = 2,6-*i*-Pr$_2$C$_6$H$_3$ (**19a**)) have been synthesised. The di(amido)ether complex Bi(O{Me$_2$SiNAr"}$_2$)Cl (**20a**) was synthesised from the reaction of O{Me$_2$SiNHAr"}$_2$ with 2.2 equivalents of *n*-BuLi followed by the *in situ* reaction with BiCl$_3$. Attempts to isolate and fully characterise the 2,6-Me$_2$C$_6$H$_3$ derivative were unsuccessful. Further derivitisation of **20a** by reaction with AlCl$_3$ resulted in formation of the cationic species [Bi(O{Me$_2$SiNAr"}$_2$)]$^+$ as the tetra-chloroaluminate salt (**21**).

Chapter 4

Experimental

4.1   General Procedures

All manipulations were performed under a dry and oxygen-free atmosphere of N_2 using Schlenk-line and cannula techniques, or in a conventional nitrogen glovebox. Solvents were dried using a Puresolv. system (Innovative Technologies). NMR spectra were recorded in C_6D_6 at 298K using either a Bruker Avance DPX 300 MHz at 300.1 (^{1}H) and 75.4 (^{13}C) MHz or a Varian VNMRS 500 MHz spectrometer at 500.1 (^{1}H), 160.4 (^{11}B), 125.4 (^{13}C) and 99.3 (^{29}Si) MHz. All ^{1}H and ^{13}C chemical shifts are referenced internally to residual solvent resonances. ^{29}Si NMR chemical shifts were obstained from ^{1}H-^{2}9Si *HMBC* spectra. Elemental analyses were performed by S. Boyer at London Metropolitan University. All compounds were purchased from the Sigma-Aldrich chemical company and used as received, unless stated otherwise. Liquids were subjected to 3x freeze-pump-thaw cycles, and stored under nitrogen in the glovebox. $Me_2Si\{NHAr\}_2$ (**8**)[94], $Bi(Me_2Si\{NAr\}_2)Cl$ (**9**)[95], $Bi(Me_2Si\{NAr\}_2)(N\{SiMe_3\}_2)$ (**16**)[62], $O(SiMe_2NHAr")_2$ ($Ar" = 2,6-i-Pr_2C_6H_3$) (**19a**)[96] and $Bi(N\{SiMe_3\}_2)_3$[119] were synthesised according to literature procedures. $BiCl_3$ was sublimed before use. 2,6-diisopropylaniline and 2,6-dimethylaniline were distilled before use.

4.1.1 Crystal Structure Data

X-ray diffraction data (Appendix C) were collected by the X-ray Crystallography Laboratory at the University of Canterbury using an Agilent SuperNova diffractometer fitted with an Atlas detector. Crystals were covered in inert oil and suitable single crystals were selected. Data was collected at 120.01(10)K using Mo Kα radiation at 0.71073 Å or Cu Kα radiation at 1.5418 Å. The structures were solved and refined using Olex2. ORTEP representations were prepared using ORTEP-III.[47]

4.2 Experimental for Section 2.2

4.2.1 Me$_2$Si{N(Na.(THF)$_3$)Ar}{NAr} (10a.(THF)$_3$)

A solution of **8** (0.30 g, 0.73 mmol.) in toluene (5 mL) was added dropwise to a suspension of NaH (0.017 g, 0.73 mmol.) in toluene (10 mL). The resulting suspension was stirred for 24 hours followed by removal of the volatiles *in vacuo*. The white precipitate was dissolved in THF (5 mL), filtered through celite and concentrated. Clear colourless crystals of **10a** were obtained after storage of the solution at -30 °C for 24 hours. Yield 0.224 g, 48 %.

^{1}H NMR (C$_6$D$_6$, 300 MHz) δ 7.20 (d, J_{HH} = 7.5 Hz, 2H, *m*-C$_6$H$_3$), 7.11 (d, J_{HH} = 7.5 Hz, 2H, *m*-C$_6$H$_3$), 6.93 (t, J_{HH} = 7.5 Hz, 1H, *p*-C$_6$H$_3$), 6.85 (t, J_{HH} = 7.8 Hz, 1H, *p*-C$_6$H$_3$), 4.23 (sept, J_{HH} = 6.9 Hz, 2H, C*H*(CH$_3$)$_2$), 3.87 (sept, J_{HH} = 6.9 Hz, 2H, C*H*(CH$_3$)$_2$), 3.41 (m, 12H, THF-C*H₂*), 3.18 (s, 1H, N-H), 1.39-1.25 (m, 28H, CH(C*H₃*)$_2$ and THF-C*H₂*), 0.47 (s, 6H, Si*Me₂*).

^{13}C NMR (C$_6$D$_6$, 75 MHz) δ 144.1, 142.3, 141.4, 123.1, 122.9, 121.6, 114.6 (*C₆*H$_3$*), 68.0 (THF-*C*H$_2$), 28.6, 28.4, 27.1, 25.7, 25.2, 24.1, 23.8 (*C*H(CH$_3$)$_2$, CH(*C*H$_3$)$_2$ and THF-*C*H$_2$), 4.7 (Si*Me₂*). *one of the aromatic resonances is not observed

4.2.2 Me$_2$Si{N(K)Ar}{NAr} (10b)

A solution of **8** (0.30 g, 0.73 mmol.) in toluene (10 mL) was added dropwise to a suspension of KH (0.030 g, 0.73 mmol.) in toluene (5 mL). The suspension was stirred for 24 hours followed by filtration through celite. The resulting solution was concentrated and stored at -30 °C. After 24 hours, clear colourless crystals of **10b** were obtained. Yield 0.170 g, 52 %

^{1}H NMR (C$_6$D$_6$, 300 MHz) δ 7.07 (d, J_{HH} = 7.2 Hz, 2H, C$_6$H$_3$), 6.86 (d, J_{HH} = 7.2 Hz, 2H, C$_6$*H$_3$*), 6.68, 6.63 (overlapping t, 2H, *p*-C$_6$*H$_3$*), 3.85, 3.78 (overlapping sept, 4H, C*H*(CH$_3$)$_2$), 3.08 (s, 1H, N-H), 1.27-1.12 (m, 24H, CH(C*H$_3$*)$_2$), 0.56 (s, 6H, Si*Me$_2$*).

^{13}C NMR (C$_6$D$_6$, 75 MHz) δ 154.5, 146.3, 143.2, 140.8, 123.3, 122.7, 120.8, 112.9 (*C$_6$*H$_3$), 28.7, 26.5, 25.3, 23.5, 23.3 (*C*H(CH$_3$)$_2$ and CH(*C*H$_3$)$_2$), 5.9 (Si*Me$_2$*).

^{29}Si NMR (C$_6$D$_6$, 99.3 MHz) δ -32.1.

4.2.3 Bi(Me$_2$Si{NHAr}{NAr})Cl$_2$ (11)

Method 1: From the reaction of **10a**.(THF)$_3$ with BiCl$_3$

A solution of **10a**.(THF)$_3$ (0.15, 0.23 mmol.) in Et$_2$O (5 mL) was added dropwise to a suspension of BiCl$_3$ (0.073 g, 0.23 mmol.) in Et$_2$O (5 mL) at -30 °C. The resultant suspension was stirred for 24 hours at room temperature followed by filtration through celite and concentration of the solution. After 24 hours at -30 °C, a yellow precipitate began to form, identified as **11**. Yield 0.065 g, 41 %.

Method 2: From the reaction of **10b** with BiCl$_3$

A solution of **10b** (0.10 g, 0.22 mmol.) in Et$_2$O (5 mL) was added dropwise to a suspension of BiCl$_3$ (0.070 g, 0.22 mmol.) in Et$_2$O (5 mL) at -30 °C. The resultant suspension was stirred for 24 hours at room temperature followed by filtration

through celite and concentration of the solution. After 24 hours at -30 °C, a yellow precipitate began to form, identified as **11** by ^{1}H NMR spectrscopy. Yield 0.051 g, 34 %.

Method 3: From the *in situ* reaction of 'Me$_2$Si{N(Li)Ar}{NHAr}' with BiCl$_3$

A solution of *n*-BuLi (0.17 mL of 1.6M solution in hexane, 0.27 mmol.) in Et$_2$O (5 mL) was added dropwise to a stirring solution of **8** (0.10 g, 0.24 mmol.) in Et$_2$O (5 mL) at -30 °C. The resulting solution was allowed to stir for 5 hours at room temperature and then added to a suspension of BiCl$_3$ (0.077 g, 0.20 mmol.) in Et$_2$O (10 mL). The suspension was filtrated through celite and concentrated. After 24 hours at -30 °C, a yellow precipitate was deposited, identified as **11** by ^{1}H NMR spectroscopy. Yield 0.063 g, 38 %.

Anal. Calcd. for C$_{26}$H$_{41}$BiCl$_2$N$_2$Si (*688.22*): C, 45.29; H, 5.99; N, 4.06 %. Found: C, 45.43; H, 5.87, N 4.15 %.

^{1}H NMR (C$_6$D$_6$, 300 MHz) δ 7.33 (d, J_{HH} = 7.8 Hz, 2H, *m*-C$_6$*H$_3$*), 7.00 (s, 3H, C$_6$*H$_3$*), 6.77 (t, J_{HH} = 7.8 Hz, 1H, *p*-C$_6$*H$_3$*), 4.61 (s, 1H, N-H), 3.79 (sept, J_{HH} = 6.9 Hz, 2H, C*H*(CH$_3$)$_2$), 3.26 (sept, J_{HH} = 6.9 Hz, 2H, C*H*(CH$_3$)$_2$), 1.49 (d, J_{HH} = 6.9 Hz, 6H, CH(C*H$_3$*)$_2$), 1.39 (dd, J_{HH} = 6.9 Hz, 6H, CH(C*H$_3$*)$_2$), 1.10 (d, J_{HH} = 6.9 Hz, 12H, CH(C*H$_3$*)$_2$), 0.1 (s, 6H, Si*Me$_2$*).

^{13}C NMR (C$_6$D$_6$, 75 MHz) δ 150.2, 141.3, 137.6, 136.4, 124.9, 124.1, 122.9 (*C$_6$*H$_3$*), 29.2, 28.2, 27.5, 25.7, 25.1, 24.5 (*C*H(CH$_3$)$_2$ and CH(*C*H$_3$)$_2$) , 3.8 (Si*Me$_2$*). *one of the aromatic resonances is not observed

4.2.4 Reaction of 11 with NEt$_3$

NEt$_3$ (4 μL, 0.029 mmol.) was added to a J. Young NMR tube charged with a solution of **11** (0.02, 0.029 mmol.) in C$_6$D$_6$. The reaction mixture was heated to 80 °C for 24 hours followed by ^{1}H NMR analysis. The ^{1}H NMR showed no consumption

of starting materials.

4.2.5 Reaction of 11 with *n*-BuLi

A solution of *n*-BuLi in hexane (18.1 μL of a 1.6M hexane solution, 0.029 mmol.) was added to a solution of **9** (0.020, 0.029 mmol.) in C_6D_6 at -30 °C. ^{1}H NMR analysis after 10 minutes at room temperature revealed formation of an unidentifiable mixture of products.

4.3 Experimental for Section 2.3

4.3.1 [Bi(Me$_2$Si{NAr}$_2$)][AlCl$_4$] (12a)

A solution of **9** (0.1 g, 0.15 mmol.) in toluene (5 mL) was added dropwise to a stirring suspension of AlCl$_3$ (0.019 g, 0.15 mmol.) in toluene (5 mL). The resulting dark red solution was allowed to stir for 4 hours followed by concentration of the solution and storage at -30 °C. After 24 hours, clear dark red crystals of **12a** were obtained. Yield 0.105 g, 88 %

Anal. Calcd. for $C_{26}H_{40}AlBiCl_4N_2Si$ (*786.47*): C, 39.71; H, 5.13; N, 3.56 %. Found: C, 39.85; H, 5.01, N 3.68 %.

^{1}H NMR (C_6D_6, 300 MHz) δ 7.26 (d, J_{HH} = 7.8 Hz, 4H, *m*-C$_6$*H$_3$*), 6.60 (t, J_{HH} = 7.7 Hz, 2H, *p*-C$_6$*H$_3$*), 3.49 (br m, 4H, C*H*(CH$_3$)$_2$), 1.21 (br s, 24H, CH(C*H$_3$*)$_2$), 0.13 (s, 6H, Si*Me$_2$*).

^{13}C NMR (C_6D_6, 75 MHz) δ 148.5, 128.8, 122.5 (*C$_6$*H$_3$), 28.2 (*C*H(CH$_3$)$_2$), 27.0 (br, CH(*C*H$_3$)$_2$), 10.4 (Si*Me$_2$*). * *o*-C not observed.

^{29}Si NMR (C_6D_6, 99.3 MHz) δ 38.0.

4.3.2   [Bi(Me$_2$Si{NAr}$_2$)][GaCl$_4$] (12b)

Method 1: NMR scale

A solution of **13b** (0.020 g, 0.026 mmol.) in C$_6$D$_6$ (0.5 mL) was added to **9** (8.5 mg, 0.013 mmol.). The ^{1}H NMR spectrum indicated complete consumption of starting materials after 10 mins at room temperature.

Method 2: Preparative scale

A solution of **9** (0.040 g, 0.061 mmol.) in toluene (2 mL) was added to a solution of GaCl$_3$ (11 mg, 0.061 mmol.) in toluene (2 mL). Removal of the volatiles followed by ^{1}H NMR analysis of the crude products revealed formation of **12b**.

^{1}H NMR (C$_6$D$_6$, 300 MHz) δ 7.28 (d, J_{HH} = 7.8 Hz, 4H, m-C$_6$$H_3$), 6.58 (t, J_{HH} = 7.8 Hz, 2H, p-C$_6$$H_3$), 3.51 (sept, J_{HH} = 6.7 Hz, 4H, CH(CH$_3$)$_2$), 1.24 (br, 24H, CH(CH_3)$_2$), 0.13 (s, 6H, SiMe_2).

4.3.3   [{Bi(Me$_2$Si{NAr}$_2$)}$_2$(μ-Cl)][AlCl$_4$] (13a)

Method 1: NMR scale

A solution of **12a** (0.020 g, 0.026 mmol.) in C$_6$D$_6$ (0.5 mL) was added to **9** (8.5 mg, 0.013 mmol.). The ^{1}H NMR spectrum indicated complete consumption of starting materials after 10 mins at room temperature.

Method 2: Preparative scale

Addition of a solution of **9** (0.040 g, 0.061 mmol.) in toluene (2 mL) to a stirring suspension of AlCl$_3$ (4 mg, 0.031 mmol.) in toluene (2 mL). The resulting suspension was allowed to stir for 4 hours followed by the removal of volatiles. ^{1}H NMR analysis of the crude product revealed formation of **13a**.

^{1}H NMR (C$_6$D$_6$, 300 MHz) δ 7.24 (d, J_{HH} = 7.8 Hz, 4H, m-C$_6$$H_3$), 6.74 (t, J_{HH} =

7.8 Hz, 2H, p-C$_6$$H_3$), 3.86 (br sept, 4H, C$H$(CH$_3$)$_2$), 1.25 (d, J_{HH} = 6.6 Hz, 24H, CH(CH_3)$_2$), 0.20 (s, 6H, SiMe_2).

4.3.4 [{Bi(Me$_2$Si{NAr}$_2$)}$_2$(μ-Cl)][GaCl$_4$] (13b)

Method 1: Reaction of **9** with 1 equiv. GaCl$_3$

A solution of **9** (0.10 g, 0.15 mmol.) in toluene (5 mL) was added dropwise to a stirring suspension of GaCl3 (0.027 mg, 0.15 mmol.) in toluene (5 mL). The resulting dark red solution was allowed to stir for 4 hours followed by concentration of the solution and storage at -30 °C. After 24 hours, an off-white precipitate was deposited in addition to several clear dark red crystals of **13b** suitable for single crystal X-ray diffraction were obtained. Yield 0.021 g, 18 %.

Method 2: Reaction of **9** with 0.5 equiv. GaCl$_3$

A solution of **9** (0.10 g, 0.15 mmol.) in toluene (5 mL) was added dropwise to a stirring suspension of GaCl3 (0.014 mg, 0.15 mmol.) in toluene (5 mL). The resulting dark red solution was allowed to stir for 4 hours followed by concentration of the solution and storage at -30 °C. After 24 hours, small deep red crystals were obtained, identified as **13b** by ^{1}H NMR spectroscopy. Yield 0.047 g, 40 %

Anal. Calcd. for C$_{52}$H$_{80}$GaBi$_2$Cl$_5$N$_4$Si$_2$ (*1482.34*): C, 42.13; H, 5.44; N, 3.78 %. Found: C, 41.97; H, 5.31, N 3.90 %.

^{1}H NMR (C$_6$D$_6$, 300 MHz) δ 7.25 (d, J_{HH} = 7.8 Hz, 4H, m-C$_6$$H_3$), 6.74 (t, J_{HH} = 7.8 Hz, 2H, p-C$_6$$H_3$), 3.90 (sept, J_{HH} = 6.8 Hz, 4H, CH(CH$_3$)$_2$), 1.27 (d, J_{HH} = 6.8 Hz, 24H, CH(CH_3)$_2$), 0.21 (s, 6H, SiMe_2).

^{29}Si NMR (C$_6$D$_6$, 99.3 MHz) δ 31.2.

^{13}C NMR data could not be obtained due to decomposition of **13b** in solution over extended periods of time.

4.3.5 Bi(Me$_2$Si{NAr}$_2$)Ph (14)

Method 1: Preparative scale from **9** + NaBPh$_4$

A solution of **9** (0.10 g, 0.15 mmol.) in toluene (5 mL) was added dropwise to a stirring suspension of NaBPh$_4$ (0.051 g, 0.15 mmol.) in toluene (5 mL). The resulting solution was allowed to stir for 72 hours at 90 °C followed by filtration through celite and concentration of the solution. After 24 hours at -30 °C, a number of white crystals of BPh$_3$ were deposited. Further concentration and storage at -30 °C yield a 2nd crop of crystals, identified as a mixture of BPh$_3$ and **14**. Characterisation of **14** was achieved through mechanical separation of the crystals. Yield 0.070 g, 67 %.

Method 2: NMR scale from **12a** + NaBPh$_4$

A solution of **12a** (0.020 g, 0.025 mmol.) in C$_6$D$_6$ (0.5 mL) was added to NaBPh$_4$ (0.009 g, 0.025 mmol.) in a J. Young NMR tube. ^{1}H NMR analysis after 5 hours at 80 °C indicated complete consumption of starting materials and formation of **14** and BPh$_3$.

Anal. Calcd. for C$_{32}$H$_{45}$BiN$_2$Si (*694.78*): C, 55.32; H, 6.53; N, 4.03 %. Found: C, 55.44; H, 6.61; N, 3.95 %.

^{1}H NMR (C$_6$D$_6$, 300 MHz) 8.48 (d, J_{HH} = 7.5 Hz, 2H, o-C$_6$$H_5$), 7.57 (t, J_{HH} = 7.5 Hz, 1H, p-C$_6$$H_5$), 6.95 (t, J_{HH} = 7.5 Hz, 2H, m-C$_6$$H_5$), 4.30 (sept, J_{HH} = 6.8 Hz, 4H, CH(CH$_3$)$_2$), 1.28 (d, J_{HH} = 6.8 Hz, 24H, CH(CH_3)$_2$), 0.63 (s, 3H, SiMe_2), 0.15 (s, 3H, SiMe_2).

^{13}C NMR (C$_6$D$_6$, 75 MHz) 148.0 (br, C_6H$_5$), 147.2, 140.9 (C_6H$_3$), 136.2, 131.6 (C_6H$_5$), 129.4, 128.4 (C_6H$_3$), 124.5 (C_6H$_5$), 27.8 (br, CH(CH$_3$)$_2$), 25.1 (br, CH(CH$_3$)$_2$, 17.5, 4.8 (SiMe_2).

^{29}Si NMR (C$_6$D$_6$, 99.3 MHz) δ 19.5.

4.3.6 Bi(Me$_2$Si{NAr}$_2$)Et (15)

A solution of **9** (0.10 g, 0.15 mmol.) in toluene (5 mL) was added dropwise to a stirring suspension of NaBEt$_4$ (0.023 g, 0.15 mmol.) in toluene (5 mL). The resulting solution was allowed to stir for 24 hours at room temperature followed by removal of the volatiles and extraction into hexane. The resulting suspension was filtered through celite and concentrated, followed by storage at -30 °C. After 24 hours, clear yellow crystals were deposited, identified as **15**. Yield 0.061 g, 63 %.

Anal. Calcd. for C$_{28}$H$_{45}$BiN$_2$Si (*646.73*): C, 52.00; H, 7.01; N, 4.33 %. Found: C, 51.81; H, 7.12, N 4.24 %.

^{1}H NMR (C$_6$D$_6$, 300MHz) δ 7.19 (d, J_{HH} = 7.6 Hz, 4H, *m*-C$_6$*H$_3$*), 6.99 (t, J_{HH} = 7.6 Hz, 2H, *p*-C$_6$*H$_3$*), 4.28 (sept, J_{HH} = 6.9 Hz, 4H, C*H*(CH$_3$)$_2$), 2.47 (t, J_{HH} = 8.1 Hz, 3H, CH$_2$C*H$_3$*), 2.04 (q, J_{HH} = 8.1 Hz, 2H, C*H$_2$*CH$_3$), 1.31 (br, 24H, CH(C*H$_3$*)$_2$), 0.42 (s, 3H, Si*Me$_2$*), 0.04 (s, 3H, Si*Me$_2$*).

^{13}C NMR (C$_6$D$_6$, 75 MHz) δ 147.9, 141.4, 124.2, 123.5 (C6H3), 27.7 (*C*H(CH$_3$)$_2$), 25.9, 25.4 (CH(C*H$_3$*)$_2$), 15.6 (Si*Me$_2$*), 8.7 (CH$_2$*C*H$_3$), 5.2 (Si*Me$_2$*). Bi*C*H$_2$CH$_3$ resonance not observed.

^{29}Si NMR (C$_6$D$_6$, 100 MHz) δ 17.8.

4.4 Experimental for Section 2.4

4.4.1 Bi(Me$_2$Si{NAr}$_2$)(OAr') (Ar' = 2,6-*t*-Bu$_2$C$_6$H$_3$) (17)

A solution of **9** (0.10 g, 0.15 mmol.) in toluene (5 mL) was added dropwise to a stirring suspension of KOAr' (0.037 g, 0.15 mmol.) in toluene (5 mL). The resulting solution was allowed to stir for 24 hours at RT followed by filtration through celite and concentration of the solution. Storage at -30 °C for 24 hours yielded deep green crystals, identified as **17**. Yield 0.101 g, 82 %.

Anal. Calcd. for $C_{40}H_{61}BiN_2OSi$ (*822.44*): C, 58.38; H, 7.47; N, 3.40 %. Found: C, 58.25; H, 7.52, N 3.49 %.

^{1}H NMR (C_6D_6, 300 MHz) δ 7.28 (d, J_{HH} = 7.8 Hz, 2H, m-C_6H_3(i-Pr)$_2$), 7.20 (d, J_{HH} = 7.8 Hz, 4H, m-C_6H_3(t-Bu)$_2$), 6.85 (t, J_{HH} = 7.2 Hz, 2H, p-C_6H_3(i-Pr)$_2$), 6.70 (t, J_{HH} = 7.8 Hz, 1H, p-C_6H_3(t-Bu)$_2$), 3.88 (br, 4H, CH(CH$_3$)$_2$), 1.39 (s, 18H, C(CH_3)$_3$), 1.34 (d, J_{HH} = 6.9 Hz, 12H, CH(CH_3)$_2$), 1.13 (d, J_{HH} = 6.9 Hz, 12H, CH(CH_3)$_2$), 0.70 (s, 3H, SiMe_2), 0.01 (s, 3H, SiMe_2).

^{13}C NMR (C_6D_6, 75 MHz) δ 159.0, 147.9, 143.7, 139.0, 125.4, 125.3, 123.5, 120.7 (C_6H$_3$(i-Pr)$_2$ and C_6H$_3$(t-Bu)$_2$), 35.4, 33.0, 30.4, 28.4, 27.5, 25.5 (CH(CH$_3$)$_2$, CH(CH$_3$)$_2$, C(CH$_3$)$_3$ and C(CH$_3$)$_3$), 15.6, 2.8 (SiMe_2).

4.4.2   Bi(Me$_2$Si{NAr}$_2$)(PCy$_2$) (18)

A solution of **9** (0.10 g, 0.15 mmol.) in toluene (5 mL) was added dropwise to a stirring suspension of LiPCy$_2$ (0.030 g, 0.15 mmol.) in toluene (5 mL). The resulting solution was allowed to stir for 24 hours at RT followed by filtration through celite and concentration of the solution. After 24 hours at -30 °C, a number of deep red crystals were isolated and identified as **18**. Yield 0.076 g, 62 %.

Anal. Calcd. for $C_{38}H_{62}BiN_2PSi$ (*814.42*): C, 56.00; H, 7.67; N, 3.44 %. Found: C, 56.17; H, 7.80, N 3.33 %.

^{1}H NMR (C_6D_6, 300 MHz) δ 7.18 (d, J_{HH} = 7.5 Hz, 4H, m-C_6H_3), 6.95 (t, J_{HH} = 7.5 Hz, 2H, p-C_6H_3), 4.35 (br, 4H, CH(CH$_3$)$_2$), 3.53 (m, 2H, α-C_6H_{11}), 1.9-0.8 (br m, 20H, C_6H_{11}), 1.43 (d, J_{HH} = 6.3 Hz, 12H, CH(CH_3)$_2$), 1.31 (d, J_{HH} = 6.3 Hz, 12H, CH(CH_3)$_2$), 0.51 (s, 3H, SiMe_2), 0.16 (s, 3H, SiMe_2);

^{13}C NMR (C_6D_6, 75 MHz) δ 148.4, 140.6, 124.2, 123.7 (C_6H$_3$), 37.6 (br, α-C_6H$_1$1), 34.7, 34.3, 27.9, 27.8, 26.7, 26.4, 25.6 (CH(CH$_3$)$_2$, CH(CH$_3$)$_2$ and C_6H$_{11}$), 15.5, 4.4 (SiMe_2). ^{29}Si NMR (C_6D_6, 100 MHz) δ 16.4.

^{31}P NMR (C$_6$D$_6$, 121 MHz) δ 56.4.

4.4.3 Insertion reactions

Reaction of Bi(N{SiMe$_3$}$_2$)$_3$ with *N,N'*-dicyclohexylcarbodiimide

Method 1: NMR scale reaction of Bi(N{SiMe$_3$}$_2$)$_3$ with 3 equivalents of *N,N'*-dicyclohexylcarbodiimide

A solution of Bi(N{SiMe$_3$}$_2$)$_3$ (0.020 g, 0.029 mmol.) in C$_6$D$_6$ (0.5 mL) was added to *N,N'*-dicyclohexylcarbodiimide 0.018 g, 0.09 mmol.) in a vial. The resulting solution was transferred to a J. Young NMR tube and analysed by ^{1}H NMR spectroscopy.

Method 2: Preparative scale 1:1 equivalents of Bi(N{SiMe$_3$}$_2$)$_3$ and *N,N'*-dicyclohexylcarbodiimide

A solution of Bi(N{SiMe$_3$}$_2$)$_3$ (0.10 g, 0.145 mmol.) in toluene (4 mL) was added dropwise to a solution of *N,N'*-dicyclohexylcarbodiimide (0.030 g, 0.145 mmol.) in toluene (5 mL). The resulting solution was stirred for 2h followed by removal of the volatiles. ^{1}H NMR of the crude sample indicated formation of the corresponding insertion product.

^{1}H NMR (C$_6$D$_6$, 300 MHz) δ 3.38 (br t, 2H, α-C$_6$$H_{11}$), 1.95-1.05 (m, 20H, C$_6$$H_{11}$), 0.37 (s, 36H, Si$Me_3$(amide)) 0.02 (s, 18H, SiMe_3(guanidinate)).

General procedure for reaction of 16/18 and carbodiimide/isocyanate substrates

A solution of **16** (0.02 g, 0.026 mmol.) in C$_6$D$_6$ was added to *N,N'*-dicyclohexylcarbodiimide (0.005 g, 0.026 mmol.) in a vial. The resulting solution was transferred to a J. Young NMR tube and analysed by ^{1}H NMR spectroscopy.

NMR data for the reaction of **18** and phenyl isocyanate.

^{1}H NMR (C$_6$D$_6$, 300 MHz) δ 7.01 (m, C$_6$$H_3$), 6.79 (m, C$_6$$H_5$), 6.53 (t, C$_6$$H_5$), 4.28 (br m, C$H$(CH$_3$)$_2$), 3.87 (br, α-C$_6$$H_{11}$), 2.10-1.00 (br m, C$_6$$H_{11}$ and CH(CH_3)$_2$), 0.52 (s, SiMe_2) 0.02 (s, SiMe_2).

^{31}P NMR (C$_6$D$_6$, 121 MHz) δ 0.2.

No change in the ^{1}H NMR spectrum was observed upon addition of *N,N'*-dicyclohexylcarbodiimide to **16** or **18**.

4.4.4   General procedure for catalytic ROP of cyclic esters

A solution of **16** (0.001 g) in C$_6$D$_6$ (0.5 mL) was added to a J. Young NMR tube charged with *rac*-Lactide (0.020 g, 0.139 mmol.), followed by ^{1}H NMR analysis after 10 minutes at room temperature. The reaction was heated to 80 °C and analysed by ^{1}H NMR spectroscopy at regular intervals. (Electronic copies of the stacked ^{1}H NMR spectra are available on the attached CD)

4.5   Experimental for Section 2.5

4.5.1   O(SiMe$_2$NHAr")$_2$ (19b) (Ar" = 2,6-Me$_2$C$_6$H$_3$)

A solution of *n*-BuLi in hexane (20.5 mL of a 1.6 M solution, 0.033 mol.) was added dropwise to a stirring solution of Ar"NH$_2$ (4 mL, 0.033 mol.) in Et$_2$O (80 mL) at -78 °C. The resulting suspension was stirred for 4h followed by the dropwise addition of O(SiMe$_2$Cl)$_2$ at -78 °C (3.25 g, 0.016 mol.). The solution was allowed to stir for 18h followed by filtration through celite. Removal of the volatiles *in vacuo* gives **19b** as a clear colourless oil. Yield 4.56 g, 78 %.

^{1}H NMR (C$_6$D$_6$, 300 MHz) δ 7.01 (d, J_{HH} = 7.5 Hz, 4H, *m*-C$_6$$H_3$), 6.88 (t, J_{HH} = 7.5 Hz, 2H, *p*-C$_6$$H_3$), 2.22 (s, 12H, *o*-$Me_2$), 0.09 (s, 12H, Si$Me_2$).

^{13}C NMR (C$_6$D$_6$, 75 MHz) δ 142.9, 131.9, 128.7, 122.5 (C$_6$*H$_3$*), 19.9 (*o-Me$_2$*), 0.8 (Si*Me$_2$*).

EI-MS: *m/z* (%): 373.21, 122.10.

4.5.2 Bi(O(SiMe$_2$NAr")$_2$)Cl (Ar" = 2,6-*i*-Pr$_2$C$_6$H$_3$) (20a)

A solution of *n*-BuLi in hexane (2.3 mL of a 1.6 M solution, 3.6 mmol.) was added dropwise to a stirring solution of O(SiMe$_2$NHAr")$_2$ (Ar" = 2,6-*i*-Pr$_2$C$_6$H$_3$) (0.80 g, 1.7 mmol.) in Et$_2$O (7 mL) at -30 °C. The resulting suspension was allowed to warm to room temperature and then stirred for 4h. The suspension was added dropwise to a stirring suspension of BiCl$_3$ (0.53 g, 1.7 mmol.) in Et$_2$O (10 mL) in the absence of light, followed by stirring for 18h in the absence of light. Unreacted BiCl$_3$ and decomposition products were removed by filtration through celite to give a clear red solution. Colourless crystals were obtained upon concentration of the solution and storage at -30 °C for 24h. Yield 0.245 g, 35 %.

Anal. Calcd. for C$_{28}$H$_{46}$BiClN$_2$OSi$_2$ (*727.29*): C, 46.24; H, 6.38; N, 3.80 %. Found: C, 46.23; H, 6.75, N 3.93 %.

^{1}H NMR (C$_6$D$_6$, 300 MHz) δ 7.22 (dd, J_{HH} = 7.5 and 1.8 Hz, 2H, *m*-C$_6$*H$_3$*), 7.09 (dd, J_{HH} = 7.5 and 1.8 Hz, 2H, *m*-C$_6$*H$_3$*), 6.98 (t, J_{HH} = 7.5 Hz, 2H, *p*-C$_6$*H$_3$*), 4.22 (sept, J_{HH} = 6.9 Hz, 2H, C*H*(CH$_3$)$_2$), 3.66 (sept, J_{HH} = 6.9 Hz, 2H, C*H*(CH$_3$)$_2$), 1.27 (ddd, J_{HH} = 6.9, 6.9 and 0.3 Hz, 24H, CH(C*H$_3$*)$_2$), 0.60 (s, 6H, Si*Me$_2$*), 0.20 (s, 6H, Si*Me$_2$*).

^{13}C NMR (C$_6$D$_6$, 75 MHz) δ 151.3, 148.3, 137.7, 126.9, 125.0, 123.7 (*C$_6$*H$_3$), 29.0, 28.7, 27.5, 25.1, 24.6 (*C*H(CH$_3$)$_2$ and CH(*C*H$_3$)$_2$), 4.5, 3.2 (Si*Me$_2$*).

^{29}Si NMR (C$_6$D$_6$, 100 MHz) δ 5.9.

4.5.3 Bi(O(SiMe$_2$NAr")$_2$)Cl (Ar" = 2,6-Me$_2$C$_6$H$_3$) (20b)

A solution of n-BuLi in hexane (3.75 mL of a 1.6 M solution, 6.0 mmol.) was added dropwise to a stirring solution of O(SiMe$_2$NHAr")$_2$ (0.50 g, 2.7 mmol.) in Et$_2$O (7 mL) at -30 °C. The resulting suspension was allowed to warm to room temperature and then stirred for 4h. The suspension was added dropwise to a stirring suspension of BiCl$_3$ (0.85 g, 2.7 mmol.) in Et$_2$O (10 mL) in the absence of light, followed by stirring for 18h in the absence of light. Unreacted BiCl$_3$ and decomposition products were removed by filtration through celite to give a clear orange solution. A small number of colourless crystals were obtained upon concentration of the solution and storage at -30 °C for 24h.

^{1}H NMR (C$_6$D$_6$, 300 MHz) δ 7.07 (br, 4H, m-C$_6$H$_3$), 6.82 (t, J_{HH} = 7.8 Hz, 2H, p-C$_6$H$_3$), 2.73 (s, 6H, o-Me_2), 2.46 (s, 6H, o-Me_2), 0.59 (s, 6H, SiMe_2), 0.17 (s, 6H, SiMe_2);

4.5.4 [Bi(O(SiMe$_2$NAr")$_2$][AlCl$_4$] (Ar" = 2,6-i-Pr$_2$C$_6$H$_3$) (21)

A solution of **20a** (0.10 g, 0.14 mmol.) in toluene (5 mL) was added dropwise to a stirring suspension of AlCl$_3$ (0.018 g, 0.14 mmol.) in toluene (5 mL). The resulting dark red solution was allowed to stir for 4 hours followed by concentration and storage at -30 °C. After 24 hours, clear dark red crystals of **21** suitable for single crystal X-ray diffraction were obtained. Yield 0.105 g, 89 %

Anal. Calcd. for C$_{28}$H$_{46}$AlBiCl$_4$N$_2$OSi$_2$ (*860.62*): C, 39.08; H, 5.39; N, 3.26 %. Found: C, 38.91; H, 5.31, N 3.28 %.

^{1}H NMR (C$_6$D$_6$, 300 MHz) 7.16 (d, J_{HH} = 7.8 Hz, 4H, m-C$_6$H$_3$), 6.83 (t, J_{HH} = 7.8 Hz, 4H, p-C$_6$H$_3$), 3.41 (sept, J_{HH} = 6.6 Hz, 4H, CH(CH$_3$)$_2$), 1.21 (dd, J_{HH} = 42.8 and 6.9 Hz, 24H, CH(CH_3)$_2$), 0.22 (s, 12H, SiMe_2);

^{13}C NMR (C$_6$D$_6$, 75 MHz) 149.2, 129.3, 128.6, 125.7, 124.4(C_6H$_3$), 29.3, 27.6, 25.2 (CH(CH$_3$)$_2$ and CH(CH$_3$)$_2$), 3.8 (SiMe_2).

References

[1] Lide, D. R. *CRC Handbook of Chemistry and Physics, 85th Edition*; CRC Handbook of Chemistry and Physics, 85th Ed; Taylor & Francis, 2004.

[2] Harder, S. *Chem. Rev.* **2010**, 3852–3876.

[3] Alexander, J. S.; Ruhlandt-Senge, K. *Eur. J. Inorg. Chem.* **2002**, 2761–2774.

[4] Hong, S.; Marks, T. J. *Acc. Chem. Res.* **2004**, *37*, 673–86.

[5] Avent, A. G.; Crimmin, M. R.; Hill, M. S.; Hitchcock, P. B. *Organometallics* **2005**, 1184–1188.

[6] Brinkmann, C.; Barrett, A. G. M.; Hill, M. S.; Procopiou, P. A. *J. Am. Chem. Soc.* **2012**, 2193–2207.

[7] Crimmin, M. R.; Arrowsmith, M.; Barrett, A. G. M.; Casely, I. J.; Hill, M. S.; Procopiou, P. A. *J. Am. Chem. Soc.* **2009**, *131*, 9670–85.

[8] Crimmin, M. R.; Barrett, A. G. M.; Hill, M. S.; Hitchcock, P. B.; Procopiou, P. A. *Organometallics* **2008**, *27*, 497–499.

[9] Crimmin, M. R.; Barrett, A. G. M.; Hill, M. S.; Hitchcock, P. B.; Procopiou, P. A. *Organometallics* **2007**, *26*, 2953–2956.

[10] Buch, F.; Brettar, J.; Harder, S. *Angew. Chem. Int. Ed.* **2006**, *45*, 2741–2745.

[11] Harder, S.; Feil, F.; Knoll, K. *Angew. Chem. Int. Ed.* **2001**, *113*, 4391–4394.

[12] Harder, S.; Feil, F. *Organometallics* **2002**, *21*, 2268–2274.

[13] Feil, F.; Harder, S. *Eur. J. Inorg. Chem.* **2005**, *2005*, 4438–4443.

[14] Barrett, A. G. M.; Casely, I. J.; Crimmin, M. R.; Hill, M. S.; Lachs, J. R.; Mahon, M. F.; Procopiou, P. A. *Inorg. Chem.* **2009**, *48*, 4445–53.

[15] Du, Z.; Li, W.; Zhu, X.; Xu, F.; Shen, Q. *J. Org. Chem.* **2008**, *73*, 8966–72.

[16] Dunne, J. F.; Fulton, D. B.; Ellern, A.; Sadow, A. D. *J. Am. Chem. Soc.* **2010**, *132*, 17680–3.

[17] Tobisch, S. *Chem. Eur. J.* **2011**, *17*, 14974–86.

[18] Day, B. M.; Knowelden, W.; Coles, M. P. *Dalton Trans.* **2012**, *41*, 10930–10933.

[19] Day, B. M.; Mansfield, N. E.; Coles, M. P.; Hitchcock, P. B. *Chem. Commun.* **2011**, *47*, 4995–4997.

[20] Hill, M. S.; Liptrot, D. J.; Mahon, M. F. *Angew. Chem. Int. Ed.* **2013**, *52*, 5364–5367.

[21] Arrowsmith, M.; Hill, M. S.; Kociok-Koehn, G. *Organometallics* **2011**, *30*, 1291–1294.

[22] Edelmann, F. F. T.; Hill, A. F.; Press, A. *Adv. Organomet. Chem. Vol. 57*; 2008 Elsevier Inc., 2008; Vol. 57; Chapter 3, pp 183–352.

[23] Coles, M. P.; Swenson, D. C.; Jordan, R. F.; Young, V. G. *Organometallics* **1997**, *2*, 5183–5194.

[24] Green, S. P.; Jones, C.; Stasch, A. *Science* **2007**, *318*, 1754–1757.

[25] Ong, T.-G.; O'Brien, J. S.; Korobkov, I.; Richeson, D. S. *Organometallics* **2006**, *25*, 4728–4730.

[26] Zhang, W.-X.; Nishiura, M.; Hou, Z. *J. Am. Chem. Soc.* **2005**, *127*, 16788–9.

[27] Barrett, A. G. M.; Crimmin, M. R.; Hill, M. S.; Hitchcock, P. B.; Lomas, S. L.; Mahon, M. F.; Procopiou, P. A.; Suntharalingam, K. *Organometallics* **2008**, *27*, 6300–6306.

[28] Schwamm, R. J. *Honours Report*; 2012, Victoria University of Wellington.

[29] Barrett, A. G. M.; Brinkmann, C.; Crimmin, M. R.; Hill, M. S.; Hunt, P.; Procopiou, P. A. *J. Am. Chem. Soc.* **2009**, *131*, 12906–7.

[30] Addison, A. W.; Rao, T. N.; Reedijk, J.; van Rijn, J.; Verschoor, G. C. *J. Chem. Soc., Dalton Trans.* **1984**, 1349–1356.

[31] Hansch, C.; Leo, A.; Taft, R. W. *Chem. Rev.* **1991**, *91*, 165–195.

[32] Perucaud, M. C.; Ducom, J.; Vallino, M. *C. R. Acad. Sci. Ser. C Sci. Chim.* **1967**, *264*, 571–574.

[33] Guino-o, M. A.; Baker, E.; Ruhlandt-Senge, K. *J. Coord. Chem.* **2008**, *61*, 125–136.

[34] Schubert, B.; Behrens, U.; Weiss, E. *Chem. Ber.* **1981**, *114*, 2640–2643.

[35] Sadique, a. R.; Heeg, M. J.; Winter, C. H. *Inorg. Chem.* **2001**, *40*, 6349–55.

[36] Xia, A.; El-Kaderi, H. M.; Jane Heeg, M.; Winter, C. H. *J. Organomet. Chem.* **2003**, *682*, 224–232.

[37] Boere, R. T.; Cole, M. L.; Junk, P. C. *New J. Chem.* **2005**, *29*, 128–134.

[38] Srinivas, B.; Chang, C.-c.; Chen, C.-h.; Chiang, M. Y.; Chen, I.; Wang, Y.; Lee, G.-h. *J. Chem. Soc., Dalton Trans.* **1997**, 957–963.

[39] Fan, M.; Yang, Q.; Tong, H.; Yuan, S.; Jia, B.; Guo, D.; Zhou, M.; Liu, D. *RSC Adv.* **2012**, *2*, 6599.

[40] Westerhausen, M.; Hausen, H.-D. *Z. Anorg. Allg. Chem* **1992**, *615*, 27–34.

[41] Goldfiel, S. A.; Raymond, K. N. *Inorg. Chem.* **1974**, *13*, 770–775.

[42] Walther, D.; Gebhardt, P.; Fischer, R.; Kreher, U.; Grrls, H. *Inorg. Chim. Acta* **1998**, *281*, 181–189.

[43] Cole, M. L.; Evans, D. J.; Junk, P. C.; Louis, L. M. *New J. Chem.* **2002**, *26*, 1015–1024.

[44] Cheng, J. *Acta Crystallogr. Sect. E-Struct. Rep. Online* **2011**, *67*, m987.

[45] Andrews, P. C.; Brym, M.; Jones, C.; Junk, P. C.; Kloth, M. *Inorg. Chim. Acta* **2006**, *359*, 355–363.

[46] Westerhausen, M. *Inorg. Chem.* **1991**, *30*, 96–101.

[47] Burnett, M. N.; Johnson, C. K. ORTEP-III: Oak Ridge Thermal Ellipsoid Plot Program for Crystal Structure Illustrations. 1996.

[48] Earnshaw, A.; Greenwood, N. *Chemistry of the Elements*; Elsevier Science, 1997.

[49] Shannon, R. D. *Acta Crystallogr. Sect. A* **1976**, *32*, 751–767.

[50] Sox, T. E.; Olson, C. A. *Antimicrob. Agents Chemother.* **1989**, *33*, 2075–2082.

[51] A, S.; Torardi, C. C.; Calabrese, J. C.; Gopalakrishnan, J.; Morrissey, K. J.; Askew, T. R.; Flippen, R. B.; Chowdhry, U.; Sleight, A. W. *Science* **1988**, *239*, 1015–1017.

[52] Bothwell, J. M.; Krabbe, S. W.; Mohan, R. S. *Chem. Soc. Rev.* **2011**, *40*, 4649–707.

[53] Hopper, K. D.; King, S. H.; Lobell, M. E.; TenHave, T. R.; Weaver, J. S. *Radiology* **1997**, *205*, 853–858.

[54] Bertsch, M. V. B. *Z. Anorg. Allg. Chem* **1988**, *3*, 7–22.

[55] Frank, W.; Weber, J.; Fuchs, E. *Angew. Chem. Int. Ed.* **1987**, *26*, 74–75.

[56] Sitzmann, H.; Wolmershäuser, G.; Boese, R.; Bläser, D. *Z. Anorg. Allg. Chem* **1999**, *625*, 2103–2107.

[57] Conrad, E.; Burford, N.; McDonald, R.; Ferguson, M. J. *Chem. Commun.* **2010**, *46*, 4598–4600.

[58] Bondi, A. *J. Phys. Chem.* **1964**, *68*, 441–&.

[59] Casely, I. J.; Ziller, J. W.; Mincher, B. J.; Evans, W. J. *Inorg. Chem.* **2011**, *50*, 1513–1520.

[60] Glassman, T. E.; Bhandari, G.; Baum, T. H. Method of forming bismuth-containing films by using bismuth amide compounds. 1999.

[61] Nekoueishahraki, L.; Samuel, P. P.; Roesky, H. W.; Stern, D.; Matussek, J.; Stalke, D. *Organometallics* **2012**, *31*, 6697–6703.

[62] Day, B. Main Group Metal Complexes Supported By N , N ' -Bidentate Ligands Synthetic and Catalytic Investigations. Ph.D. thesis, University of Sussex, 2012.

[63] Hanna, T. *Coord. Chem. Rev.* **2004**, *248*, 429–440.

[64] Allen, G. C.; Carmalt, C. J.; Cowley, A. H.; Hector, A. L.; Kamepalli, S.; Lawson, Y. G.; Norman, N. C.; Parkin, I. P.; Pickard, L. K. *Chem. Mater.* **1997**, *9*, 1385–1392.

[65] Sasamori, T.; Takeda, N.; Fujio, M.; Kimura, M.; Nagase, S.; Tokitoh, N. *Angew. Chem. Int. Ed.* **2002**, *41*, 139–141.

[66] Barrett, A. G. M.; Crimmin, M. R.; Hill, M. S.; Hitchcock, P. B.; Lomas, S. L.; Mahon, M. F.; Procopiou, P. A. *Dalton Trans.* **2010**, *39*, 7393–400.

[67] Mansfield, N. E.; Coles, M. P.; Hitchcock, P. B. *Dalton Trans.* **2005**, 2833–2841.

[68] Hou, Z. M.; Breen, T. L.; Stephan, D. W. *Organometallics* **1993**, *12*, 3158–3167.

[69] Behrle, A. C.; Schmidt, J. A. R. *Organometallics* **2013**, *32*, 1141–1149.

[70] Kawaoka, A. M.; Douglass, M. R.; Marks, T. J. *Organometallics* **2003**, *22*, 4630–4632.

[71] Douglass, M. R.; Stern, C. L.; Marks, T. J. *J. Am. Chem. Soc.* **2001**, *123*, 10221–10238.

[72] Beswick, M.; Choi, N.; Hopkins, A.; Lawson, Y.; McPartlin, M.; Rothenberger, A.; Stalke, D.; Wheatley, A.; Wright, D. *Angew. Chem. Int. Ed.* **1999**, *38*, 3053–3055.

[73] Traut, S.; Hahnel, A. P.; von Hanisch, C. *Dalton Trans.* **2011**, *40*, 1365–1371.

[74] Arbaoui, A.; Redshaw, C. *Polym. Chem.* **2010**, *1*, 801.

[75] Nomura, N.; Ishii, R.; Akakura, M.; Aoi, K. *J. Am. Chem. Soc.* **2002**, *124*, 5938–5939.

[76] Chmura, A. J.; Chuck, C. J.; Davidson, M. G.; Jones, M. D.; Lunn, M. D.; Bull, S. D.; Mahon, M. F. *Angew. Chem. Int. Ed.* **2007**, *46*, 2280–2283.

[77] Chisholm, M. H.; Gallucci, J. C.; Phomphrai, K. *Inorg. Chem.* **2004**, *43*, 6717–6725.

[78] Chamberlain, B. M.; Cheng, M.; Moore, D. R.; Ovitt, T. M.; Lobkovsky, E. B.;

Coates, G. W. *J. Am. Chem. Soc.* **2001**, *123*, 3229–3238.

[79] Kricheldorf, H. R.; Bornhorst, K.; Hachmann-Thiessen, H. *Macromolecules* **2005**, *38*, 5017–5024.

[80] Lahcini, M.; Schwarz, G.; Kricheldorf, H. R. *J. Polym. Sci. A Polym. Chem.* **2008**, *46*, 7483–7490.

[81] Kricheldorf, H. R.; Hachmann-Thiessen, H.; Schwarz, G. *Biomacromolecules* **2004**, *5*, 492–6.

[82] Balasanthiran, V.; Beilke, T. L.; Chisholm, M. H. *Dalton Trans.* **2013**, *42*, 9274–9278.

[83] Balasanthiran, V.; Chisholm, M. H.; Durr, C. B.; Gallucci, J. C. *Dalton Trans.* **2013**, *42*, 11234–11241.

[84] Vuorinen, S.; Lahcini, M.; Hatanpää, T.; Sundberg, M.; Leskelä, M.; Repo, T. *Macromol. Chem. Phys.* **2013**, *214*, 707–715.

[85] Larsson, E.; Smith, B. *Acta Chem. Scand.* **1949**, *3*, 487–492.

[86] Chen, H.; Bartlett, R. A.; Dias, H. V. R.; Olmstead, M. M.; Power, P. P. *Inorg. Chem.* **1991**, *30*, 2487–2494.

[87] Day, B. M.; Dyer, P. W.; Coles, M. P. *Dalton Trans.* **2012**, *41*, 7457–7460.

[88] Al-Rafia, S. M. I.; Lummis, P. A.; Ferguson, M. J.; McDonald, R.; Rivard, E. *Inorg. Chem.* **2010**, *49*, 9709–9717.

[89] Veith, M.; Recktenwald, O. *Z. Anorg. Allg. Chem* **1979**, *459*, 208–216.

[90] Veith, M. *Z. Anorg. Allg. Chem* **1978**, *446*, 227–236.

[91] Rozenel, S. S.; Chomitz, W. A.; Arnold, J. *Organometallics* **2009**, *28*, 6243–6253.

[92] Zhou, L.; Yao, Y.; Li, C.; Zhang, Y.; Shen, Q. *Organometallics* **2006**, *25*, 2880–2885.

[93] Zhu, X.; Fan, J.; Wu, Y.; Wang, S.; Zhang, L.; Yang, G.; Wei, Y.; Yin, C.; Zhu, H.; Wu, S.; Zhang, H. *Organometallics* **2009**, *28*, 3882–3888.

[94] Hill, M. S.; Hitchcock, P. B. *Organometallics* **2002**, 3258–3262.

[95] Day, B. M.; Coles, M. P. *Organometallics* **2013**, *32*, 4270–4278.

[96] Leznoff, D. B.; Mund, G.; Jantunen, K. C.; Bhatia, P. H.; Gabert, A. J.; Batchelor, R. J. *J. Nucl. Sci. Technol.* **2002**, 406–409.

[97] Ma, X.; Ding, Y.; Roesky, H. W.; Sun, S.; Yang, Z. *Z. Anorg. Allg. Chem* **2013**, *639*, 49–52.

[98] Bao, M.; Hayashi, T.; Shimada, S. *Organometallics* **2007**, 1816–1822.

[99] F, Z.; Hausen, H.-D.; Hess, H. *J. Organomet. Chem.* **1974**, *72*, 157–162.

[100] Evans, W. J.; Kozimor, S. A.; Ziller, J. W. *Organometallics* **2005**, *24*, 3407–3412.

[101] M, H. D.; Ferguson, G. *J. Chem. Soc. A Inorg. Phys. Theor.* **1968**, 2059.

[102] Schier, A.; Wallis, J. M.; Muller, G.; Schmidbaur, H. *Angew. Chem. Int. Ed.* **1986**, *25*, 757–759.

[103] Schmidbaur, H.; Nowak, R.; Schier, A.; Wallis, J. M.; Huber, B.; Muller, G. *Chem. Ber.* **1987**, *120*, 1837–1843.

[104] Frank, W.; Schneider, J.; Mullerbecker, S. *J. Chem. Soc. Chem. Commun.* **1993**, 799–800.

[105] Mullerbecker, S.; Frank, W.; Schneider, J. *Z. Anorg. Allg. Chem* **1993**, *619*, 1073–1082.

[106] Frank, W.; Reiland, V. *Acta Crystallogr. Sect. C-Crystal Struct. Commun.*

1998, *54*, 1626–1628.

[107] Strauss, S. H. *Chem. Rev.* **1993**, *93*, 927–942.

[108] Stavila, V.; Thurston, J. H.; Prieto-Centurion, D.; Whitmire, K. H. *Organometallics* **2007**, *26*, 6864–6866.

[109] Thaler, E. G.; Caulton, K. G. *Organometallics* **1990**, *9*, 1871–1876.

[110] Morgan, K.; Sayer, B. G.; Schrobilgen, G. J. *J. Magn. Reson.* **1983**, *52*, 139–142.

[111] Kou, X.; Wang, X.; Mendoza-Espinosa, D.; Zakharov, L. N.; Rheingold, A. L.; Watson, W. H.; Brien, K. A.; Jayarathna, L. K.; Hanna, T. A. *Inorg. Chem.* **2009**, *48*, 11002–11016.

[112] Tam, E. C. Y.; Maynard, N. A.; Apperley, D. C.; Smith, J. D.; Coles, M. P.; Fulton, J. R. *Inorg. Chem.* **2012**, *51*, 9403–15.

[113] Cordero, B.; Gomez, V.; Platero-Prats, A. E.; Reves, M.; Echeverria, J.; Cremades, E.; Barragan, F.; Alvarez, S. *Dalton Trans.* **2008**, 2832–2838.

[114] Jantunen, K. C.; Batchelor, R. J.; Leznoff, D. B. *Organometallics* **2004**, *23*, 2186–2193.

[115] Hayes, C. E.; Leznoff, D. B. *Organometallics* **2010**, *29*, 767–774.

[116] Day, B. *Unpublished Results*.

[117] Das, A. K.; Moatazedi, Z.; Mund, G.; Bennet, A. J.; Batchelor, R. J.; Leznoff, D. B. *Inorg. Chem.* **2007**, *46*, 366–8.

[118] Mund, G.; Vidovic, D.; Batchelor, R. J.; Britten, J. F.; Sharma, R. D.; Jones, C. H. W.; Leznoff, D. B. *Chem. Eur. J.* **2003**, *9*, 4757–63.

[119] Gynane, M. J. S.; Hudson, A.; Lappert, M. F.; Power, P. P.; Goldwhite, H. *J. Chem. Soc., Dalton Trans.* **1980**, 2428–2433.

Appendix

Appendix A: Alternative Solution State Structures for a $C_{2\mathrm{h}}$ Ligand Environment
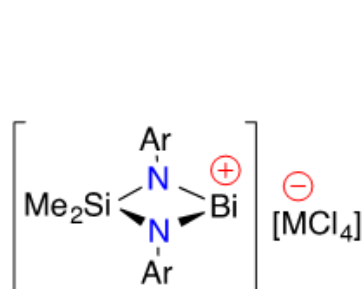
(**A**: outer sphere ion-pair)
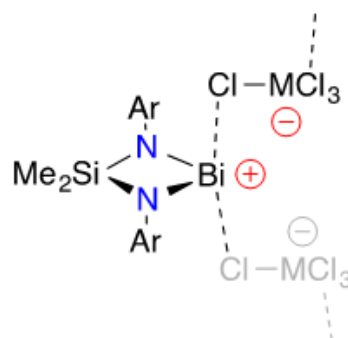
(**B**: aggregated chain)

(**C**: κ^1-*Cl*)
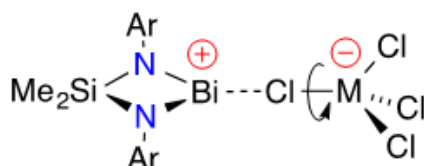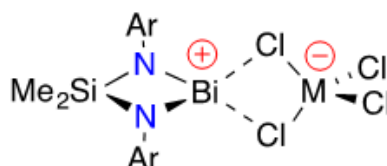
(**D**: $\kappa^2 Cl, Cl'$)
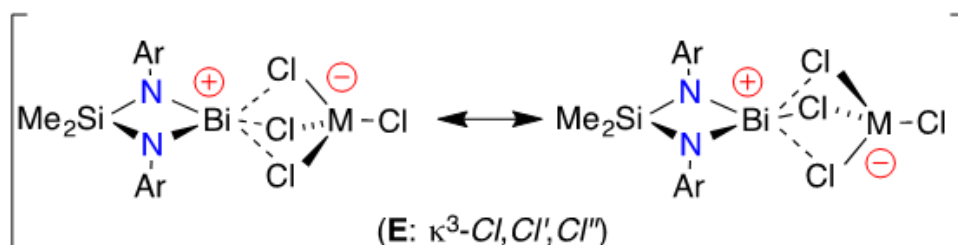
(**E**: κ^3-*Cl*, *Cl'*, *Cl''*)
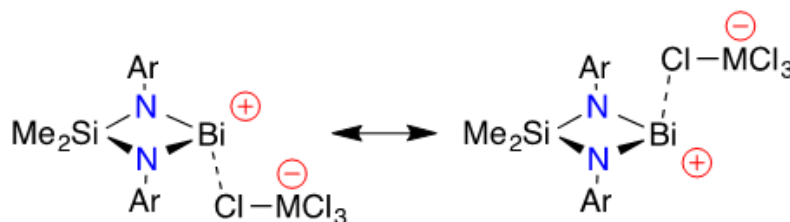
(**F**: fluxional exchange)

Appendix B: Molecular Structure of BiMe₂Si{NAr}₂)Et (15) showing the Position of Disordered Atoms.
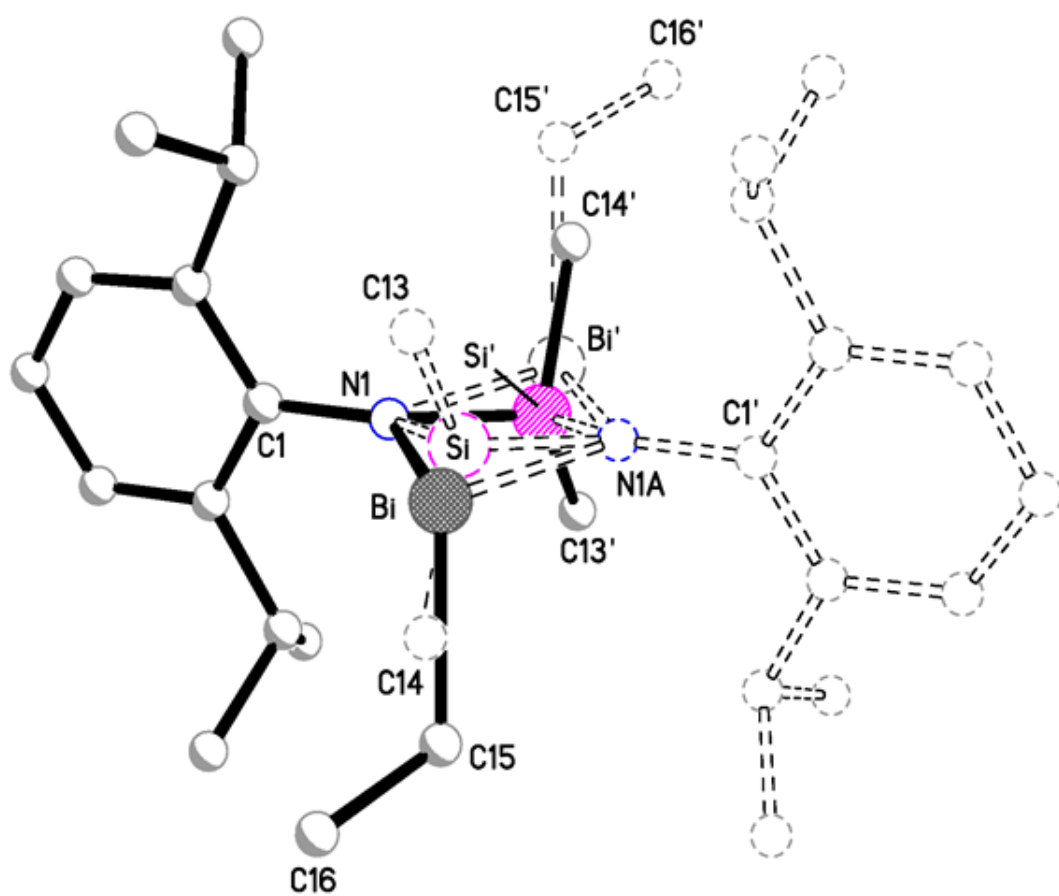
Appendix C: Crystallographic Data for Compounds.

Appendix C1: Crystal data and structure refinement for $Mg(mesCNCy_2)_2(THF)$ (**2**)

Empirical formula	$C_{48}H_{74}MgN_4O$
Formula weight	747.42
Temperature	120(1) K
Wavelength	1.54180 Å
Crystal system	Tetragonal
Space group	P 4_3 2_1 2 (No.96)
Unit cell dimensions	a = 10.24350(13) Å, α= 90°.
	b = 10.24350(13) Å, β= 90°.
	c = 43.7040(7) Å, γ= 90°.
Volume	4585.83(11) Å^3
Z	4
Density (calculated)	1.08 Mg/m^3
Absorption coefficient	0.608 mm^{-1}
F(000)	1640
Crystal size	0.25 x 0.09 x 0.05 mm^3
Theta range for data collection	4.05 to 73.79°
Index ranges	-12≤h≤12, -12≤k≤12, -54≤l≤32
Reflections collected	33678
Independent reflections	4630 [R(int) = 0.058]
Completeness to theta = 73.79°	99.90%
Absorption correction	Gaussian
Max. and min. transmission	1.782 and 0.924
Refinement method	Full-matrix least-squares on F^2
Data / restraints / parameters	4630 / 0 / 248
Goodness-of-fit on F^2	1.044
Final R indices [I≥2sigma(I)]	R1 = 0.037, wR2 = 0.092
R indices (all data)	R1 = 0.040, wR2 = 0.094
Absolute structure parameter	-0.02(5)
Largest diff. peak and hole	0.24 and -0.21 e.Å^{-3}

Appendix C2: Crystal data and structure refinement for Mg({SiMe$_3$}$_2$NC{Ni-Pr}$_2$)$_2$(THF) (**3**)

Empirical formula	C$_{30}$H$_{72}$MgN$_6$OSi$_4$
Formula weight	669.61
Temperature	120.01(10) K
Wavelength	1.5418 Å
Crystal system	Monoclinic
Space group	$P\,2_1/c$ (No.14)
Unit cell dimensions	a = 9.9306(2) Å, α= 90°.
	b = 24.2870(4) Å, β= 114.059(2)°.
	c = 18.9646(4) Å, γ= 90°.
Volume	4176.61(14) Å^3
Z	4
Density (calculated)	1.07 Mg/m^3
Absorption coefficient	0.186 mm^{-1}
F(000)	1480
Crystal size	0.32 x 0.27 x 0.11 mm^3
Theta range for data collection	3.13 to 73.81°.
Index ranges	-12≤h≤12, -29≤k≤29, -21≤l≤21
Reflections collected	50946
Independent reflections	8369 [R(int) = 0.114]
Reflections with I>2sigma(I)	7105
Completeness to theta = 66.97°	98.60%
Absorption correction	Semi-empirical from equivalents
Max. and min. transmission	1.00000 and 0.89807
Refinement method	Full-matrix least-squares on F^2
Data / restraints / parameters	8369 / 0 / 379
Goodness-of-fit on F^2	1.055
Final R indices [I≥2sigma(I)]	R1 = 0.080, wR2 = 0.125
R indices (all data)	R1 = 0.088, wR2 = 0.130
Largest diff. peak and hole	0.34 and -0.35 e.Å^{-3}

Appendix C3: Crystal data and structure refinement for Mg(PhC≡CC{Ni-Pr}$_2$)$_2$(THF)$_2$ (**4**.(THF))

Empirical formula	C$_{38}$H$_{54}$MgN$_4$O$_2$
Formula weight	623.16
Temperature	120.01(10) K
Wavelength	1.5418 Å
Crystal system	Triclinic
Space group	$P\bar{1}$ (No.2)
Unit cell dimensions	a = 9.3730(3) Å, α= 78.282(3)°.
	b = 10.0360(4) Å, β= 70.533(4)°.
	c = 10.5466(4) Å, γ= 77.850(3)°.
Volume	904.86(6) Å^3
Z	1
Density (calculated)	1.14 Mg/m^3
Absorption coefficient	0.703 mm^{-1}
F(000)	338
Crystal size	0.34 x 0.30 x 0.21 mm^3
Theta range for data collection	4.55 to 73.91°.
Index ranges	-11≤h≤11, -12≤k≤11, -13≤l≤11
Reflections collected	10124
Independent reflections	3565 [R(int) = 0.016]
Completeness to theta = 66.97°	99.80%
Absorption correction	Semi-empirical from equivalents
Max. and min. transmission	1.000 and 0.632
Refinement method	Full-matrix least-squares on F^2
Data / restraints / parameters	3565 / 0 / 205
Goodness-of-fit on F^2	1.025
Final R indices [I≥2sigma(I)]	R1 = 0.035, wR2 = 0.090
R indices (all data)	R1 = 0.036, wR2 = 0.091
Largest diff. peak and hole	0.19 and -0.17 e.Å^{-3}

Appendix C4: Crystal data and structure refinement for Mg(C≡CPh)$_2$(THF)$_4$ (**6**.(THF)$_4$)

Empirical formula	C$_{32}$H$_{42}$MgO$_4$
Formula weight	514.97
Temperature	120.01(10) K
Wavelength	1.54180 Å
Crystal system	Monoclinic
Space group	$C2/c$ (No.15)
Unit cell dimensions	a = 11.0212(6) Å, α= 90°.
	b = 22.0516(10) Å, β= 105.758(7)°.
	c = 12.0459(8) Å, γ= 90°.
Volume	2817.6(3) Å^3
Z	4
Density (calculated)	1.21 Mg/m^3
Absorption coefficient	0.814 mm^{-1}
F(000)	1112
Crystal size	0.55 x 0.41 x 0.24 mm^3
Theta range for data collection	4.01 to 73.82°.
Index ranges	-13≤h≤13, -26≤k≤27, -14≤l≤14
Reflections collected	16457
Independent reflections	2836 [R(int) = 0.059]
Completeness to theta = 73.82°	99.30%
Absorption correction	Semi-empirical from equivalents
Max. and min. transmission	1.00000 and 0.63012
Refinement method	Full-matrix least-squares on F^2
Data / restraints / parameters	2836 / 3 / 191
Goodness-of-fit on F^2	0.994
Final R indices [I≥2sigma(I)]	R1 = 0.075, wR2 = 0.221
R indices (all data)	R1 = 0.078, wR2 = 0.229
Largest diff. peak and hole	1.385 and -0.341 e.Å^{-3}

Appendix C5: Crystal data and structure refinement for [Mg(PhC≡CC{N*i*-Pr}$_2$)Br(Et$_2$O)]$_2$ ([**7**]$_2$)

Empirical formula	C$_{19}$H$_{29}$BrMgN$_2$O
Formula weight	405.66
Temperature	120(1) K
Wavelength	1.54180 Å
Crystal system	Orthorhombic
Space group	*Pca*2$_1$ (No.29)
Unit cell dimensions	a = 18.05830(13) Å, α= 90°.
	b = 12.40280(8) Å, β= 90°.
	c = 19.33740(13) Å, γ= 90°.
Volume	4331.06(5) Å^3
Z	8
Density (calculated)	1.24 Mg/m3
Absorption coefficient	2.916 mm-1
F(000)	1696
Crystal size	0.65 x 0.57 x 0.41 mm^3
Theta range for data collection	3.56 to 73.91°.
Index ranges	-22≤h≤20, -15≤k≤10, -24≤l≤24
Reflections collected	29431
Independent reflections	8510 [R(int) = 0.029]
Completeness to theta = 73.91°	98.70%
Absorption correction	Semi-empirical from equivalents
Max. and min. transmission	1.00000 and 0.70232
Refinement method	Full-matrix least-squares on F^2
Data / restraints / parameters	8510 / 1 / 434
Goodness-of-fit on F^2	1.058
Final R indices [I≥2sigma(I)]	R1 = 0.034, wR2 = 0.089
R indices (all data)	R1 = 0.034, wR2 = 0.089
Absolute structure parameter	0.00(7)
Largest diff. peak and hole	0.52 and -0.69 e.Å^{-3}

Appendix C6: Crystal data and structure refinement for $Me_2Si\{N(Na.(THF)_3)Ar\}\{NHAr\}$ (**10a**.$(THF)_3$)

Empirical formula	$C_{42}H_{72}N_2NaO_4Si$
Formula weight	720.09
Temperature/K	120.02(10)
Crystal system	triclinic
Space group	$P\bar{1}$ (No.2)
a/Å	11.3893(4)
b/Å	12.2039(4)
c/Å	16.5160(6)
$\alpha/°$	80.126(3)
$\beta/°$	74.202(3)
$\gamma/°$	77.259(3)
Volume/Å^3	2139.28(13)
Z	2
calc mg/mm^3	1.12
m/mm^1	0.105
F(000)	790
Crystal size/mm^3	0.8 x 0.43 x 0.41
Radiation	$MoK\alpha$ (= 0.71073)
2 range for data collection	5.564 to 59.998°
Index ranges	-16≤h≤15, -17≤k≤14, -22≤l≤21
Reflections collected	19499
Independent reflections	11706 [R(int) = 0.025]
Data/restraints/parameters	11706/0/484
Goodness-of-fit on F^2	1.016
Final R indexes [I≥2σ(I)]	R1 = 0.047, wR2 = 0.118
Final R indexes [all data]	R1 = 0.060, wR2 = 0.127
Largest diff. peak/hole / e Å^{-3}	0.45/-0.32

Appendix C7: Crystal data and structure refinement for [{Bi(Me$_2$Si{NAr}$_2$)}$_2$(μ-Cl)][GaCl$_4$] (**13b**)

Empirical formula	C$_{58}$H$_{94}$Bi$_2$Cl$_5$GaN$_4$Si$_2$
Formula weight	1568.48
Temperature/K	120.01(10)
Crystal system	triclinic
Space group	$P\bar{1}$ (No.2)
a/Å	12.8472(5)
b/Å	17.0713(7)
c/Å	17.4081(7)
α/°	117.739(4)
β/°	92.142(3)
γ/°	90.447(3)
Volume/Å^3	3375.4(3)
Z	2
calc mg/mm^3	1.54
m/mm^1	12.97
F(000)	1560
Crystal size/mm^3	0.1 x 0.08 x 0.02
2 range for data collection	5.742 to 147.992°
Index ranges	-14≤h≤15, -21≤k≤20, -15≤l≤21
Reflections collected	26092
Independent reflections	13265 [R(int) = 0.034]
Data/restraints/parameters	13265/36/671
Goodness-of-fit on F^2	1.036
Final R indexes [I≥2σ(I)]	R1 = 0.031, wR2 = 0.073
Final R indexes [all data]	R1 = 0.040, wR2 = 0.080
Largest diff. peak/hole / e Å^{-3}	1.66/-2.15

Appendix C8: Crystal data and structure refinement for Bi(Me$_2$Si{NAr}$_2$)Ph (**14**)

Empirical formula	C$_{67.5}$H$_{90}$Bi$_2$N$_4$Si$_2$
Formula weight	1431.57
Temperature/K	120.02(10)
Crystal system	triclinic
Space group	$P\bar{1}$ (No.2)
a/Å	12.9068(2)
b/Å	15.6323(4)
c/Å	17.3240(5)
α/°	108.940(2)
β/°	93.6783(18)
γ/°	100.2794(18)
Volume/Å^3	3224.91(14)
Z	2
calc mg/mm^3	1.47
m/mm^1	5.528
F(000)	1434
Crystal size/mm^3	0.35 x 0.16 x 0.05
Radiation	Mo Kα (= 0.71073)
2 range for data collection	5.328 to 60°
Index ranges	-18≤h≤18, -21≤k≤21, -24≤l≤24
Reflections collected	66037
Independent reflections	18799 [R(int) = 0.035]
Data/restraints/parameters	18799/0/714
Goodness-of-fit on F^2	1.036
Final R indexes [I≥2σ(I)]	R1 = 0.024, wR2 = 0.053
Final R indexes [all data]	R1 = 0.033, wR2 = 0.056
Largest diff. peak/hole / e Å^{-3}	1.82/-0.97

Appendix C9: Crystal data and structure refinement for Bi(Me$_2$Si{NAr}$_2$)Et (**15**)

Empirical formula	C$_{14}$H$_{22.5}$Bi$_{0.5}$NSi$_{0.5}$
Formula weight	323.36
Temperature/K	120.01(10)
Crystal system	trigonal
Space group	R
	(No.148)
a/Å	28.7503(11)
b/Å	28.7503(11)
c/Å	9.8541(5)
$\alpha/°$	90
$\beta/°$	90
$\gamma/°$	120
Volume/Å^3	7053.9(6)
Z	18
calc mg/mm^3	1.37
m/mm^1	5.678
F(000)	2916
Crystal size/mm^3	0.21 x 0.15 x 0.14
Radiation	Mo Kα (= 0.71073)
2 range for data collection	5.66 to 66.22°
Index ranges	-29$\leq$h$\leq$43, -42$\leq$k$\leq$43, -12$\leq$l$\leq$14
Reflections collected	16452
Independent reflections	5348[R(int) = 0.072]
Data/restraints/parameters	5348/114/179
Goodness-of-fit on F^2	1.323
Final R indexes [I$\geq$2σ(I)]	R1 = 0.129, wR2 = 0.272
Final R indexes [all data]	R1 = 0.151, wR2 = 0.280
Largest diff. peak/hole / e Å^{-3}	1.88/-3.13

Appendix C10: Crystal data and structure refinement for Bi(Me$_2$Si{NAr}$_2$)(OAr') (Ar' = 2,6-t-Bu$_2$C$_6$H$_3$) (**17**)

Empirical formula	C$_{40}$H$_{61}$BiN$_2$OSi
Formula weight	822.97
Temperature/K	120.01(10)
Crystal system	triclinic
Space group	$P\bar{1}$ (No.2)
a/Å	10.5385(2)
b/Å	11.2364(3)
c/Å	17.0806(4)
α/°	85.5200(19)
β/°	72.430(2)
γ/°	88.1001(18)
Volume/Å^3	1922.24(8)
Z	2
calcmg/mm^3	1.422
m/mm^1	4.649
F(000)	840
Crystal size/mm^3	0.14 x 0.08 x 0.03
2 range for data collection	5.42 to 55°
Index ranges	-13≤h≤13, -14≤k≤14, -22≤l≤22
Reflections collected	38886
Independent reflections	8839 [R(int) = 0.0456]
Data/restraints/parameters	8839/0/422
Goodness-of-fit on F^2	1.057
Final R indexes [I≥2σ(I)]	R1 = 0.029, wR2 = 0.064
Final R indexes [all data]	R1 = 0.034, wR2 = 0.067
Largest diff. peak/hole / e Å^{-3}	2.81/-0.73

Appendix C11: Crystal data and structure refinement for Bi(Me$_2$Si{NAr}$_2$)(PCy$_2$) (**18**)

Empirical formula	C$_{41.5}$H$_{65.5}$BiN$_2$PSi
Formula weight	860.5
Temperature/K	120.01(10)
Crystal system	triclinic
Space group	$P\bar{1}$ (No.2)
a/Å	11.6799(2)
b/Å	12.7221(3)
c/Å	15.6698(3)
α/°	69.6451(19)
β/°	68.6372(16)
γ/°	73.3507(18)
Volume/Å^3	1998.69(8)
Z	2
calcmg/mm^3	1.43
m/mm^1	4.511
F(000)	881
Crystal size/mm^3	0.25 x 0.18 x 0.15
Radiation	Mo Kα (= 0.71073)
2 range for data collection	5.426 to 54.998°
Index ranges	-15≤h≤15, -16≤k≤16, -20≤l≤20
Reflections collected	58123
Independent reflections	9184[R(int) = 0.029]
Data/restraints/parameters	9184/0/435
Goodness-of-fit on F^2	1.075
Final R indexes [I≥2σ(I)]	R1 = 0.019, wR2 = 0.048
Final R indexes [all data]	R1 = 0.020, wR2 = 0.049
Largest diff. peak/hole / e Å^{-3}	3.91/-0.56

Appendix C12: Crystal data and structure refinement for Bi(O{Me$_2$SiNAr"}$_2$)Cl (Ar" = 2,6-i-Pr$_2$C$_6$H$_3$) (**20a**)

Empirical formula	C$_{28}$H$_{46}$BiClN$_2$OSi$_2$
Formula weight	727.28
Temperature/K	220.01(10)
Crystal system	triclinic
Space group	$P\bar{1}$ (No.2)
a/Å	10.0438(3)
b/Å	12.5485(3)
c/Å	13.2758(4)
α/°	80.632(2)
β/°	86.225(3)
γ/°	75.858(3)
Volume/Å^3	1600.26(8)
Z	2
calcmg/mm^3	1.51
m/mm^1	5.689
F(000)	728
Crystal size/mm^3	0.51 x 0.46 x 0.37
2 range for data collection	5.146 to 59.996°
Index ranges	-14≤h≤14, -17≤k≤17, -18≤l≤18
Reflections collected	23378
Independent reflections	9330[R(int) = 0.037]
Data/restraints/parameters	9330/0/328
Goodness-of-fit on F^2	1.044
Final R indexes [I≥2σ(I)]	R1 = 0.032, wR2 = 0.070
Final R indexes [all data]	R1 = 0.037, wR2 = 0.072
Largest diff. peak/hole / e Å^{-3}	2.11/-2.60

Appendix C13: Crystal data and structure refinement for [Bi(O{Me$_2$SiNAr"}$_2$)][AlCl$_4$] (Ar" = 2,6-i-Pr$_2$C$_6$H$_3$) (**21**)

|	
Empirical formula	C$_{35}$H$_{54}$AlBiCl$_4$N$_2$OSi$_2$
Formula weight	952.74
Temperature/K	120.01(10)
Crystal system	triclinic
Space group	$P\bar{1}$ (No.2)
a/Å	10.53512(18)
b/Å	10.83490(18)
c/Å	18.5054(3)
α/°	87.1030(13)
β/°	88.7719(13)
γ/°	75.1549(15)
Volume/Å^3	2039.14(6)
Z	2
calcmg/mm^3	1.55
m/mm^1	4.695
F(000)	956
Crystal size/mm^3	0.46 x 0.31 x 0.22
2 range for data collection	5.206 to 60°
Index ranges	-14≤h≤14, -15≤k≤15, -26≤l≤26
Reflections collected	73699
Independent reflections	11894[R(int) = 0.028]
Data/restraints/parameters	11894/0/428
Goodness-of-fit on F^2	1.134
Final R indexes [I≥2σ(I)]	R1 = 0.015, wR2 = 0.038
Final R indexes [all data]	R1 = 0.016, wR2 = 0.039
Largest diff. peak/hole / e Å^{-3}	1.00/-0.55

Publication(s)

Catalytic C−C Bond Formation Promoted by Organo- and Amidomagnesium(II) Compounds

Ryan J. Schwamm and Martyn P. Coles*

School of Chemical and Physical Sciences, Victoria University of Wellington, P.O. Box 600, Wellington, New Zealand

S *Supporting Information*

ABSTRACT: Mg(mesC{NCy}$_2$)(N{SiMe$_3$}$_2$)(THF) is a (pre)-catalyst for C−C bond formation. Attempted isolation of intermediates in a proposed catalytic cycle was hindered by facile ligand redistribution. A subsequent investigation of commercially available organo- or amidomagnesium(II) compounds (including Grignard reagents) demonstrated similar catalytic behavior.
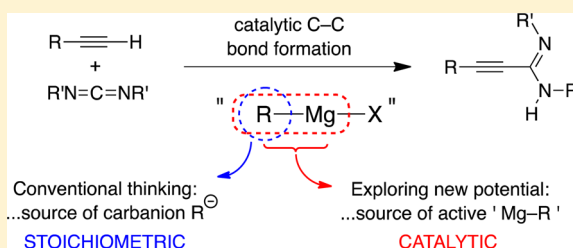
Magnesium catalysts for carbon−carbon bond formation focus primarily on the Lewis acidic properties of the metal.[1] Examples that proceed via sequential σ-bond metathesis/insertion reactions are less well represented in the chemical literature.[2] We have recently synthesized magnesium guanidinate[3] and amidinate[4] compounds and demonstrated that Mg(mesC{NCy}$_2$)(N{SiMe$_3$}$_2$)(THF) (**1**) is active for the dimerization of aldehydes (Tishchenko reaction).[4] We report here that **1** is also active toward the coupling of terminal alkynes and carbodiimides under catalytic conditions, leading to the discovery that other commercially available Mg(II) compounds, including Grignard reagents, effect this transformation. In a related study, Hill et al. have recently shown that the Mg-mediated reaction between alkynes and isocyanates forms bis(imidazolidine-2,4-diones).[5]

Carbodiimide insertion into M−C bonds of terminal acetylides to afford the corresponding propargylamidinate has been documented for Li,[6] K,[7] Ca,[8] Y,[9] Sm,[10] Yb,[9a] Lu,[9a] and U.[11] Several compounds produce the C−C coupled product catalytically,[6a,8,9c,12] with the most extensively studied system promoted by {Me$_2$Si(C$_5$Me$_4$)(NPh)}Y(CH$_2$SiMe$_3$)(THF).[9a] A general mechanism of catalysis has been presented (Scheme 1). The entry point is the conversion of a metal−alkyl or −amide (pre)catalyst to acetylide **I**. Carbodiimide insertion into the M−C bond affords propargylamidinate **III**, which is protonated by alkyne to liberate the amidine **V** and regenerate **I**.

The efficacy of **1** in the catalytic addition of terminal alkynes to carbodiimides was initially investigated on an NMR scale using *N,N*′-diisopropylcarbodiimide and phenylacetylene (Table 1). At room temperature a catalyst loading of 10 mol % yielded 44% of the amidine after 24 h (entry 1); decreasing the amount of catalyst to 1 mol % reduced the yield to 24% (entry 2). More respectable yields were obtained at the lower loading with increased temperature (entries 3 and 4), with good yields (~70%) obtained at 80 °C. Control reactions showed no catalyst decomposition at this temperature and confirmed that the propargylamidine was not formed in the

Scheme 1
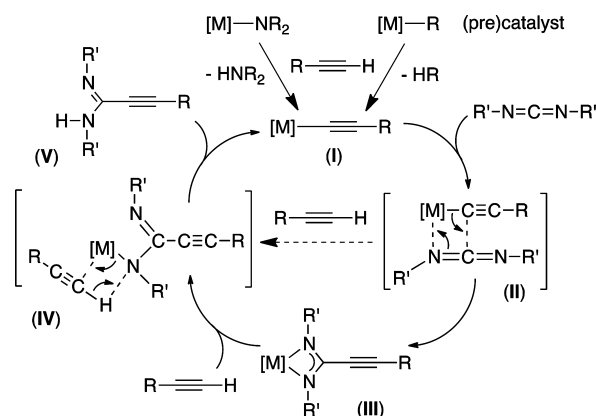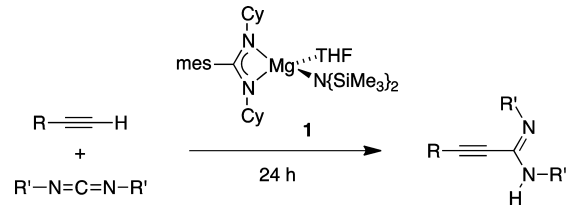
absence of **1**. Further studies were performed in C$_6$D$_6$ with 1 mol % of **1** at 80 °C.

Varying the carbodiimide had a significant effect on the activity. The *i*-Pr and Cy derivatives gave similar yields after 24 h (entries 4 and 5), consistent with a similar steric profile of the two nitrogen substituents. Increasing the bulk of the substituent to *t*-Bu gave a much lower yield (entry 6), and no amidine was produced with the 2,6-diisopropylphenyl-substituted carbodiimide (entry 7). These results are consistent with associative σ-bond metathesis during formation of the C−C bond (**II**; Scheme 1). Para substitution of the acetylene aryl group had little effect in comparison to phenylacetylene (entries 8 and 9). Lower activities were observed for silyl-substituted acetylenes (entries 10 and 11), with a further reduction in yield obtained for alkyl derivatives (entries 12 and 13). In preparative-scale reactions (entries 14 and 15), toluene gave superior results in comparison with THF, consistent with the competitive binding of THF to Mg during catalysis.

Table 1. Catalytic Addition of Alkynes to Carbodiimides promoted by 1

	R	R′	loading (mol %)	temp (°C)	yield (%)[a]
1	Ph	*i*-Pr	10	25	44
2	Ph	*i*-Pr	1	25	24
3	Ph	*i*-Pr	1	50	53
4	Ph	*i*-Pr	1	80	72
5	Ph	Cy	1	80	74
6	Ph	*t*-Bu	1	80	7
7	Ph	Ar[b]	1	80	0
8	4-*t*-BuC$_6$H$_4$	*i*-Pr	1	80	76
9	4-MeC$_6$H$_4$	*i*-Pr	1	80	77
10	SiMe$_3$	*i*-Pr	1	80	63
11	Si(*i*-Pr)$_3$	*i*-Pr	1	80	42
12	*n*-Bu	*i*-Pr	1	80	41
13	*t*Bu	*i*-Pr	1	80	12
14	Ph	*i*-Pr	5	80	73[c,d]
15	Ph	*i*-Pr	5	80	51[c,e]

[a]Yields from ^{1}H NMR integrals using THF (from **1**) as internal standard (average of two runs); [b]Ar = 2,6-diisopropylphenyl. [c]Isolated yield. [d]Toluene. [e]THF.

In a standard catalytic experiment, a solution of **1** was added to a premixed 1:1 solution of the acetylene and carbodiimide. As such, entry into the catalytic cycle may occur by two possible initiation pathways (Scheme 2). Studies on related

Scheme 2. [a]
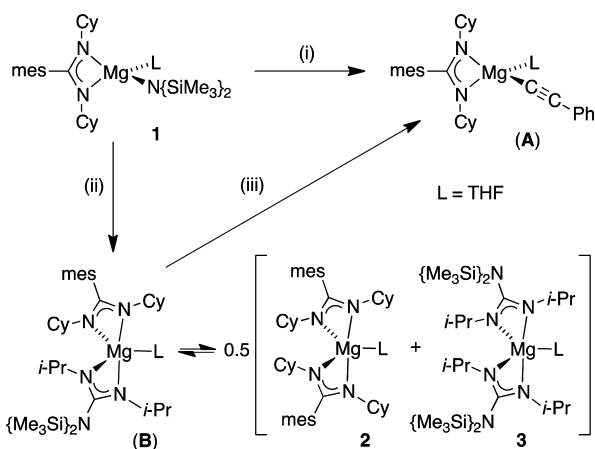
[a]Legend: (i) HC≡CPh, −HN{SiMe$_3$}$_2$; (ii) *i*-PrN=C=N-*i*-Pr; (iii) HC≡CPh, −{Me$_3$Si}$_2$NC{N-*i*-Pr}{NH-*i*-Pr}.

calcium systems suggest initial σ-bond metathesis of the amide bond to form the metal acetylide and HN{SiMe$_3$}$_2$;[8] this corresponds to formation of **A** in Scheme 2. An alternative activation process for **1** involves insertion of carbodiimide into the magnesium−amide bond to afford the mixed amidinate/guanidinate species **B**; similar heteroallene insertion into Mg−C bonds has been reported.[13] Intermediate **B** is able to react

with acetylene to afford **A** with liberation of the guanidine, {Me$_3$Si}$_2$NC{N-*i*-Pr}{NH-*i*-Pr}.[14]

An NMR-scale reaction of **1** and phenylacetylene showed quantitative liberation of HN{SiMe$_3$}$_2$ and formation of a new species represented by a single set of acetylide and amidinate resonances. NOE correlations between the *o*-C$_6$H$_5$ protons of the acetylide and the α-protons of the THF and cyclohexyl groups are consistent with the heteroleptic terminal acetylide **A**. Compound **A** is stable to additional phenylacetylene at 80 °C, demonstrating the stability of the amidinate ligand toward protonolysis under catalytically relevant conditions.

The ^{13}C NMR of the 1:1 reaction of **1** and *N,N′*-diisopropylcarbodiimide showed three low-field resonances for the metallacyclic carbon (Figure S15, Supporting Information). The peaks at δ_C 174.0 and 166.4 ppm correspond to the bis(amidinate) Mg(mesC{NCy}$_2$)$_2$(THF) (**2**) and the bis(guanidinate) Mg({Me$_3$Si}$_2$NC{N-*i*-Pr}$_2$)$_2$(THF) (**3**), respectively, confirmed by independently synthesized samples (vide infra). The remaining peak (δ_C 173.8) is attributed to the amidinate CN$_2$ of the mixed amidinate/guanidinate species **B** (Scheme 2). The CN$_3$ resonance in **B** is presumed to overlap with the peak at δ_C 166.4 ppm. The ^{1}H NMR spectrum is complicated by overlapping signals, but resonances for the mesityl group of **2** (δ_H 6.84, 2.47, and 2.13 ppm) and the *i*-Pr and SiMe$_3$ groups of **3** (δ_H 1.17 (d), 0.32 ppm) are identifiable (Figure S14, Supporting Information). The proposed equilibrium between these complexes (Scheme 2) was demonstrated by the formation of the mixed-ligand complex **B** when equimolar amounts of isolated bis(amidinate) and bis-(guanidinate) species **2** and **3** were combined.

Addition of 1 equiv of *N,N′*-diisopropylcarbodiimide to **A**, representing the second step of the proposed catalytic cycle, also generated a mixture of species (Scheme 3). Compound **2**

Scheme 3. [a]
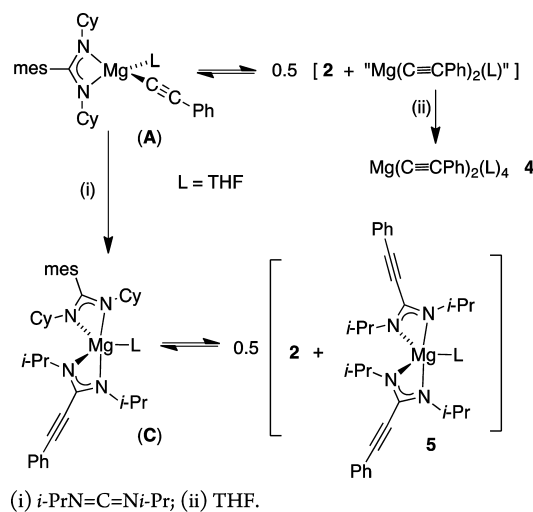
(i) *i*-PrN=C=N*i*-Pr; (ii) THF.

[a]Legend: (i) *i*-PrN=C=N-*i*-Pr; (ii) THF.

and the bis(propargylamidinate) Mg(PhC≡CC{N-*i*-Pr}$_2$)$_2$(THF) (**5**) are identified in the ^{13}C{^{1}H} NMR spectrum of the mixture from comparison with independently synthesized samples (Figure S17, Supporting Information). The remaining resonances are assigned to the mixed amidinate Mg(mesC{NCy}$_2$)(PhC≡CC{N-*i*-Pr}$_2$)(THF) (**C**) with CN$_2$

resonances at δ_C 173.8 and 157.7 ppm and acetylenic peaks at δ_C 95.8 and 81.0 ppm.

Attempts to isolate acetylide **A** from the reaction of **1** and phenylacetylene were unsuccessful. Fractional crystallization of the resultant white powder from THF/hexane afforded the bis(acetylide) Mg(C≡CPh)$_2$(THF)$_4$ (**4**;[15] first crop) and bis(amidinate) **2** (second crop), in yields of 16% and 26%, respectively. The composition of **4** was confirmed by independent synthesis. A similar ligand redistribution occurred during attempts to isolate **C**. Reaction of **A** (generated in situ) with *N,N'*-diisopropylcarbodiimide, followed by workup and crystallization from THF/hexane, gave **2** (first crop) and solvated Mg(PhC≡CC{N-*i*-Pr}$_2$)$_2$(THF)$_2$ (**5**(THF); second crop) in isolated yields of 47% and 36%, respectively.

Compound **3** was independently synthesized from the reaction of *N,N'*-diisopropylcarbodiimide with Mg(N-{SiMe$_3$}$_2$)$_2$,[16] confirming the viability of carbodiimide insertion into Mg—amide bonds in the proposed route to **B**. Compound **4** was obtained from the reaction of MgBu$_2$ with phenylacetylene. Compounds **2** and **5** were isolated during the attempted preparation of **A** and **C**, respectively. All new compounds were characterized by ^{1}H and ^{13}C NMR spectroscopy and elemental analysis; X-ray diffraction studies were performed on **2–5** (Figures S23–S27, Supporting Information).

The propensity for the magnesium compounds to undergo facile ligand redistribution precludes definitive identification of the active species in this case. This prompted us to investigate related magnesium compounds to determine whether the catalytic cycle could be accessed from simpler reagents (Table 2).

Initial work examined the products of the ligand redistribution reactions as possible active species. Catalytic turnover was observed for the bis(amidinate/guanidinate) complexes **2**,

3, and **5** with activities comparable to those obtained from **1** under identical conditions (∼70%, entries 2–5). Loss of N,N'-chelating groups to gain entry into catalysis has been observed for lanthanides in ring-opening polymerization[17] and the Tishchenko reaction.[18] The bis(acetylide) **4** exhibited a similar activity (entry 5), suggesting that a chelating ligand is not required in the (pre)catalytic species. To eliminate the possibility that the reaction was proceeding via Lewis acid catalysis, the tetraphenylborate salt Mg(BPh$_4$)$_2$[19] was tested. No activity was observed (entry 6), suggesting that Mg—N or Mg—C bonds (with the potential to form amidinate/guanidinate ligands or terminal acetylides) are important in the precatalytic species.

Other magnesium compounds with this general criterion were identified as candidates for testing. Both MgBu$_2$ and Mg(N{SiMe$_3$}$_2$)$_2$ were active (entries 7 and 8), with yields comparable to those noted above. Similar catalytic activity has been recorded for the addition of amines to carbodiimides using MgBu$_2$.[20] The Grignard reagents MgMeBr and MgPhBr were also active, albeit with lower activity (∼60%, entries 9–11). It was postulated that the presence of a magnesium—bromide bond was responsible for the reduced yield, supported by the inactivity of MgBr$_2$·Et$_2$O in catalysis (entry 12). Further evidence for the detrimental effect of the Mg—Br group resulted from testing Mg(PhC≡CC{N-*i*-Pr}$_2$)Br(OEt$_2$) (**6**), synthesized from the reaction of the neutral amidine PhC≡CC{N*i*-Pr}{NH*i*-Pr} with MgMeBr (entry 13). A yield of ∼60% was recorded, comparable to those obtained with the Grignard reagents. We also demonstrated that the commercially available Grignard reagent MgMeBr was active on a preparative scale, affording a ∼50% yield of the propargylamidine on workup (entries 14– and 15), independent of whether toluene or THF was used as solvent.

In summary, we have shown that catalytic C—C coupling of alkynes and carbodiimides is promoted by simple organo- and amidomagnesium species, including the ubiquitous Grignard reagents. While ligand exchange processes likely dominate the solution behavior of these Mg compounds,[21] this does not have an adverse effect on the overall activity, with the most important factor being the presence of groups that are able to be converted to amidinate/guanidinate ligands. Rather than being considered as a simple source of carbanion, we hope these results promote the use of commercially available reagents to access active metal centers for the development of new catalytic applications based on magnesium.

Table 2. Catalytic Addition of Alkynes to Carbodiimides Promoted by Magnesium Reagents

Ph—≡—H + *i*-Pr—N=C=N—*i*-Pr → (1 mol% catalyst, 80 °C, 24 h) → Ph—≡—C(=N-*i*-Pr)(N(H)—*i*-Pr)

	catalyst	yield (%)^a
1	Mg(mesC{NCy}$_2$)(N{SiMe$_3$}$_2$)(THF) (**1**)	72
2	Mg(mesC{NCy}$_2$)$_2$(THF) (**2**)	74
3	Mg({Me$_3$Si}$_2$NC{N-*i*-Pr}$_2$)$_2$(THF) (**3**)	73
4	Mg(PhC≡CC{N-*i*-Pr}$_2$)$_2$(THF) (**5**)	72^b
5	Mg(C≡CPh)$_2$(THF)$_4$ (**4**)	73^b
6	Mg(BPh$_4$)$_2$	0
7	MgBu$_2$ (1.0 M, heptane)	74^b
8	Mg(N{SiMe$_3$}$_2$)$_2$	70
9	MgMeBr (3.0 M, Et$_2$O)	63^b
10	MgMeBr·*n*Et$_2$O (solid)	59^b
11	MgPhBr·*n*Et$_2$O (solid)	63^b
12	MgBr$_2$·Et$_2$O	0
13	Mg(PhC≡CC{N-*i*-Pr}$_2$)Br(OEt$_2$) (**6**)	60^b
14	MgMeBr, 5 mol % (3.0 M, Et$_2$O)^{c,d}	56
15	MgMeBr, 5 mol % (3.0 M, Et$_2$O)^{c,e}	53

^{a}Yields from ^{1}H NMR integrals using THF (from **1**) as internal standard (average of two runs), unless otherwise stated. ^{b}Yield calculated from consumption of carbodiimide. ^{c}Isolated yield. ^{d}Toluene. ^{e}THF.

■ ASSOCIATED CONTENT

ⓢ Supporting Information

Text, tables, figures, and CIF files giving synthetic details, full characterization data for all new compounds, crystallographic data for **2–6**, and representative NMR spectra of catalytic performance. This material is available free of charge via the Internet at http://pubs.acs.org.

■ AUTHOR INFORMATION

Corresponding Author

*M.P.C.: tel, +64 (0)4 4636357; e-mail, martyn.coles@vuw.ac.nz.

Notes

The authors declare no competing financial interest.

■ REFERENCES

(1) (a) Yamashita, Y.; Tsubogo, T.; Kobayashi, S. *Chem. Sci.* **2012**, *3*, 967. (b) Kazmaier, U. *Angew. Chem., Int. Ed.* **2009**, *48*, 5790.

(2) (a) Crimmin, M. R.; Arrowsmith, M.; Barrett, A. G. M.; Casely, I. J.; Hill, M. S.; Procopiou, P. A. *J. Am. Chem. Soc.* **2009**, *131*, 9670. (b) Dunne, J. F.; Fulton, D. B.; Ellern, A.; Sadow, A. D. *J. Am. Chem. Soc.* **2010**, *132*, 17680.

(3) Day, B. M.; Mansfield, N. E.; Coles, M. P.; Hitchcock, P. B. *Chem. Commun.* **2011**, *47*, 4995.

(4) Day, B. M.; Knowelden, W.; Coles, M. P. *Dalton Trans.* **2012**, *41*, 10930.

(5) Hill, M. S.; Liptrot, D. J.; Mahon, M. F. *Angew. Chem., Int. Ed.* **2013**, *52*, 5364.

(6) (a) Ong, T.-G.; O'Brien, J. S.; Korobkov, I.; Richeson, D. S. *Organometallics* **2006**, *25*, 4728. (b) Brown, D. J.; Chisholm, M. H.; Gallucci, J. C. *Dalton Trans.* **2008**, 1615.

(7) Dröse, P.; Hrib, C. G.; Edelmann, F. T. *J. Organomet. Chem.* **2010**, *695*, 1953.

(8) Barrett, A. G. M.; Crimmin, M. R.; Hill, M. S.; Hitchcock, P. B.; Lomas, S. L.; Mahon, M. F.; Procopiou, P. A.; Suntharalingam, K. *Organometallics* **2008**, *27*, 6300.

(9) (a) Zhang, W.-X.; Nishiura, M.; Hou, Z. *J. Am. Chem. Soc.* **2005**, *127*, 16788. (b) Casely, I. J.; Ziller, J. W.; Evans, W. J. *Organometallics* **2011**, *30*, 4873. (c) Yi, W.; Zhang, J.; Li, M.; Chen, Z.; Zhou, X. *Inorg. Chem.* **2011**, *50*, 11813.

(10) Cole, M. L.; Deacon, G. B.; Forsyth, C. M.; Junk, P. C.; Cerón, D. P.; Wang, J. *Dalton Trans.* **2010**, *39*, 6732.

(11) Evans, W. J.; Walensky, J. R.; Ziller, J. W.; Rheingold, A. L. *Organometallics* **2009**, *28*, 3350.

(12) Zhang, W.-X.; Hou, Z. *Org. Biomol. Chem.* **2008**, *6*, 1720.

(13) Srinivas, B.; Chang, C.-C.; Chen, C.-H.; Chiang, M. Y.; Chen, I.-T.; Wang, Y.; Lee, G.-H. *J. Chem. Soc., Dalton Trans.* **1997**, 957.

(14) Loss of the amidine to afford the guanidinate analogue of **A**, Mg({Me$_3$Si}$_2$NC{Ni-Pr}$_2$)(CCPh)(THF) (**A'**) is possible at this stage. However the stoichiometric reaction of **2** with PhCCH showed no reaction, whereas **3** reacted with PhCCH to liberate the guanidine, (Me$_3$Si)$_2$NC{Ni-Pr}{NHi-Pr}, suggesting loss of this group occurs more readily.

(15) Perucaud, M.-C.; Ducom, J.; Vallino, M. *C. R. Acad. Sci., Ser. C* **1967**, *264*, 571.

(16) Sarazin, Y.; Howard, R. H.; Hughes, D. L.; Humphrey, S. M.; Bochmann, M. *Dalton Trans.* **2006**, 340.

(17) Li, C.; Wang, Y.; Zhou, L.; Sun, H.; Shen, Q. *J. Appl. Polym. Sci.* **2006**, *102*, 22.

(18) Zuyls, A.; Roesky, P. W.; Deacon, G. B.; Konstas, K.; Junk, P. C. *Eur. J. Org. Chem.* **2008**, 693.

(19) Corey, E. J.; Ishihara, K. *Tetrahedron Lett.* **1992**, *33*, 6807.

(20) Alonso-Moreno, C.; Carrillo-Hermosilla, F.; Garcés, A.; Otero, A.; López-Solera, I.; Rodríguez, A. M.; Antiñolo, A. *Organometallics* **2010**, *29*, 2789.

(21) Chisholm, M. H.; Choojun, K.; Chow, A. S.; Fraenkel, G. *Angew. Chem., Int. Ed.* **2013**, *52*, 3264.

Low-Coordinate Bismuth Cations

Ryan J. Schwamm,[†] Benjamin M. Day,[§] Martyn P. Coles,*,[†] and Christopher M. Fitchett[‡]

[†]School of Chemical and Physical Sciences, Victoria University of Wellington, PO Box 600, Wellington, New Zealand
[§]Department of Chemistry, University of Sussex, Falmer, Brighton BN1 9QJ, U.K.
[‡]Department of Chemistry, University of Canterbury, Private Bag 4800, Christchurch 8041, New Zealand

S Supporting Information

ABSTRACT: Chloride abstraction from the diamido-bismuth compound $Bi(Me_2Si\{NAr\}_2)Cl$ (**1**, Ar = 2,6-i-$Pr_2C_6H_3$) using MCl_3 (M = Al, Ga) is a facile route to cationic species. Stoichiometric reactions afford the tetrachlorometallate salts $[Bi(Me_2Si\{NAr\}_2)][MCl_4]$ (**2a**, M = Al; **3a**, M = Ga), whereas reaction with 0.5 equiv of the group 13 reagent gives the μ-chlorido bridged cations $[\{Bi(Me_2Si\{NAr\}_2)\}_2(\mu\text{-}Cl)][MCl_4]$ (**2b**, M = Al; **3b**, M = Ga). The crystal structure of **2a** shows a formally two-coordinate bismuth cation, with a Bi···Cl contact to the $[AlCl_4]^-$ anion, whereas the structure of **3b** shows a total of three Bi···Cl contacts to $[GaCl_4]^-$. Both species associate as $\{1:1\}_2$ dimers in the solid state through additional Bi···Cl interactions. Attempted preparation of cationic complexes using either $NaBR_4$ (R = Ph, Et) or $[HNEt_3][BPh_4]$ were unsuccessful. Instead of forming the borate salts, the neutral compounds $Bi(Me_2Si\{NAr\}_2)R$ (**4**, R = Et; **5**, R = Ph) were isolated as a result of aryl/alkyl transfer from boron to bismuth.
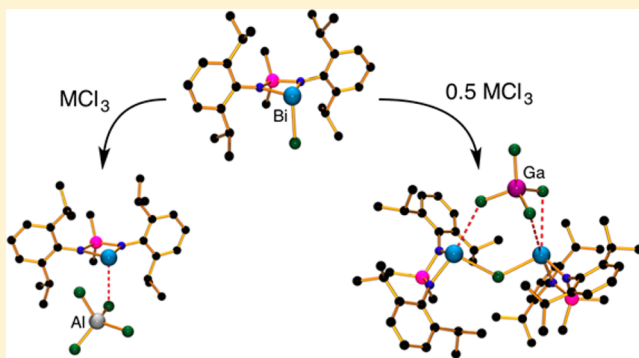
1. INTRODUCTION

Commercially available BiX_3 compounds (X = halogen, triflate, nitrate) are used as Lewis acidic reagents to promote a range of organic transformations[1] and polymerization reactions.[2] More recently cationic bismuth compounds have been investigated,[3,4] developing the concept that an increased electrophilicity associated with the positively charged metal center will enhance the activity of the reagents. Due in part to the large radius of the element [Shannon ionic radii Bi^{3+}: 6-coordinate = 1.03 Å; 8-coordinate = 1.17 Å],[5] much of the research on cationic bismuth compounds has focused on the application of multidentate ligands able to provide additional interactions to support the metal center.[6] Prominent among these examples are the potentially tridentate systems based on either a dianionic (C,E,C) framework (E = N, O, S),[4,7] or the mono-anionic (E,C,E)-system.[8,9] Relatively little work has been directed toward the study of low-coordinate bismuth cations.

A survey of the Cambridge Structural Database[10] was conducted to examine the distribution of coordination numbers associated with crystallographically characterized cationic bismuth compounds. The results, displayed in Figure 1, were divided into three classes: bismuth(III), bismuth(V), and bismuth clusters (defined in this survey as species containing three or more Bi atoms). Most examples have been reported in which the bismuth is 4-coordinate (52.5%), with 6- and 8-coordinate bismuth each representing 12.0% of the total number of structures listed in the database. Both high- (>8-co-ordinate: 7.6%) and especially low- (<4-coordinate: 3.8%) co-ordinate species are poorly represented. For each coordination
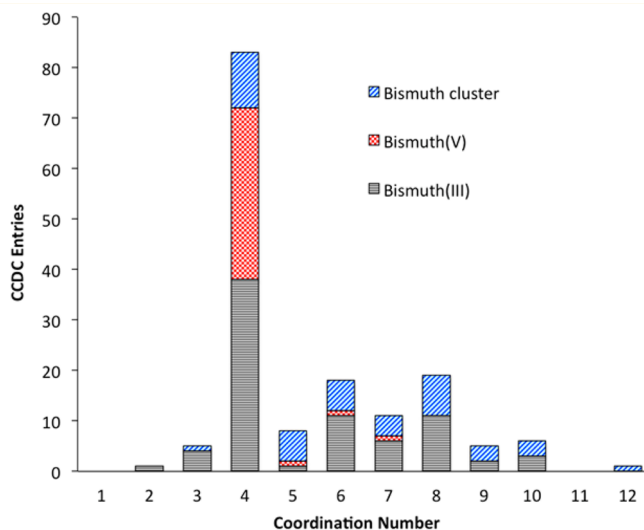
Figure 1. Graph showing the coordination number of structurally characterized bismuth cations (bismuth clusters defined as compounds containing three or more Bi atoms in the structure).

number there is a fairly even split between Bi(III) and higher nuclearity "cluster" compounds, with far fewer examples of Bi(V) cations. The exception is the 4-coordinate species, for which a large number of $[BiAr_4]^+$ cations have been structurally determined.

The only structurally characterized two-coordinated bismuth cation is supported by the bulky diamido-ligand $[Me_2Si\{Nt\text{-}Bu\}_2]^{2-}$ (**I**, Figure 2).[11] The salt is generated by chloride abstraction
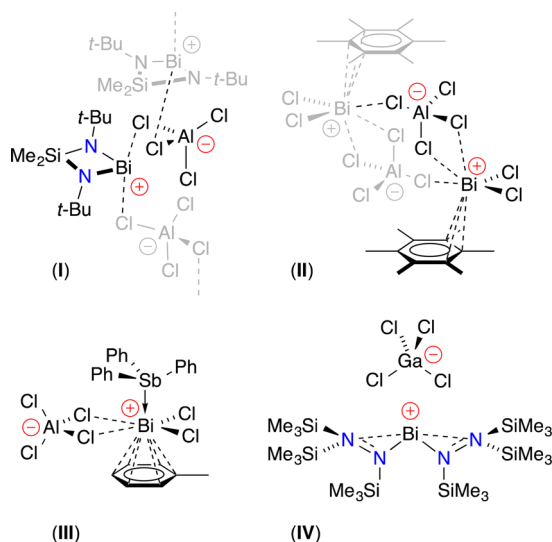

Figure 2. Examples of structurally characterized bismuth cations containing tetrachlorometallate anions (see text for references).

from the neutral Bi(III) precursor $Bi(Me_2Si\{Nt\text{-}Bu\}_2)Cl$, using MCl_3 (M = Al, Ga, and In), to afford the corresponding tetrachlorometallate species. This strategy for cation production has been applied to other bismuth systems.[12−17] The aluminum reagent $AlCl_3$ dominates as the chloride abstraction agent, with relatively few reports on the use of $GaCl_3$,[11,15,17] and only a single report of this reactivity being achieved with $InCl_3$;[11] these trends presumably reflect the differing Lewis acidity of the group 13 reagents.

The solid-state structure of the tetrachloroaluminate salt **I** contains long-range Bi⋯Cl interactions between the $[Bi(Me_2Si\{Nt\text{-}Bu\}_2)]^+$ cation and chlorides from two $[AlCl_4]^-$ anions, generating a polymeric chain parallel to the b-axis of the unit cell. Such moderation of positive charge in bismuth salts through the formation of intermolecular Bi⋯Cl contacts to the $[MCl_4]^-$ counterions is relatively common, and may be augmented by additional associations in the solid state. For example, the reaction of $BiCl_3$ and $AlCl_3$ in the presence of hexamethyl benzene affords the $\{1{:}1\}_2$ dimeric salt with an η^3-bonded aromatic ring (**II**),[12] whereas generating the $[BiCl_2]^+$ cation in the presence of $SbPh_3$, using toluene as solvent, restricted the aggregation to the monobismuth species (**III**).[16] The only structurally characterized tetrachlorogallate salt of bismuth involves the N,N',N'-tris(trimethylsilyl)hydrazido ligand (**IV**).[15] In this example bismuth is involved in three-center four-electron bonding to the two ligands, precluding the formation of interior Bi⋯Cl interactions with the $[GaCl_4]^-$ anion.

In this Contribution we examine the scope and limitations of cation formation, using $Bi(Me_2Si\{NAr\}_2)Cl$, (**1**, Ar = 2,6-i-$Pr_2C_6H_3$),[18] as a starting material. Compound **1** is stable under anaerobic conditions, and we have demonstrated that the chelating diamide ligand is a stable platform for further derivation of the Bi−Cl bond. While formation of cationic species is relatively straightforward using MCl_3 (M = Al, Ga), attempts at synthesizing salts containing borate anions $[BR_4]^-$

were complicated by transfer of the R-group and formation of $Bi(Me_2Si\{NAr\}_2)R$.

2. EXPERIMENTAL SECTION

2.1. General. All manipulations were carried out under dry nitrogen using standard Schlenk-line and cannula techniques, or in a conventional nitrogen-filled glovebox. Solvents were dried over appropriate drying agents and degassed prior to use. NMR spectra were recorded using a Bruker Avance DPX 300 MHz spectrometer at 300.1 (^{1}H) and 75.4 (^{13}C) MHz or a Varian VNMRS 500 MHz spectrometer at 500.1 (^{1}H), 160.4 (^{11}B), 125.4 (^{13}C), and 99.3 (^{29}Si) MHz. Proton and carbon chemical shifts were referenced internally to residual solvent resonances. ^{29}Si NMR chemical shifts were obtained from ^{1}H−^{29}Si heteronuclear multiple-bond correlation (HMBC) spectra. Elemental analyses were performed by S. Boyer at London Metropolitan University. $BiCl_3$ was freshly sublimed prior to the synthesis of $Bi(Me_2Si\{NAr\}_2)Cl$ (**1**), which was made according to our previously published procedure.[18] $[HNEt_3][BPh_4]$ was synthesized from $[HNEt_3]Cl$ and $Na[BPh_4]$ according to the procedure described by Evans and co-workers.[9] All other chemicals were purchased from commercial sources and used as received.

2.2. Preparation of $[Bi(Me_2Si\{NAr\}_2)][AlCl_4]$ (2a). A solution of **1** (0.100 g, 0.15 mmol) in toluene (5 mL) was added dropwise to a stirred suspension of $AlCl_3$ (0.019 g, 0.15 mmol) in toluene (5 mL). The resulting dark red solution was stirred for 4 h followed by concentration and storage at −30 °C. After 24 h, dark red crystals were obtained. Yield 0.105 g, 88%. Anal. Calcd. for $C_{26}H_{40}N_2AlBiCl_4Si$ (786.47): C, 39.71; H, 5.13; N, 3.56%. Found: C, 39.85; H, 5.01; N, 3.68%. ^{1}H NMR: δ 7.26 (d, $^3J_{HH}$ = 7.7 Hz, 4H, m-CH), 6.60 (t, $^3J_{HH}$ = 7.7 Hz, 2H, p-CH), 3.49 (m br, 4H, CHMe$_2$), 1.21 (br, 24H, CHMe_2), 0.13 (s, 6H, SiMe_2). ^{13}C$\{^1$H$\}$ NMR: δ *, 148.5, 128.8, 122.5 (C$_6$H$_3$), 28.2 (CHMe$_2$), 27.0 (br, CHMe_2), 10.4 (SiMe). * o-C not observed. ^{29}Si NMR: δ 38.0.

2.3. Generation of $[\{Bi(Me_2Si\{NAr\}_2)\}_2(\mu\text{-}Cl)][AlCl_4]$ (2b). *Method 1—NMR Scale.* A solution of **2a** (0.020 g, 0.026 mmol) in C_6D_6 (0.5 mL) was added to **1** (0.085 g, 0.013 mmol). The ^{1}H NMR spectrum indicated complete consumption of starting materials after 10 min at room temperature.

Method 2—Preparative Scale. A solution of **1** (0.040 g, 0.061 mmol) in toluene (2 mL) was added to a stirring suspension of $AlCl_3$ (0.004 g, 0.031 mmol) in toluene (2 mL). The resulting suspension was stirred for 4 h followed by the removal of volatiles. ^{1}H NMR analysis of the crude product revealed formation of **2b**. ^{1}H NMR: δ 7.24 (d, $^3J_{HH}$ = 7.8 Hz, 4H, m-CH), 6.74 (t, $^3J_{HH}$ = 7.8 Hz, 2H, p-CH), 3.86 (br sept, 4H, CHMe$_2$), 1.25 (d, $^3J_{HH}$ = 6.6 Hz, 24H, CHMe_2), 0.20 (s, 6H, SiMe_2).

2.4. Generation of $[Bi(Me_2Si\{NAr\}_2)][GaCl_4]$ (3a). *Method 1—NMR Scale.* A solution of **2b** (0.020 g, 0.026 mmol) in C_6D_6 (0.5 mL) was added to **1** (0.009 g, 0.013 mmol). The ^{1}H NMR spectrum indicated complete consumption of starting materials after 10 min at room temperature.

Method 2—Preparative Scale. A solution of **1** (0.040 g, 0.061 mmol) in toluene (2 mL) was added to a solution of $GaCl_3$ (0.011 g, 0.061 mmol) in toluene (2 mL). Removal of the volatiles followed by ^{1}H NMR analysis of the crude products revealed formation of **3a**. ^{1}H NMR: δ 7.28 (d, $^3J_{HH}$ = 7.8 Hz, 4H, m-CH), 6.58 (t, $^3J_{HH}$ = 7.8 Hz, 2H, p-CH), 3.51 (sept, $^3J_{HH}$ = 6.7 Hz, 4H, CHMe$_2$), 1.24 (br, 24H, CHMe_2), 0.13 (s, 6H, SiMe_2).

2.5. Preparation of $[\{Bi(Me_2Si\{NAr\}_2)\}_2(\mu\text{-}Cl)][GaCl_4]$ (3b). A solution of **1** (0.100 g, 0.15 mmol) in toluene (4 mL) was added dropwise to a stirring suspension of $GaCl_3$ (0.013 g, 0.075 mmol) in toluene (4 mL). The resulting dark red solution was stirred for 2 h followed by concentration of the solution and storage at −30 °C. After 24 h, small dark red crystals of **3b** were obtained. Yield 0.047 g, 40%. Anal. Calcd. for $C_{52}H_{80}N_4Bi_2Cl_5GaSi_2$ (1482.34): C, 42.13; H, 5.44; N, 3.78%. Found: C, 41.97; H, 5.31; N, 3.90%. ^{1}H NMR: δ 7.25 (d, $^3J_{HH}$ = 7.8 Hz, 4H, m-CH), 6.74 (t, $^3J_{HH}$ = 7.8 Hz, 2H, p-CH), 3.90 (sept, $^3J_{HH}$ = 6.8 Hz, 4H, CHMe$_2$), 1.27 (d, $^3J_{HH}$ = 6.8 Hz, 24H, CHMe_2), 0.21 (s, 6H, SiMe_2). ^{29}Si NMR: δ 31.2. ^{13}C$\{^1$H$\}$ NMR data

could not be obtained due to decomposition of **3b** in solution over extended periods of time.

2.6. Preparation of Bi(Me₂Si{NAr}₂)Ph (4). *Method 1—Preparative Scale from Bi(Me₂Si{NAr}₂)Cl + NaBPh₄.* A solution of **1** (0.100 g, 0.15 mmol) in toluene (5 mL) was added dropwise to a stirring suspension of NaBPh₄ (0.051 g, 0.15 mmol) in toluene (5 mL). The resulting solution was stirred for 72 h at 90 °C, followed by removal of the volatiles. Extraction into hexane and filtering through Celite resulted in a clear yellow solution. The solution was concentrated and stored at −30 °C. After 24 h, a number of white crystals of BPh₃ were deposited. Further concentration and storage at −30 °C yielded a second crop of crystals, identified as a mixture of BPh₃ and **4**. Yield 0.070 g, 67%.

Method 2—NMR Scale from Bi(Me₂Si{NAr}₂)Et + [HNEt₃][BPh₄]. A solution of **5** (0.020 g, 0.031 mmol) in C₆D₆ was added to [HNEt₃][BPh₄] (0.013 g, 0.031 mmol). The ¹H NMR spectrum revealed complete formation of **4** and BPh₃ after 0.5 h at room temperature.

Anal. Calcd. for $C_{32}H_{45}N_2BiSi$ (694.78): C, 55.32; H, 6.53; N, 4.03%. Found: C, 55.48; H, 6.64; N, 3.95%. ¹H NMR: δ 8.48 (d, $^3J_{HH}$ = 7.5 Hz, 2H, *o*-C₆*H*₅), 7.57 (t, $^3J_{HH}$ = 7.5 Hz, 1H, *p*-C₆*H*₅), 6.95 (t, $^3J_{HH}$ = 7.5 Hz, 2H, *m*-C₆*H*₅), 4.30 (sept, $^3J_{HH}$ = 6.8 Hz, 4H, C*H*Me₂), 1.28 (d, $^3J_{HH}$ = 6.8 Hz, 24H, CH*Me*₂), 0.63, 0.15 (s, Si*Me*₂). ¹³C{¹H} NMR: δ 148.0 (br, *C*₆H₅), 147.2 (*C*₆H₃), 140.9 (*C*₆H₃), 136.2 (*C*₆H₅), 131.6 (*C*₆H₅), 129.4 (*C*₆H₃), 128.4 (*C*₆H₃), 124.5 (*C*₆H₅), 27.8 (br, *C*HMe₂), 25.1 (br, CH*Me*₂), 17.5, 4.8 (Si*Me*). ²⁹Si NMR: δ 19.5.

2.7. Preparation of Bi(Me₂Si{NAr}₂)Et (5). A solution of **1** (0.100 g, 0.15 mmol) in toluene (5 mL) was added dropwise to a stirring suspension of NaBEt₄ (0.023 g, 0.15 mmol) in toluene (5 mL). The resulting solution was stirred for 24 h at room temperature, followed by removal of the volatiles and extraction into hexane. The resulting suspension was filtered through Celite and concentrated, followed by storage at −30 °C. After 24 h, clear yellow crystals were formed. Yield 0.061 g, 63%. Anal. Calcd. for $C_{28}H_{45}N_2BiSi$ (646.73): C, 52.00; H, 7.01; N, 4.33%. Found: C, 51.91; H, 7.12; N, 4.24%. ¹H NMR: δ 7.19 (d, $^3J_{HH}$ = 7.6 Hz, 4H, *m*-C*H*), 6.99 (t, $^3J_{HH}$ = 7.6 Hz, 2H, *p*-C*H*), 4.28 (sept, $^3J_{HH}$ = 6.9 Hz, 4H, C*H*Me₂), 2.47 (t, $^3J_{HH}$ = 8.1 Hz, 3H, CH₂C*H*₃), 2.04 (q, $^3J_{HH}$ = 8.1 Hz, 2H, C*H*₂CH₃), 1.31 (br, 24H, CH*Me*₂), 0.42 (s, 3H, Si*Me*₂), 0.04 (s, 3H, Si*Me*₂). ¹³C{¹H} NMR: δ 147.9, 141.4, 124.2, 123.5 (*C*₆H₃), 27.7 (*C*HMe₂), 25.9, 25.4 (CH*Me*₂), 15.6 (Si*Me*), 8.7 (*C*H₂CH₃), 5.2 (Si*Me*). Bi*C*H₂CH₃ was not observed. ²⁹Si NMR: δ 17.8.

2.8. Crystal Structure Data. Crystals were covered in inert oil, and suitable single crystals were selected under a microscope and mounted on a Enraf Nonius Kappa CCD diffractometer (**2a**) or an Agilent SuperNova diffractometer fitted with an Atlas detector (**3b**, **4**, **5**). Data was collected at 173(2) K (**2a**) or 120.01(10) K (**3b**, **4**, **5**) using Mo Kα radiation at 0.71073 Å (**2a**, **4**, **5**) or Cu Kα radiation at 1.5418 Å (**3b**).[19] The structures were refined with SHELXL-97.[19] Additional features of note are listed below:

[{Bi(Me₂Si{NAr}₂)}₂(μ-Cl)][GaCl₄] (3b). The compound crystallizes with a molecule of hexane in the unit cell.

Bi(Me₂Si{NAr}₂)Ph (4). The toluene solvate was located on an inversion center and was refined at half-occupancy; hydrogen atoms were not included in this model.

Bi(Me₂Si{NAr}₂)Et (5). The data solves in both the R3 and R$\overline{3}$ space groups; the latter model (in which the molecule is located on an inversion center) is presented. The disorder was modeled as alternative positions of the BiEt/SiMe₂ groups, with a single position for the NAr groups. There are large solvent channels in the crystal structure containing a poorly resolved and unidentified solvent; this was not modeled in the solution.

3. RESULTS AND DISCUSSION

3.1. Reaction of Bi(Me₂Si{NAr}₂)Cl with MCl₃ (M = Al, Ga, In). NMR spectroscopy is a convenient tool for the detection of changes to the Bi environment in relation to the chelating diamide ligand. The C_1 symmetry imposed by the pyramidal geometry of the bismuth atom in Bi(Me₂Si{NAr}₂)

Cl (**1**) is most clearly evident from inequivalent Si*Me*₂ resonances at δ_H 0.60 and 0.07 ppm.[18] Formation of a planar 2-coordinate Bi cation would, however, generate a single set of ligand resonances in the NMR spectrum, predicted for a C_{2h} ligand environment.

The reaction between Bi(Me₂Si{NAr}₂)Cl and one equiv of AlCl₃ in toluene proceeds with an immediate color change from yellow to deep red. Concentration and cooling of the resultant solution to −30 °C afforded deep red crystals of the tetrachloroaluminate salt, [Bi(Me₂Si{NAr}₂)][AlCl₄] (**2a**, Scheme 1). The ¹H NMR spectrum shows a single sharp

Scheme 1. Synthetic Routes to Bismuth Cations 2 and 3[a]
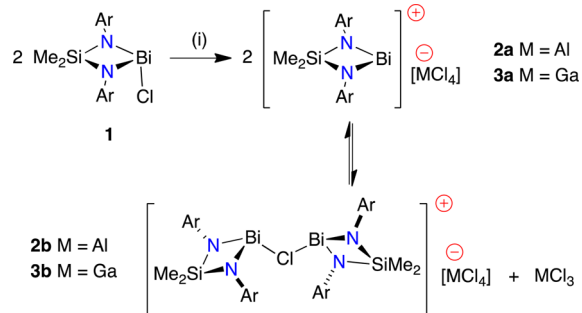
[a](i) 2MCl₃ (**2** M = Al; **3** M = Ga).

peak for the Si*Me*₂ protons at δ_H 0.13 ppm and broad resonances at δ_H 3.49 and 1.21 ppm for the *iso*-propyl methine and methyl protons, respectively (Figure 3a). These data are consistent with the formation of [Bi(Me₂Si{NAr}₂)]⁺, although we recognize that a number of alternative structures involving cation···anion interactions in the solution state also fit these data (Supporting Information, Figure S1). There is a notable low-field shift of the ²⁹Si NMR resonance upon generation of the cation, from δ_{Si} = 29.7 ppm in **1** to δ_{Si} = 38.0 in **2a** ($\Delta\delta_{Si}$ = +8.3 ppm). This indicates that changes to the environment at the bismuth center influence spectroscopic properties of the remote silicon atom, which therefore serves as a convenient handle to probe the electronic state of the metal in solution.

The analogous NMR scale reaction between **1** and GaCl₃ (1 equiv) in C₆D₆ proceeded in a similar manner, with an immediate color change on mixing to afford a deep red solution. The ¹H NMR spectrum was similar to that observed for isolated **2a**, with Si*Me*₂, C*H*Me₂, and CH*Me*₂ resonances at δ_H 3.51, 1.24, and 0.13 ppm, respectively, and are assigned to the tetrachlorogallate analogue of **2a**, [Bi(Me₂Si{NAr}₂)]-[GaCl₄], **3a** (Figure 3d). Attempted isolation of **3a** at −30 °C, however, gave two visually distinct species that cocrystallized as pale yellow and deep red solids. The lighter-colored solid was ¹H NMR silent and had a melting point of 78−79 °C, consistent with GaCl₃ (mp 77.9 ± 02 °C).[20] Mechanical separation enabled full characterization of the red crystals, including single-crystal X-ray diffraction analysis, which identified the crystals as the dibismuth cation [{Bi(Me₂Si{NAr}₂)}₂(μ-Cl)][GaCl₄] (**3b**).

The ¹H NMR spectrum of an isolated sample of **3b** is also consistent with a C_{2h} symmetric structure in solution, with selected peaks shifted notably downfield from the corresponding resonances for the [Bi(Me₂Si{NAr}₂)]⁺ cation in **3a** (Figure 3c). These chemical shift differences are most prominent for the *p*-C₆H₃ (δ_H 6.74 ppm), C*H*Me₂ (δ_H 3.90 ppm), and Si*Me*₂ (δ_H 0.21 ppm) resonances in **3b**, with $\Delta\delta_H$ values of
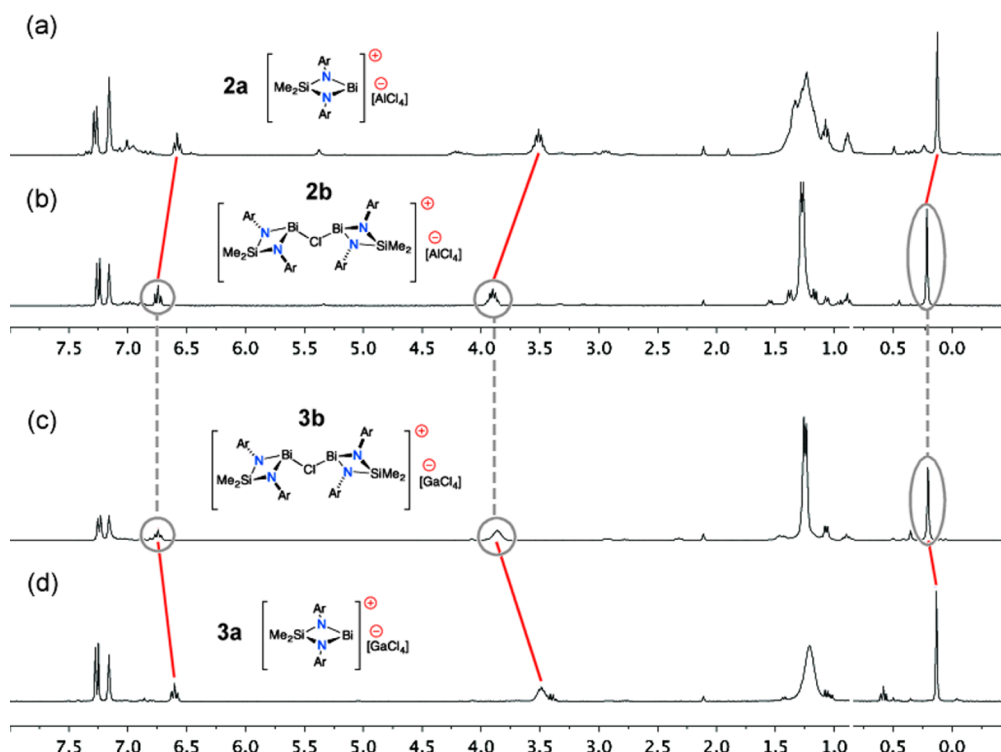
Figure 3. ^{1}H NMR spectra of cationic Bi compounds **2a**, **2b**, **3a**, and **3b**. (a) **2a** from isolated $[Bi(Me_2Si\{NAr\}_2)][AlCl_4]$; (b) **2b** from $[Bi(Me_2Si\{NAr\}_2)][AlCl_4]$ + 1 equiv of $Bi(Me_2Si\{NAr\}_2)Cl$ (**1**); (c) **3b** from isolated $[\{Bi(Me_2Si\{NAr\}_2)\}_2(\mu\text{-}Cl)][GaCl_4]$; (d) **3a** from $[\{Bi(Me_2Si\{NAr\}_2)\}_2(\mu\text{-}Cl)][GaCl_4]$ + 1 equiv of $GaCl_3$.

0.16, 0.39, and 0.08 ppm, respectively. As for **2a**, the ^{29}Si NMR resonance is shifted to low field (δ_{Si} = 31.2 ppm), although the magnitude of the shift is much less than it is in the mono-bismuth cation ($\Delta\delta_{Si}$ = +1.5). These data show that the bimetallic $[\{Bi(Me_2Si\{NAr\}_2)\}_2(\mu\text{-}Cl)]^+$ cation is not retained as a rigid unit in solution.

Addition of 1 equiv of $GaCl_3$ to an NMR sample of **3b** in C_6D_6 resulted in complete conversion to **3a**. In light of these results, the aluminum system was re-examined to determine whether similar interconversion between **2a** and the tetra-chloroaluminate analogue of **3b** is possible. Addition of one equiv of **1** to a solution of **2a** gave a ^{1}H NMR spectrum consistent with $[\{Bi(Me_2Si\{NAr\}_2)\}_2(\mu\text{-}Cl)][AlCl_4]$ (**2b**, Figure 3b), with a maximum $\Delta\delta$ of 0.04 ppm (CHMe$_2$) compared with the spectrum obtained from **3b**.

Veith reported that $Bi(Me_2Si\{Nt\text{-}Bu\}_2)Cl$ also underwent chloride abstraction to afford the cation formed when reacted with $InCl_3$.[11] However no color change was observed when $InCl_3$ was added to a solution of **1**, and NMR analysis indicated that no reaction had occurred. Attempts to promote cation formation by heating the mixture to 80 °C afforded an intractable mixture of species by ^{1}H NMR, and no clean product could be isolated. No detailed analysis of changes to the electronic structure upon replacing the nitrogen substitutents from t-Bu in Veith's compound to $2,6\text{-}i\text{-}Pr_2C_6H_3$ in **1** have been performed to explain this lack of reactivity. However, differences in the steric profile of the ligands are evident from the solid-state structures of the chlorides, where $Bi(Me_2Si\{Nt\text{-}Bu\}_2)Cl$ forms a one-dimensional (1-D) chain linked by Bi···Cl interactions and **1** is trimeric with Bi···aryl π-bonding interactions.

The molecular structure of the tetrachloroaluminate salt $[Bi(Me_2Si\{NAr\}_2)][AlCl_4]$ **2a** is shown in Figure 4, with crystal structure and refinement data collected in Table 1; selected
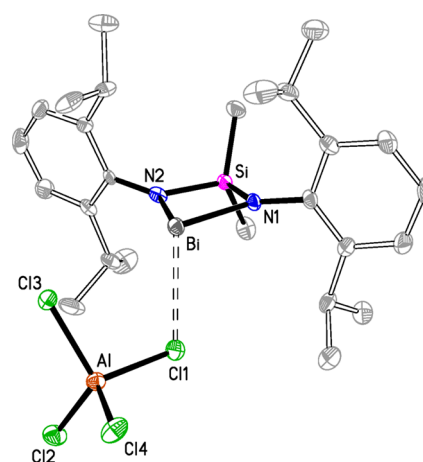
Figure 4. Thermal ellipsoid plot (30% probability, H-atoms omitted) of $[Bi(Me_2Si\{NAr\}_2)][AlCl_4]$ (**2a**).

bond lengths and angles, along with those of the previously reported structure of compound **1** are presented in Table 2. The compound crystallizes as the {1:1} salt with the closest Bi···Cl contact of 2.953(3) Å, considerably longer than the terminal Bi–Cl bonds in **1** [2.556(1) Å and 2.4857(16) Å]. The Bi–N distances in **2a** are within 3σ of those in the neutral compound, albeit with a trend toward shorter bonds. The bismuth atom in **2a** deviates slightly from the N$_2$Si least-squares plane (0.09(1) Å), which contrasts with the *endo* conformation[21] of **1** in which displacements of 0.294(6) and 0.229(8) Å of the bismuth from this plane are observed. This shift contributes to the larger ligand bite angle of 73.7(3)° in **2a** compared with values of 70.74(16)° and 71.78(11)° observed in **1**.

Table 1. Crystal Structure and Refinement Data for $[Bi(Me_2Si\{NAr\}_2)][AlCl_4]$ (2a), $[\{Bi(Me_2Si\{NAr\}_2)\}_2(\mu\text{-}Cl)][GaCl_4]$ (3b), $Bi(Me_2Si\{NAr\}_2)Ph$ (4), and $Bi(Me_2Si\{NAr\}_2)Et$ (5)

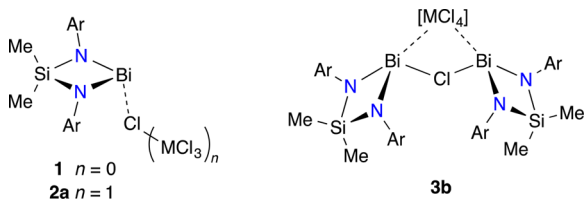|	2a	3b·C$_6$H$_{14}$	2(4)·C$_7$(H$_8$)	5
empirical formula	C$_{26}$H$_{40}$AlBiCl$_4$N$_2$Si	C$_{58}$H$_{94}$Bi$_2$Cl$_5$GaN$_4$Si$_2$	C$_{133}$H$_{180}$Bi$_4$N$_8$Si$_4$	C$_{28}$H$_{45}$BiN$_2$Si
M_r	786.45	1568.48	2863.15	646.73
T [K]	173(2)	120.01(10)	120.02(10)	120.0
crystal size [mm]	0.08 × 0.08 × 0.01	0.10 × 0.08 × 0.02	0.35 × 0.16 × 0.05	0.21 × 0.15 × 0.14
crystal system	orthorhombic	triclinic	triclinic	trigonal
space group	$Pbcn$ (No.60)	$P\bar{1}$ (No.2)	$P\bar{1}$ (No.2)	$R\bar{3}$ (No.148)
a [Å]	24.9726(10)	12.8472(5)	12.9068(2)	28.7503(11)
b [Å]	16.6486(4)	17.0713(7)	15.6323(4)	28.7503(11)
c [Å]	16.1717(6)	17.4081(7)	17.3240(5)	9.8541(5)
α [deg]	90	117.739(4)	108.940(2)	90
β [deg]	90	92.142(3)	93.6783(18)	90
γ [deg]	90	90.447(3)	100.2794(18)	120
V [Å^3]	6723.5(4)	3375.4(3)	3224.91(14)	7053.9(6)
Z	8	2	1	9
$D_{calc.}$ [mg m^{-3}]	1.55	1.54	1.47	1.37
absorption coefficient [mm^{-1}]	5.64	12.97	5.53	5.67
2θ range for data collection [deg]	7.02 to 54.16	2.87 to 74.00	5.32 to 60.0	5.66 to 66.22
reflections collected	26421	26092	66037	16452
independent reflections	7374 [R_{int} 0.161]	13265 [R_{int} 0.034]	18799 [R_{int} 0.035]	5348 [R_{int} 0.072]
reflections with $I > 2\sigma(I)$	4578	11200	15967	4288
data/restraints/parameters	7374/0/316	13265/36/671	18799/0/714	5348/114/179
final R indices [$I > 2\sigma(I)$]	R1 = 0.077, wR$_2$ = 0.163	R1 = 0.031, wR$_2$ = 0.073	R1 = 0.024, wR$_2$ = 0.053	R1 = 0.129, wR$_2$ = 0.272
final R indices (all data)	R1 = 0.131 wR$_2$ = 0.189	R1 = 0.040, wR$_2$ = 0.080	R1 = 0.033, wR$_2$ = 0.056	R1 = 0.151 wR$_2$ = 0.280
GOF on F^2	1.018	1.036	1.036	1.323
largest diff. peak/hole [e Å^{-3}]	3.64 and −3.18^a	1.66 and −2.15	1.82 and −0.97	1.88 and −3.13

^{a}Close to Bi.

There is a relatively large range of Al−Cl bond lengths in the tetrachloroaluminate anion (Δ_{AlCl} = 0.08 Å), reflecting differing degrees of Bi···Cl interaction. The longest Al−Cl bond (2.172(4) Å) involves chloride Cl1, which is most closely associated with the bismuth. The shortest bond (Al−Cl2, 2.091(5) Å) is at the low end of the range noted for a series of noncoordinated $[AlCl_4]^-$ anions within the structurally characterized compounds $[M(crown)_n(THF)_m][AlCl_4]$ (M = Li/Na, crown =12-c-4, n = 2, m = 0; M = Na/K, crown =18-c-6, n = 1, m = 2; M = K, crown =15-c-5, n = 2, m = 0: range of Al−Cl bond lengths = 2.102(2)−2.1469(9) Å),[22] consistent with a terminal chloride ligand. The remaining Al−Cl bonds are intermediate between these two values and involve chlorides that are engaged in intermolecular Bi···Cl interactions to another cation, resulting in an overall {1:1}$_2$ molecular structure (Figure 5). The bonding mode of the $[AlCl_4]^-$ anion in hexa-μ-chlorido-1:3κ^4Cl,1:4κ^2Cl,2:3κ^2Cl,2:4κ^4Cl-dichlorido-1κCl,2κCl-[N,N′-dimethylsilanediylbis(2,6-dipropan-2-ylphenylamido-3κN)][N,N′-dimethylsilanediylbis(2,6-dipropan-2-ylphenylamido-4κN)]dialuminiumdibismuth ($[2a]_2$) is unusual, but has been previously observed in polymeric tin[23] and samarium[24] complexes.

The bismuth component of the tetrachlorogallate salt 3b consists of a μ-chlorido-bridged monocation in which each pyramidal Bi atom retains a bidentate diamido-ligand. The interplanar angle between the SiN$_2$Bi metallacycles is 144.03(11)° with a *trans*–*trans* arrangement of the ligands with respect to Si···Bi−Cl−Bi···Si. This unit is supported by three Bi···Cl interactions to the $[GaCl_4]^-$ anion (Figure 6). The Bi−Cl1 bond lengths within the cation are inequivalent (2.7888(12) and 2.6902(12) Å to Bi1 and Bi2, respectively; Δ_{BiCl} = 0.10 Å), suggesting a localization of positive charge on Bi2. Both of the

Bi−Cl distances are longer than the terminal chloride bonds in 1 and shorter than the closest Bi···Cl ion-contact in 2a, suggesting an intermediate bonding type with delocalization across the Bi−Cl−Bi moiety. The asymmetry is in good agreement with the only other structurally characterized mono chloride-bridged cation, $[\{t\text{-}BuN(CH_2C_6H_4)_2Bi\}_2(\mu\text{-}Cl)][B\text{-}(C_6F_5)_4]$,[7] for which Δ_{BiCl} = 0.11 Å. As noted for 2a, there is no significant decrease in Bi−N bond lengths upon generation of the cation, and the Bi atoms are essentially coplanar with the chelating diamide (deviation from the N$_2$Si least-squares plane = 0.088(8) and 0.050(7) Å for Bi1 and Bi2, respectively), generating relatively large ligand bite angles of 72.08(15)° and 72.21(15)°.

The interior Bi···Cl distances in the asymmetric unit of 3b span the range of 3.3168(2)−3.5618(2) Å and are considerably shorter than they are in the crystal structure of IV in which no bismuth-to-tetrachlorogallate contacts are described.[15] Two of the interactions in 3b involve Bi2, also consistent with this being the more positive metal. The Ga−Cl bond lengths (range from 2.1622(14) Å to 2.1878(14) Å) span those reported for IV and the series of $[M(crown)_n(THF)_m][GaCl_4]$ compounds (M = Li/Na, crown = 12-c-4, n = 2, m = 0; M = Na, crown = 18-c-6, n = 1, m = 0; M = K, crown = 18-c-6, n = 1, m = 2).[25] The difference in the Ga−Cl bond lengths within the anion (Δ_{GaCl} = 0.03 Å) is considerably smaller than the corresponding difference in the Al−Cl distances of 2a, consistent with all four chlorides being involved in Bi···Cl interactions. Indeed, examination of the unit cell of 3b confirms that Cl4 is associating with a second cation (Cl4···Bi1′ 3.3277(1) Å) to generate the {1:1}$_2$ aggregate bis{μ-chlorido-[N,N′-dimethylsilanediylbis(2,6-dipropan-2-ylphenylamido-1κN)]-[N,N′-dimethylsilanediylbis(2,6-dipropan-2-ylphenylamido-2κN)]dibismuth(1+)}deca-μ-chlorido-1:3κ^4Cl,1:4κ^2Cl,1:5κ^2Cl,

Table 2. Selected Bond Lengths (Å) for 2a and 3b, Presented with Those of 1 for Comparison

	1^a	$2a^b$	$3b^c$
Bi—N	2.132(3)	2.118(8)	2.121(4)
	2.144(3)	2.120(8)	2.131(3)
	2.181(3)		2.143(3)
			2.152(3)
Bi—Cl	2.4857(16)		2.6902(12)
	2.5560(10)		2.7888(12)
Bi⋯Cl		2.953(3)	3.3168(14)
			3.3277(13)
			3.5373(16)
			3.5618(14)
Si—N	1.733(3)	1.763(9)	1.734(4)
	1.735(3)	1.765(8)	1.736(4)
	1.736(3)		1.748(4)
			1.752(4)
M—Cl		2.091(5)	2.1622(14)
		2.134(4)	2.1689(15)
		2.152(4)	2.1770(13)
		2.172(4)	2.1878(14)
N—Bi—N	70.74(16)	73.7(3)	72.08(15)
	71.78(11)		72.21(15)
N—Si—N	92.58(15)	92.1(4)	92.67(17)
	93.3(2)		
Bi—N—Si	97.17(14)	97.1(3)	97.00(17)
	97.54(13)	97.0(3)	97.64(18)
	97.71(14)		97.88(18)
			98.16(17)
N—Bi—Cl	96.34(9)	94.2(2)	94.28(11)
	96.37(9)	98.1(2)	97.56(11)
	97.89(9)		97.76(10)
			101.12(11)

^{a} 1.5 molecules in the unit cell. ^{b} M = Al. ^{c} M = Ga.

Figure 5. Molecular structure of $[2a]_2$, showing the bridging $[AlCl_4]^-$ anions ($' = 1 - x, y, 1/2 - z$; aryl groups reduced to show only *ipso*-carbon atoms).

$1:6\kappa^2Cl,2:4\kappa^2Cl,2:5\kappa^2Cl,2:6\kappa^4Cl,3:4\kappa^2Cl,5:6\kappa^2Cl$-$[N,N'$-dimethylsilanediylbis(2,6-dipropan-2-ylphenylamido-3κN)]-
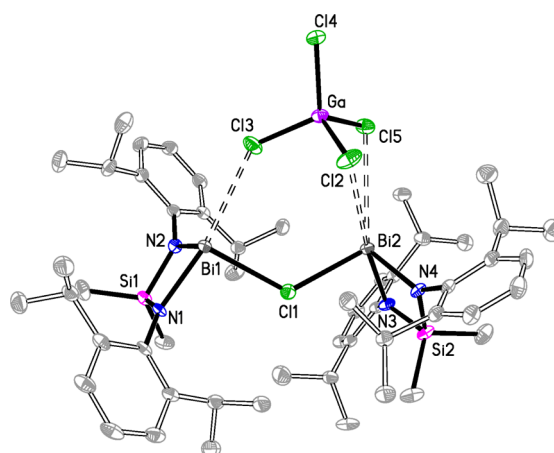
Figure 6. Thermal ellipsoid plot (30% probability, H-atoms and hexane solvate omitted) of $[\{Bi(Me_2Si\{NAr\}_2)\}_2(\mu\text{-}Cl)][GaCl_4]$ (3b).

$[N,N'$-dimethylsilanediylbis(2,6-dipropan-2-ylphenylamido-4κN)][N,N'-dimethylsilanediylbis(2,6-dipropan-2-ylphenyla-mido-5κN)][N,N'-dimethylsilanediylbis(2,6-dipropan-2-ylphe-nylamido-6κN)]digalliumtetrabismuthate(2-) in the solid state ($[3b]_2$, Figure 7). This is the only structurally characterized
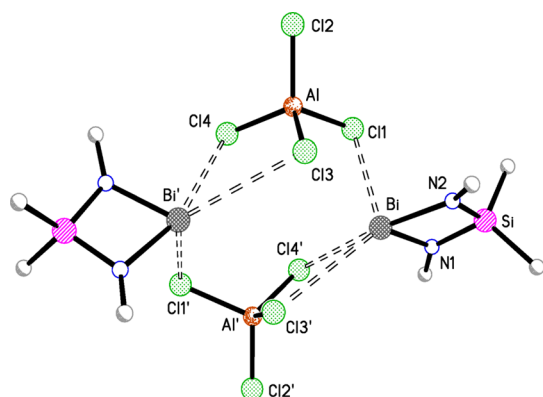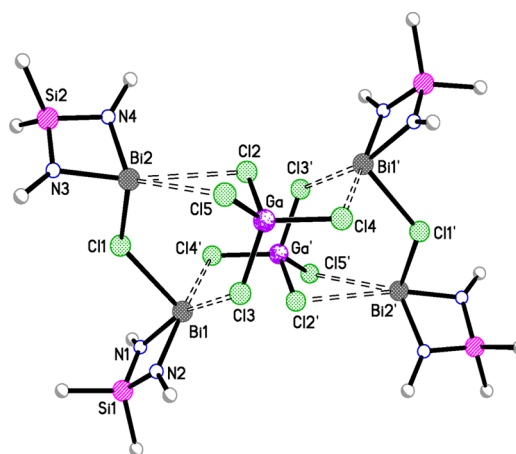

Figure 7. Molecular structure of $[3b]_2$, showing the bridging $[GaCl_4]^-$ anions ($' = -x, -y, -z$; aryl groups reduced to show only *ipso*-carbon atoms).

example of the tetrachlorogallate anion interacting through all four chloride ligands.

3.2. Reaction with M[BR₄] (M = Na, R = Ph, Et; M = HNEt₃, R = Ph). Evans and co-workers have shown that the bis(aryl) bismuth chloride compound BiAr′₂Cl (Ar′ = 2,6-(Me₂NCH₂)₂C₆H₃) is converted to the tetraphenylborate salt upon reaction with NaBPh₄ (Scheme 2). The cation is also generated from the protonolysis reaction of the allyl compound BiAr′₂(CH₂CH=CH₂) with [HNEt₃][BPh₄].[9] Monitoring a mixture of 1 and NaBPh₄ by ¹H NMR spectroscopy indicated that the reaction did not proceed at room temperature. Heating the reaction to 90 °C for 3 d, however, afforded a mixture of yellow 4 and colorless crystals upon workup. Physical separation allowed pure samples of 4 to be prepared for analysis by NMR spectroscopy, elemental analysis, and X-ray diffraction.

¹H NMR data for 4 indicate a C_1 symmetry structure, with SiMe₂ resonances at δ_H 0.63 and 0.15 ppm. Integration of the aromatic region of the spectrum is consistent with the presence

F

dx.doi.org/10.1021/ic500113g | *Inorg. Chem.* XXXX, XXX, XXX−XXX

Scheme 2. Reaction of Bi(Me₂Si{NAr}₂)X (1 X = Cl, 5 X = Et) with [A][BR₄] (A = Na, R = Ph, Et; A = HNEt₃, R = Ph)[a]
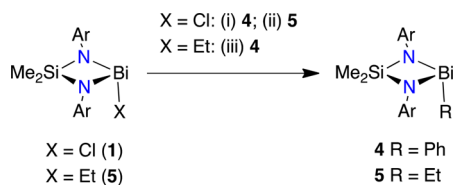
^{a}(i) NaBPh₄; (ii) NaBEt₄; (iii) [HNEt₃][BPh₄].

of a single phenyl group, with the peaks assigned to the *ortho*-protons at low field (δ_H = 8.48 ppm, C₆D₆). This chemical shift is significantly different from that observed for the [BPh₄]⁻ anion (e.g., [Bi(Ar′)₂][BPh₄]: δ_H = 6.99 ppm, CD₃CN[9]) and BiPh₃ (δ_H = 7.73 ppm, C₆D₆). These data are consistent with formation of the phenyl compound Bi(Me₂Si{NAr}₂)Ph, confirmed by elemental analysis and an X-ray crystal structure determination (*vide infra*). The colorless crystals that formed during the reaction were identified as BPh₃ by ¹¹B NMR spectroscopy (δ_B 68 ppm[26]) and by comparison of their unit cell with published data.[27]

Aryl transfer reactions from [BAr₄]⁻ anions are well documented,[28] and the reaction of Na[BAr₄″] (Ar″ = Ph, *p*-tolyl, 4−F-C₆H₄) with bismuth(III) carboxylates has been reported recently as a convenient route to BiAr₃″ species.[29] To probe this mode of reactivity further we examined the reaction of **1** with Na[BEt₄], where the tetraethylborate anion is known to behave as an alkyl transfer reagent.[30] In this case the reaction proceeded at room temperature, affording pale yellow crystals on workup. ¹H NMR data was consistent with the bismuth ethyl compound Bi(Me₂Si{NAr}₂)Et (**5**) showing a C_1 symmetry (Si*Me₂*: δ_H = 0.42 and 0.04 ppm). The resonances for methyl and methylene groups of the ethyl ligand appear as a triplet and quartet at δ_H 2.47 and 2.04 ppm, respectively. The ²⁹Si NMR resonances for **4** (δ_{Si} = 19.5 ppm) and **5** (δ_{Si} = 17.8 ppm) are shifted to higher field compared with **1** ($\Delta\delta_{Si}$ = −10.2 ppm and −11.9 ppm, respectively), reflecting the relatively electron-rich metallacycle upon exchanging the bismuth substituent from chloride to aryl/alkyl groups.

The structures of **4** and **5** were determined by single-crystal X-ray diffraction experiments (Tables 1 and 3; Figures 8 and 9).

Table 3. Selected Bond Lengths (Å) and Angles (deg) for 4

Bi1−N1	2.168(2)	Bi2−N3	2.1790(19)
Bi1−N2	2.177(2)	Bi2−N4	2.172(2)
Bi1−C27	2.253(3)	Bi2−C58	2.252(3)
Si1−N1	1.713(2)	Si2−N3	1.721(2)
Si1−N2	1.726(2)	Si2−N4	1.731(2)
N1−Bi1−N2	70.50(7)	N3−Bi2−N4	70.86(7)
N1−Bi1−C27	98.02(9)	N3−Bi2−C58	100.32(8)
N2−Bi1−C27	100.50(9)	N4−Bi2−C58	97.44(9)
Bi1−N1−Si1	98.21(9)	Bi2−N3−Si2	97.63(9)
Bi1−N2−Si1	97.49(9)	Bi2−N4−Si2	97.59(9)
N1−Si1−N2	93.65(10)	N3−Si2−N4	93.90(10)

Unfortunately the data solution for compound **5** was complicated by molecular disorder that was modeled in the $R\bar{3}$ space group as being about an inversion center (Supporting Information, Figure S2). This disorder is most likely caused by the small size of the ethyl substituent compared to other X-groups in the Bi(Me₂Si{NAr}₂)X compounds, resulting in a
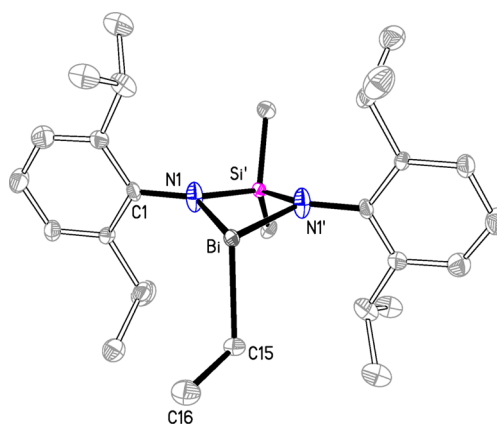
Figure 8. Thermal ellipsoid plot (30% probability) of Bi(Me₂Si{NAr}₂)Et, **5** (′ = 1 − *x*, 1 − *y*, −*z*; H-atoms omitted).
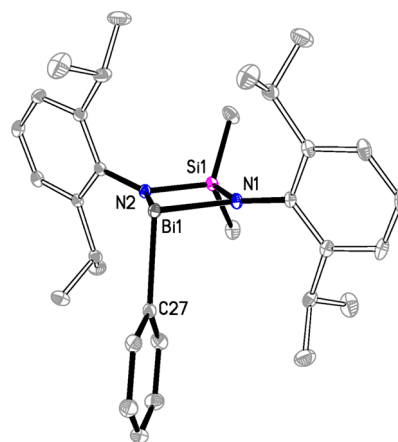
Figure 9. Thermal ellipsoid plot (30% probability) of one of the independent molecules of Bi(Me₂Si{NAr}₂)Ph, **4** (H-atoms and toluene solvate omitted).

small energy difference between the two orientations of the metallacycle with respect to the aryl substituents. As a result the solution of the data is not of sufficient quality for a meaningful discussion of bond lengths and angles; it does, however, confirm the connectivity of **5** as a rare example of a monomeric bismuth-ethyl compound (Figure 8).[31]

Compound **4** crystallizes as the toluene solvate, with two independent molecules in the unit cell that differ primarily with respect to the orientation of the phenyl substituent (Figure 9). Each molecule is monomeric with a pyramidal geometry of the Bi atom and an essentially planar metallacycle (deviation of Bi from mean SiN₂ plane: Bi1 0.121(4) Å, Bi2 0.037(4) Å). The Bi−N bond lengths in **4** are longer than in the other structures examined during this study, resulting in a smaller average bite angle of 70.68(7)° for the diamide ligand. The Bi−C bond length (2.253(3) Å) is unexceptional and is within the range noted for BiPh₃ (2.237(7) to 2.273(8) Å).[32]

Comparing the two molecules within the unit cell we note that phenyl groups are rotated in opposite directions along the Bi−C$_{ipso}$ bond relative to the plane bisecting the metallacycle through the silicon, bismuth, and C$_{ipso}$ atoms (molecule Bi1 = +14.85(7)°; molecule Bi2 = −29.56(11)°, where +ve = clockwise direction—Figure 10a,b). This twisted orientation brings the portion of the phenyl group located below the metallacycle into close proximity with one of the *i*-Pr groups of the aryl substituents. The resulting steric conflict is alleviated by the nitrogen
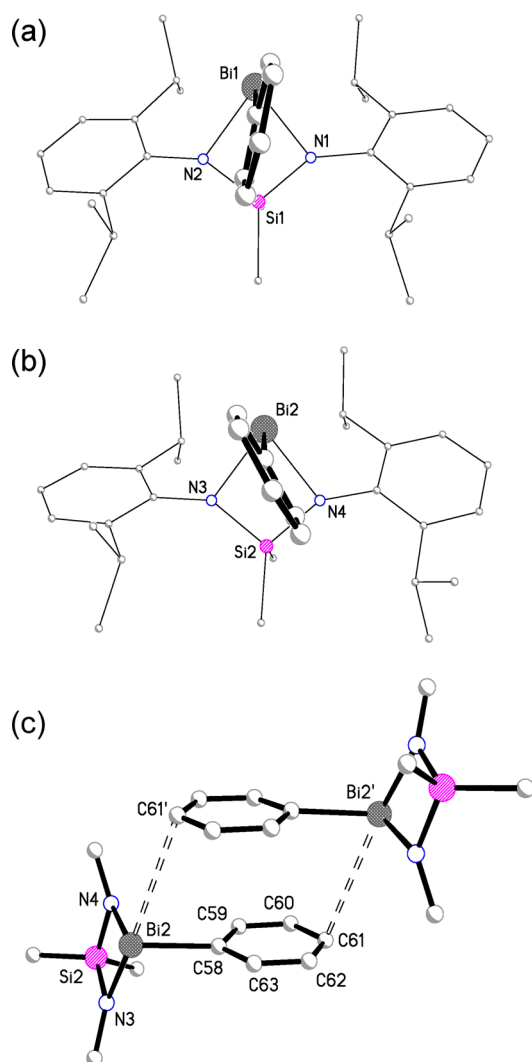
Figure 10. Schematic representations of the two molecules of **4**, showing (a) the different rotation of the phenyl ligand relative to the Si···Bi−C_{ipso} vector, (b) the displacement of one of the aryl groups out of the plane of the metallacycle, and (c) the dimerization of molecule Bi2 (′ = 2 − x, −y, 1 − z).

aryl-substituent being located above the BiNSiN-plane, illustrated by the different angles that the N−C_{ipso} bonds adopt with respect to this plane (molecule Bi1: N1−C1 = 5.9°, N2−C13 = 15.3°; molecule Bi2: N3−C34 = 9.3°, N4−C46 = 21.2°; see Supporting Information, Figure S3).

The twisting of the phenyl ligand is more pronounced in molecule Bi2. Examination of the packing shows that this molecule is involved in intermolecular interactions with a symmetry generated equivalent positioned about an inversion center (Figure 10c). The *para*-carbon atom of the phenyl substituent (C61) is located at 3.629(3) Å from Bi2′ (′ = 2-x, -y, 1-z), within the range of distances previously attributed to a bonding interaction within the series of compounds $[BiCl_3 \cdot (C_6H_{6-n}Me_n)]$ (Bi···C distances 3.168(7) to 3.751(8) Å).[33] However, the large ring slippage of 2.57 Å from the centroid of the C_6-ring suggests that it is the $\pi-\pi$ interactions between the two phenyl rings that dominate (centroid−centroid distance 3.827(3) Å, plane-to-plane shift 1.295(5) Å), although the role of crystal packing forces should not be dismissed.

4. DISCUSSION

The paucity of low-coordinate bismuth cations is illustrated by the facts that **2a** is only the second formally two-coordinate Bi$^+$ center to be structurally characterized and that **2a** is a derivative of the first example.[11] This is perhaps not surprising given the large radius of the element and the focus on multidentate ligands in this area of chemistry. As a consequence, additional interion (and other intermolecular) interactions become important in the condensed (solid) state, as shown by the Bi···Cl contacts present in the structures of **2a** and **3b**.

Previous work has quantified the bond order (BO) of Bi···Cl interactions (eq 1),[34] using values of r_0 = 2.423 Å[35] and B = 0.39.[36] We recently used this equation to show that the intermolecular Bi···Cl BO between associated molecules in the trimeric unit of **1** was 0.14[18] and that this was significantly less than that calculated for a similar Bi···Cl interaction in the Nt-Bu analogue (BO = 0.20).[37] Table 4 summarizes a series of BOs for some bismuth chloride compounds and the corresponding cations, generated by halide abstraction using MCl_3 (M = Al, Ga).

$$ BO = \exp\left[\frac{(r_0 - r)}{B} \right] $$

(eq 1)

According to eq 1, the terminal bismuth chloride bonds in **1** have BOs of 0.85 and 0.71, reflecting the relatively long Bi−Cl distances. The smaller BO (weaker bond) corresponds to the chloride involved in bridging interactions to another molecule, showing the sensitivity of this measurement to small changes in the environment of the bond. Given that these Bi−Cl BOs are significantly less than unity, it is perhaps not surprising that chloride abstraction and generation of bismuth cations is a relatively facile process.

Conversion of **1** to the cation and association of the formally positive bismuth metal and the tetrachloroaluminate anion gives a BO of 0.26 for the primary Bi···Cl interaction, suggesting a strongly associated ion pair in the solid state with a reduction of ~0.5 on generation of the cation (ΔBO = −0.59 and −0.45). Unfortunately, it is not possible to make a direct comparison with the ΔBO in the corresponding Nt-Bu cation (**I**, Figure 2), as the primary Bi−Cl bond in the neutral compound (BO = 0.43) is already weakened by intermolecular interactions along a 1-D chain in the crystal structure (*vide supra*). Nevertheless a reduction is observed upon generation of the cation, with the principal Bi···[Cl−AlCl₃] BO of 0.19 in this case approximately equal to the weaker Bi−Cl···Bi bridging bond along the chain. The calculated BO values for the Bi···[Cl−AlCl₃] interactions of the associated dimer in **2** (Figure 5) are 0.11 and 0.04 for Cl4 and Cl3, respectively. These values indicate weak, nonsymmetrical bonding to the second bismuth cation with values lower than the major interion interactions in **I**.

Comparing these BOs with the corresponding values for other ligand systems shows that the ΔBOs upon cation generation are highly dependent on the ligand. For example, the bulky cyclopentadienyl derivative $[Bi(Cp'')Cl_2]_2$ has BO values of 0.75 for the terminal Bi−Cl bonds, with the BOs of the nonsymmetrical bridging μ-chlorides being 0.53 and 0.19 (average from two crystal modifications). Formation of the cation retains the dimeric unit, with only minor modifications to the Bi(μ-Cl)Bi BOs (0.57 and 0.20), and the closest contact to the $[AlCl_4]^-$ corresponding to a BO of 0.06.

H

dx.doi.org/10.1021/ic500113g | *Inorg. Chem.* XXXX, XXX, XXX−XXX

Table 4. Bond Orders (BOs) for Bi−Cl Bonds and Bi···Cl Interactions, Calculated Using eq 1

compound	Bi−Cl bond order (BO)	[Bi]···[Cl-MCl$_3$] bond order (BO)	reference
[Bi(Me2Si{NAr}$_2$)Cl]$_3$^{a} (**1**)	0.85 0.71 0.14 (μ-)		18
[Bi(Me$_2$Si{NAr}$_2$)][AlCl$_4$] (**2a**)		0.26 0.11 0.04	this work
[Bi(Me$_2$Si{Nt-Bu}$_2$)Cl]$_\infty$	0.43 (μ-) 0.20 (μ-)		37
[Bi(Me$_2$Si{Nt-Bu}$_2$)][AlCl$_4$] (**I**)		0.19 0.17 0.03 0.02	11
[Bi(Cp″)Cl$_2$]$_2$^{a}	0.75/0.74 0.48/0.57 (μ-) 0.22/0.16 (μ-)		14, 38
[Bi(Cp″)Cl][AlCl$_4$]	0.57 (μ-) 0.20 (μ-)	0.06 0.06	14
Bi(N{SiMe$_3$}N{SiMe$_3$}$_2$)$_2$Cl	0.77		15
[Bi(N{SiMe$_3$}N{SiMe$_3$}$_2$)$_2$)][GaCl$_4$] (**IV**)		0.03 0.03	15
[{Bi(Me$_2$Si{NAr}$_2$)}$_2$(μ-Cl)][GaCl$_4$] (**3b**)	0.50 (μ-) 0.39 (μ-)	0.10 0.10 0.06 0.05	this work

^{a}Two different crystal modifications; Cp″ = [1,2,3,4-iPr$_4$C$_5$H]$^-$.

The tetrachlorogallate salt **3b** has a nonsymmetrically bridging chloride in the cationic unit, with BOs of 0.50 and 0.39. Despite being aligned well within the dimeric unit (Figure 7), the interion BOs for Bi···[Cl−GaCl$_3$] are only 0.10 to 0.05, indicating a weak interaction. These are only slightly more than the calculated BOs of 0.03 in [Bi(N{SiMe$_3$}N-{SiMe$_3$}$_2$)$_2$)][GaCl$_4$] (**IV**).

In summary, the BOs associated with terminal Bi−Cl bonds in neutral species are significantly less than those expected for a single bond, being typically in the range of 0.7−0.8. In contrast the intermolecular BOs calculated for Bi−Cl···Bi bridges during the formation of μ,μ-dichlorobridged dimers can be as much as ∼0.55 and during the association of neutral molecules can be up to ∼0.43. Surprisingly, formation of "contact" ion pairs does not give such large values of BO between the Bi$^+$ center and the tetrachloroaluminate anion, despite the electrostatic attraction between the ions. This is may be due to a delocalization of the positive charge into the ancillary ligands at Bi (as noted for the N,N′,N′-tris(trimethylsilyl)hyradzido salt **IV**) and the relative exposure of the (long) terminal Bi−Cl bonds compared with the much shorter Al−Cl bonds.

■ ASSOCIATED CONTENT

ⓢ Supporting Information

Alternative solution-state structures for a C_{2h} ligand environment; additional projections of the crystal structures of **4** and **5**; crystallographic information files (CIF format) for **2a** (CCDC 990963), **3b** (CCDC 990964), **4** (CCDC 990965), and **5** (CCDC 990966). This material is available free of charge via the Internet at http://pubs.acs.org.

■ AUTHOR INFORMATION

Corresponding Author
* E-mail: martyn.coles@vuw.ac.nz. Phone: +64 (0)4 4636357.
Author Contributions
The manuscript was written through contributions of all authors.

■ REFERENCES

(1) (a) Ollevier, T. *Org. Biomol. Chem.* **2013**, *11*, 2740−2755. (b) Bothwell, J. M.; Krabbe, S. W.; Mohan, R. S. *Chem. Soc. Rev.* **2011**, *40*, 4649−4707. (c) Leonard, N. M.; Wieland, L. C.; Mohan, R. S. *Tetrahedron* **2002**, *58*, 8373−8397.
(2) Kricheldorf, H. R. *Chem. Rev.* **2009**, *109*, 5579−5594.
(3) (a) Lichtenberg, C.; Pan, F.; Spaniol, T. P.; Englert, U.; Okuda, J. *Angew. Chem., Int. Ed. Engl.* **2012**, *51*, 13011−13015. (b) Zhang, X.; Qiu, R.; Tan, N.; Yin, S.; Xia, J.; Luo, S.; Au, C.-T. *Tetrahedron Lett.* **2010**, *51*, 153−156. (c) Zhang, X.; Yin, S.; Qiu, R.; Xia, J.; Dai, W.; Yu, Z.; Au, C.-T.; Wong, W.-Y. *J. Organomet. Chem.* **2009**, *694*, 3559−3564.
(4) (a) Tan, N.; Yin, S.; Li, Y.; Qiu, R.; Meng, Z.; Song, X.; Luo, S.; Au, C.-T.; Wong, W.-Y. *J. Organomet. Chem.* **2011**, *696*, 1579−1583. (b) Qiu, R.; Yin, S.; Song, X.; Meng, Z.; Qiu, Y.; Tan, N.; Xu, X.; Luo, S.; Dai, F.-R.; Au, C.-T.; Wong, W.-Y. *Dalton Trans.* **2011**, *40*, 9482−9489. (c) Qiu, R.; Qiu, Y.; Yin, S.; Xu, X.; Luo, S.; Au, C.-T.; Wong,

W.-Y.; Shimada, S. *Adv. Synth. Catal.* **2010**, *352*, 153−162. (d) Qiu, R.; Yin, S.; Zhang, X.; Xia, J.; Xu, X.; Luo, S. *Chem. Commun.* **2009**, 4759−4761.

(5) Shannon, R. D. *Acta Crystallogr.* **1976**, *A32*, 751−767.

(6) Raţ, C. I.; Silvestru, C.; Breunig, H. J. *Coord. Chem. Rev.* **2013**, *257*, 818−879.

(7) Bao, M.; Hayashi, T.; Shimada, S. *Organometallics* **2007**, *26*, 1816−1822.

(8) (a) Casely, I. J.; Ziller, J. W.; Fang, M.; Furche, F.; Evans, W. J. *J. Am. Chem. Soc.* **2011**, *133*, 5244−5247. (b) Dostál, L.; Jambor, R.; Růžička, A.; Jirásko, R.; Holeček, J.; De Proft, F. *Dalton Trans.* **2011**, *40*, 8922−8934. (c) Breunig, H. J.; Nema, M. G.; Silvestru, C.; Soran, A. P.; Varga, R. A. *Dalton Trans.* **2010**, *39*, 11277−11284. (d) Soran, A. P.; Silvestru, C.; Breunig, H. J.; Balazs, G.; Green, J. C. *Organometallics* **2007**, *26*, 1196−1203. (e) Dostál, L.; Novák, P.; Jambor, R.; Růžička, A.; Císařová, I.; Jirásko, R.; Holeček, J. *Organometallics* **2007**, *26*, 2911−2917.

(9) Casely, I. J.; Ziller, J. W.; Mincher, B. J.; Evans, W. J. *Inorg. Chem.* **2011**, *50*, 1513−1520.

(10) Fletcher, D. A.; McMeeking, R. F.; Parkin, D. *J. Chem. Inf. Comput. Sci.* **1996**, *36*, 746−749.

(11) Veith, M.; Bertsch, B.; Huch, V. *Z. Anorg. Allg. Chem.* **1988**, *559*, 73−88.

(12) Frank, W.; Weber, J.; Fuchs, E. *Angew. Chem., Int. Ed. Engl.* **1987**, *26*, 74−75.

(13) Sitzmann, H.; Wolmershäuser, G. *Z. Naturforsch., B: Chem. Sci.* **1997**, *52*, 398−400.

(14) Sitzmann, H.; Wolmershäuser, G.; Boese, R.; Bläser, D. *Z. Anorg. Allg. Chem.* **1999**, *625*, 2103−2107.

(15) Baumann, W.; Schulz, A.; Villinger, A. *Angew. Chem., Int. Ed.* **2008**, *47*, 9530−9532.

(16) Conrad, E.; Burford, N.; McDonald, R.; Ferguson, M. J. *Chem. Commun.* **2010**, *46*, 4598−4600.

(17) Lehmann, M.; Schulz, A.; Villinger, A. *Angew. Chem., Int. Ed.* **2012**, *51*, 8087−8091.

(18) Day, B. M.; Coles, M. P. *Organometallics* **2013**, *32*, 4270−4278.

(19) Sheldrick, G. M. *SHELXL-97*, Program for the Refinement of Crystal Structures; University of Gottingen: Göttingen, Germany, 1997.

(20) *CRC Handbook of Chemistry and Physics,* 59th ed.; Weast, R. C., Ed.; CRC Press, Inc.: Boca Raton, FL, 1978−1979

(21) Harris, L.-A.; Coles, M. P.; Fulton, J. R. *Inorg. Chim. Acta* **2011**, *369*, 97−102.

(22) Bollmann, M.; Olbrich, F.; Trzaska, S. Private contributions from Institut fur Anorganische und Angewandte Chemie, Universitat Hamburg, Hamburg, Germany, 2003−2005; CCDC Numbers 205576, 224141, 240402, 240639, 278699.

(23) (a) Weininger, M. S.; Rodesiler, P. F.; Amma, E. L. *Inorg. Chem.* **1979**, *18*, 751−755. (b) Frank, W. *Z. Anorg. Allg. Chem.* **1990**, *585*, 121−141. (c) Schmidbaur, H.; Probst, T.; Steigelmann, O.; Müller, G. *Heteroat. Chem.* **1990**, *1*, 161−165.

(24) (a) Troyanov, S. I. *Russ. J. Coord. Chem.* **1998**, *24*, 359−366. (b) Troyanov, S. I. *Russ. J. Coord. Chem.* **1998**, *24*, 591−597. (c) Fagin, A. A.; Bochkarev, M. N.; Kozimor, S. A.; Ziller, J. W.; Evans, W. J. *Z. Anorg. Allg. Chem.* **2005**, *631*, 2848−2853.

(25) (a) Trzaska, S.; Bollmann, M.; Olbrich, F. Private contributions from Institut fur Anorganische und Angewandte Chemie, Universitat Hamburg, Hamburg, Germany 2002 and 2004; CCDC Numbers 185721, 228000, 248405. (b) Petrosyants, S. P.; Ilynkhin, A. B. *Russ. J. Coord. Chem.* **2007**, *33*, 734−740.

(26) Evans, W. J.; Kozimor, S. A.; Ziller, J. W. *Organometallics* **2005**, *24*, 3407−3412.

(27) Zettler, F.; Hausen, H. D.; Hess, H. *J. Organomet. Chem.* **1974**, *72*, 157−162.

(28) (a) Strauss, S. H. *Chem. Rev.* **1993**, *93*, 927−942. (b) Stavila, V.; Thurston, J. H.; Whitmire, K. H. *Inorg. Chem.* **2009**, *48*, 6945−6951.

(29) Stavila, V.; Thurston, J. H.; Prieto-Centurión, D.; Whitmire, K. H. *Organometallics* **2007**, *26*, 6864−6866.

(30) Thaler, E. G.; Caulotn, K. G. *Organometallics* **1990**, *9*, 1871−1876.

(31) (a) Whitmire, K. H.; Hutchison, J. C.; McKnight, A. L.; Jones, C. M. *J. Chem. Soc., Chem. Commun.* **1992**, 1021−1022. (b) Mitzi, D. B. *Inorg. Chem.* **1996**, *35*, 7614−7619.

(32) Jones, P. G.; Blaschette, A.; Henschel, D.; Weitze, A. *Z. Kristallogr.* **1995**, *210*, 377−378.

(33) (a) Schier, A.; Wallis, J. M.; Müller, G.; Schmidbaur, H. *Angew. Chem., Int. Ed. Engl.* **1986**, *25*, 757−759. (b) Schmidbaur, H.; Nowak, R.; Schier, A.; Wallis, J. M.; Huber, B.; Müller, G. *Ber. Bunsen-Ges.* **1987**, *120*, 1829−1835. (c) Schmidbaur, H.; Wallis, J. M.; Nowak, R.; Huber, B.; Müller, G. *Ber. Bunsen-Ges.* **1987**, *120*, 1837−1843. (d) Frank, W.; Schneider, J.; Müller-Becker, S. *J. Chem. Soc., Chem. Commun.* **1993**, 799−800. (e) Müller-Becker, S.; Frank, W.; Schneider, J. *Z. Anorg. Allg. Chem.* **1993**, *619*, 1073−1082. (f) Frank, W.; Reiland, V. *Acta Crystallogr.* **1998**, *C54*, 1626−1628.

(34) Brown, I. D.; Altermatt, D. *Acta Crystallogr.* **1985**, *B41*, 244−247.

(35) Haaland, A.; Hougan, J.; Samdal, S.; Tremmel, J. *Acta Chem. Scand.* **1988**, *42A*, 409−412.

(36) Frank, W. *J. Organomet. Chem.* **1990**, *386*, 177−186.

(37) Veith, M.; Bertsch, B. *Z. Anorg. Allg. Chem.* **1988**, *557*, 7−22.

(38) Sitzmann, H.; Wolmershäuser, G. *Ber. Bunsen-Ges.* **1994**, *127*, 1335−1342.